Microspectroscopic Analysis of Traditional Oil Paint

Jaap van der Weerd

cover: balancing on the Art-Science interface. Results from infrared analysis of a sample from *Falling Leaves (Les Alyscamps)* by Vincent van Gogh. A processed version of this figure is included in this Thesis as Fig. 8.5.

Microspectroscopic Analysis of Traditional Oil Paint

ACADEMISCH PROEFSCHRIFT

Ter verkrijging van de graad van doctor
aan de Universiteit van Amsterdam
op gezag van de recor magnificus
Prof. mr. P.F. van der Heijden
Ten overstaan van een door het college voor promoties ingestelde
Commissie, in het openbaar te verdedigen in de Aula der Universiteit
Op vrijdag 6 december 2002, te 10.00 uur
door

Jaap van der Weerd

geboren te IJsselmuiden

Promotiecommissie

Promotores:	Prof. dr. J.J. Boon
	Prof. dr. R.M.A. Heeren
Co-promotor:	Prof. dr. J.R.J. van Asperen de Boer
Overige commissieleden:	Prof. Dr. H. Schenk
	Prof. Dr. J.W. Verhoeven
	Prof. Dr. H.J. Bakker
	Dr. A. Burnstock
	Dr. T. Visser

Faculteit der Natuurwetenschappen, Wiskunde en Informatica

MOLART Reports

MOLART - Molecular Aspects of Ageing of Painted Art - is a 5-year cooperative project between art historians, restorers, analytical chemists and technical physicists funded by the Dutch Organisation for Scientific Research (NWO). Technical support and advice is given by Shell-SRTCA (Amsterdam), AKZO-NOBEL (Arnhem), Instituut Collectie Nederland (ICN, Amsterdam) and the Dutch art museums. The project was launched on 1 February 1995 and will end early 2003. The object of MOLART is to contribute to the development of a scientific framework for the conservation of painted art on the molecular level. The focus of MOLART is the determination of the present chemical and physical condition of works of art produced in the period from the 15th to the 20th century. Studies of historical paint manufacturing and workshop practice must give insight into the nature of the painters' media and the painting technique used originally.

Fundamental studies on varnishes, paint, and colorants are undertaken to understand the molecular aspects of ageing since this is thought to be a main cause for the continued need to treat paintings.

This thesis is the seventh in a series of MOLART reports that will summarise all research results obtained in the course of the project. Information about MOLART can be obtained from the project co-ordinator Prof. Dr. J.J. Boon, FOM-Institute for Atomic and Molecular Physics, Kruislaan 407, 1098 SJ Amsterdam, The Netherlands.

Previously issues of the MOLART series:

1. Molecular studies of fresh and aged triterpenoid varnishes, Gisela A. van der Doelen, 1999. ISBN 90-801704-3-7

2. A mathematical study on craquelure and other mechanical damage in paintings, Petri de Willigen, 1999. ISBN 90-407-1946-2

3. Solvent extractable components of oil paint films, Kenneth R. Sutherland, 2001. ISBN 90-801704-4-5

4. Molecular changes in egg tempera paint dosimeters as tools to monitor the museum environment, Oscar F. van den Brink, 2001. ISBN 90-801704-6-1

5. Discoloration in renaissance and baroque oil paintings, Margriet van Eikema Hommes, 2002.

6. Analytical chemical studies on traditional linseed oil paints, Jorrit D.J. van den Berg, 2002. ISBN 90-801704-7-X

Publications

This thesis is based on the following publications:

Chapter 2 - Van der Weerd J, Van Veen MK, Heeren RMA and Boon JJ, The Identification of Pigments in Paint Cross-Sections by Reflection Visible Light Imaging Microspectroscopy (Vis-Imaging). *Submitted to Analytical Chemistry.*

Chapter 3 - Van der Weerd J, Heeren RMA and Boon JJ, Evaluation of Preparation Methods and Infrared Techniques for the Infrared Spectroscopic Analysis of Traditional Paint. *Submitted to Studies in Conservation.*

Chapter 4 - Van der Weerd J, Brammer H, Boon JJ and Heeren RMA, Fourier Transform Infra-red Microscopic Imaging of an Embedded Paint Cross-Section. *Applied Spectroscopy* **56(3):** p. 275-283, 2002.

Chapter 5 - Van der Weerd J, Van Loon A, Heeren RMA and Boon JJ, FTIR Studies of the Effect of Pigments in the Ageing of Oil. *Submitted to Studies in Conservation.*

Chapter 6 - Van der Weerd J, Boon JJ, Geldof M, Heeren RMA and Noble P, Chemical Changes in Old Master Paintings: Dissolution, Metal Soap Formation and Remineralisation Processes in Lead Pigmented Paint Layers of 17th Century Paintings. *Zeitschrift für Kunsttechnologie und Konservierung,* **16(1**): p. 35-51, 2002.

Chapter 7 - Van der Weerd J, Van den Berg JDJ, Keune K, Zucker J and Boon JJ, Metal Carboxy-lates in the Grounds of 19th Century Preprimed Canvases used by F. Church. *Submitted to the Journal of the American Institute of Conservation.*

Chapter 8 - Van der Weerd J, Geldof M, Struick van der Loeff L, Heeren RMA and Boon JJ, Zinc Soap Aggregate Formation in 'Falling Leaves (Les Alyscamps)' by Vincent Van Gogh. *Submitted to Zeitschrift für Kunsttechnologie und Konservierung.*

Other publications:

Van de Weert M, Van't Hof R, Van der Weerd J, Heeren RMA, Posthuma G, Hennink WE and Crommelin DJA, Lysozyme Distribution and Conformation in a Biodegradable Polymer Matrix as Determined by Ftir Techniques. *Journal of Controlled Release* **68:** p. 31-40, 2000.

Wolters-Arts M, Van der Weerd L, Van Aelst AC, Van der Weerd J, Van As H and Mariani C, Water Conducting Properties of Lipids During Pollen Hydration. *Plant, Cell and Enviromnent* **25(4):** p. 513-519.

Van der Weerd J, Heeren RMA and Van Asperen de Boer JRJ, A European 640 X 486 Ptsi Camera for Infrared Reflectography. In: *Le dessin Sous-jacent et la technologie dans la peinture. Colloque XIII, La Peinture et le Laboratoire. Procédés. Méthodologie. Applications, Leuven,1999* (Eds. Van Schoute R and Verougstraete H), p. 231-243. Uitgeverij Peeters.

Heeren RMA, Van der Weerd J and Boon JJ, Ftir Imaging Spectroscopy for Organic Surface Analysis of Embedded Paint Cross-Sections. In: *Fifth International Conference on Optics Within Life Sciences OWLS V, Crete, 1998* (Eds. Fotakis C, Papazoglou TG and Kalpouzos C), p. 179-182. Springer.

Boon JJ, Keune K, Van der Weerd J, Geldof M and Van Asperen de Boer JRJ, Imaging Microspectroscopic, Secondary Ion Mass Spectrometric and Electron Microscopic Studies on Discoloured and Partially Discoloured Smalt in Cross-Sections of 16th Century Paintings. *Chimia* **55(11):** p. 952-960, 2001.

JvdW had been involved in the acquisition of several Infrared Reflectograms, some of which have been published in the following references:

Châtelet A, *Jean Prévost Le Maître De Moulins*, Monographies. Gallimard, Paris, 2001.

Van den Brink P, Two Unknown Wings from a Tryptich by the Master of the Antwerp Adoration. *ArtMatters* **1**: p. 6-20, 2002.

Contents

List of abbreviations

AFM	Atomic force microscopy
ATR	Attenuated total reflection
CCD	Charge coupled device
DRIFTS	Diffuse reflectance infrared Fourier transform spectroscopy
DSC	Differential scanning calorimetry
DTMS	Direct temperature resolved mass spectrometry
EDX	Energy dispersive X-ray spectroscopy
FA	Fatty acid
FPA	Focal plane array
FTIR	Fourier transform infrared
GC	Gas chromatography
GC-MS	Gas chromatography-mass spectrometry
HPLC	High pressure liquid chromatography
IRR	Infrared reflectography
LCTF	Liquid crystal tuneable filter
LD-MS	Laser desorption-mass spectrometry
LM	Light microscopy
MALDI	Matrix assisted laser desorption ionisation
MCT	Mercury cadmium telluride
MIR	Mid infrared
MS	Mass spectrometry
μ-TA	Micro thermal Analysis
NIR	Near infrared
PAS	Photo acoustic spectroscopy
PIXE	Particle (or Proton) Induced X-ray Emission
Py-GC-MS	Pyrolysis-gas chromatography-mass spectrometry
S/N	Signal-to-Noise ratio
SEC	Size exclusion chromatography
SEM	Scanning electron microscopy
SIMS	Secondary ion mass spectrometry
TOF-SIMS	Time of flight secondary ion mass spectrometry
UDR	Under sampling ratio
UV	Ultra violet
VIS	Visible light
XRD	X-ray diffraction
XRF	X-ray fluorescence

1 IMAGING STUDIES IN PAINTINGS RESEARCH

1.1 INTRODUCTION

Paintings are an important part of our cultural heritage. Art from all periods and places is stored, conserved, studied, and admired in various museums. Paintings are studied by investigators in different disciplines:

Art historians study the history of the visual arts, being concerned with identifying, classifying, describing, evaluating, interpreting, and understanding the art products and historic development of the fields of painting, sculpture, (…), etc.[1]

Art restorers or conservators are concerned with the conservation and repair of works of architecture, painting, (…) from the effects of negligence, wilful damage, or, more usually, inevitable decay caused by the effects of time and human use on the materials of which they are made.[1] Common tasks for paintings restorers are replacement of yellowed varnishes, filling and retouching of paint losses and repair of weakened supports.

Paintings researchers in the physical sciences identify painting materials and their current state. Identification of the original materials is important for art historical research to study the authenticity, working methods, and the materials used by the artist. A correct assessment of the current chemical and physical state of the painting is crucial for responsible decisions on the safety of conservation and restoration treatments.

There is a growing awareness that aged paintings are very complex and dynamic systems and cannot be adequately investigated with the tools available to most restorers and art historians. Paintings researchers in the physical sciences therefore refine and extend these studies. They assimilate the vast amount of knowledge that has been gathered in related scientific disciplines and apply the advanced techniques that have been developed in the long tradition of the physical sciences. The hands-on experience of painting restorers and the knowledge on painting materials and techniques gathered by art historians are very important in this research. They indicate the problems encountered in practice, prevent the formulation of historically incorrect hypotheses, and normally arrange the access to paintings and samples from paintings. As a result, paintings research is more and more becoming a multidisciplinary area, in which physicists, chemists, art historians, and restorers co-operate to characterise paintings and their changes in time. This Thesis describes several studies carried out in this multidisciplinary environment. The focus is on the application of microscopic imaging techniques in the analysis of paint samples. The rationale of this research will be presented after an introduction on the physical structure of paintings and an overview of several techniques that are used in their investigation.

1.2 PHYSICAL STRUCTURE OF PAINTINGS

A painting is made of several superimposed layers on a support, normally a wooden panel or a canvas. The first paint layer applied to this support is a white or grey coloured ground layer to provide a homogeneously coloured and smooth surface. Painters often made a sketch of the scenery on top of the ground layer using chalk, charcoal, or ink. Subsequently, the paint layers were applied. Generally, several paint layers were applied for the larger coloured areas, smaller details, shadow regions, and highlights. A varnish layer was applied after thorough drying of the paint layers to provide gloss to the painting and saturate the colours.

The study of multi-layered paint systems presents difficulties for most analytical techniques. The chemical properties of adjacent areas can be completely different and should ideally be analysed individually. It is however impossible to physically dissect the smaller of these structures by means of a scalpel as paint and varnish layers are only between ~1 and 100 μm thick. Inhomogeneities occur on an even smaller scale within the paint layers, as paint itself is a mixture of pigments and binding medium. Pigment particles provide colour and opacity. A fluid binding medium is mixed with the pigment so that it can be applied to a surface. The binding medium cures afterwards to a solid paint layer. The size of individual pigment particles ranges from 0.1 to a few microns and their individual sampling is tricky, if not impossible.

Impurity of the materials used to manufacture paint give rise to inhomogeneities on the molecular level. Painting materials in traditional paints were not nearly pure, as the chemical production and purification methods were far from optimal. Further impurities could easily be introduced during the formulation of the paint, which was commonly carried out in the studio of the artist, as ready-to-use paint was not commercially available until the 19th century.

The final source of inhomogeneities in paint is caused by the several alterations that take place during the lifetime of a painting, possibly influenced by restoration treatments. Paint curing is the first important reaction of freshly applied paint. Drying is normally completed within a couple of hours or days, depending on a large number of factors, including light intensity, temperature, humidity, and the presence of certain pigments or other additives. After drying, chemical reactions keep occurring, albeit at much longer time scales: years rather than days. Indications for these reactions can be obtained from macroscopic changes in paint and varnish layers, including the formation of craquelé, discoloration, yellowing, fading, or darkening of paint. Another effect of ageing is the changing transparency of paints. Many of these long-term reactions are taking place in the insoluble, polymerised oil binder, which is difficult to assess accurately by common analytical techniques.

The general working method sketched is based on the situation before 1900AD. The production methods of painting materials have since been largely modernised. Furthermore, the 19th C painters started to develop more individual working procedures. A complete introduction on methods and materials in the creation of paintings has been given by several authors[2-4] and is outside the scope of the present study.

The complexity of paintings has induced a long history of scientific investigation, which can be categorised in a number of different approaches: non-destructive or non-sampling analysis leaves the painting untouched; analysis of samples, which have been physically removed from the painting; and finally the analysis of cross-sections with imaging techniques.

1.3 NON-DESTRUCTIVE ANALYSIS

The non-destructive or non-sampling approach utilises techniques that enable the study of an intact work of art. Obviously, this is the only choice when sampling of a painting is prohibited by its owner. Non-sampling techniques can reveal a wealth of information on the support, lead containing pigments, underdrawings, and the identity of pigments.

One of the most important non-sampling techniques is X-radiography. X-rays have a high penetration depth and can be used to literally look through a painting. The contrast in the images

is due to X-ray absorbing compounds in the painting, such as lead-containing paints, puttied retouchings, and nails in the support.[5] X-ray photography can be used to study a larger area of the painting in spatially resolved ways and is therefore classified as an imaging technique. Pigments on the surface of a painting can be analysed by PIXE (Particle (or Proton) Induced X-ray Emission).[6] PIXE provides an elemental analysis based on the energies of X-rays emitted upon irradiation with high-energy protons. Similar information can be obtained by XRF (X-ray Fluorescence), where the sample is excited by irradiation with X-rays. PIXE and XRF can analyse only a single spot on the painting simultaneously, and subsequent measurements are needed to analyse different areas (spot-analysis). Normally, this technique suffices for pigment identification in the top paint layer. Alternatively, pigments in the upper layer can be analysed by their visual reflectance spectrum.[7,8]

IRR (Infrared Reflectography) is a non-sampling imaging technique, which is mainly used for the visualisation of carbon-containing underdrawings.[9] IRR detects the NIR (Near Infrared) radiation (wavelength $\sim 1 - 2.5$ µm) that is reflected by a painting. The penetration depth of NIR light is normally high, due to the low scattering power and absorption of most paints in this spectral region. The underdrawing however is commonly drawn with efficient infrared absorbers, e.g. black chalk or lamp black, and can be revealed by IRR. These underdrawing studies are particularly interesting for art historical research, as they provide a clear insight in the early stages of the genesis of the painting.[10] IRR reveals some information on the absorption characteristics of the observed pigment, and can be used for identification of these pigments in some cases. However, the specificity of the chemical information is low and certainly not sufficient for an unambiguous pigment analysis, especially in multi-layered systems. The specificity of IRR can be increased by detecting different spectral ranges independently. The easiest way to achieve this is the use of optical filters.[11] A modern approach of this principle is the implementation of LCTFs to enable NIR spectroscopy (Liquid Crystal Tuneable Filters). This approach seems to produce consistent results, but the claim that 'the specificity is sufficient to enable the differentiation of pigments[12] should certainly not be accepted as a definite identification. Another new development in IRR is the application of FPA (focal plane array) digital cameras, which improve the observed images due to an extended spectral range, and less distortions in the image.[13,14] A different approach to improve the chemical specificity of non-sampling techniques is the use of MIR light instead of NIR light.[15] Limitations of this technique and the more useful alternatives will be discussed in Chapter 3 of this Thesis.

In summary, non-sampling techniques can reveal a wealth of information on the support, lead containing pigments (X-ray), and underdrawings (IRR). However, the chemical information that can be derived is limited to the identification of pigments in the surface layers (XRF, PIXE, VIS-spectroscopy). Identification of the binding medium using non-sampling techniques has not yet been reported. Another disadvantage of non-sampling techniques is the inaccessibility of the deeper layers in a painting, or the impossibility to discriminate these layers, depending on the penetration characteristics of the technique. Individual analysis of different layers might be possible by depth profiling techniques, such as confocal microscopy or photo-acoustic spectroscopy. However, application of these techniques to intact paintings has not yet been reported. Sampling is currently inevitable for a detailed chemical analysis of the binding medium and for the individual analysis of different layers.

1.4 SAMPLING

Samples should be very small to minimise the damage to a painting. They are normally taken using a stereomicroscope and a surgical scalpel. A new range of analysing methods becomes available in this case, because the samples can be used for invasive measurements. Application of these methods results in a detailed identification of painting materials and their degradation products.

Small organic molecules in paint can be identified by GC (Gas Chromatography) and GC-MS (Gas Chromatography-Mass Spectrometry), the most common organic analytical techniques applied in paintings research. These measurements can be used to identify different types of drying oils in an aged paint,[16,17] identify and quantify different oxidation products, investigate solvent extractable compounds[18] in a paint layer and determine the degree of oxidation of an oil medium.[19] Furthermore, the composition of terpenoid varnishes can be identified accurately.[20] A disadvantage of GC and GC-MS is the inability to study the non-volatile products that form the major part of aged paint. Py-GC-MS (Pyrolysis-Gas Chromatography-Mass Spectrometry) can be used in cases where the involatile network is of crucial importance, or in the absence of volatile materials. Volatile and network fragments can be roughly separated before mass-spectrometric analysis by DTMS (Direct Temperature resolved Mass Spectrometry).[21] This method provides a good and fast fingerprinting method for drying oils, resins, waxes, and other classes of materials. Other mass spectrometric techniques have been used in paintings research on a less regular basis. These include MALDI (Matrix Assisted Laser Desorption Ionisation[22]) and SIMS (Secondary Ion Mass Spectrometry[23,24]).

Information on organic functional groups in paint can be obtained from FTIR (Fourier Transform Infrared Spectroscopy) spectroscopy. A complete paint sample, including the oil network, can be analysed, as FTIR does not require samples to be soluble, volatile, or ionised. Therefore, extractions or chemical derivatisation reactions are not needed prior to analysis. Furthermore, only a small sample is needed to obtain quantitative results. FTIR is sensitive to functional groups in a molecule rather than for complete molecules and complete structural identification of the sample molecules is therefore normally not achieved. FTIR has been used extensively in the investigation of the early reactions in the drying of oil, mostly using model compounds.[25-33] Many studies mention the use of infrared spectroscopy in the investigation of oil paints,[34-44] resins,[45-47] and tempera paint.[37,48] Reference libraries are available from several sources, e.g. Sadtler (www.sadtler.com), Aldrich,[49] IRUG (infrared users group, www.irug.org) or the SDBS (Integrated Spectral Data Base System for Organic Compounds, www.aist.go.jp/RIODB/SDBS/menu-e.html). These sources contain a wealth of infrared spectra but the direct applicability of these reference spectra in paint research is limited due to the enormous variety of products that are formed upon ageing of paint. A detailed overview of aged paint systems and their infrared spectra would be of great help for the interpretation of FTIR results, but is not yet available.

Raman spectrometry, like FTIR, characterises the vibrational properties of chemical functional groups. It has been used mainly in the analysis of dyes and pigments.[50-55] The identification of fresh binding media has been reported,[56] but the value of these results in the analysis of aged binding media is not convincing.

Tempera paint[57,58] and several dyes[59] have been investigated using HPLC (High Pressure (or

Performance) Liquid Chromatography). This technique can identify and quantify different amino acids and thereby differentiate the different protein sources used for paints, e.g. glues and egg. SEC (Size exclusion Chromatography) is a form of HPLC where a separation is made on the basis of the hydrodynamic volume of the molecules. It has been used in the analysis of drying oil,[32,60] but the application to older paint samples is hindered by the low solubility of the network fragments in these samples.

Melting tests provide a useful indication on the presence of several materials, such as waxes, proteins etc. However, the tests are fairly unspecific and the results should be taken as indications rather than as proof. A more sophisticated and quantitative technique is DSC (Differential scanning calorimetry), which has been reported as a useful tool for binding medium analysis.[34,61]

The chemical information on the samples can be obtained with remarkable detail by a combination of these techniques. The spatial resolution of the measurement is determined by the sample size needed for analysis and the skills of the analyst, as the sample should be separated manually before analysis. This restricts the spatial resolution, normally to about 50 μm.

1.5 THE IMAGING APPROACH

A powerful approach to increase the spatial resolution is the use of microscopic technique. This approach enables the analysis of cross-sections, which are prepared from multi-layered samples taken from a painting, thereby eliminating the need for a perfect separation during sampling. Paint cross-sections are normally embedded entirely in a polyester or poly-acrylate resin[62,63] to facilitate handling and prevent loss of the minute paint chip (~μgrams). Furthermore, an embedded sample can be polished to obtain a smooth surface in which all layers are visible. The spatial resolution of analyses on embedded paint cross-sections is only determined by the used technique. They are independent of the physical size of the entire sample and can therefore be used to study layers or particles with far greater detail than would be possible by physical separation.

Normal visual light microscopy is the most common imaging techniques and is indispensable in the investigation of paint cross-sections. It is used to investigate the colour, thickness, and particle size distribution of the different layers. The colour and form of pigment particles can in many cases be used for their identification.[64] The spatial resolution of optical microscopy is about 1 μm. An even higher spatial resolution can be achieved by backscattered SEM (Scanning Electron Microscopy), another technique that is routinely used in the investigation of paint cross-sections. The enormous resolving power of a modern SEM (~10 nm) is hardly exploited fully in paint research. The main rationale for analysis by SEM is the possibility to identify elements present in a paint cross-section by EDX (Energy Dispersive X-ray spectroscopy). EDX can be implemented in a SEM and measures the energy of X-rays emitted from a sample upon irradiation with high-energy electrons. SEM-EDX is particularly useful for the spatially resolved analysis of pigments, which normally have a characteristic elemental composition.

Staining tests form a low-cost method to analyse the presence of different organic materials, such as different proteins, oil, and several metals.[5] A disadvantage of these tests is their low specificity. Furthermore, a separate staining test should be performed for every element to be analysed, which makes the chances of missing important compounds high. A final disadvantage

of staining test is the introduction of reactive materials in the sample. These might hinder subsequent analytical investigations.

Imaging techniques that can provide a reliable analysis of the organic materials in a paint cross-section have not yet been used on a routine basis. However, the possibilities of imaging techniques capable of investigating organic substances have increased enormously during the last decade. New technological advances led to several techniques that can be used to assess organic materials with a resolution better than 10 μm, which was previously only accessible by staining tests. These techniques include a microscopic imaging visual light spectrometer,[65] different infrared imaging systems,[66-68] Raman and confocal Raman spectroscopy,[69,70] micro-thermal analysis system,[71,72] spatially resolved mass-spectrometry systems, TOF-SIMS (Time of Flight-Secondary Ion Mass Spectrometry[73]) and LD-MS (Laser Desorption-Mass Spectrometry[74]). An overview of imaging techniques is given in Table 1.1. This large number of new analytical possibilities provides more and more resources to evaluate both the organic and inorganic materials in a paint cross-section. Furthermore, a single paint cross-section can in principle be analysed using all these techniques, leading to a wealth of complementary results. The application of these techniques to paint samples from traditional paintings will improve our insight into their organic chemistry.

Technique	Detection of	Spatial resolution
Microscopy	Colour	1 μm
VIS-imaging	Colour	1 μm
SEM-EDX	Elemental analysis	10 nm
FTIR imaging	Functional groups	6 μm
SIMS-TOF	Molecular weight	< 1 μm
μ-TA	Melting points, heat capacity	1 μm
Raman Microscopy	Functional groups	1 μm

***Table 1.1.** Overview of the main characteristics of different imaging techniques.*

1.6 Scope of the thesis

This Thesis describes the results of the application of different imaging techniques to various paint samples. A thorough description is given of visual light micro-spectroscopic imaging and some applications are presented in Chapter 2. Analytical spectroscopy using imaging micro-FTIR and FTIR in various other modes is the topic of Chapters 3-8.

The innovative visual light spectral imager is mounted on a light microscope and provides a complete visual light spectrum (400-750 nm) of a cross-section with a maximum spatial resolution of about 1 µm and a spectral resolution of about 4 nm. These visual light spectra can in several cases identify pigments in a cross-section. The colour description obtained by the system is objective and unbiased and leads in many cases to identification of pigments in a cross-section. Extensive experience of the analyst, which is required for identification by normal light microscopy, is not necessary. Vis-Imaging can also be used to monitor the effects of discoloration reactions.[24] Imaging-FTIR (Fourier Transform Infrared Spectroscopy) is a relatively new imaging technique. It is a promising technique for the analysis of the binder, as it is highly specific in the identification of organic functional groups and has a diffraction limited spatial resolution (~6 µm). This technique and its application to an embedded cross-section are highlighted in Chapter 4. The application of FTIR and FTIR-imaging to paint cross-sections and other paint samples is not straightforward. The sample preparation procedure can vastly influence the spectral quality and spatial resolution of the final results. Therefore, Chapter 3 gives an overview of the different sample preparation techniques and their application in paintings research. Spectra of paint cross-sections as well as dissected samples are included for a valid comparison.

A recurrent topic in the described analyses is the interaction between pigment and binder. The presence and nature of a pigment can strongly influence the properties of a paint layer. These interactions have been recognised on a macroscopic scale for many years, but their chemical basis is far from completely understood. FTIR is valuable technique for the analysis of these pigment binding medium interactions, as it can be used to study intact samples. However, an unambiguous interpretation of FTIR is difficult due to the complex composition of aged paint.

The mechanisms of early reactions in the oil curing process, as well as the accompanying changes of the infrared spectra are extensively described in the literature. It is however questionable whether these systems give a justifiable model for normally aged paint, because the measurements that were the basis for most of this work on the early stages have been performed on pure esterified fatty acids and not on an oil. Furthermore, the interaction with pigments is not taken into account. The study of paint samples from traditional paintings is also complicated, as the methods and materials used by the painter, as well as later restoration methods are normally not documented and can give rise to large uncertainties about the composition of the starting material. A more controlled alternative is the study of naturally aged test paints. The work of Meilunas *et al.* shows good spectra and a clear interpretation of different 50 years old paints,[37] but highlights only two pigmented oil paints. Further FTIR studies on historically accurate aged paints with a known composition are very limited.

In general, the extended libraries of FTIR-spectra for fresh materials are hardly useable for aged paints, while the number of library spectra for well characterised aged paint materials is

very limited. This provided the rationale to perform a number of analyses on naturally aged test paintings to investigate the long-term effects of several pigments on the oil paint composition. These studies, as well as a short review on the early stages of drying, are described in Chapter 5 of this Thesis. One important outcome of these studies is the indication that different pigments can induce the formation of metal carboxylates in paint.

Chapters 6-8 describe the investigation of paint defects, caused by aggregation of these metal carboxylates. These aggregates, named protrusions, are small whitish lumps of metal soap material that literally protrude through the paint surface. Several paint samples from affected paintings were investigated by various micro-analytical and imaging techniques, including light microscopy, FTIR, FTIR-imaging, VIS-imaging, SEM-EDX, GC-MS, DTMS, and SIMS. Chapter 6 describes an FTIR analytical study on protrusions in paint cross-sections from five 17th century Dutch paintings from different masters. A hypothesis on the origin of lead soap containing protrusions and efflorescence could be developed further on the basis of analysis of unfinished primed canvases by the 19th century American painter Frederic Church. The metal carboxylate containing protrusions found in *Falling Leaves (Les Alyscamps)*, painted by Van Gogh are a result of chemical reactions in the lead chromate/zinc white paint. Analysis of the protrusions in this paint show that the formation process is still active.

2 THE IDENTIFICATION OF PIGMENTS IN PAINT CROSS-SECTIONS BY REFLECTION VISIBLE LIGHT IMAGING MICROSPEC-TROSCOPY (VIS-IMAGING)

A set-up for reflection visible light imaging microspectroscopy (VIS-imaging) as well as its evaluation and application is described and tested. The spatial resolution of the system is about 1 μm at a spectral resolution of 4 nm. The optical contrast between different coloured particles parts in the surface of a sample is optimised with a new image processing method for mapping of the distribution of the identified pigment particles. The potential of VIS-imaging in the study of paint cross-sections obtained from paintings is explored. Spectra obtained from pigment particles in these cross-sections result in the classification or identification of several pigments. The investigated paint samples are challenging test cases, as they contain several coloured materials with a very fine distribution. VIS-imaging can identify and map the most common traditional blue pigments i.e. smalt, azurite, ultramarine and indigo in 17th century oil paintings. Smalt can be identified even after complete discoloration. VIS-imaging analysis assisted in the identification and mapping of modern synthetic red and yellow pigments in a 20th century painting.

2.1 Introduction

A painting consists of several superimposed paint layers and a finishing varnish layer. Information about this layer structure and pigment distribution can only be obtained by taking samples from the painting and preparing paint cross-sections from these samples. A paint cross-section is made by embedding the paint sample in a resin and polishing it in such a way that the different layers are visible as adjacent layers on the surface of the paint cross-section.[62,63,75] The embedding is a convenient way to investigate the layer structure by analytical surface techniques. Reflected light microscopy is frequently used as the first technique to examine embedded paint cross-sections.[64] It reveals the fine dispersion of pigment particles in the binding medium but offers no objective means of pigment identification. Pigment identification is often carried out using X-ray techniques like SEM-EDX (Scanning Electron Microscopy-Energy Dispersive X-ray spectroscopy). This technique determines the elementary composition with a very high spatial resolution and suffices in most cases to identify the pigment. A cheaper alternative would be visual light spectroscopy, which acquires characteristic spectra that can act as a fingerprint for identification of many pigments. The elegant and completely non-invasive fibre technique recently developed by Leona and Winter[8] aims at the acquisition of visual light spectra directly from the surface of the painting. Visual light spectra can also be recorded from pigment scrapings.[76] A limitation of these approaches is that only the surface layer is measured, as the structure of the sample is lost. It is difficult to acquire spectra of lower paint layers. The manual separation of different layers is hindered by the thinness of individual paint layers in paint cross-sections, which normally range from $1-50$ μm. The combination of high spatial and spectral resolution required for measurements of cross-sections has not been available so far.

A potentially suitable high resolution spatially resolved visual light microspectroscopic system was described by Johansson and Pettersson.[65] This set-up enables the acquisition of transmission visual light spectra with a spatial resolution that is in principle diffraction limited. This set-up was adapted to allow the reflection microspectroscopic analysis of paint samples. The biggest change to the system is the possibility to record reflectance spectra. This is necessary, as older paint systems are normally very brittle due to ageing. Thin slices that can be used for transmission measurements can seldom be made due to crumbling of the samples. Implementation of the reflection mode was established by the introduction of a standard analytical microscope in the measurement set-up. This microscope ensures a homogeneous illumination of the sample, a high and reproducible image quality and the easy application of other accessories available on the microscope. These features include darkfield microscopy and the use of crossed polarisers in the illuminating and reflected beam. Both tools can be used to eliminate the mirror reflection from the surface of the sample that normally dominates the reflected light.

The spatial and the spectral resolution that can be obtained with this approach are directly determined by the slit width. A small slit width enables measurements at high spatial and spectral resolution, but decreases the sensitivity as less light is transmitted. The absorption bands in most pigments are very broad and a spectral resolution of 5 nm was considered sufficient for our studies. This requirement resulted in the choice of an 80 μm slit width in the spectrometer set-up. A spatial resolution of at least 5 μm is considered necessary in order to be able to analyse individual pigment particles. The spatial resolution in the Y-direction (perpendicular to the slit,

see Fig. 2.2) then equals the slit width d divided by the magnification M and a resolution of 5 µm is achieved for magnifications higher than 16. The spatial resolution in the X-direction (parallel to the slit) equals the size of the pixels in the CCD camera divided by the magnification M.

The raw data recorded by this microspectroscopic system consist of a series of images, each of which has been acquired at a specific position of the translation table. The most straightforward means of data processing displays a reflection spectrum at a selected location, or shows the intensity of the light reflected from the surface as a false colour image. However, the contrast in these images is normally low. Localisation of specific compounds on the imaged surface can be a complicated and time-consuming task, especially when several different pigments are present. Therefore, an algorithm is developed that uses the complete spectra instead of reflection at a single wavelength to localise a specific compound on the imaged surface with high sensitivity and enhanced contrast.

A comparative study of the most common traditional blue pigments in paintings before 1800 AD, i.e. smalt, indigo, azurite and natural ultramarine is presented to show the potential of this new method and to demonstrate the sensitivity of the set-up. Previous investigations have shown that these pigments can be distinguished by their transmission spectrum.[76] Here, we investigate blue pigments in the various paint layers directly from the paint cross-section by reflectance microspectroscopy.

A second case study is a paint sample taken from *Interior with a Picture* by the 20th century British painter Patrick Caulfield (1936-). Elemental analysis normally does not suffice for the identification of the large number of pigments that have become available during the 20th century. Numerous variations of the organic functionalities in these modern pigments result in a large number of often "tuneable" spectral features. VIS-imaging is expected to provide a useful additional means for the identification of these pigments.
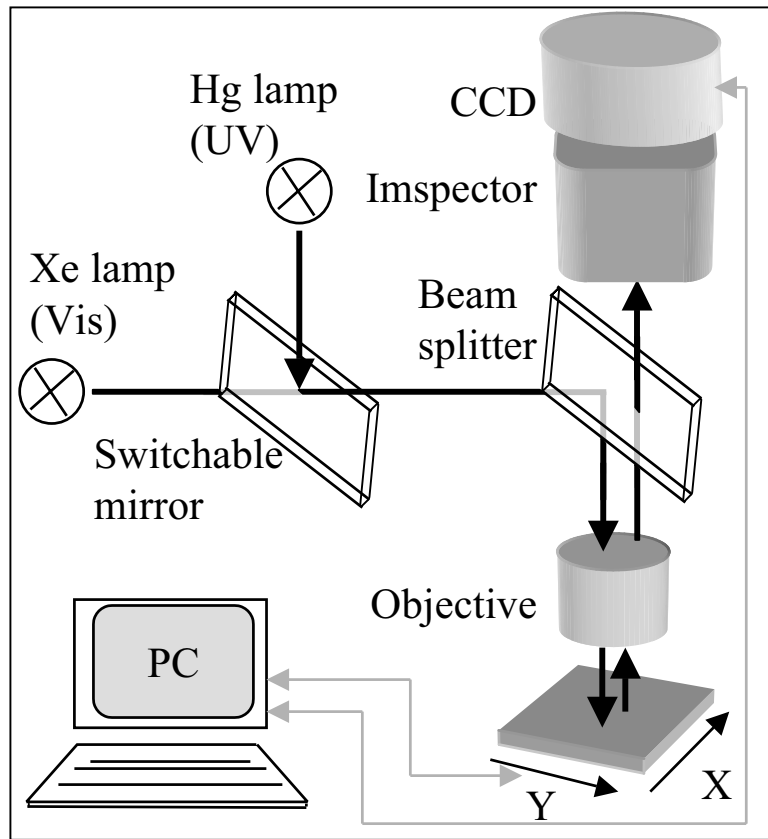
Fig. 2.1. *VIS-imaging experimental set-up displaying the microscope set-up with a visual and an ultraviolet source, the Imspector spectroscope, a translation stage, the CCD-camera and a personal computer that drives the system.*
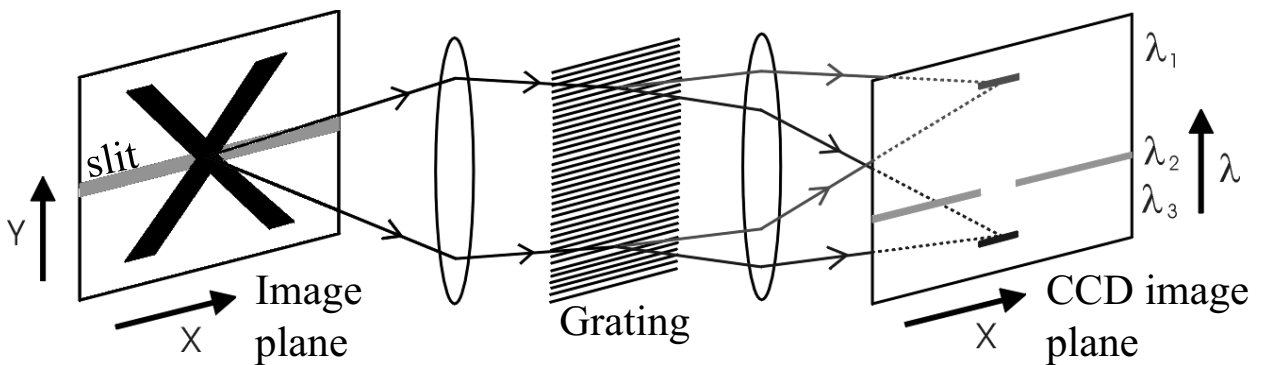

Fig. 2.2. *The working principle of the Imspector. The slit in an image plane (left) transmits a single line of light. The grating diffracts the light in its spectral components and focuses these on the CCD-camera.*

2.2 Experimental

2.2.1 Sample origin and preparation

The studies presented in this paper focus on the application of the technique described above on embedded paint cross-sections. The cross-sections used were obtained from various sources. Two of the samples investigated were taken from 17th century paintings (1648-1652) in the "Oranjezaal", the central room in Paleis Huis ten Bosch, one of the Dutch royal palaces. The samples were taken during a recent extensive restoration (1998-2001). Sample HTBS 19/7 is taken from *Frederik Hendrik ontvangt de survivantie voor Willem II* by Gonzales Coques (1615-1684), while sample HTBS 3/2 is taken from the *Vijf Muzen* by Jan Lievens (1607-1674). Cross-section (A102/11) was taken from a heavily discoloured blue paint layer in *The Seven Sorrows of Mary* (c.1554, St. Leonardus Parish, Zoutleeuw), painted by Pieter Aertsen (1509-1575). The paint cross-section T07112-C2 is taken by T. Learner from Patrick Caulfield's (1936) *Interior with a Picture* (1985-6, Tate Gallery, London, Accession no. T07112).

Samples A102/11 and T07112 were embedded in Polypol (Poly-service, The Netherlands) synthetic resin. The other samples were embedded in Technovit 2000LC (Heraeus Kulzer, Wehrheim, Germany). The embedded paint samples were polished with Micromesh® (Scientific Instrument Services Inc., Minnesota) polishing cloths prior to analysis. Reference pigments were taken from the collection of H.C. von Imhoff that is presently kept at the Canadian conservation Institute (CCI, Ottawa, Canada). The powdered pigments were distributed on a microscope slide for analysis.

2.2.2 Hardware

The visual light imaging system consists of a Leica DMRX analytical microscope (Leica Inc., Wetzlar, Germany), an Imspector V7 spectrometer (Specim Inc., Oulu, Finland), a cooled 1030×1300 pixel Princeton Micromax CCD camera (Roper Scientific, Trenton, USA) and a DynaOptic CTC-512-1 Motion translation stage (DynaOptic Motion Inc., Laguna Hills, USA). A schematic of the system is shown in Fig. 2.1.

The analytical microscope is used for the illumination of the sample and magnification of the sample image. The sample is illuminated by a Xenon visual light source similar to the source used by Johansson.[65] Crossed polarisers are placed in the incident and reflected beam to prevent the transmission of specularly reflected light. The magnification of the sample image can easily be adjusted by changing the objective of the microscope. The entrance slit of the Imspector V7 spectrometer is placed in the image plane of the microscope.

The pixel size of the Micromax CCD-camera is 6.7 µm. The maximum resolution in the X direction is more than ten times (80/6.7) higher than the resolution in the Y direction at equal magnification. The resolution in the X-direction of the CCD-camera is therefore reduced by combining pixels in groups of 10. The sample is moved by the translational stage in the Y-direction, orthogonal to the slit in the Imspector (see Fig. 2.2), such that adjacent lines on the sample are imaged. A data-set is build up by combining the images acquired at succesive translation steps. A single self-written program in Visual Basic (version 6, Microsoft) drives both the translation stage and the camera.

2.2.3 Calibration

A measurement session has to be preceded by calibration of the spectrometer, as the calibration is not completely stable in time. The drift is assigned to slight positional changes of parts of the set-up. Calibration is performed on the line spectrum of a Helium lamp using the Winspec software provided with the CCD camera. Every measurement is accompanied by measurement of a dark current image recorded when the lamp is turned off, and a Teflon surface, which is taken as a white standard in the visual range. The shutter time of the camera is set to a value where the intensity reflected by the white Teflon surface amply falls within the dynamic range of the camera, thus preventing saturation during any stage of the measurement. The camera interface allows the accumulation of several images during a single step of the translation stage to improve the signal to noise ratio.

2.2.4 Data processing

The resulting image-stacks are transferred to Matlab (version 5.3, The Mathworks Inc.) for data-processing. Routines in Matlab transform the image series to a 3D data-set (X, Y, λ) and correct the spectrum for dark-current and background by calculating for every spectrum:

$$\% R_{xy} = 100 * (S_{xy} - B_x)/(W_x - B_x) \qquad [2.1]$$

where %R is the percentage reflection, S is the raw sample data, B is the dark current signal, and W is the reflection of the white Teflon background. The subscripts x and xy indicate the dimensions, in which the variable was determined. Images of white response W and dark current B are independent of the movement in the Y direction and therefore the acquisition of a single image for both W and B suffices to correct the entire data-set.

The software can display the visual light spectrum of a particular spot on the sample and enables the creation of spectral images, in which the reflection at a selected wavelength range is displayed as a false colour image. These images can be used to correlate the measured spectroscopic data-set to the visual light microscopic image. After selection of a single pixel, corresponding to the pigment particle or other region of interest, all spectra are projected onto this spectrum from the data-set, which results in a score vector P. This vector quantifies the similarity between the measured data and the reference spectrum. Mathematically, the projection is a simple dot product:

$$P = \mathbf{D} \bullet \mathbf{r} \qquad [2.2]$$

In which D is the normalised data-set, containing all spectra in rows, and vector r contains the normalised reference spectra as a column. P is the calculated projection, consisting of one scalar for every spectrum (pixel) in the data-set. Vector P can be presented as a false colour image, which visualises the similarity of the reference spectrum and the spectra in the data-set. The localisation of a reference or library component can be determined by taking the corresponding vector as r. In principle, the procedure can be made completely non-supervised by the projection of the data-set onto principal components[77] rather than user selected reference spectra.

2.3 Results and discussion

2.3.1 System performance

The spectral and spatial resolution of the microspectroscopy system described were determined to characterise the performance of the system. The emission bands of a He-discharge lamp are employed to determine the spectral resolution. The He-lines provide a good indication of the overall spectral resolution due to their small natural line-width. The measured peak-width at half height of two lines was measured to be slightly above 3.6 nm, which is better than the 5 nm spectral resolution required for pigment analysis. The line-width covers about 12 pixels on the CCD-camera in the current set-up, which is an unnecessary oversampling. The pixels are binned in the wavelength direction in pairs of five to reduce the size of the data-set. The measured line-width of the most intense He-line after binning is slightly increased to 3.8 nm, as shown in Fig. 2.3a. This minimal decline of the resolution justifies the use of binning.

The spatial resolution in the X-Y direction was determined experimentally from an image data-set taken from a USAF '51 resolution target (Edmunds scientific, Barrington, USA). This target was homogeneously illuminated with white light. The highest line frequency on this target is 228 cycles/mm, which means that individual bars are about 2.2 µm wide. These lines could be resolved in both X and Y direction without any problems (see Fig. 2.3b), indicating that the spatial resolution is well below 2.2 micrometer.

Reference spectra taken directly from common traditional blue pigments in reflection are shown in Fig. 2.4. The spectral characteristics of the investigated blue pigments are clearly distinguishable as has been reported for the transmission spectra.[76] Azurite has an obvious reflectance of blue light, as is expected for a blue pigment. The spectrum of natural ultramarine can be distinguished from azurite by the increased reflection in the red part of the spectrum (650–750 nm), which is almost as high as the blue reflection (400–500 nm). The spectrum of smalt is clearly recognisable from its extra reflection maximum in the reflection spectrum at 565 nm. Indigo extinguishes the incoming beam in the visual region to a large extent. This is due to the low reflectivity of the nearly black indigo clusters. The blue reflection of the indigo is almost featureless, but the intensity of the long wavelength reflection of the spectrum (700–750 nm) is high, which still results in a useful spectral fingerprint for indigo. The small wiggles observed in the indigo reference spectrum are probably due to imperfect projection of the image on the CCD camera by the Imspector or the presence of a coating on top of the CCD array.[65]

The signal to noise ratio in these spectra decreases slightly on the short wavelength side. In the camera selection process special attention was paid to the blue region of the spectrum where conventional CCD cameras have limited responsivity. This is especially important for the analysis of blue pigments. Further pilot experiments showed that heating up of a standard CCD-chip causes high and unstable noise levels, especially in the short wavelength region of the visible spectrum. Therefore, a low-noise, cooled camera was used in the research described in this paper. The lower signal to noise ratio in the short wavelength part of the spectrum (<430 nm) which is found in the current set-up is explained by absorbance in the blue region of the polarisers in the microscope.
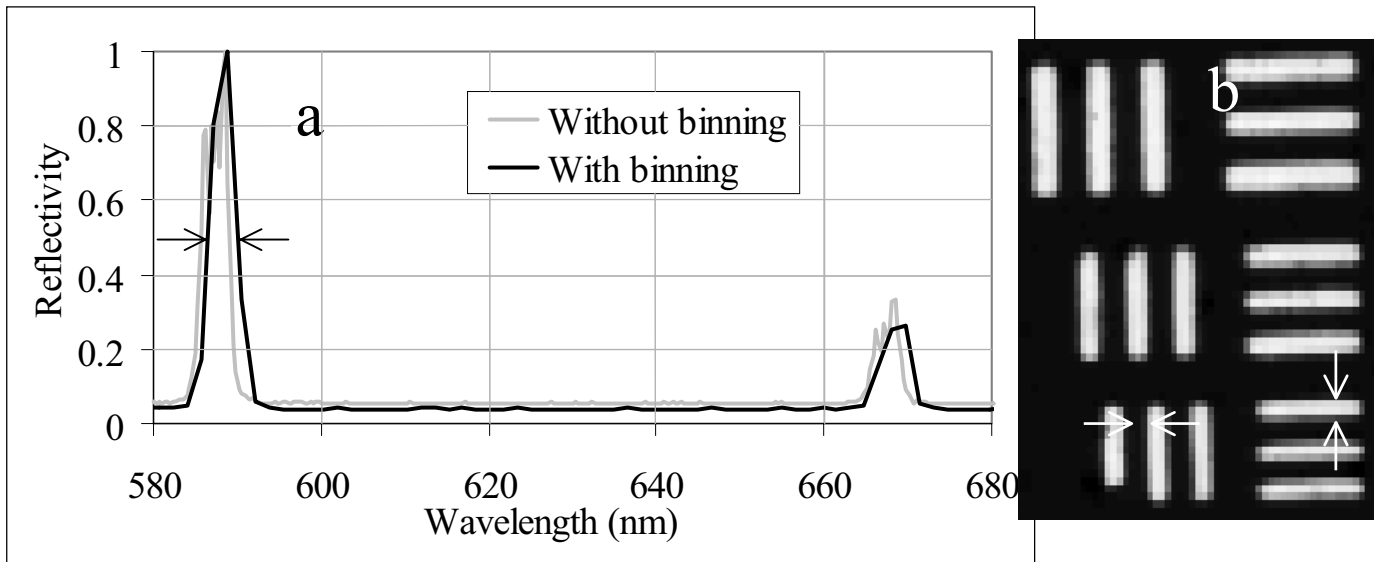
Fig. 2.3. *Validation of VIS-imaging. (**a**) Emission lines of a He-lamp. The arrows indicate the position where the line width is measured. (**b**) Imaging of a USAF 1951 Test target. The width of the lower bars (arrows) is 2.2 μm.*
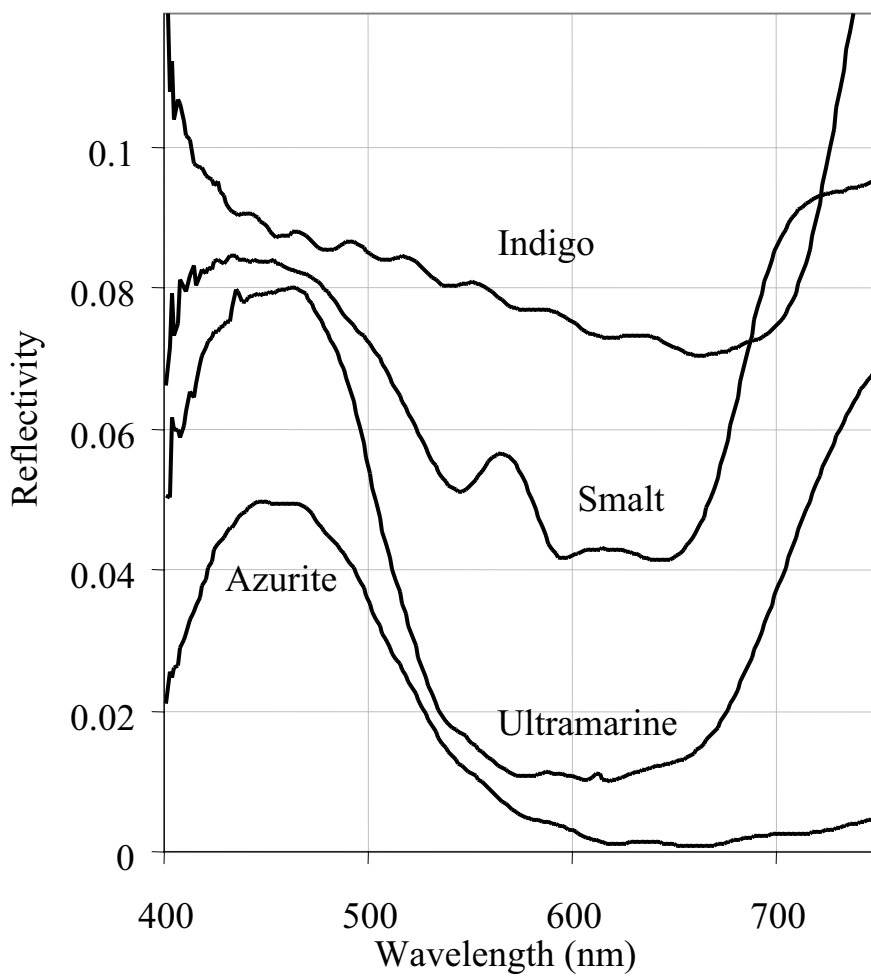
Fig. 2.4. *Reflection spectra of four traditional blue pigments. Smalt (Co-glass), azurite (basic copper carbonate), natural ultramarine and indigo. An offset was added to the spectra for easier comparison. Reflectivity of the pure materials is normally between 0 and 10%.*
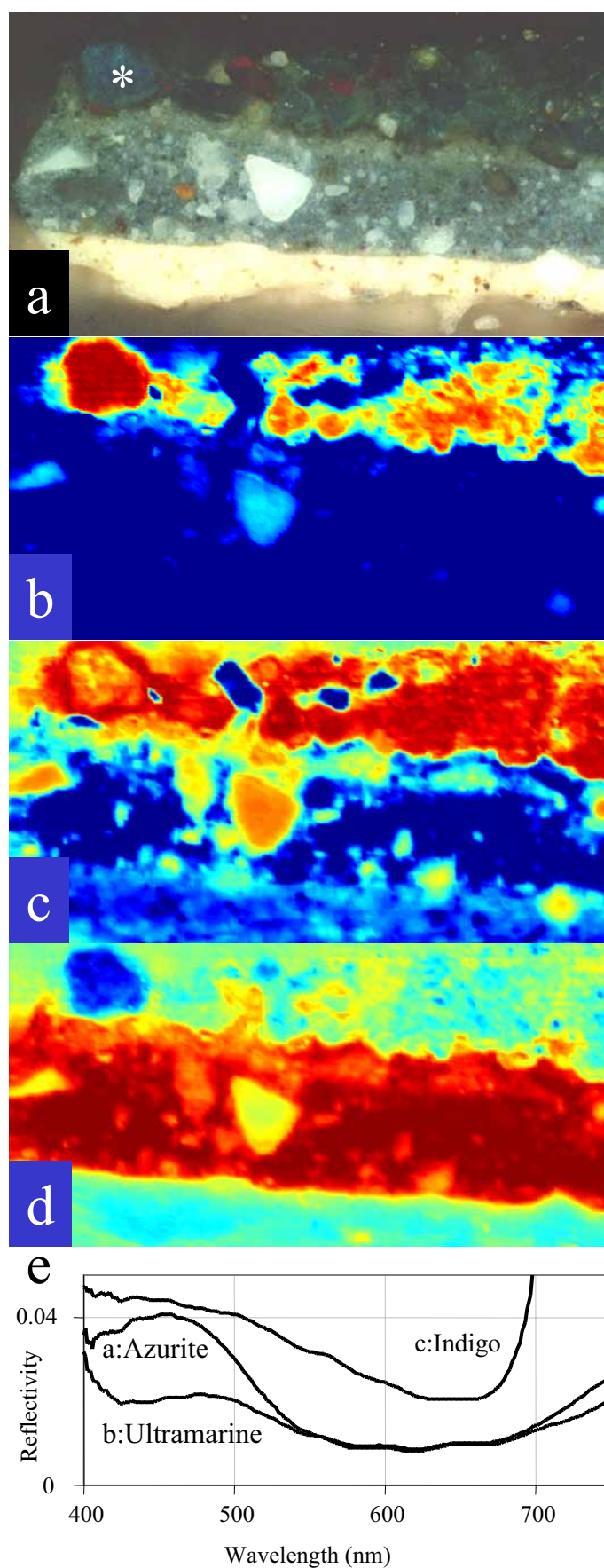
Fig. 2.5. *VIS-imaging data of paint cross-section HTBS 3/2, taken from the painting* Vijf Muzen *(1650) by Jan Lievens. (**a**) Optical microscopic image, (**b-d**) false colour score plots showing the localisation of azurite, ultramarine and indigo respectively, and (**e**) averaged reflection VIS-spectra from the highlighted regions in Fig. 2.5c-d. (see also coloured version at the end of this Thesis)*

2.3.2 Imaging of azurite, ultramarine and indigo

The results of spectral analysis of some paint cross-sections with blue pigments are shown in Figs. 2.5–2.7. Paint cross-section HTBS 3/2 (Fig. 2.5a) taken from *Vijf Muzen* by Jan Lievens (1607-1674) contains different blue paint layers on top of a beige ground layer. The lower blue layer contains some bright white pigment particles in a blue matrix. The darker top layer contains several types of larger blue particles. Such a build-up of layers, in which a thin layer of more expensive pigments follows an underpaint layer with cheaper pigments, is often observed. The apparent presence of different blue pigments makes this sample a good test-case to evaluate VIS-imaging as a tool for pigment identification and mapping in embedded paint cross-sections. The spectroscopic data-set of this sample was imported into MATLAB and processed according to equation 2.1. A spectrum of the big blue particle in the upper left corner of the sample (marked *) was used as a reference spectrum for the projection method. The complete data-set is projected on a single spectrum taken from this position, according to equation 2.2. This projection yields the score plot shown in Fig 2.5b. The score of the large blue particle and all related particles that have similar spectral features is clearly larger than its environment, as indicated by the red shades. The spectral fingerprint corresponding to this pigment is subsequently determined. The co-ordinates of the spectra of which the dot product in P has a higher value than a user-defined threshold value (typically 0.99 on a scale of 0 to 1) are determined first. The non-normalised spectra of the pixels that fulfil this threshold criterion are averaged to yield the spectral fingerprint. This averaged spectrum (Fig. 2.5e) has a greatly improved signal-to-noise ratio and identifies this pigment as azurite.

The spectral fingerprints of the other particles in the top layer were obtained in a similar manner. They are markedly different from the azurite particle in the upper left part. The corresponding score-plot is shown in Fig. 2.5c. Their identification as ultramarine is based on the high reflection intensity of red light ($\lambda > 650$ nm). The low absolute reflection intensity of these particles can be explained by the use of the crossed polarisers, which filter out the light that is specularly reflected by the polished pigment surface. Projection of the data-set onto a single spectrum of the lower blue layer resulted in the score image presented in Fig. 2.5d. The lower blue layer is clearly highlighted and outlines the bigger white particles. However, the smaller white particles and the very small blue particles were not clearly resolved, and therefore the averaged spectrum, shown in Fig. 2.5e, has a relatively high overall reflectance. This layer has an especially high reflectance at longer wavelengths and the colouring material is therefore identified as indigo. The spectrum is not completely identical to the indigo reference spectrum shown in Fig. 2.4, as the high reflection of the red light starts above 650 nm rather than above 700 nm observed for the reference material. This alteration was observed in more indigo samples and is presumably related to chemical changes in indigo due to ageing.

2.3.3 Smalt discoloration

Fig. 2.6a shows a microscopic visual light image of a very large pigment particle (~60×80 μm) in a paint cross-section taken from *The Seven Sorrows of Mary* (c.1554) by Pieter Aertsen (1509-1575). This particle was chosen for analysis as it is partially discoloured. The core of the particle retained its colour while the outer rim is discoloured. A single band reflection image at 550 nm is shown in Fig. 2.6b. The pigment particle is seen as a dark gray area in which the blue core is vaguely observable. The contrast between core and rim is just enough to select a refer-

ence spectrum. The projection method enhances the contrast between the blue core (Fig. 2.6c) and the discoloured rim (Fig. 2.6d). This high gain in contrast clearly shows the advantage of the projection method over the direct reflection images of raw data (Fig. 2.6b). The spectral finger-prints of both regions are plotted in Fig. 2.6e. The absorption bands observed in the reflectance spectrum of the discoloured rim are not very pronounced compared to the spectrum of the blue core, but the two absorption bands at 465 and 565 nm are still visible. Comparison of the spectra to the references in Fig. 2.4 shows a clear resemblance to the spectrum of smalt, a cobalt con-taining glass. This identification is confirmed by EDX and SIMS analysis, in which silicon, potassium, and cobalt were found.[24] The cited study revealed that discolouration of smalt is caused by a change in the co-ordination state of cobalt ions in the glass. This change occurs as the internal basicity of the glass is altered as a result of the loss of potassium ions to the sur-rounding medium. Here we demonstrate that even completely discoloured smalt can be objec-tively identified as smalt.
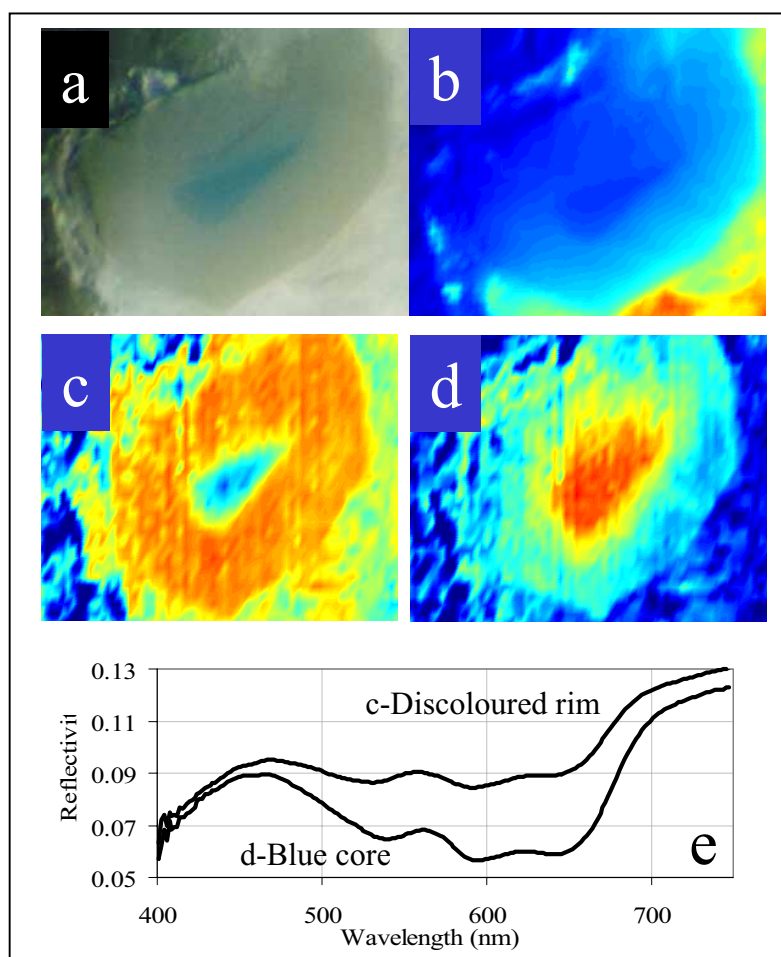
Fig. 2.6. *VIS-imaging data of cross-section A102/11, taken from the discoloured robe of Mary Magdalene in* The Seven Sorrows of Mary *(c.1554) by Pieter Aertsen (1509-1575).* **(a)** *Optical microscopic image showing a partly discoloured blue particle,* **(b)** *false colour image of the intensity of the light reflected at 550 nm,* **(c-d)** *false colour score plots outline the contours of the discoloured rim and the coloured core, and* **(e)** *averaged spectra from the highlighted regions in Fig. 2.6c and d.*
(see also coloured version at the end of this Thesis)

Paint sample HTBS 19/7 is taken from *Frederik Hendrik ontvangt de survivantie voor Willem II* by Gonzales Coques (presumably 1650) and contains colourless transparent masses between opaque white pigment particles (Fig. 2.7a). The projection of the data-set onto a spectrum selected from one of the transparent areas (marked *) resulted in the score plot shown in Fig. 2.7b. This score plot clearly highlights the transparent masses observed in Fig. 2.7a. The spectral fingerprint of these masses (Fig. 2.7d) is comparable to the spectrum of the discoloured rim in Fig. 2.6d and shows the typical features of smalt. In this case, the intensity of the 565 nm band is even higher than the band at 465 nm, indicating that the smalt in this painting discoloured even stronger than the discoloured rim in sample A102/11 (Fig. 2.6f). Smalt is thus identified in a completely discoloured layer based on the spectral fingerprint. This leads to a better understanding of the original intention of the painter, even after complete discoloration of a smalt-containing paint. Also included in Fig. 2.7a are bright blue particles situated next to the discoloured particles. These are not highlighted in the score plot in Fig. 2.7b. Projection of the data-set on a spectrum selected from one of these particles is shown in Fig. 2.7c. An average spectrum (see Fig. 2.7d) identifies this second pigment as azurite. Our data demonstrate that the painter originally used different types of blue pigments in subsequent layers to achieve the colour shade intended.
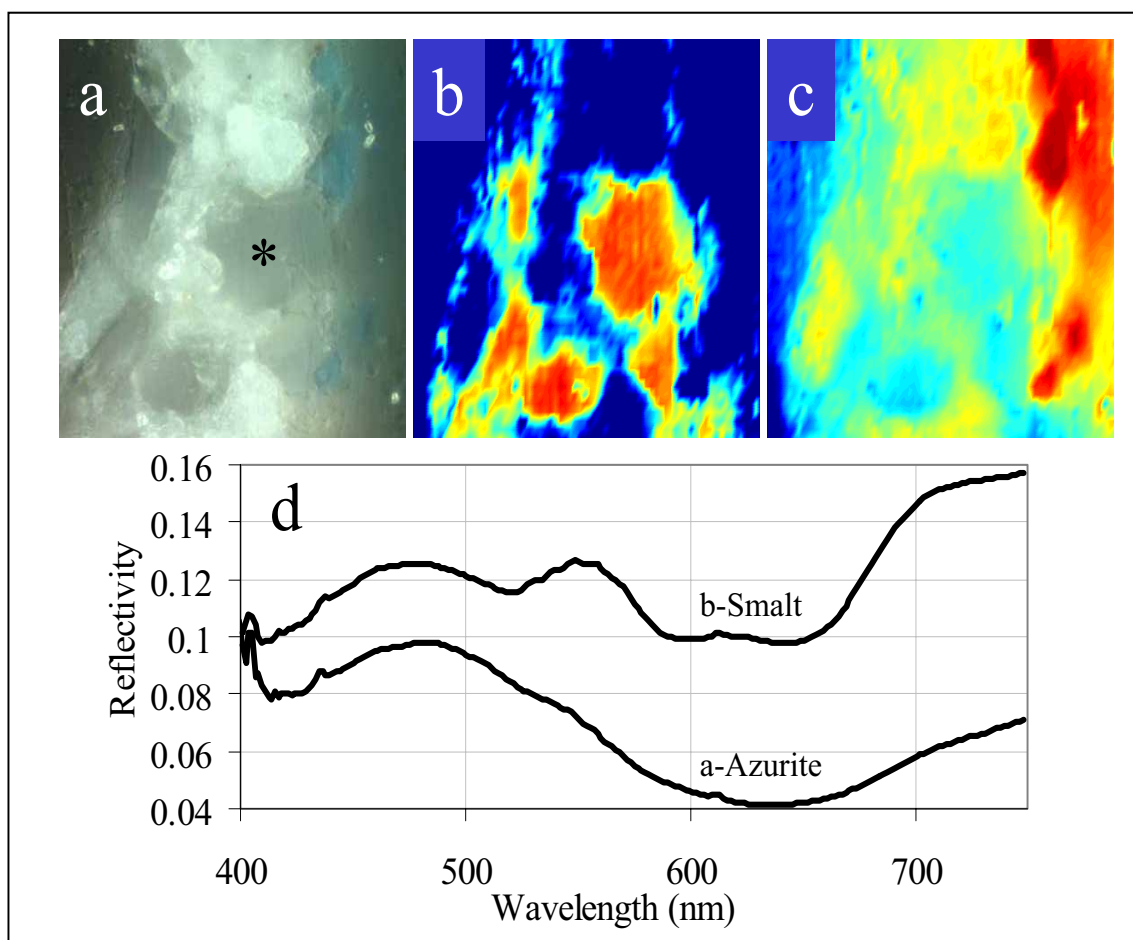
Fig. 2.7. VIS-imaging data of cross-section HTBS 19/7 taken from Frederik Hendrik ontvangt de survivantie voor Willem II *(presumably 1650) by Gonzales Coques. (a) Optical microscopic image, (b-c) false colour score plots outline the distribution of the transparent particles and the azurite particles on the right, and (d) averaged spectra form the highlighted regions in Fig. 2.7b and c. (see also coloured version at the end of this Thesis)*

2.3.4 Modern paint with organic pigments

An even more complex layer structure is found in the modern painting *Interior with a Picture* by Patrick Caulfield (1936-). The cross-section in Fig. 2.8a shows a titanium white ground (no. 7) and a complex build-up of at least 6 paint layers, including three red and two yellow layers. The colour differences between the three red and two yellow layers are too small to allow an unambiguous colour description or identification of the pigments by normal microscopy. The morphology of the pigments cannot be used as an aid in identification, as the pigment particles in the coloured layers are too small to be resolved in visual light microscopy. This is consistent with the small particle sizes of modern pigments and explains the homogeneous appearance of the layers. The microscopic identification of modern pigments is more difficult than the identification of traditional pigments. A positive identification of a modern pigment must be supported by several analytical techniques such as mass spectrometry and SEM-EDX because of the large number of closely related isomeric structures in modern organic pigments. The visual light reflection spectra of most modern pigments are however relatively specific, so that the application of VIS-imaging can assist in their identification. Unfortunately, the reference spectral library for modern pigments is not yet complete, which hampers the identification of pigments with this methodology. Here we demonstrate how VIS-imaging spectroscopy can distinguish subtle spectral differences in complex laminated paint cross-sections. The reflection images are used to localise the different layers in the data-set. Projection of the data-set onto a single spectrum chosen from these layers provides high quality spectra and localises the corresponding pigment in the sample (see inserts in Figs. 2.8b and c).

Fig. 2.8b presents the spectra of the three red layers (numbered 1, 4 and 6 in Fig. 2.8a). It is clear that the subtle colour differences that can be seen between the layers are caused by vast differences in their reflection spectra. The spectrum of layer 1 matches the spectral fingerprint of PR170, a diazotised p-aminobenzamide coupled with 3-hydroxy-2-naphto-O-phenetide.[78] This pigment was also identified by laser desorption ionisation mass-spectrometric techniques. A more detailed description of the MS and SEM-EDX analyses is published elsewhere.[79] The drop-off seen at $\lambda > 650$ nm is not characteristic for PR170. SEM-EDX and mass spectrometric analysis did not indicate the presence of an additional pigment. A possible explanation is the increase of the effective path length of light in a scattering medium at higher wavelength of the light, since the path length of diffusely reflected light in a sample increases with the wavelength due to the reduced scattering.

The spectrum of layer 6 could be assigned to PR101, a synthetic red iron oxide. The presence of iron is confirmed by SEM-EDX. The pigment of the thin and bright red layer 4 suggests an organic azo pigment, but the pigment could not be identified due to the incompleteness of the available spectral library.

The identification of the pigments in the yellow layers (spectra in Fig. 2.8c) is ambiguous due to the unusual steps in the spectra. These steps are not normally found in pure materials. This suggests that the obtained spectra consists of different superimposed spectra. The yellow pigments in layers 3 and 5 are assigned to a PY37 and PY3 respectively. These assignments are supported by EDX, which shows the presence of chlorine in layer 3 and cadmium in layer 5. Reflection spectra of these pigments indeed overlap with the lower wavelength part of the presented reflection spectra. The additional steps observed in the VIS-imaging spectra might very
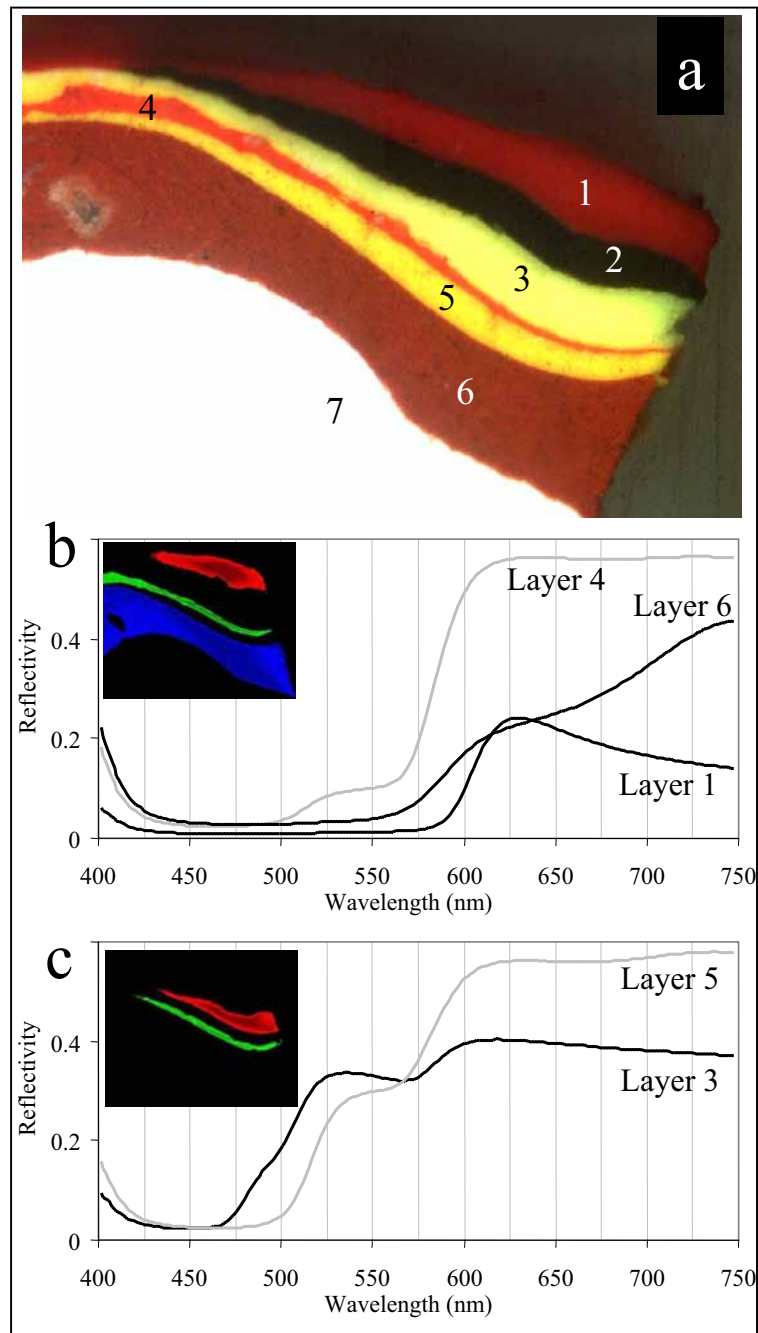
Fig. 2.8. *VIS-imaging data of cross-section T07112-C2 taken from Patrick Caulfield's (1936)* Interior with a Picture *(1985-6), **(a)** optical microscopic image, **(b)** averaged spectra of the three red layers. The insert displays the scores of these layers as a RGB-plot. Red represents the score for layer 1, green for layer 4 and blue for layer 6.*
(c) *Averaged spectra of the two yellow layers. The insert displays the scores of these layers as a RG-plot. Red represents the score for layer 3 and green for layer 5.*
(see also the coloured version at the end of this Thesis)

well be caused by a contamination of the surface of the paint sample by red pigments from the adjacent layers.

The combination of VIS-imaging, mass spectrometry and SEM-EDX lead to an identification for two of the three red pigments and two yellow pigments. Selection of the reference pixels of these pigments and projection on the whole spectral data-set identifies the layers with these pigments in the cross-section.

The case studies presented above prove the value of the visual light microspectroscopy in the study of paint cross-sections. The spatial resolution of the system allows the analysis of very thin paint layers independent from their surroundings, while the spectral resolution of about 4 nm was sufficient for the identification of the most common pigments. The value of the technique can be further increased by the implementation of a pigment database. Furthermore, the set-up can be easily changed to acquire fluorescence spectra with a similar spatial and spectral resolution. This might lead to a better selectivity for fluorescing pigments. The extension of the system to detect light in other spectral regions, e.g. the ultraviolet or the near infrared might also increase the analytical possibilities but will require more extensive technical adaptation to the system.

2.4 Conclusions

A novel reflected light microscopic imaging system (VIS-imaging) was developed and applied in the field of paint analysis. The imaging resolution of the system is near the diffraction limit, and allows the spectroscopic analysis of very thin (~1 μm) paint layers and individual larger pigment particles in traditional paints. The spectral resolution of 4 nm proved to be sufficient for the identification of several pigments. VIS-imaging was employed to localise as well as identify the pigments, which was demonstrated by the application to both traditional and modern paint cross-sections. Four traditional blue pigments were discriminated, among which partially and completely discoloured smalt, a blue cobalt containing potash glass. VIS-imaging is also a useful tool for investigation of modern pigments, but only in combination with other analytical techniques such as SEM-EDX, mass spectrometry and FTIR to provide a well-founded identification. The contrast of the resulting images is greatly enhanced by the application of the described projection method.

2.5 Acknowledgements

3 A PRACTICAL EVALUATION OF PREPA-RATION METHODS AND ACCESSORIES FOR THE INFRARED SPECTROSCOPIC ANALYSIS OF TRADITIONAL PAINT

Several traditional paint samples were prepared for infrared spectroscopic analysis in a number of different ways. The applied methods include the formation of KBr pellets, squeezing of isolated or multi-layered samples in a diamond cell, embedding in a modern resin, and a new method in which a paint cross-section is embedded in KBr and polished from both sides to obtain a thin layer. Microtoming of a paint cross-section embedded in a modern resin was not successful. The various samples were analysed by infrared spectroscopy to analyse the useful-ness of these sample preparation techniques in the field of paintings research. The amount of information that can be derived from the obtained infrared spectra appeared optimal for sample preparation methods that allow the application of transmission techniques. The results obtained for specular reflectance techniques were of lesser quality, while no diffuse reflectance spectra could be obtained. The results can best be traced to a specific layer or structure in an inhomo-geneous paint system if the layer structure of the sample is left intact, i.e. using specular reflec-tance of an embedded cross-section or transmission of a thin section obtained by doubly polish-ing a cross-section embedded in KBr.

3.1 Infrared spectroscopy of multi-layered paint systems

The value of infrared spectroscopy in the investigation of oil paint and paintings research has long been recognised. The application of infrared spectroscopy for the analysis of aged paint and painting materials has been reported several times.[34-43,45-47,80,81] Most of the samples analysed in these studies were ground and prepared in KBr (potassium bromide) pellets, which was the standard sample preparation technique in infrared spectroscopy for many years. However, this method of sample preparation has some serious drawbacks. The most important of these is the complete destruction of the sample structure during the formation of the pellet. Therefore, it is very difficult to individually analyse different paint layers in a complex multi-layered system, such as a 17th century painting (cf. Chapter 1 of this Thesis), as they have to be dissected before the measurement. This need for a physical dissection of the samples limits the accuracy with which the individual layers can be investigated.

The sampling accuracy can be increased in different ways. The most obvious way to allow a better dissection of different layers in a painting is the reduction of the amount of sample needed. Ongoing improvement of FTIR methodology has led to the introduction of different accessories to allow the analysis of samples that are far smaller (< 1 µg) than can be analysed using KBr pellets (≈1 mg). These are the diamond anvil cell,[82,83] and miniaturised ATR (Attenuated total reflection) crystals.[84]

The second way to enable a better individual analysis of different paint layers in a sample is the application of sample preparation methods that leave the structure of the investigated paint sample intact. In this case, details in a sample can be studied individually, as long as the spatial resolution of the applied infrared technique is sufficient. This would clearly be the preferred solution, especially since the spatial resolution that can be obtained in infrared microscopy has been increased quite a lot by the introduction of infrared imaging equipment.[66]

This Chapter aims at a comparison of the various sample preparation techniques (both isolated and cross-sections) in the investigation of paint. The criteria for a useful sampling technique are a high accuracy to trace the results of a measurement to a specific layer in the paint structure, and the quality of spectra, which determines the amount of information that can be extracted from a spectrum. The main conditions for a high quality spectrum are a high S/N (Signal to Noise ratio), symmetric absorption peaks, and a straight baseline.

The spectrometer can analyse a sample in various 'measurement modes', i.e. transmission, reflection (specular or diffuse), photo-thermal, and Raman spectroscopy. These different modes dictate specific requirements to the sample handling. The next section therefore provides the theory of the different measurement modes and reviews the various sample preparation techniques and accessories that adapt a sample to a suitable form for analysis.

3.2 Theory of measurement modes and sample preparation accessories and methods

3.2.1 Transmission

Infrared spectroscopy is most easily carried out using transmission experiments, in which light passes through a sample. The sample partly absorbs the incoming light and thereby reduces the intensity of the transmitted beam. The absorption of a material is a characteristic function of the wavelength λ, and the intensity of the transmitted light can be used as a fingerprint to classify or even identify the sample material. Transmission measurements can be quantitative, as the experimentally determined absorbance A is linearly dependent on both the concentration of the absorbing material and the path length of light in a sample. This relation forms the basis of Lambert Beer's Law:[85]

$$A_{\lambda v} = \varepsilon_\lambda \cdot c \cdot l = -\log T_\lambda \qquad [3.1]$$

in which the extinction coefficient ε ($l\ mol^{-1}\ cm^{-1}$) is a characteristic property of the absorbing material, c is its concentration, and l is the path length of the light through the sample. Absorbance A can directly be deduced from the transmission T, which is the fraction of light transmitted through a sample (scale 0–1). Both the transmission and the absorption notations define the ratio between sample and reference and are dimensionless.

The successful application of transmission infrared spectroscopy is often problematic, as many materials are efficient absorbers of infrared light. As a result, the intensity of the transmitted light can easily become very low and cannot be measured accurately. Generally, the transmission of the most intense peaks of interest in the spectrum should be more than 0.1 to be quantified accurately. This implies that the absorbance values should not exceed 1. The infrared sampling accessories available for transmission measurements reduce the high absorption values by decreasing either the concentration c (dilution) or the path length l. Dilution unavoidably leads to the loss of structural integrity and therefore this method cannot take advantage of the high spatial resolution provided by microscopic analyses. Therefore, the analysis of a cross-section with a small thickness would be the most promising approach. There are several ways to prepare a sample for transmission measurements. The most common methods will be discussed below.

3.2.1.1 KBr pellets

The most familiar infrared sampling method is based on KBr (potassium bromide) pellets. KBr is a salt that is transparent in the infrared region and is bought as a white powder. The application of high pressure ($\pm$ 5 tons) to the salt changes it into a solid transparent pellet. A sample can be diluted in a KBr pellet by mixing sample and KBr powder before pressing the pellet. Preparation of KBr pellets normally involves the grinding of the sample to prevent light scattering. Structural information is therefore lost completely and the application of imaging techniques is not useful. Spatial information can only be obtained by manual separation of the different areas of interest in the sample. Unfortunately, a rather large amount of sample is required (~3 mg, or 2–4 % w/w of the total pellet) for a good absorbance spectrum.

3.2.1.2 Diamond anvil cell

A diamond anvil cell consists of two diamond windows. The sample is squeezed between these windows before analysis. Diamond is an appropriate window for a transmission cell, as it is transparent in the important infrared regions as well as in the visual region. Furthermore, the hardness of diamond makes the squeezing of most samples straightforward. The diamond anvil cell is an established sampling accessory in infrared spectroscopy and has been used to analyse archaeological[86] and paint[87] samples. Sample preparation is easy, especially when facilitated by a stereomicroscope. Only a minor amount of sample is required for a high-quality infrared spectrum.

3.2.1.3 Microtome

Another approach to obtain a thin layer of sample is the slicing of an embedded sample using a microtome. The thickness of sliced samples should be below 15 μm to prevent complete extinction of the incident light by absorption or scattering. Advantages of slicing are the conservation of the structure of the sample and the possibility to sample existing paint cross-sections. Microtoming of samples embedded in curing resins has been described as a routine procedure.[43,82,88] A problem of microtoming samples embedded in a resin might be smearing of the polyester or poly-acrylate embedding medium on the sample surface, which will contaminate the sample spectra and thereby complicate spectral interpretation. Silver chloride (AgCl)[89a] and potassium bromide (KBr)[89b] have been proposed as embedding medium to prevent this. A problem of AgCl is its darkening due to ultraviolet and visible light. This makes visual inspection of the sample difficult to impossible, but does not significantly influence the infrared spectra. Another problem is the accelerated corrosion due to the reactivity of AgCl. Samples should therefore be investigated preferably within one day after sample preparation.

3.2.1.4 Polishing

An elegant way to obtain thin sections from a cross-section is to polish a sample on both sides until a thin slice remains. A sample should be polished on one side, which is than glued onto a glass slide. Subsequently, the other side is polished in until the sample is thin enough to transmit light. This method is known from petrology were rocks crystals can be studied in transmitted visual light in this manner[90] and has been used to study embedded paint cross-sections in transmitted light.[5]

This method cannot be directly applied to prepare samples for transmitted light infrared spectroscopy, as existing glues are strong infrared absorbers and seriously disturb the analysis and its interpretation. In this study, we propose cold flowing KBr to act both as glue and infrared transparent window. The proposed procedure is outlined in Fig. 3.1. The sample is positioned with the layers vertical in a thin layer of KBr and covered by additional KBr. The sample is subsequently pressed into a pellet, which is polished on one side. The pellet is re-introduced in the KBr die with the polished side upward and is covered by KBr. Pressure is applied again and the sample in the pellet is subsequently polished on the other side until the sample is thin enough to allow transmission FTIR measurements. This procedure completely avoids the use of infrared absorbing media, and can be applied without specialised equipment.
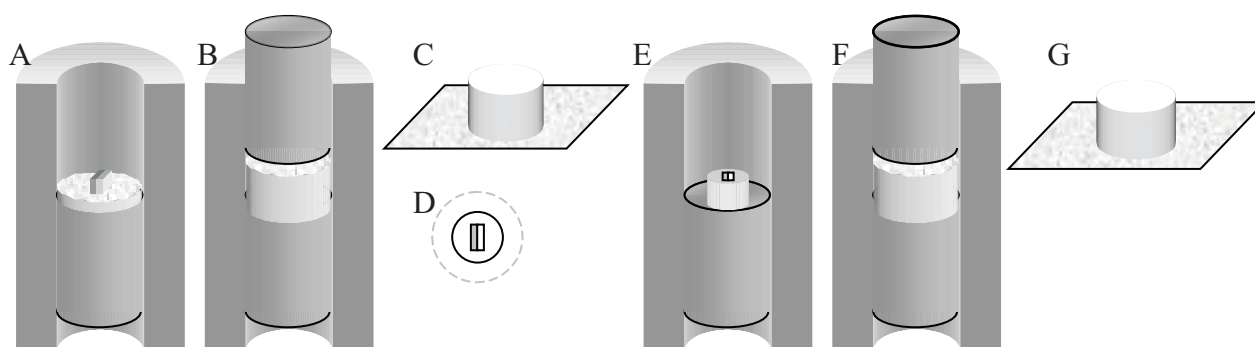
Fig. 3.1. *Proposed procedure for the preparation of thin sections of a multi-layered paint system. (**a**) A multi-layered sample is positioned in a thin layer of KBr in a KBr-die. (**b**) The sample is carefully covered with additional KBr and a transparent KBr pellet is made by the application of high pressure. (**c**) The KBr pellet is ground and polished until a flat surface is obtained in which the layers of interest are present on the surface. (**d**) The rim of the KBr pellet is removed and (**e**) the remaining pellet is re-introduced in the KBr-die upside down. (**f**) KBr is added and a new pellet is created. (**g**) Finally, this pellet is ground and polished until the section is thin enough to allow transmission measurements.*

3.2.1.5 Attenuated total reflection

Attenuated total reflection (ATR) is basically a transmission technique, although the name suggests differently. The principles of total reflection can be derived from Fresnel's law, which describes the fractions of a light beam that are reflected and transmitted on arrival at a surface.[91] Fig. 3.2 displays a result of Fresnel's law for unpolarised light arriving at a surface under an incidence angle θ_i of 30°. The transmission is 1 (100%) when the refractive indices are equal ($n_2/n_1 = 1$), but in all other cases the reflected light has a non-zero intensity. The reflection of the incident beam is 1 (total reflection) when n_2/n_1 is smaller than ~0.5. During total reflection, light is not completely localised inside the high refractive index material, as a standing wave, called the evanescent wave, protrudes from its surface.[85] This evanescent wave can be absorbed if an absorbing material is penetrated in this process. This ATR process is successfully employed in infrared spectroscopy by bringing a sample in close contact with a high refractive index material, called the ATR crystal. The small penetration depth of light in the sample (e.g. 1 μm at 2000 cm^{-1}, $\theta_i = 25°$, $n_{crystal} = 4$, $n_{sample} = 1.5$) makes ATR very suitable for the analysis of thin surface layers, e.g. varnish layers, which are normally difficult to sample. Another common application of ATR is the study of the drying mechanism of oil.[33] Larger ATR crystals have been used extensively for decades, but are now increasingly replaced by small ATR crystals,[84] such as the Golden Gate system with a diamond crystal. These systems can obtain high quality spectra from small samples and can therefore be useful for conservation research. Microscopic ATR crystals are a new, interesting development. These crystals can be connected to an infrared microscope and preserve the spatial information of the sample. In combination with FTIR-imaging,[67] this is a versatile accessory, which is very promising for the study of paint cross-sections, as it enables the analysis of intact embedded cross-sections, without the need to prepare a thin layer. A problem that can be anticipated in this application is an imperfect contact between the sample and the crystal. Furthermore, the absorption of inorganic pigments will be overemphasised, as the effective path length increases with the refractive index of the sample.
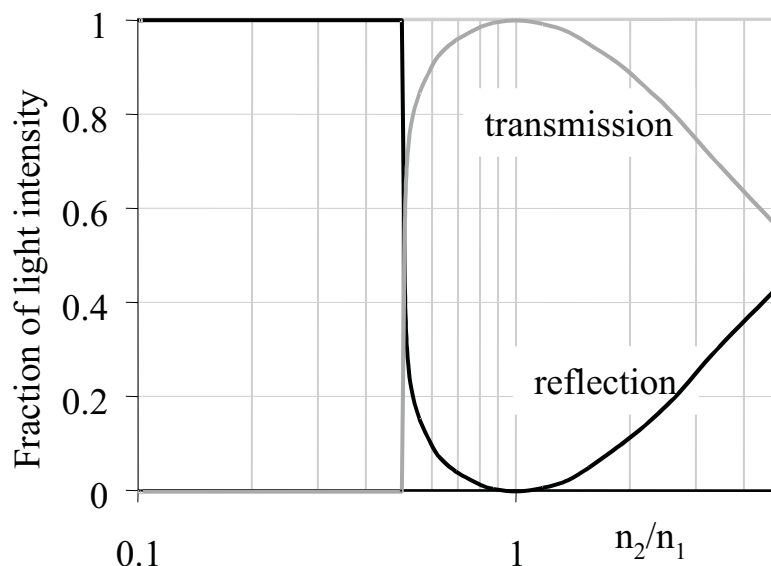
Fig. 3.2. *Results of Fresnel's law: transmission and reflection as a function of the refractive index ratios. The intensities of transmitted and reflected light are present as fractions of the intensity of the incoming beam. (calculated for unpolarised light, θ_i of 30.)*

3.2.1.6 Reflection-Absorption Spectrometry

A sample prepared for Reflection-Absorption spectrometry, also known under the ugly but popular nickname 'Transflection', should consist of a thin layer of sample on a smooth metal surface. The incoming light is transmitted through the sample, reflected by the metal surface, and transmitted again through the sample.[85] The effective path length of the light beam in the sample is at least double the layer thickness and can be further increased by using a grazing angle objective. Reflection-Absorption Spectrometry is applicable only in a limited number of cases in the field of traditional paint research, e.g. varnished gildings or silver layers, but can result in high quality spectra (unpublished results).

3.2.2 Specular reflectance

The earlier discussion on total reflection pointed to the influence of a surface between two materials on light arriving at the surface. A beam will be partly or fully reflected by this surface when the refractive indices of the two materials differ. The intensities of the reflected and transmitted beams are described by Fresnel's law,[91] and exemplified in Fig. 3.2, which presents the results of Fresnel's law for a range of different refractive index ratios. A refractive index ratio of 1.5 (n_2/n_1) results in a 4% reflectance, while the reflectance increases to 36% at a refractive index ratio of 4 (Fig. 3.2). The intensity of the reflected beam is thus related to the refractive index of the sample. The absolute values for the refractive index spectrum acquired by specular reflectance are not very accurate, as the results are influenced by absorption of the evanescent wave, surface corrugation etc.. Nevertheless, a specular reflectance spectrum can be transformed into an absorbance-like spectrum by the Kramers-Kronig transformation,[83,92] which is a standard feature in the software that comes with commercial spectrometers. Specular reflectance measurements can easily be applied to existing embedded paint cross-sections. The enormous number of samples already prepared in the past for optical microscopic investigation in various

laboratories can therefore be used with minimal additional sample preparation and without extra sampling of the painting. Furthermore, a high spatial resolution measurement can be applied, as the layer structure remains intact during embedding.

Dedicated specular reflectance accessories allow the adjustment of the incidence and polarisation angles of the light beam. However, the spatial resolution that can be achieved with these 'neat' systems is limited, as no microscope can be included in the system. On the other hand, several infrared microscopes have the possibility to analyse light reflected from a sample. This approach improves the spatial resolution to the theoretical maximum. However, the angle of the incident beam loses its definition, as it becomes a range of values determined by the numerical aperture of the microscope objective, instead of a single value. This loss of definition influences the intensity of the reflected beam and therefore reduces the accuracy of specular reflectance measurements. Another side effect might be introduced in inhomogeneous samples, as the intensity of the specular reflectance is dependent on the refractive index of the sample (which is the basis for the specular reflectance measurements). When applied to paint samples, the high refractive index of inorganic pigment particles will lead to strong reflectance bands, known as 'Reststrahlen' bands,[85,93] while the intensity of the organic binding medium is relatively low. Specular reflectance has been applied successfully on different kinds of polymer samples,[94] ceramics,[95] and paint cross-sections.[87]

3.2.3 Diffuse reflectance

Absorption and specular reflectance give a more or less complete description of the interaction between light and homogeneous samples. Homogeneous in this context means that the sample does not contain internal surfaces of materials with different refractive indices. This condition is however normally not satisfied for paint samples, which contain both binding medium and pigment particles. Fresnel's law is also valid at internal surfaces and lead to light scattering inside the paint layer, as shown in Fig. 3.3. Part of the scattered light leaves the sample on the illuminated side and is called diffuse reflectance. The effective path cannot be determined for most systems and this makes the application of Lambert-Beer's law (Eq. 3.1) unpractical. A better alternative is the Kubelka-Munk transformation, which can be used to transform the intensity of diffusely reflected light into an absorption-like spectrum.[96,97] The Kubelka-Munk transformation is nowadays a standard feature in the software delivered with spectrometers. The major task of diffuse reflectance accessories is the rejection of specularly reflected light. When a mix of specular and diffuse light is analysed, neither the Kubelka-Munk correction nor the Kramers-Kronig transformation will lead to useful results.

3.2.3.1 DRIFTS

Samples for DRIFTS are normally powdered and mixed with KBr for dilution. The incoming light beam is focussed on the sample by a parabolic mirror, while a second parabolic mirror reflects diffuse reflectance light towards the detector. The disturbing influence of specular reflectance is reduced by the rough surface of the powdered sample.
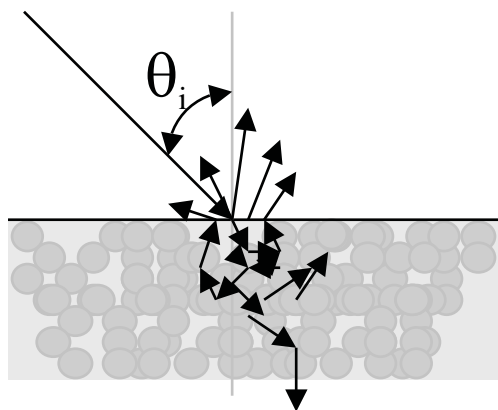
Fig. 3.3. *Scheme of diffuse reflectance. The incoming beam is scattered extensively in the paint, leading to a broad distribution of reflectance angles and loss of polarisation.*

3.2.3.2 Sandpaper

An elegant method that is also based on reflectance by a rough surface is diffuse reflectance from sandpaper.[81] Silicon carbide (SiC) particles, the most common abrasive in commercial sandpaper do not absorb mid-infrared radiation and are therefore well suited as sample support for DR spectroscopy. Applying sample on sandpaper is easy, as it is a side effect of its normal use. This method destroys the spatial structure of a sample, but allows the sampling of a surface layer. It seems impossible to sample different layers in a multi-layered sample in a controlled way, and this method is therefore not promising for traditional paint samples.

3.2.3.3 Crossed polarisers

Specular reflectance of a flat and smooth surface can be removed by the use of crossed polarisers. This method exploits the loss of polarisation upon diffuse reflectance. Specular reflectance preserves the polarisation and is filtered out by the crossed polarisers. This method is applied on a routine basis in visual light microscopy.[98] Its application in infrared spectroscopy seems straightforward, but has not been found in literature by the author.

3.2.4 Photo-thermal detection

Photo-thermal techniques measure the temperature increase of a sample due to absorption of light. This temperature rise is a fairly direct measure for the absorption of the incoming light. It can be measured by a miniature thermometer or, less directly, a microphone (Photo-acoustic spectroscopy). Photo-thermal detection might have some major advantages for paint research. One advantage is the easy sample preparation: the preparation of thin or diluted samples is not necessary as heating takes primarily place at the front side of the sample. Furthermore, specular reflections do not induce heating of the sample and therefore do not disturb the measurement.

3.2.4.1 Temperature sensors

The energy deposited in the sample can be quantified by determining the induced rise in temperature. The thermometer to be used, most likely a thermocouple or thermoresistor, should be small to prevent shading effects, allow a fast response, and provide a high spatial resolution. Hammiche *et al.*[99] used a micro thermal analyser (µTA) equipped with a thermo-resistive canti-

lever tip, which can directly perform a spot temperature analysis. The first results of this approach look promising, but at present, the measurement times are too long to be of practical relevance. Further improvements of this technique might lead to an apparatus with a very high spatial resolution, as the ultimate resolution is dependent on the tip size and the heat diffusion properties of the sample rather than on the diffraction limit of infrared light. Another approach to probe temperature changes is the tracing of volume increase and surface deformation by an accurate atomic force microscope (AFM).[100] However, no experimental spectra have been published using this technique and the usefulness of this approach cannot yet be assessed.

3.2.4.2 Photo-acoustic spectroscopy

PAS (Photo-acoustic Spectroscopy) is another approach to quantify the energy deposited in the sample by absorption of light. PAS is based on the photo-acoustic effect, found by Bell in the 1880s, but implemented in FTIR only in the 1980s.[101] A modulation of the incident beam varies the heat deposition in the sample. The fluctuating temperature of the sample surface induces a fluctuating pressure in the gas surrounding the sample. These fluctuations can be detected as sound when the modulation frequency is chosen correctly. A modulated beam produced by a normal rapid-scan spectrometer can very well be used to measure PAS spectra, but the application of a step-scan interferometer has distinct advantages,[102] such as a more controlled depth profiling. PAS is currently a well-developed, commercially available, and routinely used measurement technique. An advantage is the facile, contactless probing of the surface of thick samples. It might be a good sampling method to probe the surface of intact paintings as well as embedded paint cross-sections. However, the current commercial PAS accessories cannot handle larger (>1 cm^2) samples and do not provide a spatial resolution, which makes them of little use in the analysis of traditional paint.

3.2.5 Raman spectroscopy

Raman spectroscopy has evolved to an established technique in the past 30 years. It is therefore nowadays very uncommon to classify Raman as 'another' IR sampling technique. Instead, both infrared and Raman spectroscopy are normally classified as vibrational spectroscopy. Nevertheless, Raman spectroscopy basically is an approach to measure absorptions in the infrared region. Raman scattering is the phenomenon where energy of a photon is changed during scattering[103] due to the excitation or relaxation of molecular vibrations. The difference between the excitation and the scattered beam can be determined experimentally and equals the energy of the vibrational transition. Absorption peaks in infrared and Raman spectroscopy appear at equal spectral position. However, Raman active bands might be completely absent in infrared spectra and vice versa, as the conditions of vibrational excitation are completely different. The techniques are therefore complementary. The short wavelength of the exciting light, normally between 500 and 1100 nm allows the use of normal glass windows and lenses. The spatial resolution of Raman spectroscopic imaging can be as high as 1 μm as a result of the short excitation wavelength. The successful analyses of pigments,[51,54] polychromed sculptures,[53] different binding media[56] and even rock paintings[104] by Raman spectroscopy have been reported.

3.3 Comparative studies of a 17th century multi-layered paint

Only a small number of the various accessories and sample preparation techniques reviewed in the previous section are promising in the investigation of complex traditional paint systems. As explained, the layers in a multi-layered sample can be better sampled when only a small sample is needed. In this respect, a diamond anvil cell is the most promising and is therefore included in the following evaluation. A number of different sample preparation methods yields a prepared sample with an intact layer structure. The most common way to prepare a paint cross-section is by embedding in a synthetic resin. This method has been used for years by various painting investigators to enable optical microscopic analysis of a paint structure. As a result, large numbers of cross-sections are available and could be used for infrared analysis. Embedded paint cross-section can be measured directly in a reflectance mode, both specular and diffuse. Other ways that might enable the infrared analysis of embedded paint cross-sections are microscopic ATR, and Raman spectroscopy. The photo-thermal techniques have not been included in the present study, as they are not routinely available (small temperature sensors) or do not provide a reasonable spatial resolution (PAS).

Transmission measurements of an embedded paint cross-section other than ATR are not possible, as the sections are too thick and block the incoming light beam completely. Therefore, several methods were evaluated to enable the analysis of a multi-layered paint sample in transmission mode. These include the careful squeezing of a multi-layered sample in a diamond cell, microtoming of a thin section of an embedded paint cross-section, and the newly proposed KBr polishing technique.

A valid evaluation of these sample preparation methods must ensure that the other parameters are kept constant. Therefore, all infrared spectra are recorded on the same infrared spectrometer. Optimal evaluation of the spectral quality can be achieved by single-point FTIR detection, as this provides a more reproducible quality. Imaging results are included additionally to the single point measurements only in the cases where a higher spatial resolution is advantageous, i.e. when the sample preparation method preserves the layer structure of the sample. A very important factor to keep constant is the investigated paint system. The paint should thus be available in relatively large amounts, to ensure that the layer structure investigated by the several techniques is very similar. Furthermore, the investigated paint structure should be taken from a traditional paint to ensure the significance of the obtained results. These demanding preconditions could be fulfilled elegantly by the availability of a discarded 17th century Dutch painting. A large piece of this painting was sacrificed by the Rijksmuseum Amsterdam for research, due to its poor condition. Care was taken that all the samples taken for analysis were taken from the same area and that the same layer structure observed for all samples is similar.

Characterisation of the paint is not the main focus of this Chapter. However, knowledge on this paint is essential for a correct comparison of the various preparation techniques. Therefore, interpretation of the obtained spectra is also included, as well as the results of additional analysis by optical microscopy, SEM-EDX, and GC-MS.

3.4 Experimental

All samples used in this project were taken from the same area in a single painting, painted in 1773 by an unknown painter. The embedded sample used for optical microscopy, SEM-EDX, and several FTIR techniques was embedded in Technovit 200LC (Heraeus Kulzer, Germany) and polished using Micromesh® polishing cloths up to the finest mesh (12000) (Scientific Instrument Services Inc., Minnesota).

A Leica DMRX analytical microscope (Leica Inc., Wetzlar, Germany) was used for visual light microscopy. SEM-EDX analysis was performed using an XL30 SFEG SEM and an EDAX EDX system (FEI company, Eindhoven, the Netherlands). The accelerator voltage used was 25 kV. The sample was carbon coated to improve the conducting properties of the surface. Mass spectrometric analysis of the homogenised stack of layers was carried out following the procedure by Van den Berg *et al.*[105]

KBr (Aldrich, FT-IR grade) pellets were made in a macro-micro KBr die (Aldrich) using paper inserts to minimise the amount of sample needed. Thin slices obtained by polishing were embedded in KBr by using the same KBr and die. The resulting pellets were ground using standard sandpaper to remove excess KBr and subsequently polished using Micromesh polishing cloths up to the finest mesh (12000). The diamond cell was a P/N 2550 (Graseby Specac, Orpington, Kent, UK). The Leitz microtome was equipped with glass knives, prepared from glass strips (Agar, Van Loenen, Zaandam, The Netherlands) by a LKB KnifeMaker. A Bio-Rad slide-on ATR connected to the standard 15X Cassegrain objective was available for ATR measurements. The ZnSe infrared polarisers were obtained from Bio-Rad.

The FTIR measurements described in this paper were performed on a Bio-Rad FTS-6000 (nowadays Digilab, Cambridge, MA, USA) FTIR spectroscope, combined with a Bio-Rad UMA-500 IR microscope. All single point spectra were recorded at 4 cm⁻¹ spectral resolution, an undersampling ratio (UDR) of 2, and a mirror speed of 5 kHz. 100 spectra were accumulated to increase S/N.

Independent measurements of layers in a multi-layered sample were obtained using a single point detector and a sharp edge diaphragm. This diaphragm blocks all light that is transmitted or reflected outside a region of interest, which can be adjusted in visible light. All spectra were corrected for the background, water vapour absorption, and slopes in the baseline. The specular reflectance measurements were Kramers-Kronig transformed after background correction.

Imaging-FTIR measurements were performed using the Bio-Rad Stingray system, consisting of the described infrared spectrometer and microscope extended with a 64×64 pixel MCT Focal Plane Array (FPA, Santa Barbara Focal plane). An extensive description of this system is presented in Chapter 4 of this Thesis. The images and averaged spectra were obtained by using the projection analysis described in Chapter 2 of this Thesis.

The Raman system used was a Renishaw 1000B Raman analyser equipped with two lasers: 514 and 785 nm.

3.5 Results

3.5.1 Preparation of the multi-layered samples

Fig. 3.4 shows the different prepared multi-layered samples. A paint cross-section embedded in a modern resin (Fig. 3.4A) shows a clear overview of the complex layer structure of this painting. These different layers are tentatively assigned in Table 3.1. This table also presents an elemental analysis by SEM-EDX. Layer 1 is a dark red layer, probably coloured by ochres (elements Si, Al, Fe). The metallic part in this layer consists of iron. This layer is covered by a very thin layer of yellowish Pb containing paint. Layers 3 and 4 are again a red and a yellowish layer. Layer 5 is a remarkably thick and bright layer. This layer is pigmented by a lead-containing pigment. The presence of Ba in this paint seriously questions its 17th century origin. The top layers are a rather undefined sequence of a number of transparent (7 and 9) and opaque (6 and 8) layers.

Fig. 3.4B shows a sample of the same paint after squeezing in the diamond cell. It is clear that a layer structure has been altered in the squeezing process, but several layers can still be distinguished. The numbering of these layers is consistent with the numbering in the embedded paint cross-section. The assignment of this numbers is not directly clear from the presented image, but is based on the IR analysis described below.

The layers in this figure are numbered. Fig. 3.4C shows the sample obtained by the KBr polishing technique described in Fig. 3.1. The presented visual light microscopic image is obtained in transmission mode, and clearly shows that this sample preparation method leaves the layer structure completely intact. The layer structure of this thin section agrees very well with the embedded cross-section presented in Fig. 3.4A and the numbering of the different layers is kept consistent accordingly. However, some smaller differences are present between Figs. 3.4A and C. The colours of these cross-sections are not completely similar. This is ascribed to a difference in microscopic technique (reflection with crossed polarisers vs. transmission) rather than to differences in sample composition. Furthermore, the rather diffuse top layers 6-9 cannot be distinguished as separate layers in the thin section. This might be due to small differences between the samples or due to the loss of top part of the cross-section in the polishing process. The numbering of the layers 7-9 in used for consistency with Fig. 3.4A. The various lower layers in these different cross-sections are well comparable, and provide a good means to evaluate the different sample preparation techniques.

Microtoming of samples from the test painting was not successful, despite extensive trials. In all cases, the paint crumbled upon cutting due to the brittleness of aged paint. The pigment particles, which can very well be larger than the desired slice thickness, are expected to easily damage the paint section through the imperfect cohesion and large differences in hardness between particles and the surrounding matrix. It is expected that this preparation method will be of more value when the investigated samples are small, as the support due to the embedding medium increases with decreasing sample size. Besides, microtomy of modern paints might be more straightforward, as these are normally more flexible and contain smaller pigment particles than traditional 17th century paint.

The several physically isolated samples used were also taken from the same spot on the painting. The samples were dissected using a surgical scalpel and a stereomicroscope, while care was taken that the layer structure was similar to the structure shown in Fig. 3.4A.
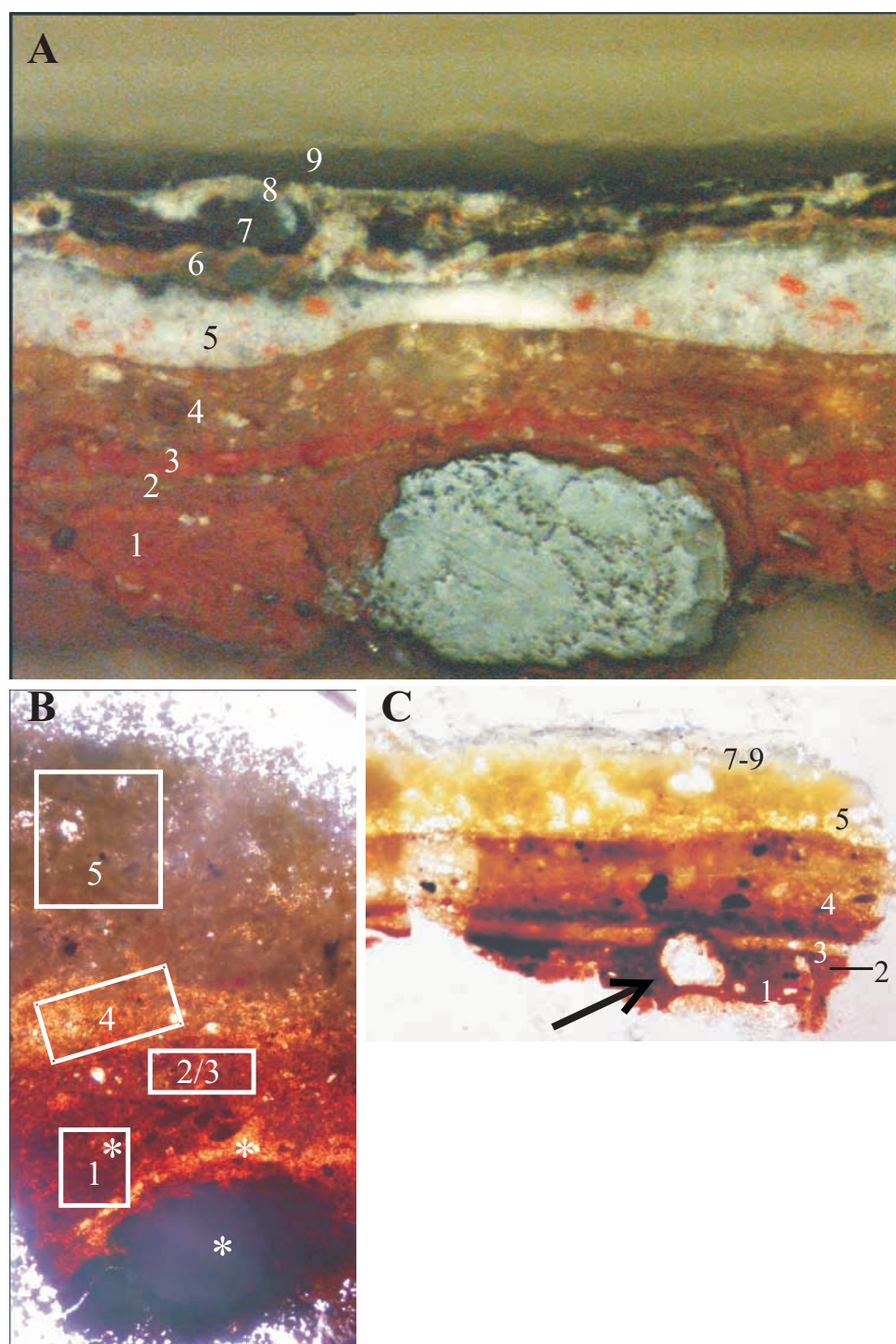
Fig. 3.4. *Optical microscopic images of the different analysed paint cross-sections.* ***(a)*** *Paint cross-section prepared in a modern resin.* ***(b)*** *Cross-section prepared after squeezing in a diamond anvil cell.* ***(c)*** *Thin section of a cross-section embedded in KBr. The numbering of the layers in the different images is consistent. Elemental analysis (SEM-EDX) is presented in Table 3.1.*
(see also the coloured version at the end of this Thesis)

Number	Colour	Thickness	Elements	Identification
9	transparent	a)		Varnish
8	white	a)	K,P	
7	transparent	a)		Varnish
6	yellow	a)	Cr,Mg	Colour paint
5	white	60	Pb, Ba (particles)	Coloured paint
4	yellow/brown	95	Ca, Al, Pb	Colour paint
3	red	12	K Al, P	Imprimatura
2	yellow/brown	8	Pb	Isolation
1	red	>150	Al, Si, K, Mg, Fe	Ground

Table 3.1. Summary of the various numbered layers in the embedded paint cross-section in Fig. 3.4, the approximate thickness of the layers (μm) and the elemental analysis are determined using SEM-EDX. a) Layer thickness not clearly determined, due to its diffuse appearance.

3.5.2 Fingerprinting the paint system

The elemental content of the different layers in the investigated paint samples was determined using SEM-EDX on the embedded cross-section shown in Fig. 3.4A. The results of these analyses are provided in Table 3.1. Mass spectrometric analysis indicated the presence of linseed oil that has been used without heat-treatment. The degree of hydrolysis of the paint is 91%.

3.5.3 Infrared analysis of physically isolated samples

3.5.3.1 KBr-pellets

Samples from different layers of the test panel were separated manually as good as possible using a fine scalpel. Only a rough separation between the upper and the lower layers could be achieved due to the relatively large amount of material needed for a KBr pellet. Fig. 3.5 shows two spectra of samples obtained from the upper and lower layers. The absorption intensity of the spectra is still low (< 0.2 for the most intense inorganic absorption), despite the relatively large samples that have been used. This low absorption results in a relatively high noise level, especially below 1000 cm^{-1}. Nevertheless, several absorptions can be assigned.

Table 3.2 presents the interpretation of the absorption bands that were found in the different FTIR spectra.[31,37,103,106] The lower layers (1–4, black line in Fig. 3.5) contain a strong silicate signal (1015, 915 cm^{-1}) due to the earth pigments in the red ground layer. These pigments also contain crystal water, leading to the sharp absorptions at 3619 and 3695 cm^{-1}. Carbonates can be assigned to lead white and calcium carbonate in layer 4 (Pb and Ca found in EDX, Table 3.1). Identification of the binding medium is not straightforward. The combination of peaks at 1630 and 1542 cm^{-1} would indicate the presence of protein, but this preliminary assignment will be rejected below. The oil absorptions (1708, 2927, 2854 cm^{-1}) are small due to the high pigment concentration. The grey line in Fig. 3.5 represents the top layers of the paint. The highest absorption in this spectrum is the carbonate at 1404 cm^{-1} that can be identified as lead white (Pb found in EDX). The pronounced carboxylate peak at 1516 cm^{-1} indicates the extensive formation of

lead soaps (cf. Chapter 6). The oil binding medium and varnish materials results in the carbonyl peak at 1710 cm^{-1}, with a distinct shoulder at 1740 cm^{-1} (cf. Chapter 5).
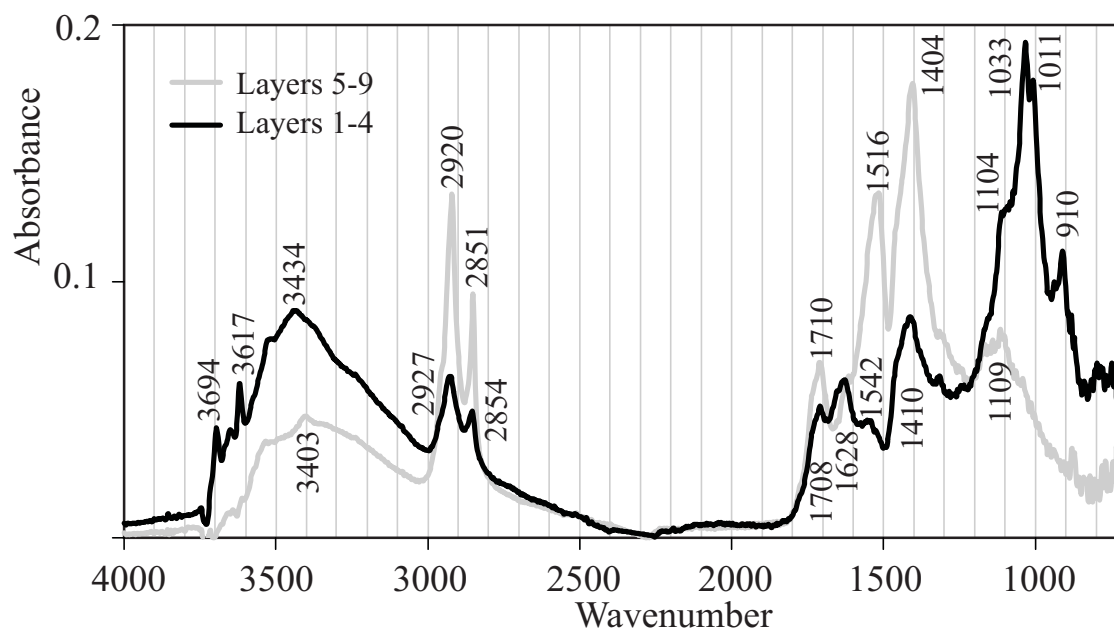
Fig. 3.5. *Transmission infrared spectra of dissected parts of the investigated paint, prepared in a diamond anvil cell. The numbers of the layers correspond to those in Fig. 3.4 and Table 3.1.*

Wavenumber(cm^{-1})	Vibration	Assignment
3699-3620	H$_2$O	Crystal water in pigment
3535, 1450–1420, 1050, 681	Various	Lead white pigment
3460–3350	OH	Binding medium
2940–2924,2865–2850	CH	Binding medium
1785–1770	C=O	Polymerised oil[37]
1740–1700	C=O	Binding medium
1650–1620		Metal carboxylates ?
1550–1510	COOM	Metal carboxylates
1460	CH	Binding medium
1415	CO$_3$	Carbonate in pigment
1050–1030,1020, 915	Si-O	Earth pigment

Table 3.2. *General assignment of the infrared absorption bands in Figs. 5-11.*

3.5.3.2 Diamond anvil cell

The spectra obtained from the test painting are shown in Fig. 3.6. A small sample (< 1 μg) suffices for these measurements and consequently the sampling of a single layer can be performed more accurately than for KBr pellets (~50 μm). In this case, it appeared possible to sample layers 1 and 4 (cf. Fig. 3.4A) individually. Despite the small sample sizes, the absorbance intensity of the resulting spectra is much higher than for the KBr pellets (1.4 for the most intense silicate band in layer 1, compared to 0.2 in Fig. 3.5).

The better separation of these layers improves the accuracy of the chemical interpretation. The most remarkable new result is the separation of the absorption bands at 1650 (layer 1) and 1533 (layer 4). The presence of proteins, which was suggested by the KBr spectra (Fig. 3.5), is thereby completely contra-indicated. The increase in spatial resolution thus prevented a wrong interpretation, based on a coincidental combination of peaks. Furthermore, the carbonates and silicates, which could not be located individually using KBr pellets, can be located in layer 4 and layer 1 respectively. The absence of the strong carbonate absorption further allows the observation of carboxylic acids (1410 cm^{-1}) and the CH bend vibration (1460 cm^{-1}, shoulder), illustrating that the higher accuracy with which a spectrum can be traced to a specific region in a painting increases the information content that can be derived from the obtained spectra.

Layer 5 contains lead white (1404, 3535 and 681 cm^{-1}) and lead carboxylates (1529 cm^{-1}). The two smaller peaks around 1100 cm^{-1} could be due to barium sulphate (BaSO4), as Ba has been identified by EDX. This seriously questions the authenticity of this layer and obviously the layers on top of it, as BaSO4 is only known as an additive in paint since the 19th century. It has been reported as an adulteration of lead white[2] and might be introduced during a restoration procedure. The top layers contain mainly organic features, which explain the dark transparent appearance in the optical image (Fig. 3.4A). The spectrum contains characteristics of oil, resin and a small amount of carbonates due to imperfect sampling.

3.5.4 Analysis of multi-layered samples

3.5.4.1 Diamond anvil cell

Squeezing of a carefully positioned multi-layered sample does not necessarily destroy the layer structure, but may also expand all layers. Several layers can therefore be measured individually in a single sample and it is possible to increase the effective spatial resolution to beyond 50 μm. A microscopic transmission image of a squeezed, multi-layered sample is shown in Fig. 3.4b. The three labelled areas (*) were all found to contain silicates, but no carbonates, as indicated by a spectrum of one of these layers (Fig. 3.7) and are therefore assigned to the ground layer 1. Squeezing of this sample in the diamond cell clearly induced a physical separation of the red ground layer 1. This separation suggests that fractions with different rigidities are present in the paint, but the chemical nature of these differences has not been studied in detail. Layer 5 is recognisable as a white, scattering layer. The clearly present carbonyl band at 1708 cm^{-1} is almost absent in the spectrum of the isolated sample (layer 5 in Fig, Fig. 3.6) might due to mixing with layers 7–9, which are not visible as individual layers (Fig. 3.4B). Layer 4 has been turned into a rather transparent, well-isolated layer upon squeezing. The corresponding spectrum is very similar to the spectrum of layer 4 obtained with an isolated sample (Fig. 3.6). The

remaining layers 2 and 3 seem to have merged, as they cannot be distinguished in the optical microscopic image.

Both methods of sample preparation in a diamond anvil cell resulted in the acquisition of high quality spectra from small samples. These small samples could be isolated from relatively thin layers (~50 μm). The preparation of a 'cross-section' in the diamond cell led to severe deformations by mixing and de-mixing during preparation in the diamond cell. Mixing seriously compromises the spatial resolution that can be obtained with this technique. Squeezing of simpler samples, i.e. samples with 1−3 layers, is expected to induce less mixing. Analysis of these samples in a diamond anvil cell is expected to be useful, as the measurement requires only a minor amount of sample, and is fast.
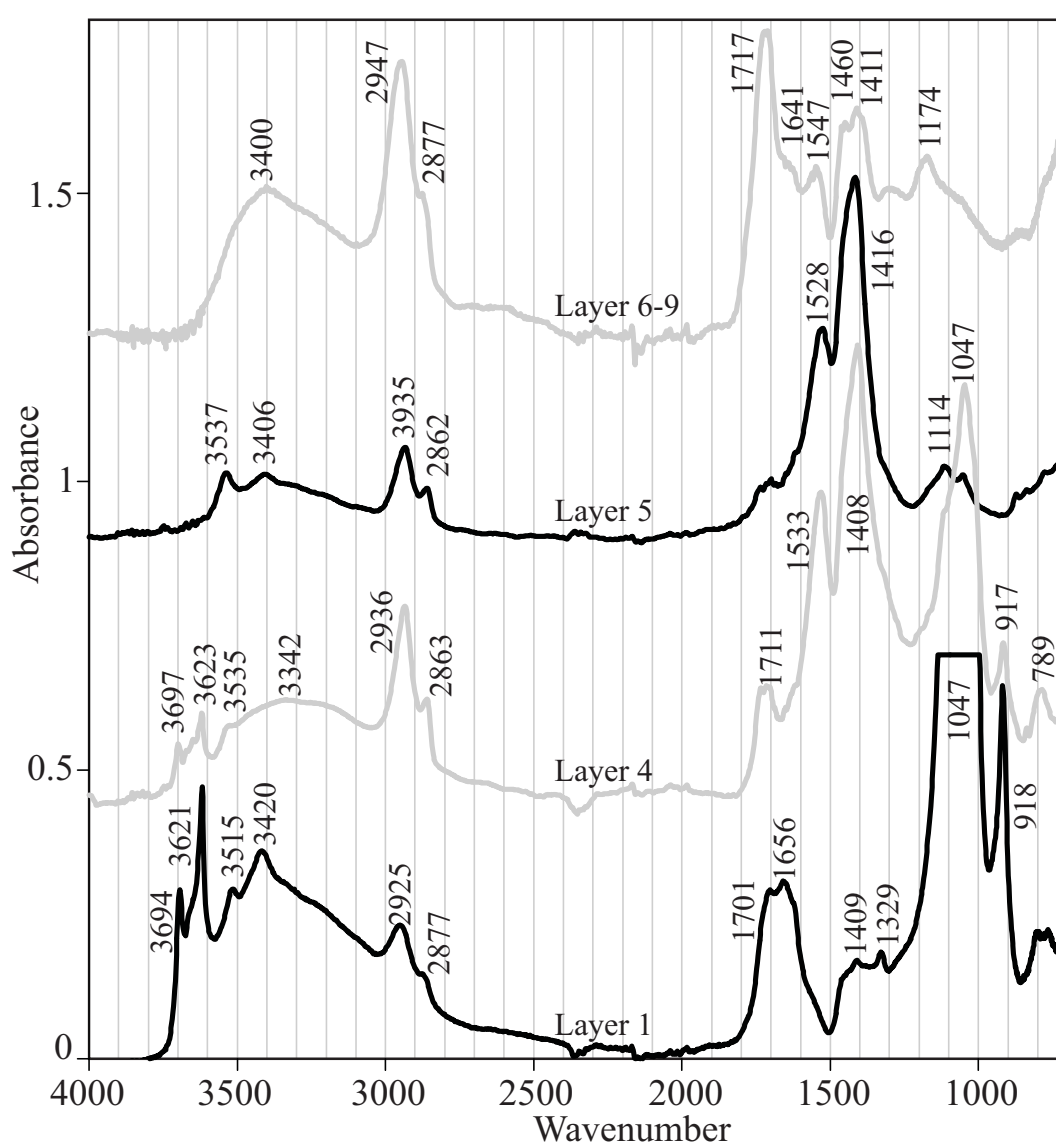

Fig. 3.6. *Transmission infrared spectra of dissected parts of the investigated paint, prepared in a diamond anvil cell. The numbers of the layers correspond to those in Fig. 3.4 and Table 3.1.*
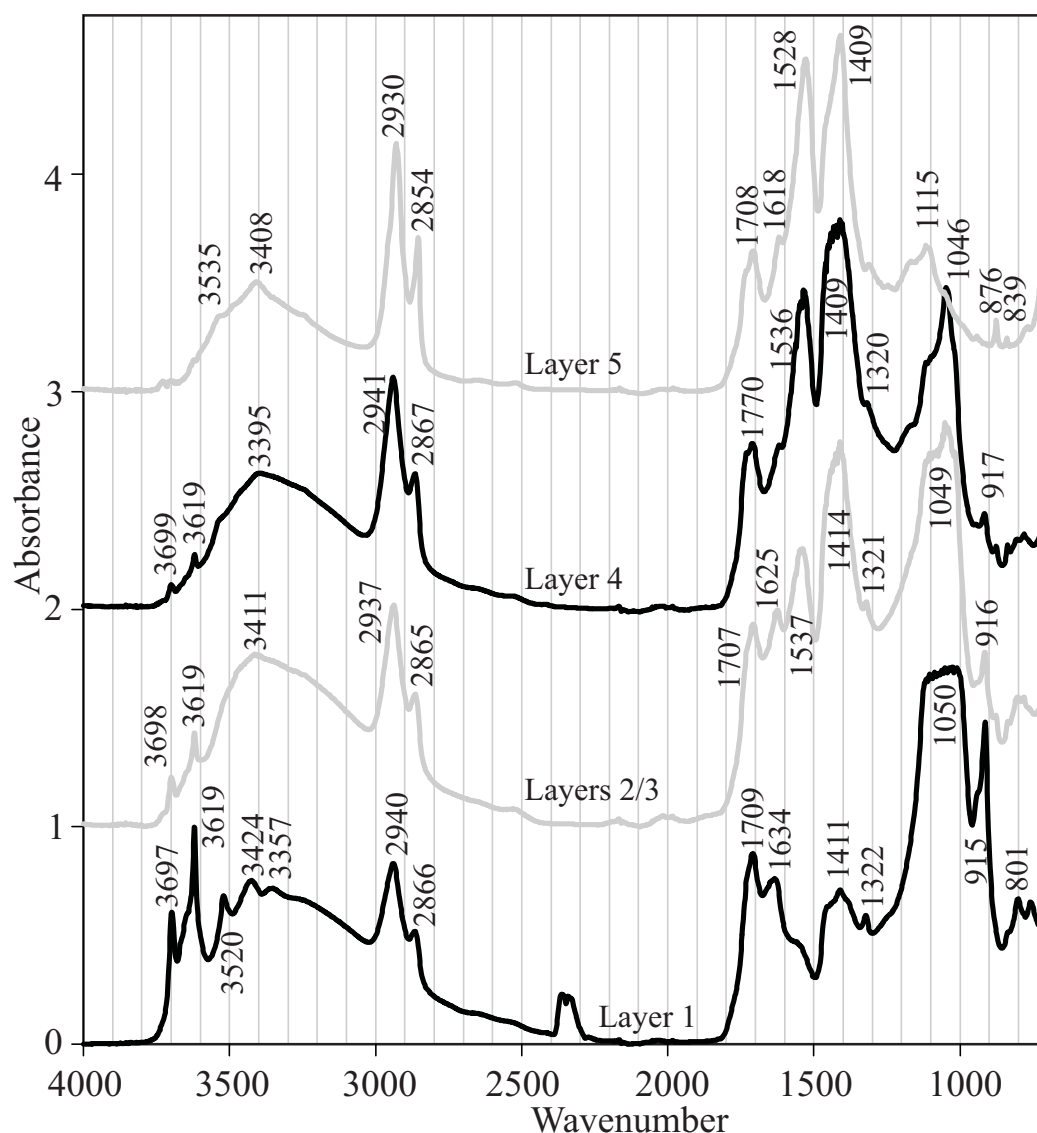
Fig. 3.7. *Transmission infrared analysis of a multi-layered sample of the investigated paint, prepared in a diamond anvil cell. The measurement positions are indicated in Fig. 3.4B. The numbers of the layers correspond to those in Fig. 3.4 and Table 3.1.*

3.5.4.2 Diffuse reflection of an embedded paint cross-section

The application of diffuse reflectance in the study of paint samples presented a number of problems. The large sample sizes needed for DRIFTS make the technique less suitable for investigation of paint samples. No literature references of the application of darkfield microscopy, a standard technique in optical microscopy have been found and a suitable objective for these measurements was not available. Sampling on sandpaper completely destroys the layer structure and provides little control over the actual sampling depth. The application of crossed polarisers therefore is the only promising method to analyse the diffuse reflectance from embedded paint cross-sections. However, the intensity of the light arriving at the detector via two crossed polarisers and the sample appeared too low to enable the acquisition of an infrared spectrum. Rotation of one of the polarisers lead to a considerable response of the detector, indicating that the spectrometer was functioning well and the sample was correctly positioned. This experiment shows that the diffuse reflectance of the polished surface is negligible.

3.5.4.3 Specular reflection of an embedded paint cross-section

Specular reflectance spectra could be easily obtained from the paint cross-section shown in Fig. 3.4A. Different regions in this cross-section were individually analysed using the sharp edge diaphragm. This procedure enabled the individual analysis of the thin layers 2 and 3 (see Fig. 3.4A). The spectra presented in Fig. 3.8 clearly show the presence of various organic and inorganic absorptions, but the overall spectral quality is poor. The CH stretch absorption peaks hardly exceed the noise level (S/N between 2 and 5) in the spectra of layers 1–5. The OH absorption bands (3600–3100 cm^{-1}), which were clearly observed in the various transmission experiments, are virtually absent in the specular reflectance spectra. The S/N is much better on the long wavelength side of the spectrum (< 1800 cm^{-1}). This part of the spectrum can well be compared to the presented transmission spectra, albeit that the intensities of the inorganic features in the spectrum (carbonates at 1400 cm^{-1} and silicates at 1100 cm^{-1}) are exaggerated due to the higher refractive index of these materials.

The same sample was investigated by FTIR-imaging, as the preservation of the layer structure in embedded paint cross-sections makes the higher spatial resolution analysis profitable.

The obtained infrared spectra indicated the organic compounds in part of this cross-section were heavily damaged. The affected area correlated with the area analysed by SEM-EDX that preceded the FTIR measurements. Therefore, the resulting data-set was processed only partly and the affected area was excluded from further data analysis. The clusters found by the projection method (see Chapter 2 of this Thesis) are shown in Fig. 3.9A. The corresponding averaged spectra are presented in Fig. 3.9B. The lower spectrum represents the embedding medium. The absorption peaks of the embedding medium can hardly be seen in the other spectra, indicating that the smearing is low. The only peak that can be recognised in the ground layer 1 is the enormous (truncated) silicate peak. The corresponding score plot also localises layer 3. The high similarity between the spectra of layers 1 and 3 is indeed confirmed by Fig. 3.8. The silicate absorption in layer 1 is more intense, but the absolute absorption values are ignored by the projection method, which scales the spectra before the projection. Layer 2 is positioned neatly between layers 1 and 3. The corresponding spectrum is comparable to the spectrum found by single point analysis (Fig. 3.8). Layer 4 contains two different fractions on the sample spot. The spectrum of the top part suggests the presence of carbonates, while lead soaps are identified in the lower region (1530, 2920 and 2850 cm^{-1}). The observed contrast in layer 4 indicates an important advantage of imaging detection. The full spatial resolution is achieved without the need for visual selection of a region of interest. A diaphragm is not needed to separate the different regions, and therefore the accurate localisation of regions that are identical in visual light is possible without trial and error.

The spectra obtained from layer 5 contain intense carbonate and sulphate absorptions. On the other hand, the spectra obtained from the varnish region (layers 6–9) are very poor. Similar results have regularly been obtained by specular reflectance of varnish layers, probably due to the low intensity of the reflected light. The high resolution of the specular reflectance measurements, and the low sample preparation time make specular reflectance measurements an interesting method. In fact, alternatives for this preparation method are hardly available when only an embedded paint cross-section is available for analysis. Unfortunately, the quality of the resulting spectra is low, and the possibilities for chemical interpretation are restricted.
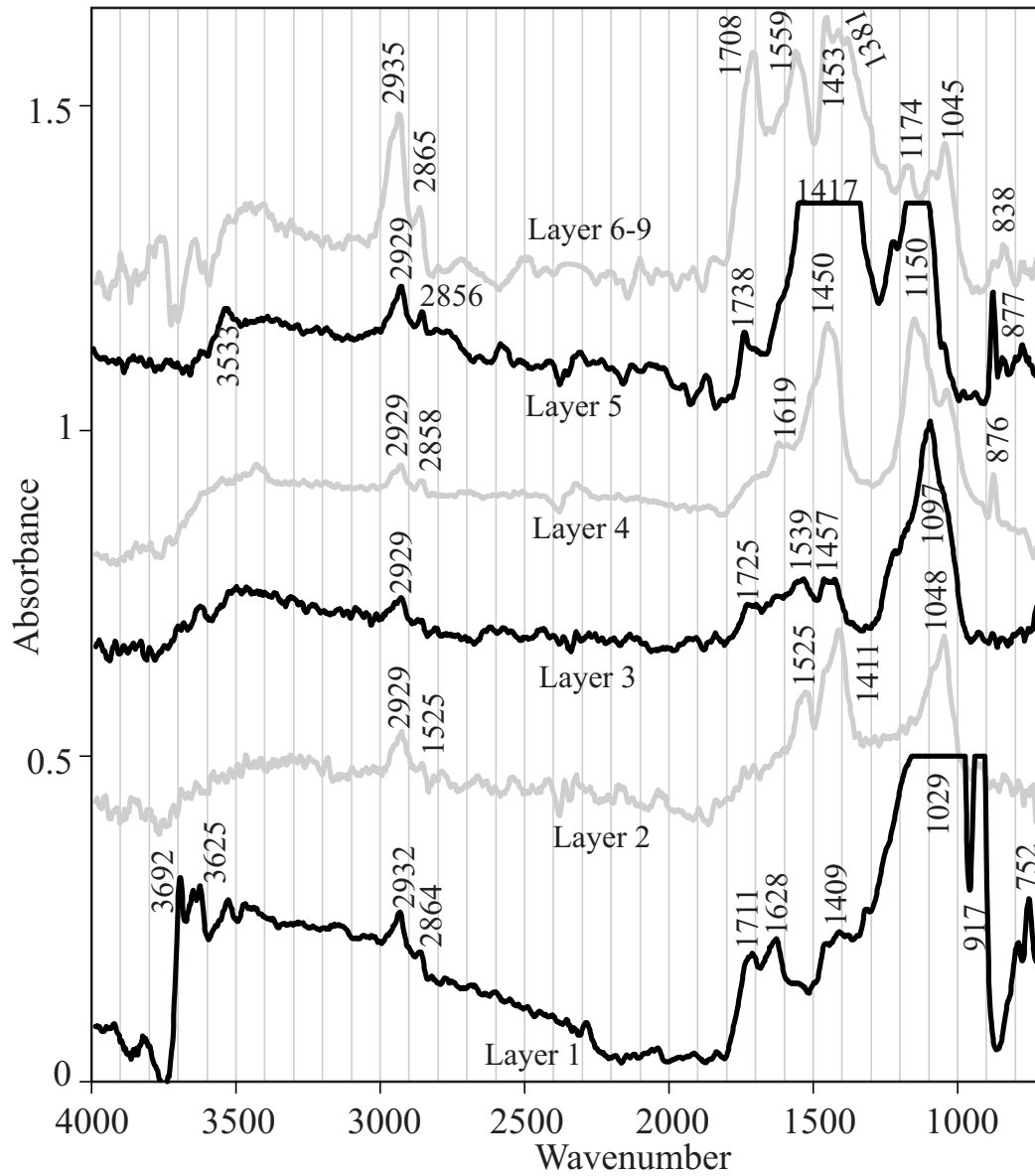
Fig. 3.8. *Specular reflectance infrared spectra obtained directly from the embedded paint cross-section in Fig. 3.4A. The numbers of the layers correspond to those in Fig. 3.4 and Table 3.1.*
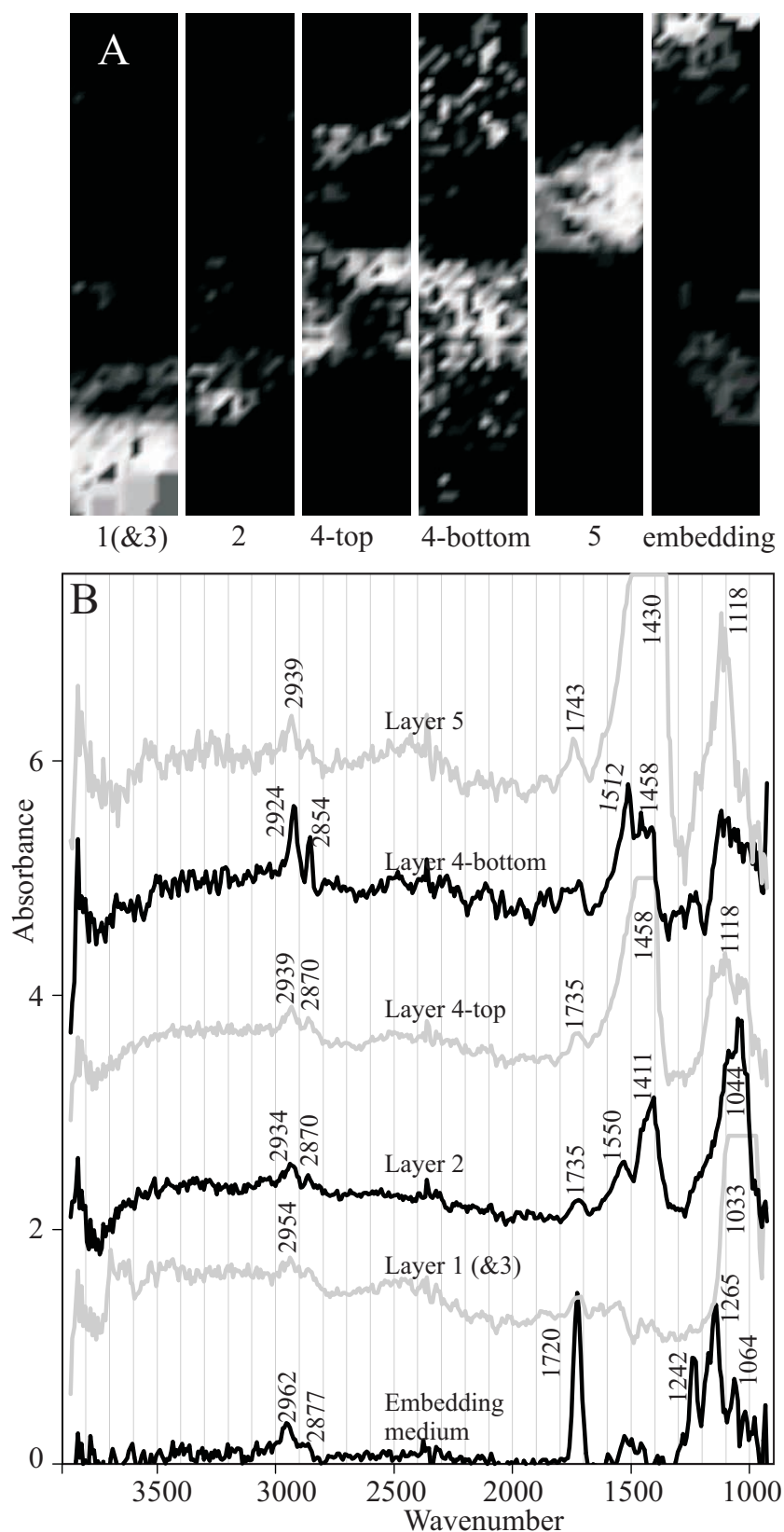
Fig. 3.9. *Specular reflectance imaging-FTIR spectra obtained directly from the embedded paint cross-section in Fig. 3.4A. Results are extracted from the obtained data-set using the projection method described in Chapter 2 of this Thesis. (a) Score plots showing the localisation of the spectra shown in B. (b) Mean spectrum of the highlighted area shown in the score plot in A. The number of the layers correspond to those in Fig. 3.4A and Table 3.1.*

3.5.4.4 ATR of an embedded paint cross-section

Microscopic ATR measurements of the embedded cross-section shown in Fig. 3.4A were not successful. The used ATR crystal is made of the optically opaque germanium, which makes the accurate positioning of the crystal difficult. Therefore, the diaphragm could not be used to select a single layer from the multi-layered paint structure. As an alternative, spatial resolution could be introduced by imaging detection. These measurements do not need the application of the diaphragm. However, the combination of ATR microscopy and detection by an infrared camera did not lead to successful measurements for technical reasons.

ATR measurements did lead to the acquisition of very useful spectra in cases where the exact location of the crystal is not critical, such as the analysis of thin surface layers directly from the surface of a painting (unpublished results).

3.5.4.5 Raman spectroscopy of an embedded paint cross-section

Raman spectroscopy applied on a cross-section of the paint cross-section led to a strong fluorescence, which was far more intense than the Raman scattering, leading to a complete masking of the Raman bands. This fluorescence was even persistent upon illumination by a 785 nm laser. A Raman system with a longer wavelength illumination should prevent this fluorescence, but test measurements have not been performed.

3.5.4.6 Transmission of a thin cross-section embedded in KBr

A microscopic image of a thin section made doubly polishing a sample embedded in KBr is displayed in Fig. 3.4C. The image clearly shows that the paint sample taken from the test painting is not damaged by the high pressure of the KBr press or by the polishing process. The layer structure is left intact, and this method is therefore a suitable method for the transmission measurement of large and multi-layered samples. A further advantage is that the thin sections can be obtained by conventional equipment that is readily available in nearly every FTIR-environment: a KBr-press, sandpaper/polishing clothes, and an optical microscope. The method is fairly time-consuming as two polishing steps are involved. However, a single sample can be used to investigate several layers in a sample. The optical transparency of pressed KBr further enables a combined optical and infrared microscopic investigation. The samples can be measured at different stages of grinding and polishing. It would be useful to be able to determine the exact layer thickness of the cross-section at these grinding steps, but no method has been found or established for that purpose yet. Nevertheless, the different grinding steps were particularly useful in the analysis of the more organic top layers (7–9). The absence of scattering in these layer results in a relatively high light transmission. The spectrum of layers 6–9 (Fig. 3.10) was accordingly measured at an early stage of polishing. At this stage, light transmission of the pigmented parts of the sample was too low to allow transmission infrared analysis, but the transparent top layers yielded the clear spectrum presented in Fig. 3.10. This spectrum suggests the presence of oil by absorptions at 3933, 2876, 1711, 1459, and 1175 cm^{-1}. Unpigmented oil does not explain the absorptions at 1624, 1541 and 1387 cm^{-1}, but an unambiguous identification for these absorptions has not been found. The other spectra presented in Fig. 3.10 (layers 1–5) were acquired after a further polishing step, as the scattering in these pigmented layers did not yield useful infrared spectra. Still, a baseline correction was necessary to correct for remaining scattering of the sample. After this step, it was possible for the first time to obtain transmission spectra of the

rather thin layers 2 and 3. These spectra show the presence of lead white (1402 cm⁻¹) and lead carboxylates (1526 cm⁻¹) in layer 2 and a mixture of carbonates (1411 cm⁻¹), carboxylates (1536 cm⁻¹) and silicates (1101 cm⁻¹) in layer 3. The clear organic features in these spectra (2927, 2856, 1709 cm⁻¹) indicate an oil binding medium for these layers. The spectra of layers 2 and 3 could be acquired without any problem from this sample and show the high spatial resolution that can be obtained with this preparation method. The remaining transmission spectra in Fig. 3.10 (layers 1, 4, and 5) are very similar to the diamond cell spectra (Figs. 3.6 and 3.7.) and their interpretation is therefore remains unchanged.
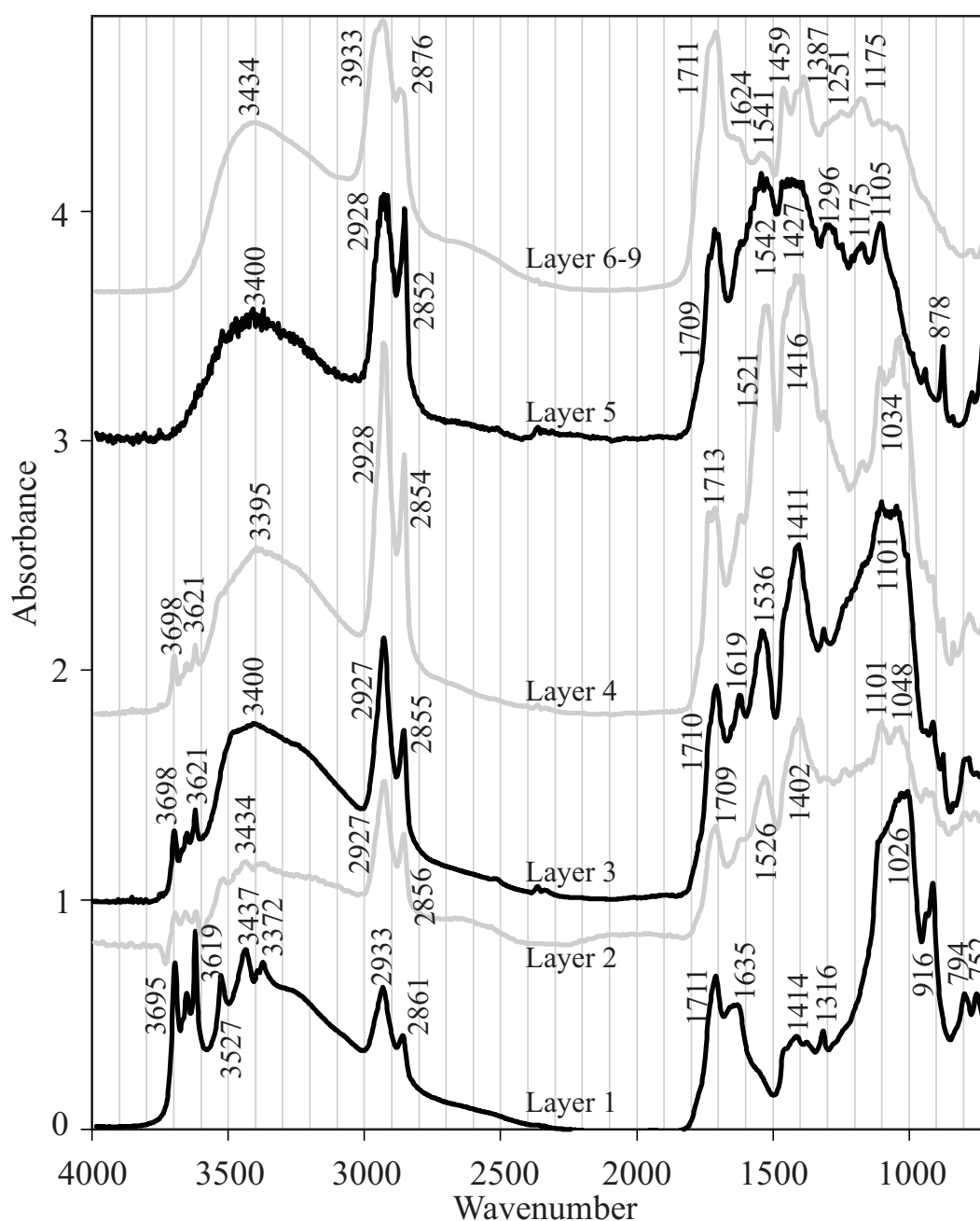
Fig. 3.10. *Transmission analyses of a multi-layered thin section of the investigated paint, prepared after embedding in KBr (see Fig. 3.1). The numbers of the layers are consistent with Fig. 3.4C.*
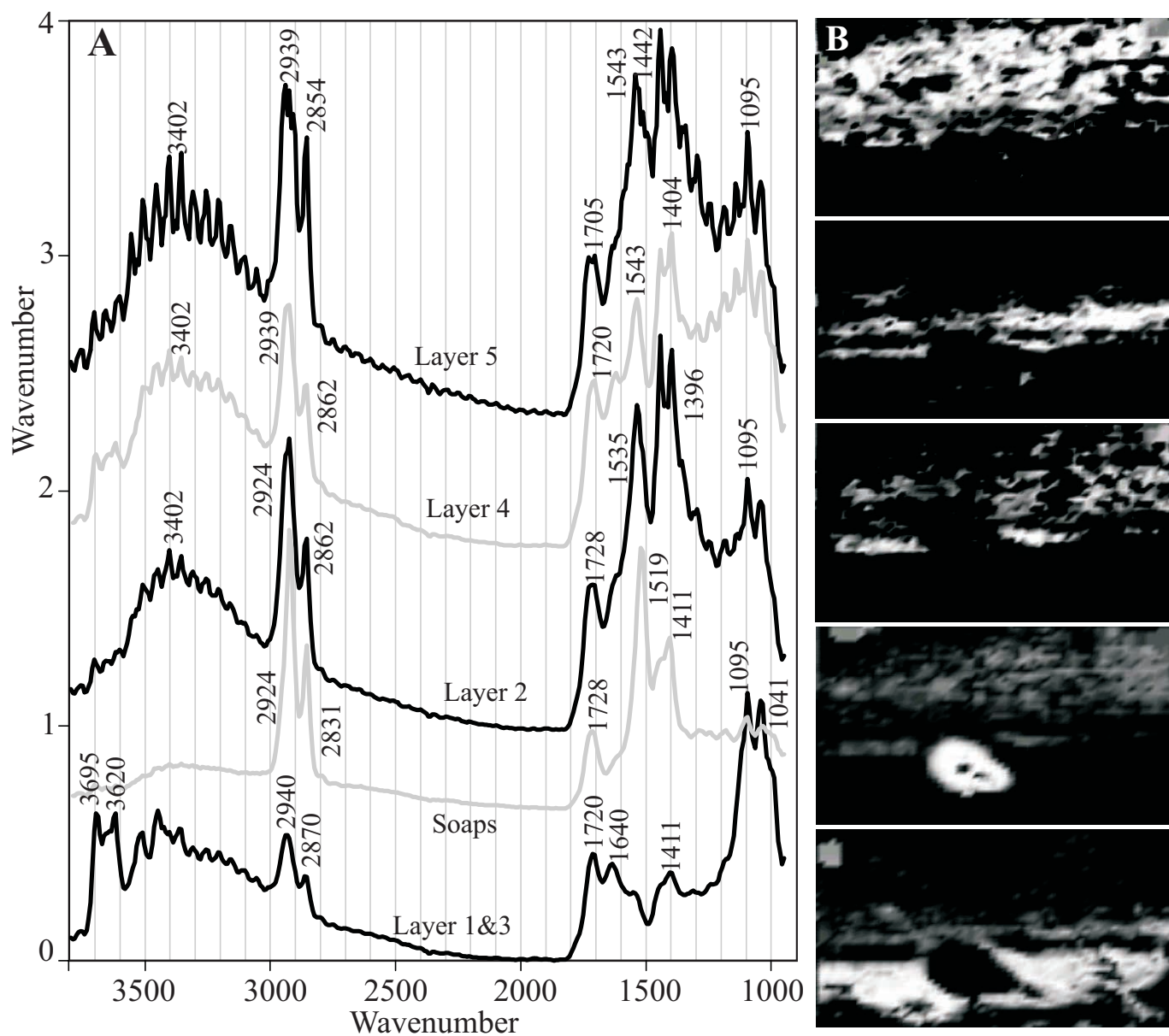
Fig. 3.11. *Imaging-FTIR spectra of the thin section shown in Fig. 3.4C. Results are extracted from the obtained data-set using the projection method described in Chapter 2 of this Thesis. (**a**) Mean spectrum of the highlighted area shown in the adjacent score plot. (**b**) Score plots showing the localisation of the spectra shown in A.*

This sample was further analysed by FTIR-imaging to fully exploit this high resolution. The various spectra were clustered using a projection algorithm, which compares all spectra from the data-set with a single, user-selected spectrum. The similarity between these spectra is expressed as a score-plot, and the similar spectra are averaged to increase the S/N. This algorithm is presented in Chapter 2 of this Thesis. The score plots most important clusters found with this algorithm, as well as their averaged infrared spectra are shown Fig. 3.9. The further increase of spatial resolution allows the analysis on a scale smaller than the size of the layers. This is nicely illustrated by the spectrum of the transparent part in Fig. 3.4C (arrow). The corresponding spectrum indicates the abundant presence of metal soaps, a distinct CH absorption and a low absorp-

tion by alcohol groups (3400 cm^{-1}, 1000–1300 cm^{-1}). These features indicate a similarity with protrusions, which will be highlighted in Chapters 6–8 of this Thesis. Layers 1 and 3, both containing silicates, are highlighted in the lower score plot in Fig. 3.11. The hiatus between these layers seen in the lower score plot in Fig. 3.11 is filled by the area highlighted in the score plot of layer 2. The score plots of layers 4 and 5 clearly localise these layers, but the quality of the corresponding spectra is low, especially in the short wavelength range, where the effects of scattering are maximal. The reduced spectral quality compared to the single point spectra in Fig. 3.10, are explained by the lower accuracy of the imaging detector compared to the single point detection.

3.6 Discussion

The results presented in this Chapter were acquired using transmission (Figs. 3.5–3.7, 3.10–3.11) and specular reflectance (Fig. 3.8–3.9) measurements. Diffuse reflectance spectra were not obtained for various reasons: limited spatial resolution or large sample size (normal DRIFTS accessory, sandpaper), unavailability of the required accessory (darkfield) or lack of results (crossed polarisers). The complete annihilation of the light beam due to the crossed polarisers indicates that the intensity of diffuse reflected light from a solid sample is low. The absence of diffuse reflectance can be explained by the combination of high absorption and low scattering. The low scattering of infrared light in paint is successfully explored in IRR (infrared reflectography[9]) to reveal underdrawings, normally using NIR (near infrared, 0.8–2.5 µm) light. Scattering of MIR (mid infrared, 2.5–25 µm) light is even lower than scattering of NIR light, leading to a longer effective path length. Furthermore, the absorption intensities in the MIR range are stronger. Darkfield illumination of embedded paint cross-sections is therefore not promising. Even if this approach would enhance the observed intensity of diffuse reflectance, the high penetration depth of infrared radiation (tens of micrometers) would restrict the spatial resolution of the measurement. The above discussion is thought to be valid also for reflectance measurements directly on the surface of a painting. The results obtained by Fabbri[15] are thus assigned to specular reflectance. A better alternative for these non-invasive measurements would be ATR or photo-acoustic spectroscopy. Pilot experiments using a microscopic ATR crystal on the surface resulted in the acquisition of high quality infrared spectra of the surface layers, especially when an unpigmented varnish is observed (unpublished results). The current portable spectrometers could therefore readily be utilised to obtain an on-spot classification of varnishes.

The specular reflectance measurements enable the analysis of embedded cross-section with a spatial resolution determined by the diffraction limit. However, the reflectance spectra exhibit some remarkable differences when compared to transmission spectra. The OH absorption (~3400 cm^{-1}) is hardly visible in any of the reflectance spectra (Fig. 3.8), while the transmission spectra readily prove the presence of these moieties (Figs. 3.5–3.7). Furthermore, the peak shifts and high intensities observed for the more intense inorganic absorptions[93] limit the analytical value of reflectance spectra. Erroneous explanation of these effects has instigated some dubious reasoning.[87] The reported absorption at about 1580 cm^{-1} observed in azurite paint is clearly a copper carboxylate and not a vague polarisation effect that can be observed with unpolarised light.

Next to these shifts, it appears that the overall quality of the reflectance spectra (Fig. 3.8) is rather poor. Other published reflectance spectra of paint also show a similar quality[87] and this is the most probably reason that the reflectance measurements of traditional paint got only minor attention.[43] To explain this, it should be stressed that the application of the Kramers-Kronig transformation is formally not allowed, as $n(\lambda)$ is not completely determined, the angle of incidence is not a single value, and the incident beam is not polarised. Nevertheless, good quality spectra have been obtained by similar set-ups,[94,107] indicating that a violation of the mentioned conditions does not necessarily lead to low-quality spectra. Therefore, the poor spectral quality of the inhomogeneous paint samples should have a different cause.

The noise-resembling features in the specular reflectance spectra (Figs. 3.8–3.9) are not grey noise, as they do not reduce upon accumulation of more spectra. Mixing of specular reflectance and diffuse reflectance is also not a very probable explanation for low quality of the specular reflectance spectra, as it has been shown before that the intensity of diffuse reflectance is below the detection limit.

A very interesting remark regarding the characteristics of specular reflectance was made by Chalmers,[107] who estimated that the effective penetration depth in a specular reflectance measurement is a number of microns. Specular reflection can thus not be seen as a pure surface technique. This indicates that part of the light that arrives at the detector actually entered the sample. However, this light is not reflected in a diffuse way, as it has not been observed through the crossed polarisers. Therefore, the origin of the distortions must be a specular reflectance on sub-surface layers or particles. It is very well possible that sub-surface pigment particles act as a mirror and result in a reflection-absorption experiment (see introduction of this Chapter) of the material, e.g. a binding medium on top of this particle. However, this mirror is not nearly perfect, and the absorption spectrum of the binding medium is convoluted with the refractive index spectrum of the reflecting particle. The mixed signal might very well explain the poor spectral quality of specular reflectance measurements, as the Kramers-Kronig transformation should only be applied to the reflectance part of the detected signal, while the transmitted light should be processed by Lambert-Beer's law. However, there is no method to separate these individual contributions. The intensity of sub-surface reflectance might be more than twice as high as the specular reflectance from the binding medium itself, assuming refractive indices of 1.5 and 2 for the binding medium and pigment respectively. This high intensity provides a further explanation for the enormous intensity of the inorganic peaks in the specular reflectance spectra (Figs. 3.8–3.9). Microscopic imaging experiments using an ATR objective would be a promising means to analyse paint cross-sections, as the penetration depth is mainly determined by the crystal, and sub-surface reflections only have minor significance. Unfortunately, these measurements could not be carried out due to technical problems. Single point spectra do not form an alternative for imaging detection in this case, as the used germanium ATR crystal is optically opaque and therefore cannot be localised accurately on a specific layer.

The discussion presented here indicates that the model presented in Fig. 3.3 is not valid for the reflectance of infrared radiation from an inhomogeneous sample. The preservation of the polarisation angle upon reflection shows that all light reflected from a paint is specularly reflected. Accordingly, the number of reflections inside the paint is very limited. A revised version of Fig. 3.3 is presented in Fig. 3.12. This discussion also suggests that the analysis of samples

prepared on sandpaper[81] should be classified as a reflection-absorption technique rather than a diffuse reflectance method. Correct data processing of results obtained by this technique should therefore be based on Lambert-Beer's law, and not on Kubelka-Munk analysis.

The Raman measurements were unsuccessful as a result of fluorescence, even at the relatively high wavelength laser beam of 785 nm. The different successful Raman spectroscopic studies of painting materials that have been published were acquired with similar or even shorter wavelengths. These analyses include several pigments[54] and spectra of fresh binding media.[56] The differences must therefore be assigned to ageing products that have been developed during the lifetime of the painting. In fact, the presence of fluorescence in aged paint systems is commonly observed in microscopic studies, even in the absence of fluorescing pigments. A further increase in the wavelength of the excitation beam seems the most logical next step to prevent fluorescence. The application of Raman spectroscopy to paint cross-sections is not fully developed and certainly merits further study.

The quality of the presented transmission spectra (Figs. 3.6–3.7, 3.10–3.11) is high and clearly indicates that transmission would currently be the preferred analytical mode. In fact, the spectra recorded with the different transmission techniques are very similar and only differences relative peak intensities have been found. These peak ratios can provide a further characterisation of the sample preparation methods. The silicate peak (1050 cm^{-1}) is the most intense peak in the spectrum of layer 1 (red ground layer). It is truncated in diamond cell and specular reflectance spectra (Figs. 3.6–3.7 and 3.10–3.11) to prevent overlap with other spectra. The height ratio of this silicate peak and the carbonyl band ($I_{(1050\,cm^{-1})}/I_{(1720\,cm^{-1})}$) is 19 for specular reflectance, 5.2 for the diamond cell, and only 2.4 for the KBr polishing technique. The carbonate peaks (1420 cm^{-1}) in the spectra of layers 4 and 5 relates in a similar way to the carbonyl (1720 cm^{-1}) peak. In fact, the carbonyl band is hardly present in the specular reflectance measurement. The high relative intensity of the inorganic peaks in the specular reflectance spectra is explained by the higher reflective index of the inorganic materials and the presence of sub-surface reflections. However, the measurements using the diamond cell and KBr polishing method are both performed in transmission mode and should have a constant path length. The clear differences between peak ratios are therefore to be interpreted as changes in the sample. The most probable reason is the loss of inorganic pigment particles due to the polishing in the KBr polishing method. In fact, the partial loss of pigment particles upon polishing is not surprising, as the size of the thin section is in the same order of magnitude as the size of the pigment particles. This indicates that the KBr polishing method changes the quantities of the materials in a sample and should be considered as a qualitative method. However, this is an advantage rather than a problem, as the analysis of pigments is well established, while the analysis of embedding medium is normally disturbed by the presence of these pigments.

As the quality of the spectra is sufficient for the diamond cell, and KBr-polishing and, if enough sample material is available, KBr pellets, other characteristics of the techniques will be decisive for the choice of a specific technique in a specific situation. Bulk techniques (KBr and diamond cell) will be the methods of choice when a spatially resolved measurement is impossible. The methods are fast and reliable, but accuracy of tracing the analytical results to a specific spot in the painting is limited by the sampling procedure. The analysis of a squeezed cross-section in a diamond cell improves the spatial resolution, and can be performed very fast. Disad-

vantages are the possible mixing of materials, especially for larger, multi-layered samples. Microtomy is a fast method, but it is not expected to work with every paint system. Furthermore, the embedding medium might be disturbing the visual (using AgCl[89a]) or infrared (using modern resin[43]) observation. Nevertheless, slicing by a microtome might be a good technique to prepare small or modern paint samples. The KBr polishing procedure proposed in this Chapter provides a very high spatial resolution. This analysed thin section was obtained with a minimum of equipment, and appeared to be straightforward, even for the rather complex layer structure of the investigated painting. This sample preparation might therefore proof a valuable tool in the investigation of multi-layered traditional paint samples.
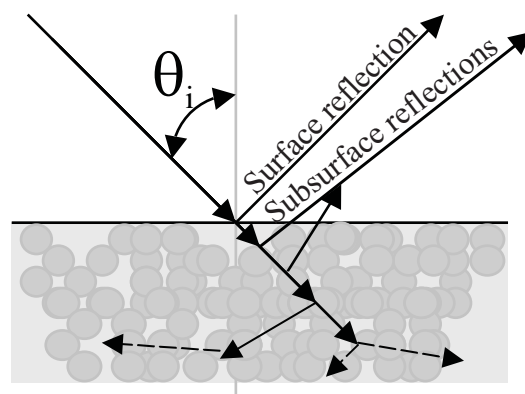

Fig. 3.12. *Model of the nature of the reflected MIR light from the surface of an inhomogeneous system, such as paint. Both surface and sub-surface reflections are present. The sub-surface reflections are specularly reflected and do not loose their polarisation.*

3.7 Conclusions

Several sample preparation methods for infrared spectroscopic analysis of traditional paints have been presented. The optimal spectral quality is obtained for the different transmission techniques. Specular reflectance measurements lead to the introduction of deformations in the spectrum, that severely hinder the spectral interpretation. These deformations are explained as due to the presence of sub-surface reflections. It is not possible to analyse the diffuse reflection of a paint cross-section, and it was concluded that diffuse reflectance of infrared radiation is hardly present. Further diffuse reflectance analyses of paint cross-sections are considered useless. Raman spectroscopy was also unsuccessful. However, ongoing progress in the Raman equipment might very well provide a way to overcome the current technical problems.

The accuracy with which the results can be traced to a specific layer in a painting is optimal in the cases where the sample preparation procedure leaves the layer structure intact, as an imaging measurement can resolve details that are far smaller than the normal sample sizes obtained by sampling with a surgical scalpel. This Chapter provides a new means to make a thin section from a paint cross-section. This method is shown to yield the best combination of high spectral quality and spatial resolution.

3.8 Acknowledgements

4 FOURIER TRANSFORM INFRARED MICROSCOPIC IMAGING OF AN EMBEDDED PAINT CROSS-SECTION

FTIR-imaging is presented as a new analytical approach in the study of paint cross-sections. Analytical FTIR reflection imaging provides the spatially resolved acquisition of infrared spectra with a resolution of about 7 μm. The technique reveals detailed information on the organic functional group distribution in the individual layers of embedded paint cross-sections and is used complementary to visual microscopy and SEM-EDX. This method was applied to a paint cross-section of Rembrandts Portrait of a standing man *(1639). FTIR imaging of this cross-section identified and localised different compounds present in the layers of this sample. Identification of these compounds, based on their infrared spectra is confirmed by results from art historical and conservation literature. Special attention was given to a discoloration that was observed in large parts of the described painting. This discoloration was clearly visible in the paint cross-section. A hypothesis on the nature of the discolored paint layer is formulated based on the FTIR imaging results.*

4.1 Introduction

The continuous need to treat and restore easel paintings is generally attributed to various molecular ageing phenomena. The components used by the painter are subject to chemical and physical changes both during and after the creation of a painting. Painting restorers strive to minimise the negative effects of these ageing reactions and try to preserve a painting as long as possible. Yellowed varnishes are being replaced with fresh ones, damaged areas are filled and overpainted in the course of the restoration of a painting. The restorer has to have a thorough knowledge of the painting materials and the current condition of the paint to take informed decisions on treatment and restoration of our cultural heritage. This knowledge is generally obtained in two complementary ways. Historical sources, such as painters' handbooks and letters from painters are studied to reveal information on painting materials and techniques. On the other hand, analytical investigations on paintings and paint samples are performed to ascertain their current chemical and physical state. In this study we will present a new analytical approach in the molecular study of easel paintings and paint materials.

4.1.1 Materials and structure of paintings

Easel paintings essentially consist of superimposed paint layers. The paints applied by the painter are prepared beforehand and mixed on the artist's palette. The binding medium and other materials (pigments, additives) in the paint substantially change in molecular structure during the subsequent period of ageing and repeated restoration treatments. The paint, which normally consists of colouring materials (pigments, dyes) and a binding medium (oil, tempera), dries due to cross-linking of the binding medium. In oil paints, de-esterification of the glycerol ester bonds and oxidation of fatty acids leads to formation of aldehydes, alcohols, carboxylic acid groups, and peroxides.[109,125,126] Pigments or other additives can have a large influence on these processes. On a macroscopic scale, the paint solidifies and later on becomes brittle due to these chemical changes.

Varnish layers applied on top of the paint layers protect the paint and saturate the colour of the paint. Most varnishes consist of di- or triterpenoids that undergo extensive oxidation and crosslinking. These reactions result in yellowing of the varnish layer.[110,111]

The few processes described above already indicate that the compounds present in a paint layer as well as the resulting ageing processes can greatly differ between the distinct layers of a painting. Analytical strategies designed to elucidate the processes of chemical change in paint layers must therefore have a sufficiently high spatial resolution to examine the layers individually.

4.1.2 Cross-sections in paintings research

Analytical strategies aimed at the molecular processes occurring beneath the surface of a painting require sampling of the layered structure. Two analytical approaches can be distinguished. The first approach involves the dissection of the sample in its individual layers, followed by a bulk analysis of each layer. The required physical separation of the different layers under a microscope is normally difficult or impossible due to the small layer thickness (~ 1–50 μm) and the strong adhesion between layers. The second approach involves the preparation of a paint cross-section, which implies that a multilayered sample is taken from a painting and em-

bedded entirely in a polyester or poly-acrylate resin. The resin facilitates handling and prevents loss of the minute paint chip (~ micrograms). The embedded sample is polished to obtain a smooth surface in which all layers are visible.

The widespread use of paint cross-sections by restorers, art historians, and other investigators makes that a large number is available for analysis. Reflected light microscopy is frequently used to study the colour and structure of the paint layers.

Scanning Electron Microscopy combined with Energy Dispersive X-ray spectroscopy (SEM-EDX) is mostly used to examine the elemental composition of a paint cross-section. However, both techniques provide no information on the organic moieties in the different layers of the painting. Revealing organic information from cross-sections by normal analytical techniques is mostly impossible, as the technique should meet two requirements to analyse cross-sections. The first requirement is the ability to study the surface properties. The second requirement is a high spatial resolution, as layer thickness normally varies between 1–50 μm. Few analytical techniques meet these two requirements. An advanced reflection FTIR spectroscopic imaging set-up is used in the study described here, as conventional FTIR spectroscopy is unavailing in the analysis of paint cross-sections.

4.1.3 FTIR-imaging in the study of paint cross-sections

Infrared spectroscopy has often been used to identify organic compounds in a painting. The possible use of infrared spectroscopy in conservation science was recognised already in 1966 by Olin and in 1970 by van 't Hul-Ehrnreich.[41] The possibilities to measure the small samples normally available in paintings research were increased extensively after dispersive infrared spectroscopy was replaced mainly by FTIR.[37,41,42,44] Most of the measurements on paint samples are transmission measurements performed on KBr discs. Preparation of KBr pellets requires the grinding of a sample. Grinding of the sample leads to a homogenisation of the sample and hence the possibility to study the spatial distribution of compounds is lost. Diffuse Reflectance Infrared Fourier Transform Spectroscopy (DRIFTS) gives results similar to transmission FTIR, but also DRIFTS requires a powdered sample and is therefore inadequate for a spatially resolved study of layered structures.

The transmission techniques described above are obviously not suitable for the analysis of opaque thick cross-sections. We therefore describe the development of reflection FTIR-imaging as a novel strategy in the analysis of embedded cross-sections in this paper. Two different approaches exist to obtain spatially resolved infrared spectra of complex surfaces. A scanning or rastering experiment uses a diaphragm to select a small spot on the surface of the sample. Modulated light from the interferometer that is reflected by this spot reaches the detector, and a spectrum of that spot is recorded. The sample is subsequently moved to a next spot for a new measurement. This sequential measurement of all spots on the surface yields an assembly of infrared spectra from the different surface positions.

It is unfortunately an extremely time consuming approach, as the diaphragm which determines the spatial resolution in a mapping experiment deprives the largest amount of the modulated light. The decreasing signal to noise ratio (S/N) of the infrared spectra has to be compensated by longer integration times. Furthermore, all of spectra are recorded sequentially. Spatial resolutions of 10–15 μm have been achieved using the scanning approach.[85]

The second approach that is employed here is FTIR-imaging. The FTIR-imaging set-up (see Fig. 4.1) consists of an array of a large number of independent detectors, called a Focal Plane Array (FPA) and a step-scan interferometer. The step-scan interferometer steps through several hundreds of mirror positions during data collection. Modulated light from the interferometer illuminates the sample. An image of the sample is projected by an infrared microscope onto the FPA, which is triggered to acquire an image at every mirror position of the step-scan interferometer.[66] In this way, all pixel elements of the FPA simultaneously record an interferogram of a different spot on the sample. The parallel recording of multiple spectra has a number of advantages compared to a mapping experiment. A diaphragm is not needed for spatial resolution in imaging experiments. Therefore the modulated light is used more efficiently than in mapping experiments and the total time to complete a spatially resolved FTIR image is reduced by several orders of magnitude. The experiment time is now solely governed by the desired spectral resolution and S/N. These two parameters can be adjusted by changing the number of mirror steps and the number of image summations respectively.

The spatial resolution in the short wavelength range is determined by the magnification of the microscope and the size of the pixels in the FPA. In the experiments described in this paper the instrumental limit of the resolution is 6–7 µm. The resolution is diffraction limited in the longer wavelength fingerprint region.

FTIR-imaging on paint cross-sections presented here provides detailed information on the organic functional groups and their distribution in the individual layers of embedded paint cross-sections and is used complementary to visual microscopy and SEM-EDX.
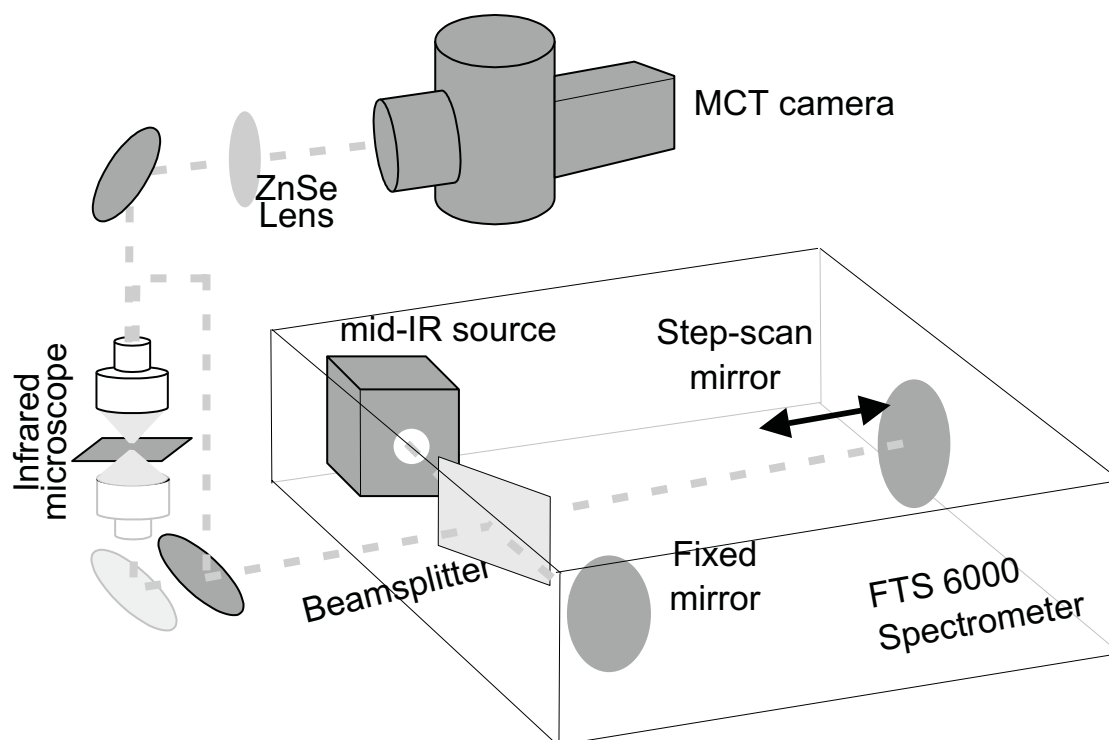

Fig. 4.1. *The FTIR imaging set-up consists of an infrared spectrometer, equipped with a step-scan interferometer. Modulated light from this system is focussed on a sample through an infrared microscope. Light reflected by the sample is projected on an MCT focal plane array by a ZnSe-lens. The light path for transmission measurements is also indicated in the figure.*

4.2 Material and Experimental

4.2.1 Sample description and preparation

Rembrandt painted the *Portrait of a standing man* in 1639 (Staatliche Museen Kassel, Gemäldegalerie der Alten Meister, GK 239, see Fig. 4.2). This painting has undergone several restoration treatments in the course of time. It was investigated as a preparation for the latest restoration. Some paint samples became available for analysis during these investigations. One of these is used as a validation of the technique in the field of conservation, as much is known about the paint materials, techniques, and layer composition used by Rembrandt[4] and especially about this particular cross-section.[112]

Next to the typical layer composition, an interesting artefact is present in this sample. The originally dark paint layer has a pale appearance on large parts of the surface of the painting, which is not to be expected in a dark shadow region. The pale appearance could be correlated to a discoloration in the uppermost part of the paint layer. However, the reason for this degradation could not be found by microscopy. Therefore we tried to obtain more chemical information from this sample by FTIR-imaging spectroscopy.

The sample was embedded in Scandiplast (H.P. Tempelman, Hagen, Germany) and polished with Micromesh® polishing cloths up to the finest mesh (12000) (Scientific Instrument Services Inc., Minnesota).

4.2.2 FTIR Experimental set-up

The experiment described in this paper was performed on a FTS-6000 Stingray FTIR-imaging system (Bio-Rad, Cambridge, MA, USA), which combines a step-scan Michelson interferometer (Bio-Rad FTS-6000),[113] an IR microscope (Bio-Rad UMA-500) and a 64 by 64 element MCT focal plane array (Santa Barbara Focal Plane, Goleta, CA). The 15× Cassegrain optics of the microscope are extended with a 76-mm ZnSe-lens in order to image the sample onto the FPA. With this optical configuration an area of 400 by 400 µm is imaged on the full FPA. This field of view combined with the 64×64 pixel FPA yields a maximum resolution of 6.25 µm. The resolution is diffraction limited in the long wavelength range. A 2.53 µm short wave cut-off filter (OCLI, Santa Rosa, CA) in front of the FPA allows scanning with an under sampling ratio (UDR) of 4. The step distance of the interferometer at UDR 4 is 1.266 µm, so the shortest wavelength that can be observed is 2.53 µm (3950 cm^{-1}) according to the Nyquist theorem. The long wavelength limit of the optical band pass is 900 cm^{-1}, as the FPA is sensitive to light up to about 10.5 µm.

The selected interferometer step frequency can be adjusted for higher speed or higher S/N. The low step rate (1 Hz) of the step-scan interferometer in the experiments described allows the frame-grabber board in the camera to average 200 images during each step, leading to a high S/N. The averaged image is transferred to the computer. Win-IR Pro 2.5 software (Bio-Rad) is used to control the interferometer and the ImagIR 2.1 image acquisition software (Santa Barbara Focal Plane). Approximately 500 interferometer steps are needed to obtain the spectroscopic resolution of 16 cm^{-1}. The total measurement time in this configuration is about 9 minutes, while the resulting data-set is about 8 Mb in size.

A two-point calibration ensures a homogeneous response of each pixel on the FPA. A zinc selenide (ZnSe) window was chosen for this calibration because of its nearly constant reflection

Fig. 4.2. Portrait of a standing Man*, painted by Rembrandt van Rijn in 1639. (Staatliche Museen Kassel, Gemäldegalerie der Alten Meister, GK 239). A cross-section is taken from the shadow region below the man's right arm. (see also the coloured version at the end of this Thesis)*

in the complete MIR range. ZnSe has a refractive index of 2.45 and reflects about 18% of the incoming light, comparable to that experienced in cross-section analysis. The background spectra were also recorded from the ZnSe-window.

Specular (Fresnel or mirror) reflected light forms the main part of detected light from a polished paint cross-section sample. The intensity of the reflected beam is not only dependent on the absorption, contrary to transmission measurements, but also on the refractive index of the sample. Hence, spectra of specularly reflected light are not directly comparable to results of transmission measurements. Fortunately, a fundamental relation between absorption and refraction exists. This relation was first described by Kramers and Kronig[114] and the transformation that yields absorbance-like spectra from specular reflectance data is called a Kramers-Kronig transformation.[92,94] The infrared microscope fixes the angle of the incident beam, and makes the application of polarised light unsuccessful due to the collimation of the incident beam. Therefore the application of the Kramers-Kronig transformation is formally not allowed for these measurements. However, the relatively small angle of incidence can be assumed near-normal in the described set-up, especially for the evaluation of low absorbing samples.

The data-set obtained during one run of the interferometer contains one complete interferogram for every pixel in the FPA. Data pre-processing of these 4096 spectra was performed by the Win-IR Pro software, using standard Mertz phase correction,[85] a triangular apodisation and zero-filling to 1024 points. After Fourier transformation, the real part of the signal was background corrected to reflectance units. The Kramers-Kronig transformation algorithm provided with the Win-IR Pro software was used to transform the specular reflectance spectra to absorbance spectra.

The resulting three-dimensional data-cube consists of a stack of images. Each image contains an absorption plot at a specific wavelength, while every pixel in the image contains a complete infrared spectrum. These infrared spectra can be displayed and analysed individually to identify the compound present at a particular image position. The most straightforward way to analyse the spatial distribution of a compound is to compare the intensities of one of its specific spectral absorbance band in all spectra. The outcome of this comparison is displayed as a false colour intensity map that shows the functional group distribution of the cross-section surface. A combination of these tools provides a simple means to identify and localise compounds present in the paint sample.

Calcium carbonate (Merck, 99%) was measured as a reference material in transmission as a KBr pellet. The diffuse reflectance measurement was obtained using the Bio-Rad DRIFTS accessory. Both measurements were performed using the Bio-Rad FTS 6000 spectrometer in rapid scan mode. The spectra have a resolution of 4 cm^{-1} and were acquired with a mirror speed of 5 kHz co-adding 50 spectra. Both spectra were corrected to absorbance units with a KBr background spectrum using the appropriate sampling method.

4.2.3 Microscopy

Visual light microscopy reveals layer structure and colour with a high resolution (~1 μm). Illumination with ultraviolet light causes specific components, especially resins, to fluoresce. Microscopic studies were performed on a Leica DMR microscope (Leica, Wetzlar, Germany). Normal light was provided by a 100W Halogen projection lamp, using bright-field illumination and crossed polarisers. An Osram HBO 50 lamp and Leica filter D (excitation 360–425 nm, emission > 460 nm) were used for fluorescence microscopy.

4.2.4 SEM-EDX

SEM-EDX measurements were performed to identify heavy elements present in pigments, dryers or other compounds. These measurements were carried out on a JEOL JSM 5900 LV scanning electron microscope scanning with a 25 kV electron beam. Samples were coated with carbon to increase the low conductivity of the sample and so prevent accumulation of charge. EDX analyses were performed on different parts of the cross-section by measuring the emitted X-rays with a Noran Vantage EDS-system equipped with a Pioneer Norvar Detector.

4.3 Results and discussion

4.3.1 Microscopy and EDX

Results of the microscopic investigation are shown in Fig. 4.3. Fig. 4.3a shows the visual light image, Fig. 4.3b shows the fluorescence of the same paint cross-section under UV illumination. Fig. 4.3c is a map in which the function of the different layers is summarised. The cross-section in these figures is positioned such that the layers at the bottom of the figures represent the lower layers in the painting (closest to the canvas).

The lowest layer in Fig. 4.3a shows a red, opaque layer. On top of this layer, a white layer that contains large pigment particles is found. The binding medium between these particles has yellowed. This remarkable combination of a red and a white ground layer, the so-called double ground, is often observed in Rembrandts paintings.[115]

The paint layer on top of the white ground is very dark and probably contains boneblack as a pigment. Various varnish layers are present on top of the black paint layer. As resins fluoresce strongly, they are clearly visible in the UV fluorescence image (Fig. 4.3b). Several varnish layers have been applied during successive restoration treatments. They are separated by darker layers, which contain overpaint or accumulated dirt.[112] The fluorescence image visualises a crack in the dark paint layer (arrows in Figs. 4.3a, 3b) as it is filled with varnish.

Fig. 4.3d is an enlargement showing a darkfield microscopic image of part of the paint cross-section (see outline in Fig. 4.3c). The arrow in Fig. 4.3d points to a 5 μm thick whitish part, which is present in the upper part of the dark paint layer.[112,116]

Results of elemental analysis by EDX measurements (Table 4.1) reveal the presence of silicon and aluminum in the red ground layer. Lead is found in the white ground layer and supports the identification of the white pigment particles (Fig. 4.3a and c) in this layer as lead white. Calcium and phosphorous found in the dark paint layer can be explained by the presence of bone black pigment, which contains calcium phosphate and calcium carbonate due to the thermal degradation of hydroxy-apatite. The small amounts of lead in the dark paint are probably due to a lead-containing dryer.
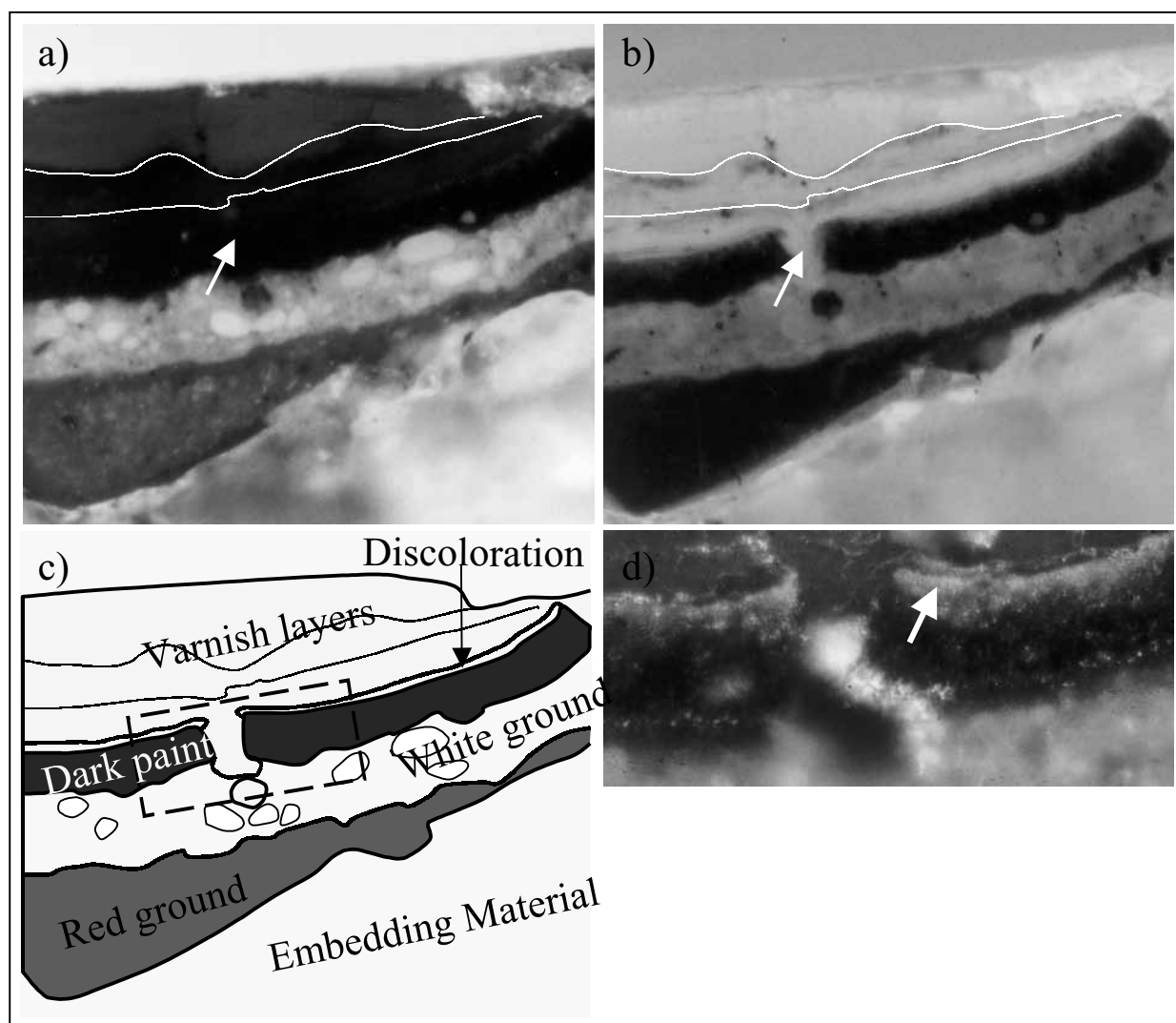
Fig. 4.3. *Microscopic images of the cross-section taken from the painting shown in Fig. 4.2.* ***(a)*** *Visible microscopic image,* ***(b)*** *fluorescence image after UV illumination,* ***(c)*** *a map to localise the different layers, and* ***(d)*** *displays a darkfield microscopic image of a small section of this cross-section, indicated by a grey box in Fig. 4.3c. This image emphasises the pale upper part of the dark paint layer (arrow).*
(see also the coloured version at the end of this Thesis)

Layer	Elemental composition
Dark paint layer	Ca, Pb, Al, Si, P, K (Fe, Na, Mg)
Discoloured paint	Ca, Pb, Al, Si, P, K (Fe, Na, Mg)
White ground	Pb
Red ground	Si, Al, Fe, K (Pb, Ca, Ti, Mn, Na)

Table 4.1. *Elemental composition of the different layers in the paint cross-section shown in Fig. 4.3, as determined by EDX.*

4.3.2 Reflection FTIR-imaging

The results of the FTIR measurement are given in Fig. 4.4. The wavenumber of the imaged absorption peak is indicated in each false colour plot. A blue colour in these plots represents a lower absorption of the indicated absorption band, while the red ('highlighted') area has a higher absorption of this band. Comparison of the layers highlighted in Figs. 4.4a–4.4e to Fig. 4.2 indicates the highlighting of the adjacent layers in these figures. A single pixel infrared spectrum from the highlighted part of this plot (marked *) is shown next to each false colour plot.

The red ground layer is highlighted in Fig. 4.4e, where a broad peak around 1034 cm^{-1} is imaged. The infrared spectrum of a spot in this layer is shown on the right and indeed contains a large band just above 1000 cm^{-1}. This band is caused by absorption of silicates in materials as glass, sand, quartz, and kaolin. These materials were used as cheap fillers in the 17th century. The purpose of this lowest paint layer was mainly the smoothing of irregularities in the canvas, for which high quality pigments were not needed. The presence of silicates as sand and quartz in red ground layers is well known.[4,115] This interpretation is supported by identification of silicon, potassium, and sodium by EDX (Table 4.1). The absence of binding medium peaks in this layer is attributed to the high pigment content. The area imaged in Fig. 4.4e is reasonably homogeneous, although the colour map shows some intensity differences (yellow to red).

Meilunas[37] assigns the bands at 1040 and 1100 cm^{-1} to hematite, an iron oxide. However, iron oxides do not absorb in this spectral region and the absorption is probably due to an impurity in his samples.

Fig. 4.4d shows the white ground layer. The FTIR spectrum taken from this layer exhibits intense absorption bands at 1404 cm^{-1} and 1520 cm^{-1}. The peak at 1404 cm^{-1} matches exactly the maximum found for the carbonate absorption in lead white references,[117] a very common pigment in the 17th century, which was used both for ground and other paint layers.[4,115] Furthermore, the presence of lead is confirmed by the EDX measurements (Table 4.1). The FTIR spectrum in Fig. 4.4d also shows an absorption peak at 1520 cm^{-1}. This absorption band is often observed in lead white containing paint layers. There is strong evidence in several studies of other 17th century paintings that it is caused by absorption of lead carboxylates. Lead carboxylates masses in highly degraded underpaint layers were identified in another study by both FTIR and mass spectrometry.[118,119] Previous assignment of a peak at 1520 cm^{-1} in a lead white containing layer to the amide II peak of a proteinaceous material[34] is in our opinion erroneous, as the assumed amide I in this study is very sharp, unlike the broad appearance of amide peaks normally. Furthermore, it is uncommon that the amide II absorption (1520 cm^{-1}) in proteins is higher than the amide I band (1650 cm^{-1}). Hence we conclude that also in this case lead carboxylates must have been observed.

Reactions between oils and metals that result in formation of carboxylate containing materials were already mentioned by Jacobsen and Gardner in 1941,[120] and the presence of similar products in paint layers has been assumed.[108] However, the detection and localisation of metal carboxylates in paint cross-sections is hardly possible using conventional techniques.

Lead carboxylates can be formed after partial or complete dissolution of lead white pigment particles.[118] It seems that we are dealing with an early phase of a similar phenomenon here. The position of the lead white particles is indicated by white boxes in Fig. 4.4d. The position of these boxes is based on the visual microscopic image in Fig. 4.2. Some of these boxes (those indicated by an arrow) perfectly match with voids in the lead carboxylates absorption intensity. Lead

Fig. 4.4. *The images on the left are false colour plots displaying the intensity of the absorbance peaks at (a) 1774 cm⁻¹, (b) 1650 cm⁻¹, (c) 1430 cm⁻¹, (d) 1522 cm⁻¹, and (e) 1034 cm⁻¹. Fig. (f) facilitates the correlation of the FTIR false colour plots to the microscopic data in Fig. 4.3. The IR-spectra on the right are obtained from the highlighted part (indicated by *) in the false colour plots, respectively the (a) varnish layer, (b) upper part of the dark paint layer, (c) dark paint layer, (d) white ground, and (e) red ground. (see also the coloured version at the end of this Thesis)*
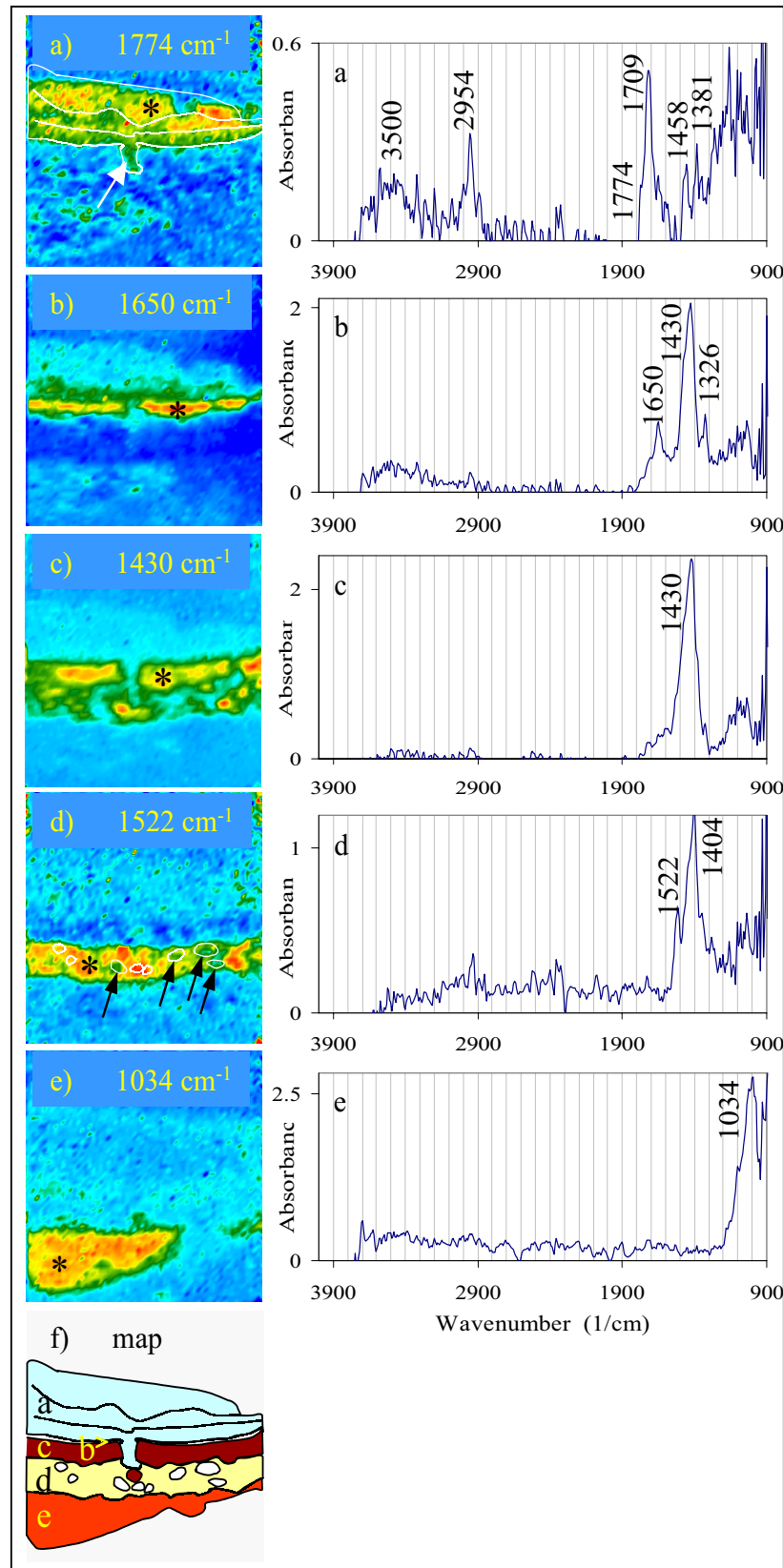
carboxylates are not observed in these places and the lead white pigments therefore seem to be intact. The remaining white boxes (not indicated by an arrow) cannot be distinguished from the matrix on the basis of the absorption at 1520 cm^{-1}. This absorption might be due to a carboxylate envelope around the lead white particle, or due to smearing of surrounding carboxylate matrix onto the particle.

The false colour plot in Fig. 4.4d obtained by FTIR-imaging allows not only the identification of this ageing product, but also reveals its distribution within the paint layer in great detail.

The black paint layer is imaged in Fig. 4.4c using the absorption band at 1430 cm^{-1}. This peak position of the carbonate in the black paint layer is similar to the absorption of calcium carbonate (or chalk), a very common pigment in 17th century paintings. The identification of calcium carbonate (1430 cm^{-1}, spectrum 4c) is confirmed by the observation of calcium in SEM-EDX (Table 4.1).The false colour plot of the 1430 cm^{-1} carbonate band in Fig. 4.4c reveals the homogeneous spatial distribution of the calcium carbonate in the dark paint layer. The crack that was seen in the fluorescence image in Fig. 4.2b displays itself as an interruption of the highlighted area in Fig. 4.4c.

Some lead white particles in the white ground layer are also highlighted in Fig. 4.4c due to the proximity of calcium carbonate (1430 cm^{-1}) and lead white (1404 cm^{-1}) absorptions.

The varnish layers are imaged in Fig. 4.4a, using the absorption at 1774 cm^{-1}. The FTIR spectrum of a spot in these varnish layers in spectrum 4a shows the 1774 cm^{-1} absorption as a small shoulder on the left of the intense 1700 cm^{-1} peak. The choice for the 1774 cm^{-1} peak instead of the much higher acid 1700 cm^{-1} band may seem strange, but imaging of the latter band emphasises the high absorption of carbonyl groups in the embedding resin. The absorption at 1774 cm^{-1}, which is also observed in polymerised drying oil[37] is only present in the broadened peaks of varnish spectra. It is not present in the embedding medium. Next to the carbonyl absorptions (1700−1800 cm^{-1}), this layer contains only absorptions of organic compounds at 2925 (CH), 1470 (CH$_2$), 1380 cm^{-1} (CH$_3$), and a broad absorbing spectral region at 1100−1400 cm^{-1} due to various C−O bonds. This high and broad absorption band indicates an extensive oxidation of the varnish layers. Absorptions by inorganic compounds are not present, as varnish layers are normally not pigmented.

The absorption of the varnish layers is not homogeneous. Some higher absorbing parts in the varnish layer can be seen as red/yellow areas in false colour plot (Fig. 4.4a), while the less intense absorbing parts are green. The white lines in Figs. 4.3a, 4.3b and 4.4a allow comparison of the infrared images with the visual images. It is clear that in the upper part of the varnish the high absorption area (Fig. 4.4a) correlates with the lighter area in the visual image (Fig. 4.3a).

Several varnish layers have been added during the various restoration treatments that this painting has undergone. Nowadays, previous varnish layers are removed before a new varnish is applied. However, from this paint sample it is clear that previous layers were not or hardly removed during the latest restauration treatments. This may point to application of the Pettenkofer process, a method to regenerate varnish layers instead of replacing them that was practised frequently in Staatliche Museen Kassel in the 19th century.

The chemical differences we observe here between the different varnishes layers are therefore probably connected to differences between the various varnish layers applied in the course of time. The interpretation of these differences is however not straightforward. They may result either from the different materials used by the restorers or from different stages in ageing. The

presence of varnish in the crack in the paint (arrow in Fig. 4.4a) is clearly seen (cf. Fig. 4.2b). This varnish must therefore be applied after the crack had developed.

Fig. 4.4b shows an FTIR-imaging map of the 1650 cm^{-1} band. This band is very specific for the upper part of the dark paint layer, and is not present in the lower part of this paint layer (see spectrum 4c). The same is true for the peak at 1326 cm^{-1}. The intensity distribution map at 1326 cm^{-1} (not shown) resembles Fig. 4.4b closely. The interpretation of this spectrum is not yet completely clear. Library search on the combination of peaks at 1650 and 1326 cm^{-1} revealed oxalates as possible component. It has long been known that di-acid compounds can result from the degradation of fatty acids, but the presence of oxalates on 17th century paintings has never been reported and is in fact unlikely. Spectrum 4b also contains a small absorption at 1520 cm^{-1}. The combination of bands at 1650 and 1520 gave rise to the idea that this layer is of proteinaceous origin.[121] However, the high intensity and the sharp appearance of the 1650 cm^{-1} band do not resemble the broad, low intensity appearance normally connected to amide peaks. We therefore rejected this hypothesis. A more likely hypothesis is an alteration of the calcium carbonate. According to Salisbury, the reflection spectrum of calcium carbonate is altered due to 'reststrahlen' effects.[93,95] This implies that the intensity and spectral position of these reststrahlen peaks are strongly dependent on the size and volume fraction of the calcium carbonate particles. Reference measurements we did ourselves on reflection of calcium carbonate indeed show peaks at 1630 and 1360 cm^{-1} (see Fig. 4.5). Similar distortions in reflected light spectra of chalk have been presented by Fabbri *et al.*[15]

The 1430 cm^{-1} peak in spectrum 4b shows that calcium carbonate indeed is present in the top paint layer. EDX measurements specifically in the upper part of the paint layer confirmed the presence of calcium. Furthermore, it can be seen from Fig. 4.3d that the discolored layer is opaque and contains pigment particles. These observations all indicate the presence of calcium carbonate particles in this layer and therefore this hypothesis seems more likely. A tempting hypothesis on the changes that lead to the extensive changes between the calcium carbonate in the intact paint layers and the discolored top-layer is an increased porosity of the top part of the paint layer due to loss of the more vulnerable binding medium. However, the aberrations of reflection spectroscopy from the normal absorption spectroscopy have not yet been explored fully, and we have at the moment no neat way to test the hypothesising. However, these results imply that reflection FTIR spectra contain information on the physical status or the surroundings of the calcium carbonate.

It appears that chemical information of an area of only 5 μm thickness can be obtained. This does not conflict with the physical limit of the diffraction limit. It is indeed possible to obtain useable spectra of features below the diffraction limit. The diffraction limit only restricts the correct determination of the size and spatial distribution of absorbing compounds. It will in principle not change the absorption spectra.
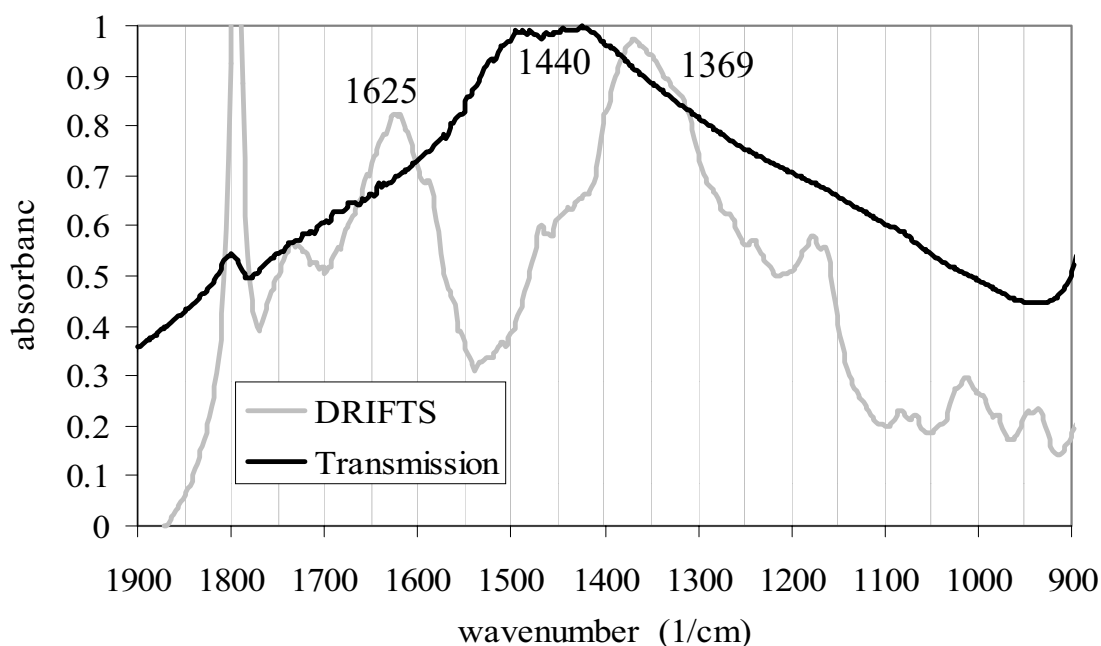
Fig. 4.5. *Comparison between the transmission (heavy line) and DRIFTS (diffuse reflection) (light line) spectra of calcium carbonate (DRIFTS).*

4.4 Conclusions

We have shown the application of FTIR spectroscopic imaging in reflection mode operation for the analysis of paint cross-sections. The reflection experiment described here is in itself unique as it is the first application of reflection FTIR spectroscopic imaging on embedded paint cross-sections. This method provides valuable information on the contents of different layers in paintings. This accurate information could be obtained despite the low intensity of the reflected light from a smooth surface and the artefacts that are introduced by specular reflection and the subsequent Kramers-Kronig transformation.

In Rembrandts *Portrait of a standing man* silicates were identified and located in the red ground layer, lead white and lead carboxylates in a white ground layer, calcium carbonate in one of the paint layers and different organic functional groups, e.g. carbonyl, CH and C−O groups, were observed and located in the varnish layers. A more precise identification of the resinous varnish material is at present not possible in reflection FTIR and would require analysis with mass spectrometric techniques.

The presence of these compounds is very similar to what can be expected from conservation and art history literature. Chemical contrast on an even smaller scale could be seen inside the layers. Examples are the lead white particles in the ground layer, the discolored upper part of the dark paint layer, and the contrast between the varnish layers added in different periods to the painting. It appeared possible to obtain spectra of features smaller than the diffraction limit. However, the accurate size and spatial distribution of these small, absorbing features can of

course not be determined.

Paint cross-sections are commonly studied by visual light microscopy only. Fortunately, the same samples are suitable for surface analytical techniques such as FTIR-imaging and SEM-EDX. Our studies show that FTIR-imaging is a useful technique for the spatially resolved analysis of paint cross-sections. The high spatial resolution is required by the fine distribution of compounds. The structure of the complex, aged materials can be partially elucidated by FTIR-imaging. The intricate interplay between organic and inorganic species in a painting requires the combination of visual light microscopy, FTIR-imaging, and SEM-EDX to provide a detailed insight in the chemistry of old master's paint.

4.5 Acknowledgements

5 FTIR STUDIES OF THE EFFECT OF PIGMENTS IN THE AGEING OF OIL

This Chapter describes the changes in the infrared spectra of paint as a result of ageing. The focus is on the influence of a pigment on the long-term changes in the oil binding medium, a poorly covered topic in literature. Several naturally aged paints made with different pigments were analysed by FTIR. One of the most pronounced effects observed in the infrared spectra of ageing paint is the shifting and broadening of the carbonyl band due to the formation of carboxylic acids. The different carbonyl absorptions (ester, carboxylic acid) could well be resolved by taking the second order derivative of the spectra. The carboxylic acids are hardly observed in paints where metal carboxylates have been formed, as is the case for paints containing Naples yellow, minium (red lead), lead white, and zinc white. Another effect of pigments on the oil binding medium is the catalysis of the hydrolysis of triglycerides, as indicated by the decreasing intensity of the ester absorption. This effect is most pronounced for minium and zinc white. Finally, the nature of the included pigment has a profound effect on the CH stretch absorptions. These differences were assigned to a varying level of oxidation, and can be rather large: the maximum of the symmetric CH stretch vibration in red lead pigmented paint (which is similar to fresh oil), differs more than 15 cm^{-1} for paints pigmented with ultramarine, Naples yellow, Cadmium red and Ochres. From these results it is clear that pigments can significantly alter the infrared spectra of drying oil, and should therefore be identified for a correct assessment of the infrared spectra of drying oil.

5.1 Introduction

Oil is a natural product that can be pressed out of a variety of plant seeds. Some types of oils, e.g. linseed, walnut or poppy seed oil, chemically dry to form a solid film on exposure to air. These so-called drying oils have good working properties when used as binding medium in paint.[122,123] These properties made vegetable drying oils the common binding medium in paints from the 15th until the 20th century, when they were mostly replaced by alkyd and acrylic media.

The drying of oil has been investigated thoroughly over the past 130 years, and a detailed description of the involved mechanisms can be found in literature.[28,60,109,124-127] It appears to be a very complicated process, in which a number of different mechanisms are occurring simultaneously. However, it is not clear to what extent the developed models are a valid description of a normal ageing paint, as important differences exist between paint and the model compounds, which were investigated to formulate the mechanism. Most of the drying studies have been performed using chemically pure esterified fatty acids, instead of the triglycerides that make up normal drying oil. Furthermore, the time scale of most chemical studies is very short; the changes on a longer time scale are simulated by using thermally or light accelerated ageing.[28,32,37-39] The assumption that this accelerated ageing does not change the ageing processes is however not easily verified. The most important restriction of the majority of ageing studies is the absence of pigments, which is a crucial and potentially reactive compound in paint. The presence of pigments or other additives might very well influence the ageing process of paint. This long-term influence of pigments on paint has long been recognised on a macroscopic level,[128] but the underlying chemistry is largely unknown.

This Chapter presents a study on aged oil paints. The paints were investigated by FTIR spectroscopy, which has proven to be a very useful tool in the analysis of the drying of oil and the investigation of traditional paint. A mechanism of early reactions in the drying of oil is presented and illustrated by a study, in which the effects of the drying on the infrared spectra are followed in a time resolved-series of measurements. Subsequently, infrared spectra of several traditionally made and naturally aged paints will be presented and discussed.

5.1.1 Mechanism of the drying process

Fig. 5.1 presents a simplified model of the reactions that take place during the chemical drying of oil. The initial process in the drying of oil is the formation of free radicals. This is possible by elimination of a hydrogen atom from an unsaturated fatty acid. The formation of reactive free radicals is energetically unfavourable, and only occurs when the formed radical can be stabilised by resonance.[109,124-126] This stabilisation is possible when the hydrogen is removed from a methylene group on an α-position to a double bound, or from methylene group between two unsaturations. The latter case is shown as the initial reaction in Fig.5.1.

The formed radicals are trapped effectively by antioxidants that are naturally present in drying oil. Trapping of radicals inhibits the drying of oils, but inactivates the antioxidant. The drying of oil does not start until this inactivation process is completed. The delocalised radical can in principle attach to a double bond in an adjacent fatty acid. The free radical is not consumed during the attachment, and the process and might repeat itself, leading to a higher molecular weight fraction. Addition of a free radical to a double bond in the same fatty acid leads to
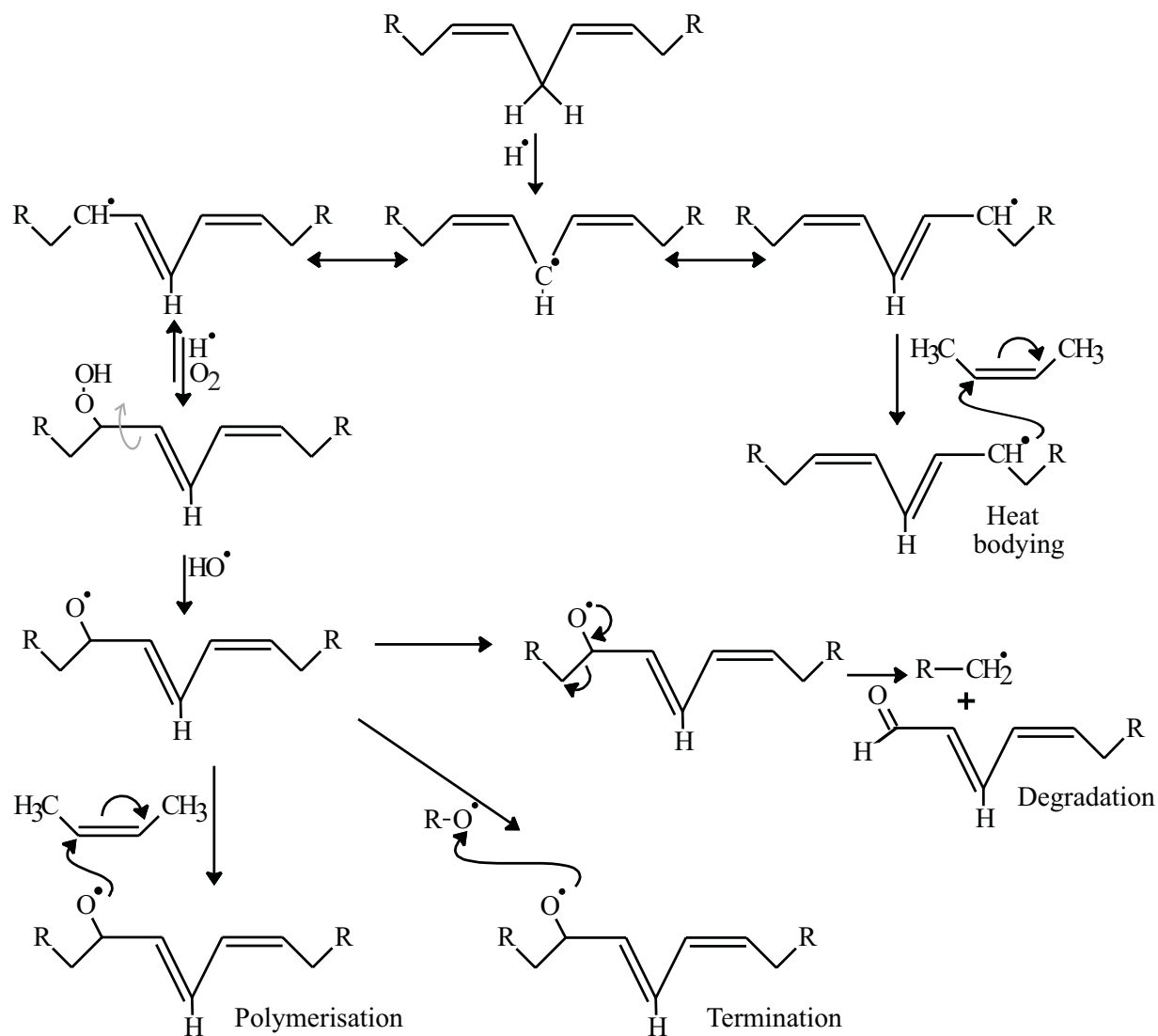
Fig. 5.1. *Simplified model of the early reactions taking place during the drying of oil. This scheme is based on the mechanisms presented by Wexler[109] and Porter.[125,126]*

intramolecular cyclisation.[129] However, these reactions are slow, and only take place when the oil is heated in the absence of oxygen, e.g. during the anaerobic heat bodying of oil.[109] The formation of carbon-carbon bonds is thought to be rare in the presence of oxygen. In this case, addition of oxygen usually leads to the formation of peroxides. The hydro-peroxide normally binds to one of the terminal atoms of the delocalised radical, resulting in the formation of energetically favourable conjugated double bonds.[130] The free peroxyl radical (ROO·) can react with another free radical and so lead to dimerisation of two fatty acids. However, a more likely process is the addition of a hydrogen atom, leading to the formation of a hydro-peroxide. Addition of oxygen to an unsaturated fatty acid can result in a shift of one of the double bonds from the original position. The newly formed double bond is normally in a trans-configuration. Furthermore, the addition of oxygen enables the free rotation around the C–C bond adjacent to the attached peroxide, as rotation is no longer restricted by resonance. Elimination of oxygen after rotation of the C–C bond results in a transformation of the original *cis* double bond into an

energetically favourable *trans* double bond.[37,126] Addition and elimination of oxygen can occur several times and lead to a more or less complete transformation of the *cis* to *trans* double bonds.

Hydro-peroxides formed by oxygen addition are not stable and will be cleaved in the course of time. This cleavage again results in the formation of free radicals. Both peroxyl (ROO·) and alkoxy (RO·) radicals can be formed in this process, the latter being shown in Fig. 5.1. These radicals give rise to different types of reactions, i.e. polymerisation, termination or degradation reactions, as shown in Fig. 5.1. In a polymerisation reaction, a nearby double bond is attacked and the corresponding fatty acid is chemically linked to the fatty acid where the radical was present. This reaction consumes the attacked double bond, but the free radical is still available afterwards and can propagate the polymerisation reaction, eventually resulting in a high molecular weight fraction. Reaction with a double bond in the same fatty acid leads to the formation of epoxides or larger ring structures. Condensation of two radicals terminates the polymerisation reaction. A further important reaction that can be caused by a free radical is the degradation of the fatty acid on which the radical resides. This process leads to the formation of smaller alcohols and aldehydes,[131] which may eventually oxidise to volatile carboxylic acids.

The several mechanisms that play a role in ageing of oil paint are certainly more complicated than can be explained in a single figure. Fig. 5.1 therefore focuses on the most general aspects. This figure ignores the presence of different types of fatty acids, the important role of catalysts in the different steps, the cis-trans transformations as a result of successive oxygen additions, the role of photoxidation in the formation of hydro-peroxides,[130] and several other reactions that take place on heat-bodying of oil.[132] However, the cited publications provide a detailed overview of these effects. In general, the research carried out during the past 130 years has resulted in an accurate description of the possible reaction pathways. The main hiatus in the analysis of dried oils is the accurate description of the polymer network. This fraction is normally insoluble and involatile, which complicates the separation and investigation of intact molecules by methods based on gas chromatography, liquid chromatography, and mass spectrometry. Other analytical techniques (infrared spectroscopy, DSC (Differential Scanning Calorimetry), Raman spectroscopy) can directly be applied to investigate the intact solids, but do not yield very specific information on the network. SEC (Size Exclusion Chromatography) and mass spectrometry using soft ionisation techniques recently enabled the observation of isolated oligomers up to hexamers,[60] but an accurate description of the higher molecular weight fraction is a challenge for future research.

Meanwhile, analysis of the smaller molecules present in aged oils has proven very informative. Several researchers isolated the soluble fraction from aged paint by solvent extractions. These extractions have been used to identify the drying oil and its preparation method.[16,43] Extractions have also been applied in the sample preparation for infrared spectroscopy, mainly to avoid the disturbing influence of inorganic pigments.[43] Extractions are normally combined with chemical derivatisation techniques to improve the volatility of the extracted material. Recently, Van den Berg *et al*. used an elegant two-step derivatisation to determine the degree of hydrolysis of the ester bond between the fatty acid and glycerol.[19] It was concluded that hydrolysis, neglected or denied[133] in older literature, is a relatively slow process compared to the initial drying of oil (~10s of years).

It is generally assumed that the role of pigments in the initial stages of drying is catalytic or

inhibitive, influencing the activation of oxygen or the breakdown of hydro-peroxides.[134] However, there are indications that several pigments undergo chemical alteration during the ageing of paint. Discoloration of the paint is the most obvious indication of such a process. Another indication is the physical change of the paint layer to a hardened, brittle system. This hardened system has been described as a poly-anionic network, in which the several carboxylic acid groups are stabilised by metal ions.[108] Pigments are the most probable source of these metal ions. Unfortunately, studies on the long-term behaviour of artist's pigments in paint are scarce. Rasti and Scott quantified oxygen absorption, weight loss, hydro-peroxide formation, and degradation products in paint films with different pigments. Vermillion pigmented paint films showed a relatively high weight loss, high hydro-peroxide concentration, and high relative amounts of degradation products. Surprisingly, heavy metal containing pigments like lead white and verdigris were found to have an inhibitive effect on these effects. It is likely that at least part of the results can be explained by the rather untraditional samples used in these experiments (1% w/w mixtures of pigment in oil, layer thickness 2 mm, UV illumination ageing). Especially the effect of lead white might be reduced by scattering and absorption of the UV light.

Meilunas *et al.* have compared spectra of fresh paint with a similar paint after accelerated ageing, and 50-years-old paint on test panels.[37] This article provides a good overview of the changes in infrared spectra upon ageing of linseed oil and lead white pigmented linseed oil. It shows several indications for the influence of the pigment on the ageing mechanism. According to Meilunas *et al.*, the presence of lead reduces the number of carbonyl products by catalysis of the hydrolysis of ester linkages. Instead, metal carboxylates were observed. Luxan and Dorrego[39] investigated the reactivity of several pigments to form metal carboxylates under unrealistic ageing conditions. However, their study seems to be based on poorly founded presumptions. It is e.g. presumed that metals can only catalyse the drying of oil in the form of metal soaps. Furthermore, metal carboxylates are assumed to be soluble, as the spectra are recorded from solvent extracts.

This small number of studies clearly indicates that pigments have an influence the long-term ageing process of paint. However, the results are not complete and sometimes even contradictory. One of these contradictions concerns the catalytic behaviour of lead white on the drying of oil. Meilunas *et al.* conclude that lead white acts as a catalyst,[37] while Rasti and Scott indicate that lead white inhibits ageing.[38] The contradictory results might very well be due to a different ageing procedure followed by these authors: Meilunas *et al.* investigated thermally and naturally aged samples, while Rasti and Scott used UV illumination for accelerated ageing. It is known that lead white efficiently absorbs UV light[117] and this absorption is a more likely explanation for the inhibitive effect than any chemical effect. The controversy illustrates that the ageing procedure may significantly influence the chemical ageing of the paint in a complex way.

5.1.2 Outline

This Chapter continues with the infrared spectra of several aged paints to further investigate the long-term changes of paint. Only naturally aged paints were investigated, to minimise the bias due to the ageing method. Furthermore, the composition of these paints is typical for traditional paints. The paints were taken from different collections of test panels. The test panels from the Von Imhoff collection are 30-years-old. Still older reconstructions are obtained from

the Doerner collection, which contains a number of 60-years-old test panels as well as some 80-years-old test panels. The oil medium in several aged samples from the Von Imhoff collection has earlier been investigated by GC-MS.[19]

5.2 Experimental

5.2.1 Samples

The drying of oil study was performed on a cold pressed linseed oil, to which 0.06% cobalt was added as a catalyst. The oil was prepared by Wim Muizebelt (FOM AMOLF). The old linseed oil that had been kept in a closed vial was taken from the paint materials collection of about 50 years old, which belonged to a sales representative of Sikkens, a Dutch paint manufacturer and was kindly provided by Martin Paans. The naturally aged linseed oil paints were taken from different collections. Paints containing vermilion, iron oxide, ultramarine, indigo and lead white were taken from the Von Imhoff collection, which was prepared by H.C. von Imhoff in 1973 with cold-pressed linseed oil (Mühlfellner-Rupf, Zürich, Switzerland). The oil was allowed to stand in flat dishes of 4 mm height for 3 weeks, after which the skin was removed. The oil was mixed with pigments until a workable paint was obtained. The different paints were applied on primed linden wood panels and hung under natural light conditions in the Canadian Conservation Institute (CCI, Ottawa). The samples were carefully scraped off the paint layer. Paints containing cadmium red, red lead, Naples yellow, yellow ochre, gold ochre, green earth, Kassel earth, zinc white, and lead white were taken from the Doerner collection. The test panels in this collection were made by between 1912 and 1941. The early test panels (until 1938) have been made by Professor Alexander Eibner. Later panels were produced by his (former) pupils. The paints were initially stored under normal conditions. However, it was found in a closed cupboard when the sample was taken. An overview of the analysed paints is presented in Table 5.2.

5.2.2 FTIR

The fluid samples were applied on a ZnSe disc for infrared transmission experiments. The solid paints were squeezed in a P/N 2550 diamond cell (Graseby Specac, Orpington, Kent, UK) before measurement. The FTIR spectra presented are acquired using a Bio-Rad FTS-6000 FTIR spectrometer (currently Digilab, Cambridge, MA, USA), connected to an IR microscope (Bio-Rad UMA-500) and a MCT detector. The resulting spectra were processed using the Bio-Rad Win-IR Pro software. Base-line correction and subtraction of a water vapour spectrum were applied to improve the spectral quality. Every scaling mark on the vertical axes in Figs. 5.5–5.21 was set to 0.2 absorbance units, to allow an easy comparison of the absolute value of the spectra. The apparent spectral resolution of the FTIR spectra was increased taking the second derivative of the spectra.[135] The use of spectral deconvolution[136] was thought inappropriate as the different materials present in paint might contain absorption peaks of largely varying width. The second derivative spectra were inversed to make the absorption peaks positive. Infrared spectra of oil during the drying process were acquired using the kinetics mode, embedded in the Win-IR Pro software. In this mode, the spectrometer measures continuously. The spectra are averaged during periods of 10 minutes and a single spectrum is stored for each of these periods. Selected

spectra of this series were processed using Matlab 5.2 (The Mathworks Inc., Natick, MA, USA) to form Figs. 5.3A and B. Fig. 5.22 compares the height and area of the peak around 2930 cm^{-1} in all of the spectra presented in Figs. 5.5–5.21. The presented values for height and area were calculated using the Win-IR Pro software. The applied peak-definitions are (all values in cm^{-1}): Height of peak: baseline (3030, 2800), centre: extreme in region (2970, 2910). Area of peak: baseline (3030, 2800), edges (2968, 2901), centre irrelevant.

5.3 Results

5.3.1 Early reactions during the drying of oil

The drying of oil was followed by FTIR to study the involved mechanisms. A thin film of oil was applied to an infrared transparent disc to enable transmission FTIR measurements and to improve the oxygen supply via diffusion. An infrared spectrum of the fresh linseed oil is displayed in Fig. 5.2. The various absorption peaks in this spectrum are assigned in Table 5.1. Subsequently, the film was analysed at fixed time intervals. Selected spectra from the data-set obtained in this way are presented in Figs. 5.3A and B. These figures only display selected parts of the spectra to visualise the changes more clearly. The time passed since the start of the experiment is indicated on the left side of the spectra.

The left part of the spectrum in the fresh oil is dominated by a series of aliphatic vibrations around 3000 cm^{-1}, caused by the large amount of CH$_2$ and CH$_3$ groups in the fatty acids. Stretch vibration of CH bonds lead to high absorptions at 2926 and 2855 cm^{-1} with a shoulder at 2958 cm^{-1}. Bending vibrations of these moieties are present at 1460 cm^{-1} and 1374 cm^{-1} (CH$_3$). These peaks do not show much variation in time. On the other hand, the smaller peak at 3009 cm^{-1}, assigned to the *cis*-type unsaturated CH group (C=C-H),[137] disappears in about 5 hours. The same group absorbs at 726 cm^{-1}, and the intensity of this peak also decreases. The simultaneous increase of the absorption at 980 cm^{-1} suggests that the *cis* double bonds are isomerised to the *trans* configuration.[30,106] The presence of unsaturations also leads to the small peak at 1653 cm^{-1}, caused by C=C double bonds in the fatty acids.

Another clearly changing feature on the left hand side of the infrared spectrum is the formation of a new absorption band at 3440 cm^{-1}. The spectral position and broad appearance of this band indicates that it should be assigned to alcohol and/or hydro-peroxide vibrations, both products of oxidation. A further distinction between alcohols and hydro-peroxides cannot be made, as the difference in their peak maxima is small. Discrimination only becomes possible after specific derivatisation of the oil.[28,29,138] These studies have indicated that hydro-peroxides formed in the early stages are subsequently replaced by alcohols and ethers. The uppermost spectrum in Fig. 5.3A shows an increased absorption in the spectral region of 3000–3200 cm^{-1} (between the peaks at 2926 and 3440, arrow in Fig. 5.3a). These absorptions are probably caused by carboxylic acid moieties, as is confirmed by the formation of an absorption band at 1414 cm^{-1} and the broadening of the carbonyl band. This intense carbonyl peak at 1744 cm^{-1} is originally due to ester bonds between glycerol and fatty acids, but the carboxylic acids absorption at about 1710 cm^{-1} is normally not resolved from this peak and partly explains the broadening.[37,106] The formation of carboxylic acids is a generally recognised degradation reaction in drying oil, and the associated increase of the acidity is confirmed by titration studies.[133] However, other types of

*Right-hand image: **Fig. 5.3.** FTIR study of the drying of linseed oil, showing the infrared spectra of linseed oil at different periods after its application as a thin film. The time since application is indicated on the left sides of the spectra. (**a**) Spectral region 2600-3600 cm⁻¹. (**b**) Spectral region 700-1800 cm⁻¹.*
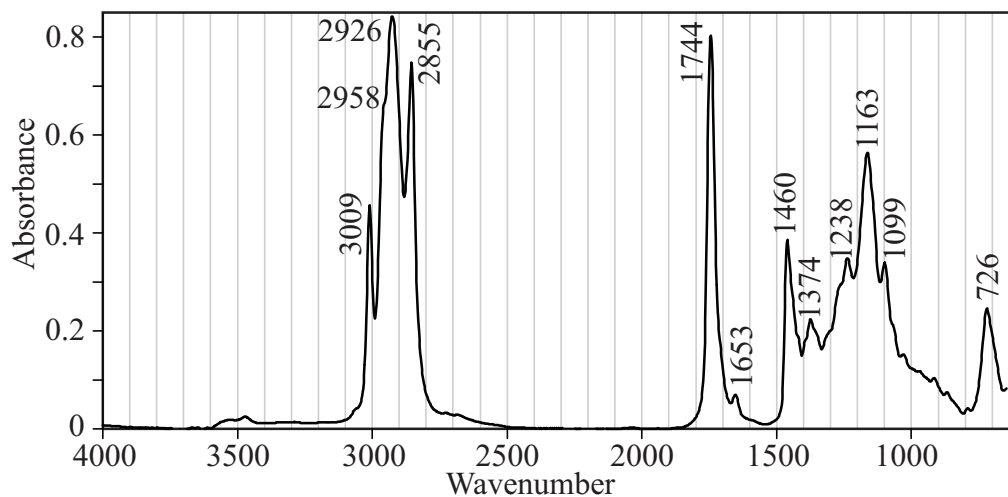
Fig. 5.2. *Infrared spectrum of fresh linseed oil.*

Wavenumber (cm⁻¹)	Moiety	Source
3009	C=C–H (cis) stretch	Fatty acid
2958(s)	CH3 stretch	Fatty acid
2926	CH2 stretch	Fatty acid
2855	CH2 stretch	Fatty acid
1744	C=O	Ester bond
1653	C=C	Fatty acid
1460	CH3 (asymm. bend) CH2 (scissors)	Fatty acid
1374	CH3 "umbrella mode"	Fatty acid
1238	C–O	Ester bond
1163	C–O	Ester bond
1099	C–O	Ester bond
720	CH2 rock	Fatty acid
726	C=C–H (cis) bend	Fatty acid

Table 5.1. *Assignment of the absorption bands in the spectrum of fresh linseed oil, shown in Fig. 5.2.*
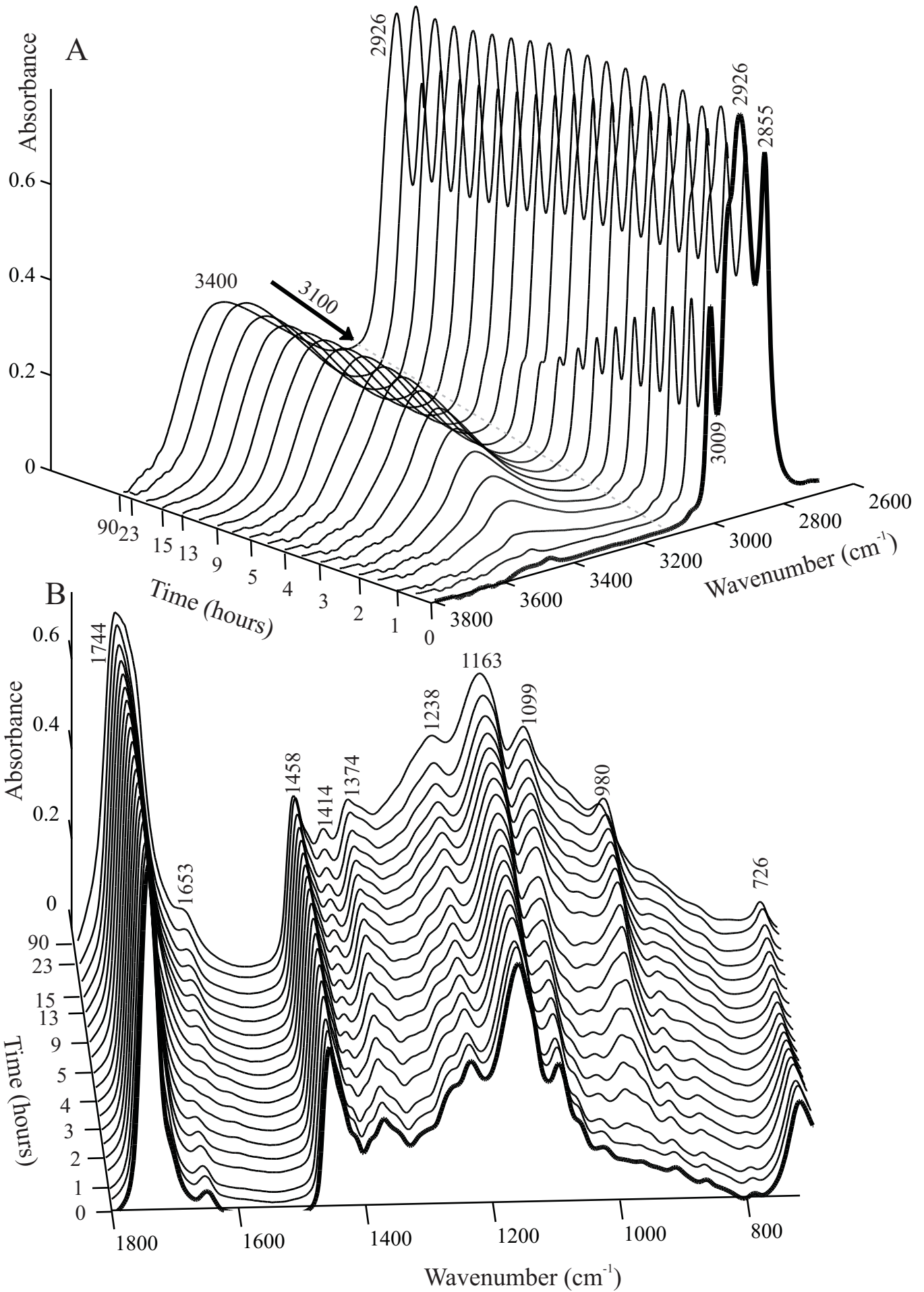
Pigment	Colour index	Source (a)	Year	Oil	Support	Fig.
Vermilion	PR106	I	1973	Linseed	Panel	5.5
Cadmium red	PR108	D	1937	Linseed	Panel	5.6
Iron oxide	PR101	I	1973	Linseed	Panel	5.7
Red lead	PR105	D	1916	Poppy	Canvas	5.8
Naples yellow	PY41	D	1939	Linseed	Canvas	5.9
Yellow ochre	PY43	D	1939	Linseed	Canvas	5.10
Gold ochre	PY43	D		Linseed	Canvas	5.11
Green earth	PG23	D	1939	Linseed	Canvas	5.12
Kassel earth	Natural	D	1973	Linseed	Canvas	(b)
	Brown 8	I	1939	Linseed	Panel	5.13
Ultramarine	PB29	I	1973	Linseed	Panel	5.14
Indigo	Vat blue 1	I	1973	Linseed	Panel	5.15
Zinc white	PW4	D	1941	Linseed	Panel	5.16
Lead white	PW1	D	1912	Linseed	Panel	5.17
		D	1941	Linseed	Panel	5.18
		D	1941	Linseed	Panel	5.19
		D	1941	Linseed	Panel	5.20
		I	1973	Linseed	Panel	5.21

Table 5.2. Overview of the aged paints investigated in this Chapter.
(a) The paints were taken from the collections prepared by H.C. Von Imhoff (I) or from the collection kept at the Doerner Institute (D).
(b) Results not shown.

carbonyls, e.g. ketones, aldehydes, lactones and anhydrides, might also play a role in the observed broadening of the carbonyl band.

The drying studies presented in Figs. 5.3A and B show the extensive changes of the infrared spectra of oil upon drying. Infrared spectroscopy has therefore been one of the most important techniques in the elucidation of the mechanism shown in Fig. 5.1.

5.3.2 Infrared spectra of unpigmented aged oils

Fig. 5.4 shows spectra of two different unpigmented aged oil samples. These provide a reference for the spectra of various pigmented paints presented in the next section. The aim of this comparison is the evaluation of the influence of pigments on the ageing of oil. Spectrum 4A represents a thin linseed oil layer cured for 90h (equal to the uppermost spectrum in Figs. 5.3A and B). This spectrum is remarkably similar to the spectrum of the 50-years-old unpigmented oil film presented by Meilunas *et al.*[37] This suggests that the cross-linked oil system is relatively stable after an initial drying period, at least, as far as infrared spectroscopy can observe. The claim that a thermal treatment (24h at 120°C) faithfully reproduces a 50-years-old paint[37] should therefore be taken with a pinch of salt. The lower spectrum in Fig. 5.4 represents a 50-years-old
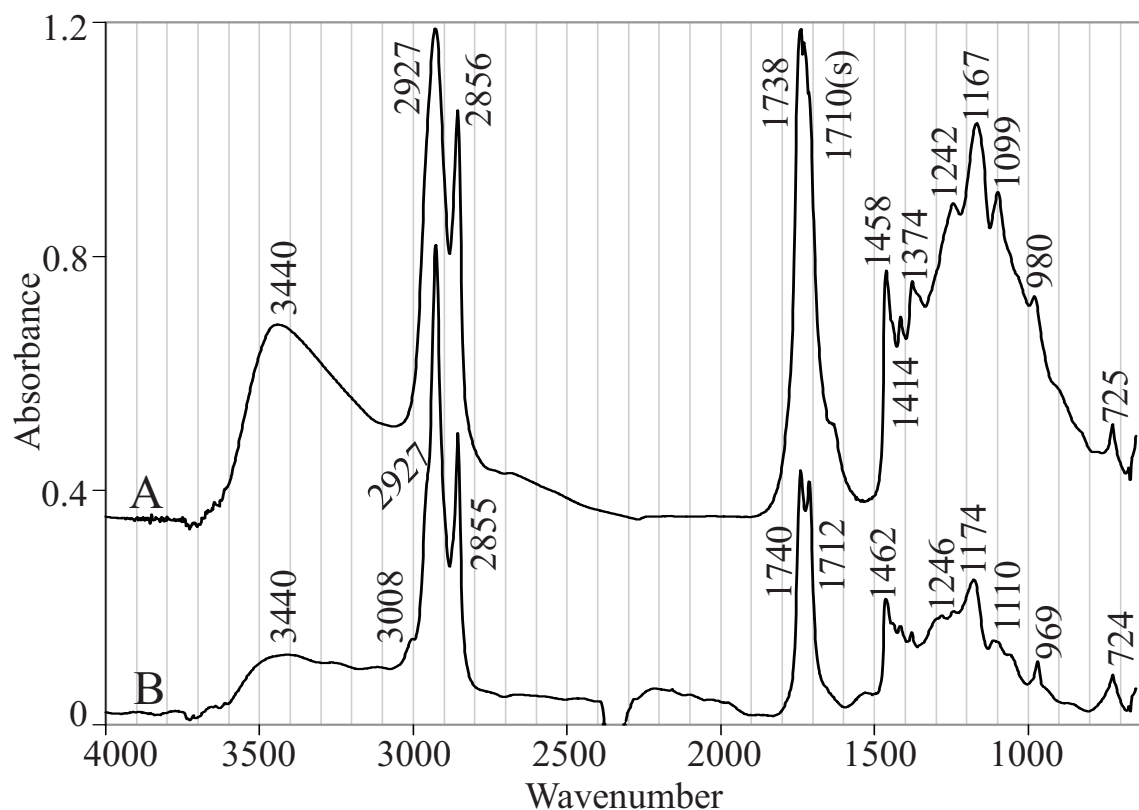
Fig. 5.4. *Infrared spectra of aged, unpigmented linseed oil. (**a**) 90 hours after application as a thin film; (**b**) 50 years after production. This oil has been kept in a closed container.*

stand oil, which was taken from the promotion material of a sales representative of a Dutch paint manufacturer. This oil has been kept in a closed container during most of its lifetime, and has only been prepared as a thin film until at the time of the infrared measurement. Therefore, the oxygen supply to this oil has been restricted, and a low amount of oxidation is expected. Absorption peaks of oxidation products are indeed small (OH at 3440 cm^{-1}, C–O background at 900–1400 cm^{-1}). The ester peak at 1740 cm^{-1} is accompanied by a distinct peak at 1712 cm^{-1}. These are assigned to fatty acids formed by hydrolysis of the glycerol esters, as the formation due to degradation, as shown in Fig. 5.1, is limited by the oxygen supply. Indications for this are the relatively low intensity of the ester band at 1740 cm^{-1} and the deformation of the ester triplet (~1246, 1174 and 1110 cm^{-1}). The peak at ~1712 cm^{-1} is also seen in library spectra of glycerol 1,2 distearate and glycerol 1,3 dilaurin (SDBS refs 34789 and 7719, Integrated Spectral Data Base System for Organic Compounds, www.aist.go.jp/RIODB/SDBS/menu-e.html). Similar molecules, i.e. diacylglycerols, can also be formed due to hydrolysis. However the presence of a fatty acid impurity in the samples measured for this database seems a more likely explanation for this absorption than an absorption by diacylglycerols.

An absorption at about 1710 cm^{-1} is also present in Fig. 5.4A and the spectrum provided by Meilunas *et al*. However, in these cases it is poorly resolved from the absorption at 1740 cm^{-1}, and is only visible as a shoulder. A similar loss of resolution is seen in the CH stretch vibration peaks, which seem much narrower in spectrum 4B. The broadening seems to be typical for

natural ageing, and the spectrum in Fig. 5.4A is therefore considered a good reference for the spectra of the pigmented films presented in the next section.

5.3.3 Infrared spectroscopy of naturally aged oil paints

Several naturally aged paints have been analysed. Their infrared spectra, as well as the second derivatives of these spectra are presented in Figs. 5.5–5.21 and discussed in the following sections.

5.3.3.1 Vermilion paint

The spectrum of a 30-year-old vermilion containing paint is shown in Fig. 5.5. The corresponding second derivative spectrum is displayed to the right of this spectrum. Vermilion does not absorb in the MIR (mid infrared) region, but causes extensive scattering. The intensity of the transmitted light therefore decreases with the wavelength. The corresponding slope in the baseline was removed by a baseline correction, but the low transmittance causes the low S/N (Signal-to-Noise ratio) on the left side of the spectrum. Vermilion does not seem to induce the formation of detectable amounts of products that are not present in unpigmented aged paint, as its spectrum closely resembles Fig. 5.4A. The carbonyl moieties lead to a broad absorption at 1734 cm^{-1} (1744 cm^{-1} in fresh oil, Fig. 5.2). Increasing of the spectral resolution by means of the second derivative spectrum reveals the presence of clearly distinct carbonyl peaks (1740, 1708, and a smaller absorption at 1781 cm^{-1}). The clear triplet of peaks at 1247, 1183 and 1102 cm^{-1} in the raw spectrum shows the presence of intact esters in the dried oil.

5.3.3.2 Cadmium red paint

The infrared spectrum of a 60-years-old cadmium red paint is presented in Fig. 5.6. CdS does not absorb infrared light, and the scattering is low, compared to vermilion. Therefore, the S/N on the left side of the spectrum is higher. Otherwise, the spectrum is very similar to that of vermilion paint. Even the carbonyl absorption pattern observed in the second derivative spectra (1782, 1739 and 1707 cm^{-1}) is very similar. Cadmium red is therefore concluded not to influence the drying paint to a large extent.

5.3.3.3 Iron oxide paint

The absorption spectrum of an iron oxide containing paint is displayed in Fig. 5.7. This spectrum, which is clearly different from the spectra of vermilion and cadmium red paint, as it shows a strong absorption at 1100 cm^{-1} as well as an absorption at the right side of the spectrum (< 700 cm^{-1}). These absorptions can be assigned to the pigment, as they are also found in pure iron oxide pigment used in this test panel. The absorption at 1177 cm^{-1} is not due to this pigment, and should be assigned to ester groups. The presence of esters is confirmed by the carbonyl absorption at 1738 cm^{-1} (second derivative). Carbonyl absorptions at 1708 and 1782 cm^{-1} (second derivative spectrum) have appeared in the spectrum. The intensity of the 1709 cm^{-1} peak is relatively high and results in the low wavenumber of the carbonyl absorption in the raw spectrum (1720 cm^{-1}). The absorptions at 3200–2500, 1414, and 921 cm^{-1} indicate that the 1709 cm^{-1} should be assigned to carboxylic acids. The abundant presence of carboxylic acids in this paint is confirmed by mass spectrometry.[19]
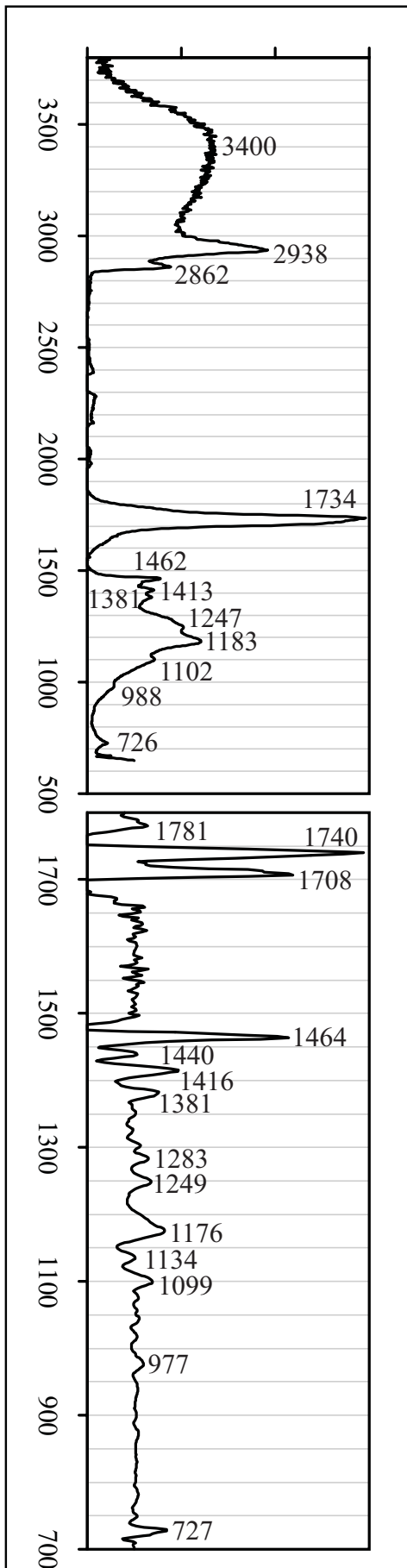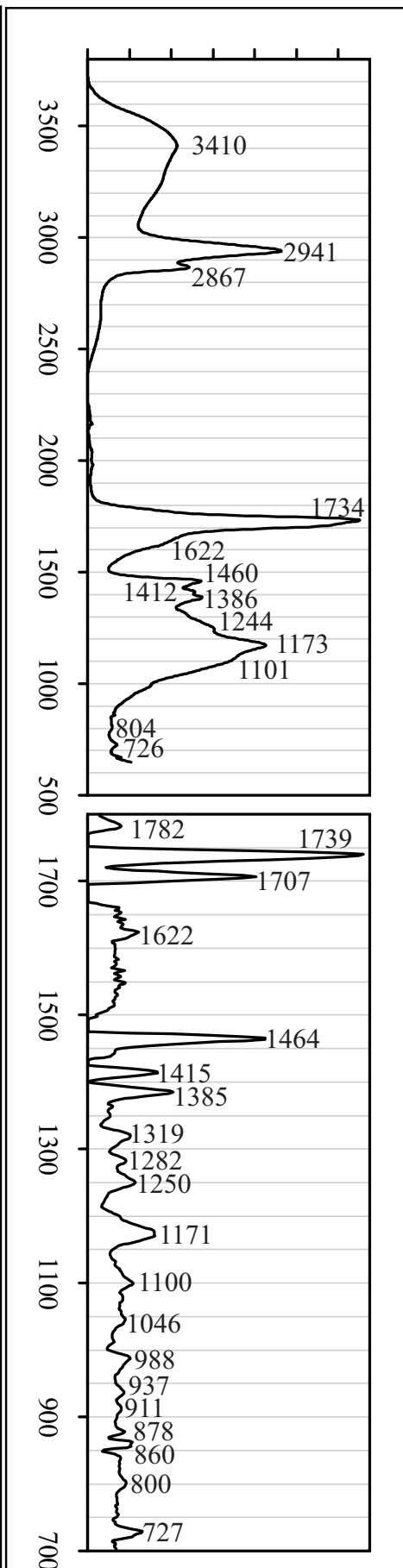
Fig. 5.5. *Vermilion*
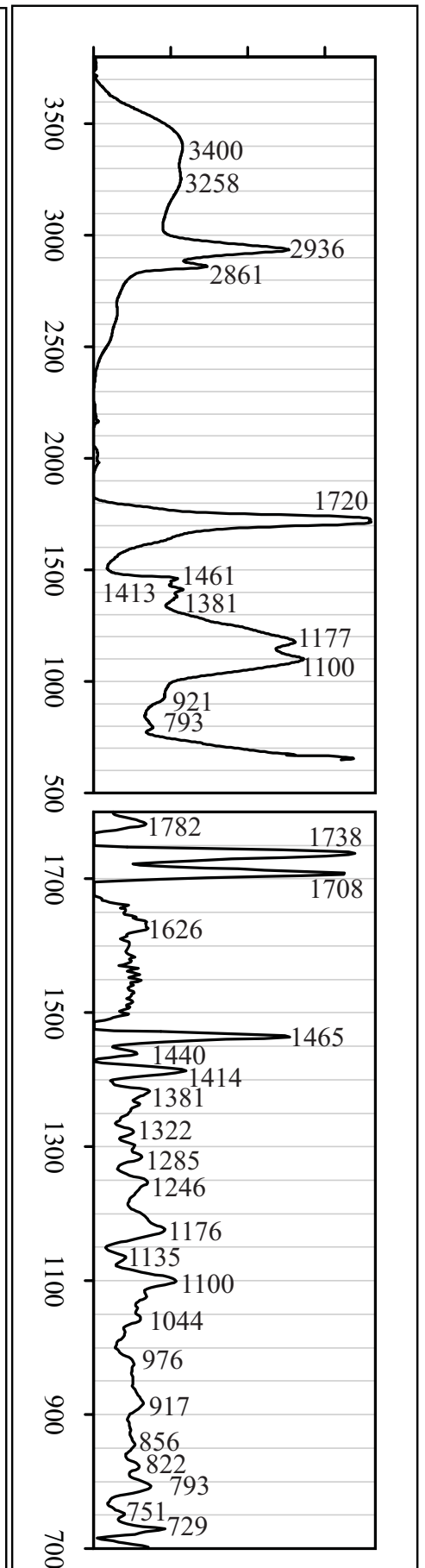

Fig. 5.6. *Cadmium Red*

Fig. 5.7. *Iron Oxide*

Fig. 5.5 - fig. 5.21. Infrared spectra of aged paints. The figures on the left show the normal infrared spectra. Their second order derivatives are partly (700-1800 cm⁻¹) shown in the figures on the right. The pigment used in the paint is mentioned in the Figures. An overview of the included pigments is provided in Table 5.1.

5.3.3.4 Minium (red lead) paint

The main features in the spectrum of the minium-containing paint in Fig. 5.8 are peaks at 1177/1117, 1090 (truncated in this figure) and 984 cm⁻¹. The peaks 1185, 1123 and 1072, and 984 (see second derivative) exactly coincide with the absorptions of $BaSO_4$ (SDBS-no.40201). The presence of Ba has been confirmed by EDX, but the source of $BaSO_4$ is not known. It can be due to an imperfect sampling of the red lead paint layer or a filler introduced with the pigment. The relatively strong peaks at 1526 and 1404 cm⁻¹ can be attributed to lead soaps.[106] The intensity of the carbonyl peak at 1741 cm⁻¹ is lower than the C─H stretch vibration at 2924 cm⁻¹, unlike the pigmented paints discussed so far. This suggests that the amount of carbonyl moieties is relatively low and accordingly that the presence of minium as a pigment increases the hydrolysis of the triglycerides. The second derivative spectrum shows the mere absence of carboxylic acids evidenced by the minute absorption at 1707 cm⁻¹. The absence of carboxylic acids is confirmed by the low intensities at ~3200–2600 cm⁻¹ (raw spectrum), and 1414 cm⁻¹.

5.3.3.5 Naples yellow paint

The infrared spectrum of an aged paint containing Naples yellow is presented in Fig. 5.9. This spectrum shows strong peaks at 1548 and 1413 cm⁻¹, which are not present in the pure pigment (spectrum of pure pigment has been reported before[139]). The peaks are assigned to metal carboxylates that were formed during ageing. The presence of intact ester bonds is clear from absorptions at 1740 cm⁻¹, and the glycerol ester triplet at 1251, 1178 and 1099 cm⁻¹. The second derivative spectrum shows that the carbonyl peak mainly consists of ester absorption at 1740 cm⁻¹ with only a small contribution of carboxylic acids at 1709 cm⁻¹. Both red lead and Naples yellow pigmented paints (Figs. 5.8 and 5.9) show that pigments that mediate the formation of metal carboxylates simultaneously reduce the number of carboxylic acids, which can readily be explained by the consumption of carboxylic acids during the formation of metal carboxylates.

5.3.3.6 Yellow ochre paint

The absorptions of ochre are highly dominating in the infrared spectrum of a 65-years-old yellow ochre paint. The most pronounced features (Fig. 5.10) are the intense truncated silicate absorptions at 1200–980 cm⁻¹, 918, 806, and 701 cm⁻¹. The presence of quartz in these samples has been confirmed by XRD (by I.N.M Wainwright, CCI). Crystal water in the pigment gives rise to the sharp peaks at 3695 and 3619 cm⁻¹ and might also contribute to the absorptions at about 1622 cm⁻¹. Finally, the characteristic absorption pattern between 2600 and 3500 cm⁻¹ is partly assigned to hydroxyl groups in or on the pigment particles, as the observed maximum (as low as 3114 cm⁻¹) is uncommon for organic materials. The aliphatic moieties in this sample lead to broad absorption bands at 2944, 2864, 1453, and 1382 cm⁻¹. The carbonyl absorptions (1724 cm⁻¹) are resolved by the second derivatisation in peaks at 1738 and 1705 cm⁻¹. Unfortunately, the ester triplet around 1170 cm⁻¹ is completely masked by the strong Si-O absorptions.
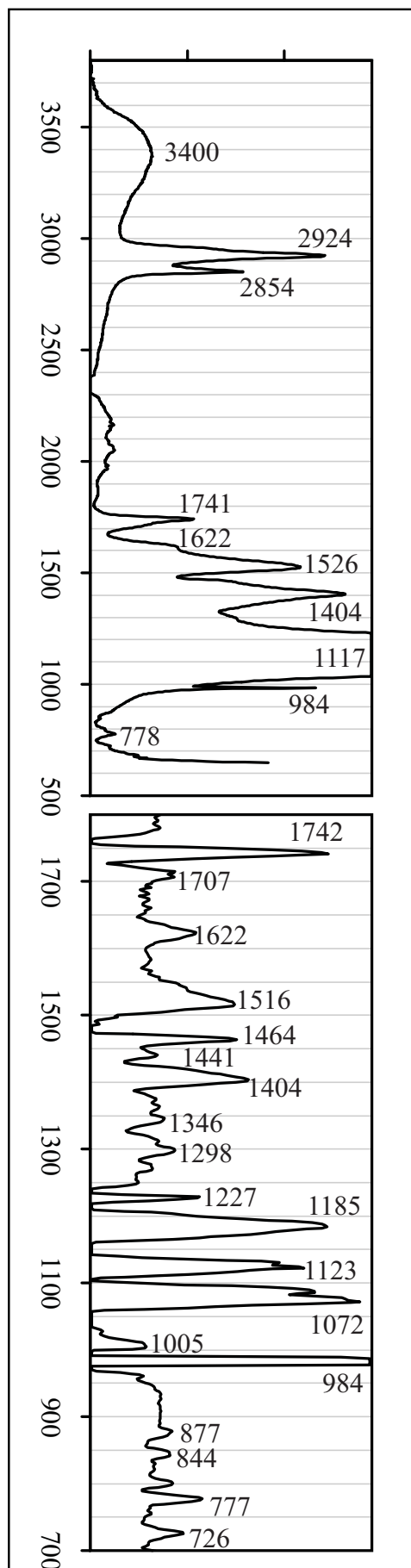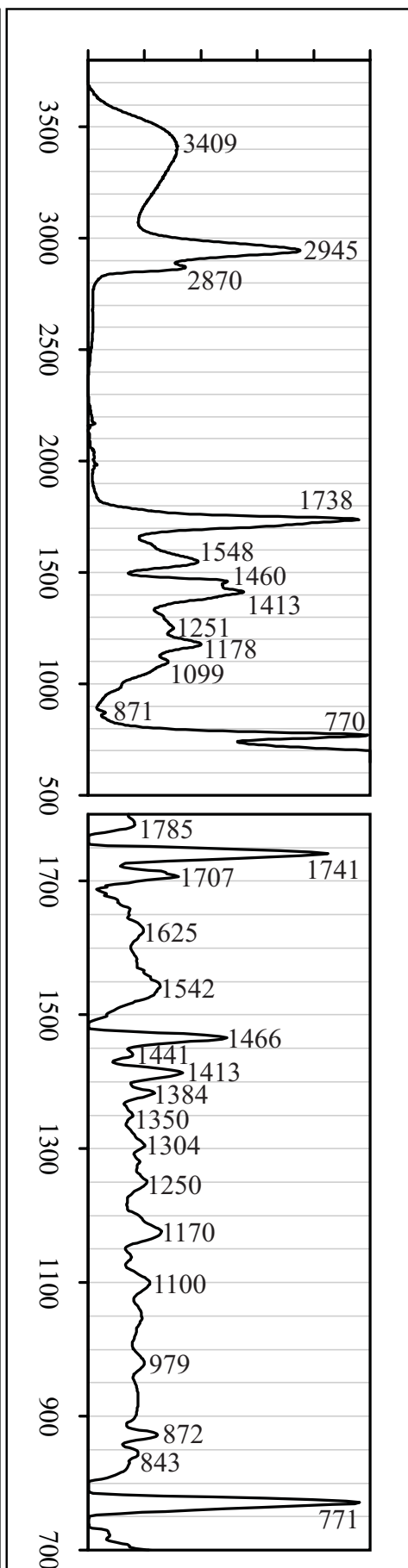
Fig. 5.8. *Red Lead*
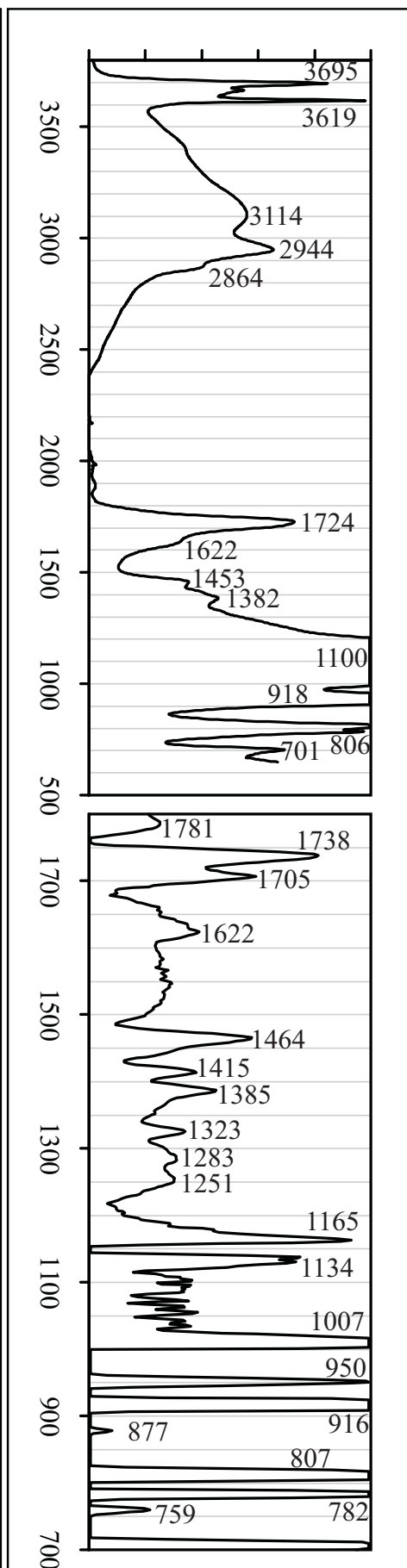
Fig. 5.9. *Naples Yellow*

Fig. 5.10. *Yellow Ochre*

5.3.3.7 Gold ochre paint

The spectrum of the aged linseed oil paint containing gold ochre (Fig. 5.11) is very similar to the spectrum obtained from the yellow ochre. The second derivative spectrum shows a higher relative intensity of the 1707 cm^{-1} carbonyl absorption. This subtle intensity change led to the significant shift of the carbonyl peak in the raw spectrum: from 1724 to 1710 cm^{-1}.

5.3.3.8 Green earth paint

The spectrum of green earth pigmented paint film is presented in Fig. 5.12. The green earth pigment used in the reconstructions was found to contain silicates (1039, 915, 801 cm^{-1}) with crystal water (3697, 3619 cm^{-1}), and calcium carbonate (2522, 1799 (small), 1416, 875 cm^{-1}). Green earth reference spectra[140] are clearly different from the pigments in the test panel. The definition of green earth is not unambiguous. The inorganic materials mask many of the organic features in the spectrum. The remaining organic features include aliphatic peaks at 2938 and 2867 cm^{-1} as well as 1464 cm^{-1} in the second derivative spectrum. The second order derivatisation again resolves the carbonyl band into distinct absorptions at 1779, 1738 and 1708 cm^{-1}. The absorption at 1624 cm^{-1} is well resolved from the carbonyl peak (1717 cm^{-1}), contrary to the spectra of the ochre-pigmented paints (Figs. 5.10–5.11). The assignment of this peak (1624 cm^{-1}) to crystal water (as suggested in the discussion of the ochre paints) is contradicted by this spectrum, as the amount of crystal water in this paint (3697 and 3619 cm^{-1}) is very low. A better assignment might be the presence of metal carboxylates. However, no further indications could be found to confirm this attribution.

5.3.3.9 Kassel earth (Van Dyke Brown) paint

The infrared spectrum (Fig. 5.13) represents an aged paint prepared with Kassel earth, a fossil of mainly organic subbituminous coal fossil,[141] regularly used as a brown pigment. The organic absorption at 1611 cm^{-1} is the most intense absorption in the infrared spectrum. This peak is caused by the pigment itself, and has been assigned tentatively to iron carboxylates.[142] Assignment to a carboxylate or metal carboxylate is confirmed by the presence of an almost equally intense and broad absorption at 1416 cm^{-1}, which can be assigned to the symmetric carboxylate stretch. The absorption at 1611 cm^{-1} has a very noisy appearance in the second derivative spectrum. However, the fine-structure (including peaks at 1626, 1567, 1587, 1608, and 1645 cm^{-1}) is reproducible: the same absorptions have been found in the Kassel earth pigmented paint taken from the Von Imhoff collection (results not shown). These various peaks should be assigned to different chemical surroundings of the carboxylates, but a detailed identification of these absorptions has not been established and is left for further research. Second derivative analysis of the broad absorption band at 1416 cm^{-1} also reveals a number of underlying absorptions, including those at 1383 (CH$_3$), 1464 (CH$_2$), and 1413 cm^{-1} (COOH). The presence of carboxylic acids is confirmed by absorptions at 915, 3200–2600, and at 1709 cm^{-1}. Especially this spectrum clearly illustrates the increment in information that can be derived after second derivatisation, as two broad peaks can reproducibly be resolved into a number of narrow absorptions.

Only a trace of inorganic materials can be observed as a relatively sharp peak at 1099 cm^{-1}. This peak is not part of the glycerol triplet, as its intensity is too high compared to the connected peaks (~1170 and 1240 cm^{-1}). Small amounts of glycerol-esters are however indicated by the

modest absorption at 1736 cm^{-1} (second derivative spectrum). The second derivative of the carbonyl peaks resolves the two absorptions (1736 and 1709 cm^{-1}), but the resolution is worse than in other cases observed so far. This might very well be due to the presence of carbonyl moieties in the Kassel earth pigment. Unfortunately, the presence of the several related functional groups in the oil and pigment fraction makes a detailed evaluation of the oil fraction impossible.

5.3.3.10 Ultramarine paint

The strongest absorption in the spectrum of artificial ultramarine pigmented paint (Fig. 5.14) is the truncated silicate absorption at 1001 cm^{-1} (SDBS, ref 3143). Other pigment absorptions are present at 714 and 680 cm^{-1}. The absorptions due to the binding medium are rather broad and featureless. In fact, the CH bend absorption (1466 cm^{-1}) can only be distinguished in the second derivative spectrum. The broad CH stretch absorptions have their maxima at 2945 and 2873 cm^{-1}, compared to 2926 and 2855 cm^{-1} for the fresh oil (see Fig. 5.2). The exact positions of these absorptions appear to be very unstable, and values of the naturally aged paints vary between 2924 (red lead in Fig. 5.8) and 2945 (ultramarine paint in Fig. 5.14). The shift to higher wavenumber normally seems to accompany a broader appearance of the peaks.[28] A broad shoulder is present at 1640 cm^{-1}. This peak again gives the impression of a metal carboxylate, as it is accompanied by a broad absorption at 1414 cm^{-1}.

5.3.3.11 Indigo paint

The indigo pigment in the 35-years-old paint is well preserved, as indicated by its intense blue colour. The many indigo absorptions are clearly present in spectrum 15 (3239, 3064, 1627, 1612, 1588, 1485, 1392, 1321, 1300, 1200, 1173, 1130, 1077, 1014, 882, 861, and 752 cm^{-1}). These peaks mask most of the binding medium peaks in the fingerprint region. In fact, only the carbonyl band (1728) and the CH stretch vibrations (2940 and 2865 cm^{-1}) can be assigned unambiguously.

Second order derivatisation does not improve the interpretation of the spectral data, as aromatic structures like indigo normally have many narrow absorption bands. These sharp peaks are prominently present in the second derivative spectrum. The well-resolved bands for esters (1737) and carboxylic acids (1707 cm^{-1}) are seen as minor features in this spectrum.

5.3.3.12 Zinc white paint

The spectrum of zinc white pigmented paint (Fig. 5.16) shows intense CH vibrational peaks at 2933 and 2858 cm^{-1}. The narrow carbonyl peak (1740 cm^{-1}) is lower than the CH stretch vibration at 2933 cm^{-1}, indicating that the amount of intact ester bonds is relatively low. The second derivative spectrum shows the absence of carboxylic acids by the negligible absorption at 1709 cm^{-1}. The clear and broad carboxylate absorption (1589 cm^{-1}) consists of several separate peaks (second derivative, 1620, 1586, 1540 cm^{-1}). The absorption peak at 1460−1418 cm^{-1} resolves into the CH bend vibration (1467 cm^{-1}) as well as peaks at 1415 and 1376 cm^{-1}. A minor addition of whiting ($CaCO_3$) to the zinc white is suggested by the combination of peaks at 1418, 876 and 778 cm^{-1} (second derivative). The 1150 cm^{-1} absorption indicates the abundant presence of alcohol groups in the oil. This peak is not due to a silicate or sulphate adulteration, as these moieties normally show a series of absorbances in this spectral region. Lead sulphate
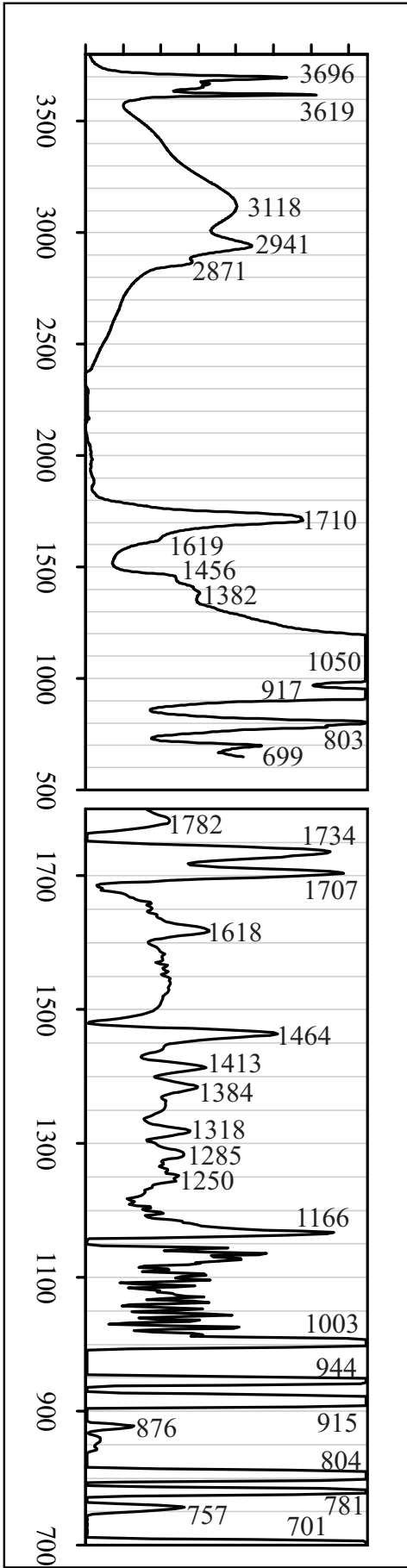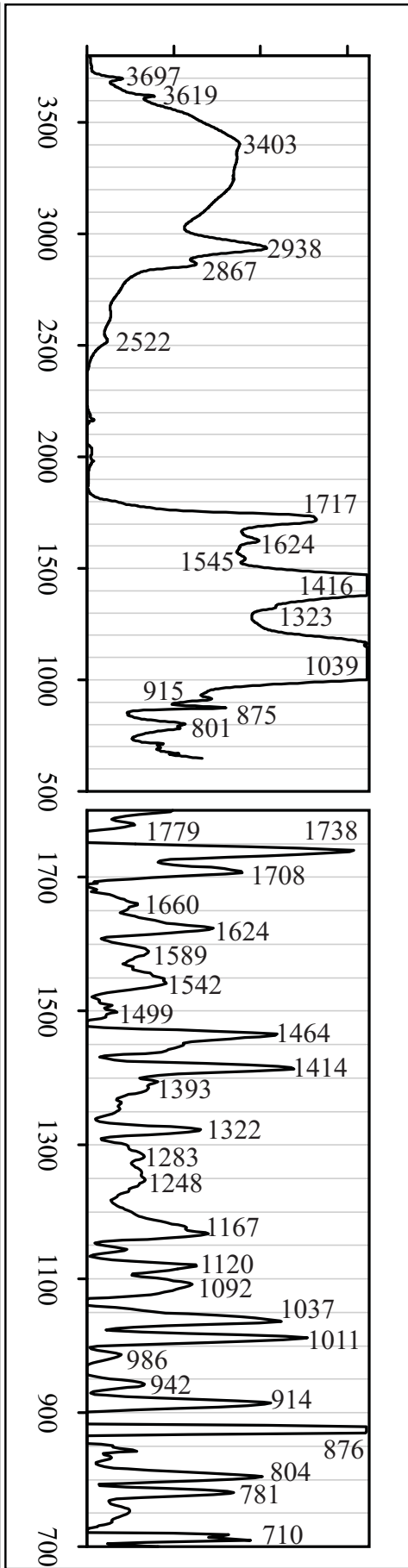
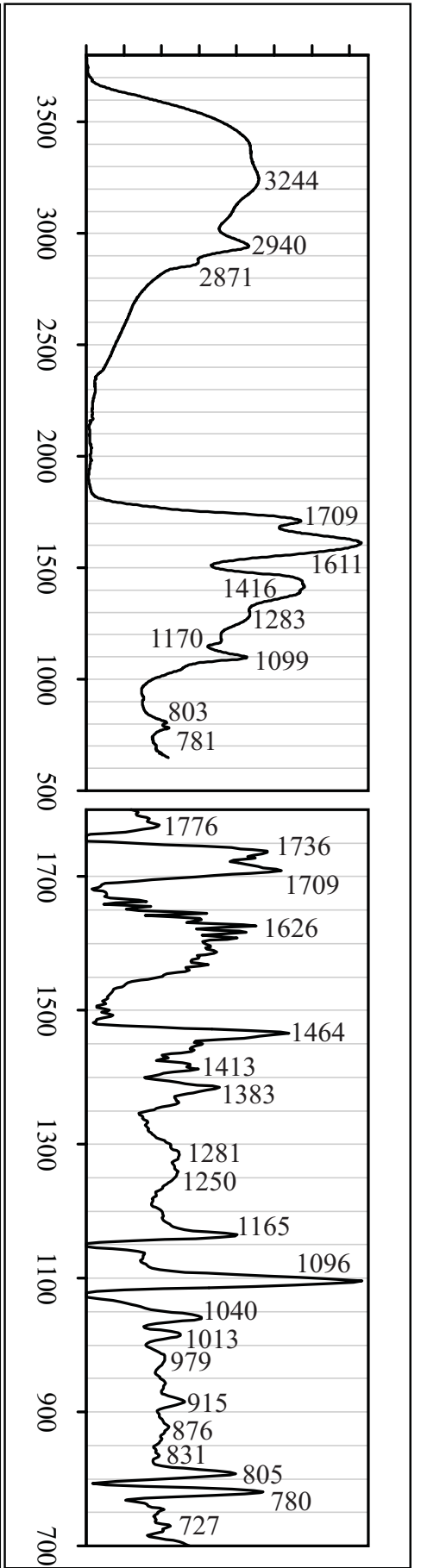*Fig. 5.11. Gold Ochre*
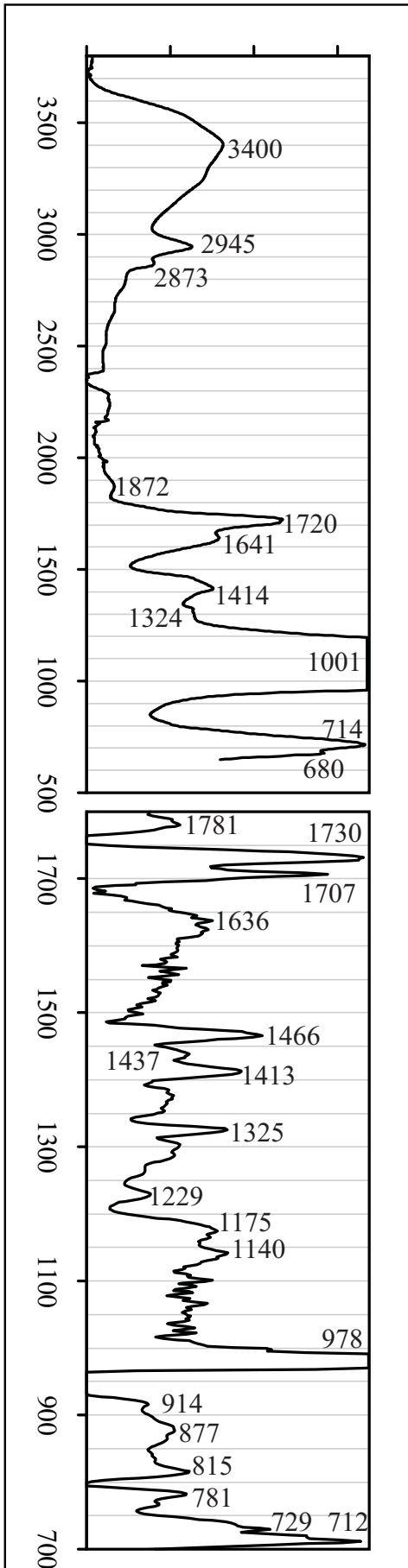

Fig. 5.12. Green Earth

Fig. 5.13. Kassel Earth

Fig. 5.14. *Ultramarine*
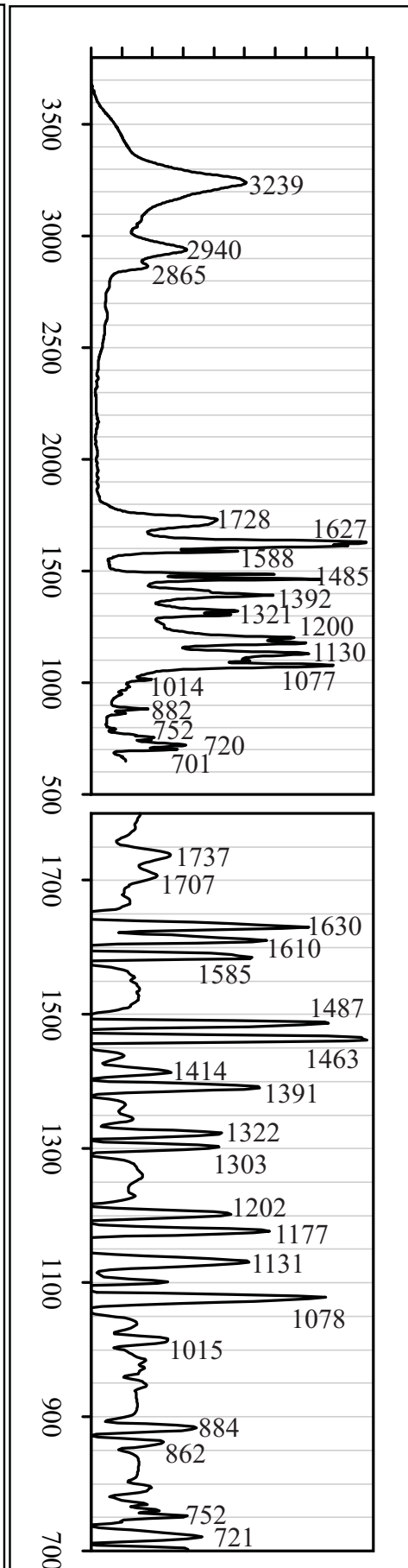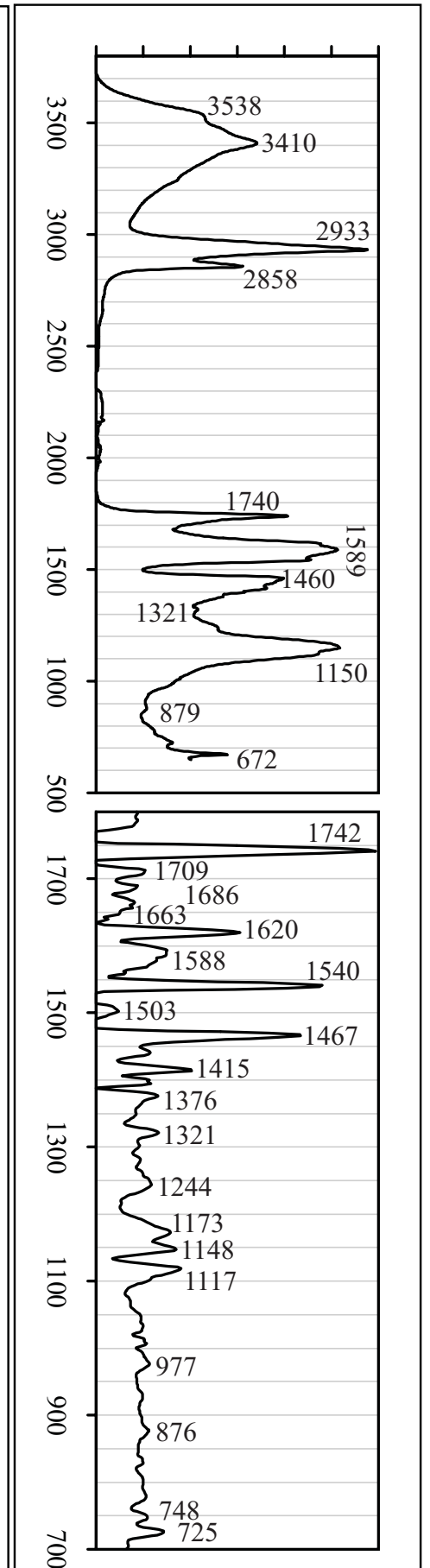

Fig. 5.15. *Indigo*

Fig. 5.16. *Zinc White*

impurities[143] would further have a different maximum absorption (1060 cm^{-1}). The assignment to alcohols is confirmed by the relatively strong absorption at 3410 cm^{-1}. The presented spectrum suggests that zinc white influences the ageing of oil in different ways: it stimulates the formation of alcohol groups, catalyses the hydrolysis of glycerol-esters, and forms metal carboxylates with the present carboxylic acids.

5.3.3.13 Lead white paint

Lead white is probably the most commonly used pigment in the history of panel painting. Therefore it has been included in many test panel series, e.g. the painting by Gettens, which has been analysed and reported by Meilunas *et al.*[37] The Doerner test series even contains several lead white paints, with a number of different lead white types, oils, and additions. The infrared spectrum of a paint prepared in 1912 is shown in Fig. 5.17. Spectra of other paints from this series, made in 1941, are shown in Figs. 5.18–5.20. The lead white paint from the CCI test series is shown in Fig. 5.21.

The most intense absorption in spectrum 5.17 is due to the carbonates present in the lead white pigment (truncated, 1300 to 1450 cm^{-1}). Less intense pigment absorptions are seen at 3539 cm^{-1} (OH stretch), 1048 cm^{-1}, 776 cm^{-1} and 681 cm^{-1}. The absorption at 838 cm^{-1} is due to neutral lead carbonate (PbCO$_3$), which is a common component of lead white.[117] The most intense organic features are present at 2933 and 2875 cm^{-1} (CH stretch) and 1740 cm^{-1} (carbonyl). The second derivative of the carbonyl region shows the presence ester moieties at 1740 cm^{-1}, but the almost complete absence of carboxylic acids. The ester C–O triplet (1169, 1248 and 1100 cm^{-1}) confirms the presence of esters. The shoulder on the short wavelength side of the intense carbonate band should be assigned to the absorption of lead carboxylates,[37] but it is masked by the adjacent very intense carbonate absorption. Nevertheless, spectral subtraction of a pure lead white spectrum revealed a clear absorption at 1540 cm^{-1} (results not shown). Second derivative analysis of the absorption spectrum of lead white paint (Fig. 5.17) reveals the presence of several small absorption maxima (1533, 1543, 1551, 1625 cm^{-1}). These peaks look like noise, but their relevance is indicated by their presence in the other lead white pigmented oil paints, see Figs. 5.18–5.21. The several peaks in this region are probably due to different co-ordination structures of the lead carboxylates, comparable to the situation observed for fine structure on top of the carboxylate absorption peak in the Kassel earth pigmented paint, be it that the exact spectral locations have altered. An even clearer fine pattern is seen in the region between 1365 and 1480 cm^{-1} with peaks at 1364, 1386, 1410, 1428, 1447, 1466 (CH bend), 1474, and 1481 cm^{-1}. All these small absorption peaks appear in the various lead white spectra that were investigated, which stresses their significance. The absorption at 1410 cm^{-1} has been assigned to carboxylic acids in the preceding part of this Chapter. However, this seems not valid here, as carboxylic acids should give rise to an absorption band at 1707 cm^{-1}, which is clearly not present. The same has been observed in the spectrum of the zinc white paint, but a valid alternative assignment for the 1415 cm^{-1} absorption has not yet been found.

A remarkable difference between the several lead white pigmented paint films is the different intensity observed for the OH stretch vibration at ~3535 cm^{-1}. The intensity of this absorption varies in intensity between strong (Figs. 5.17, 5.18, 5.21) and negligible (Fig. 5.19). The same intensity differences are found for the OH bend vibration (775–780 cm^{-1}). The absence of these peaks (3535 and 778 cm^{-1}) correlates with the presence of peaks at 838 and 2420 cm^{-1}, and leads
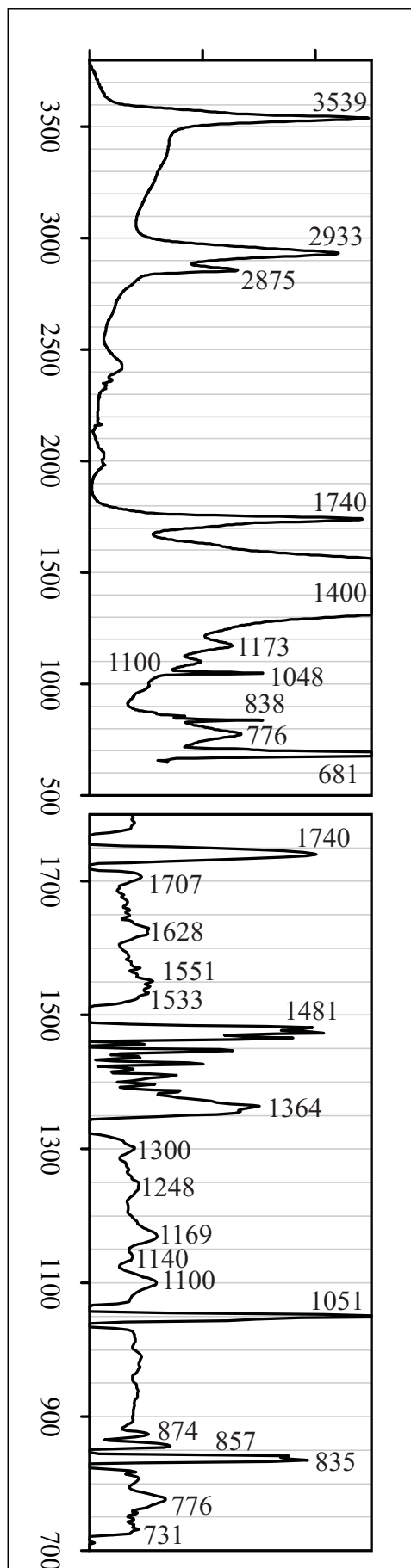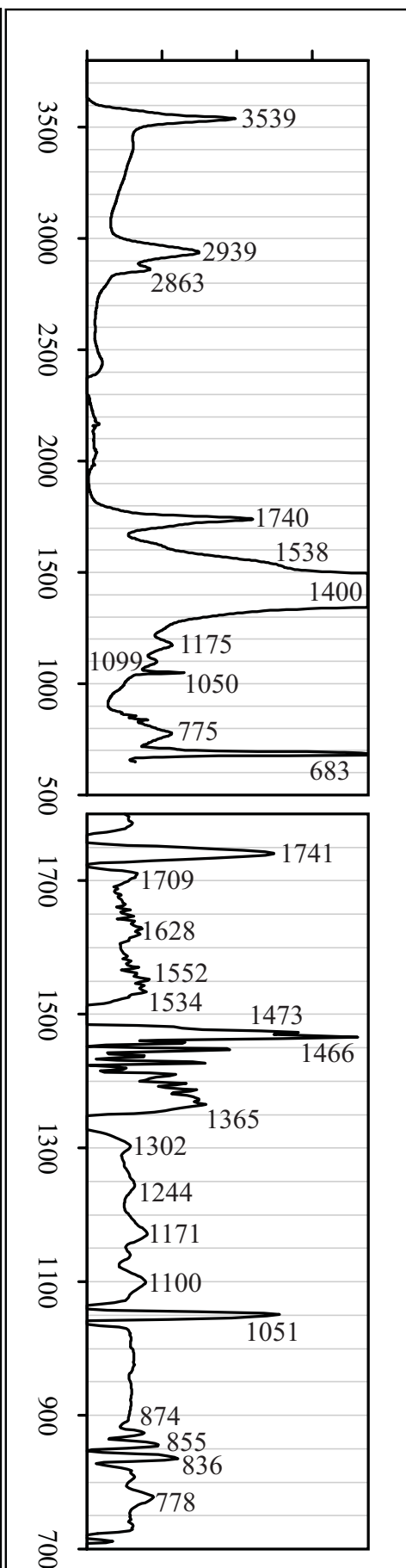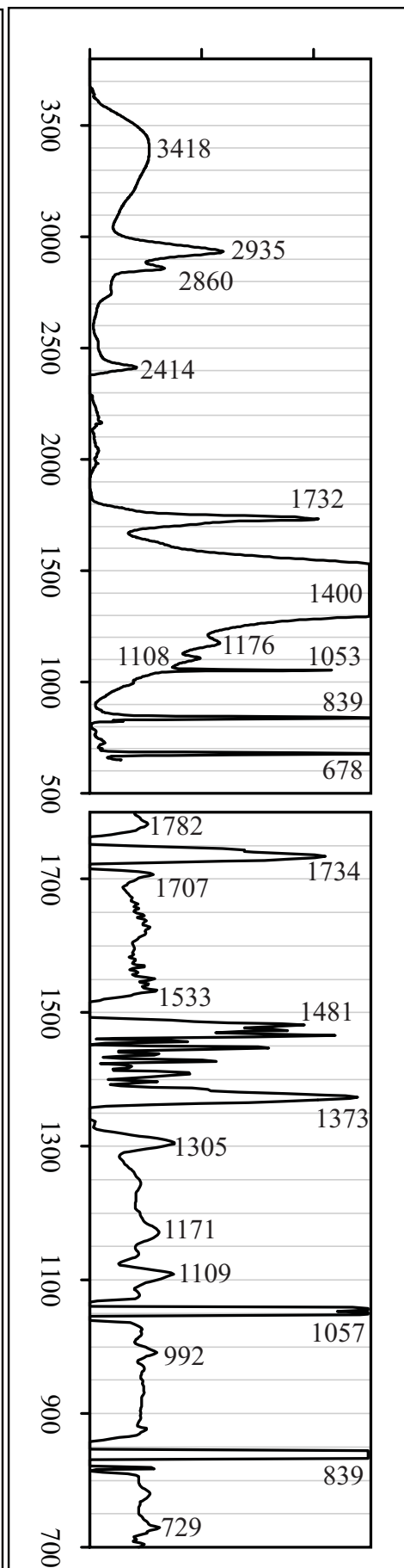
Fig. 5.17. *Lead White; D1*

Fig. 5.18. *Lead White; D4*
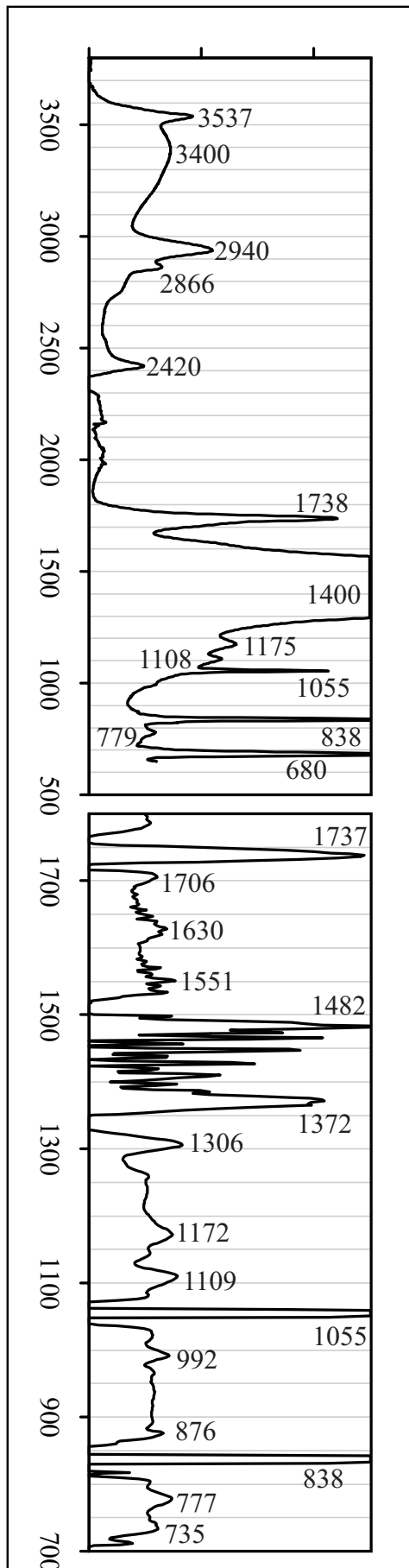
Fig. 5.19. *Lead White; D5*

Fig. 5.20. Lead White; D6
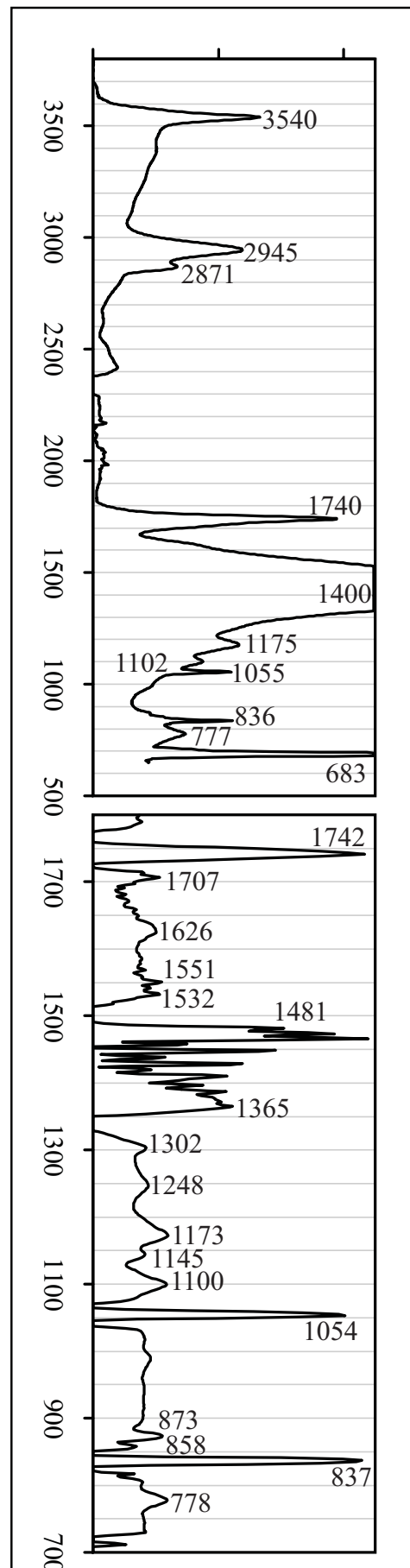
Fig. 5.21. Lead White; CCI
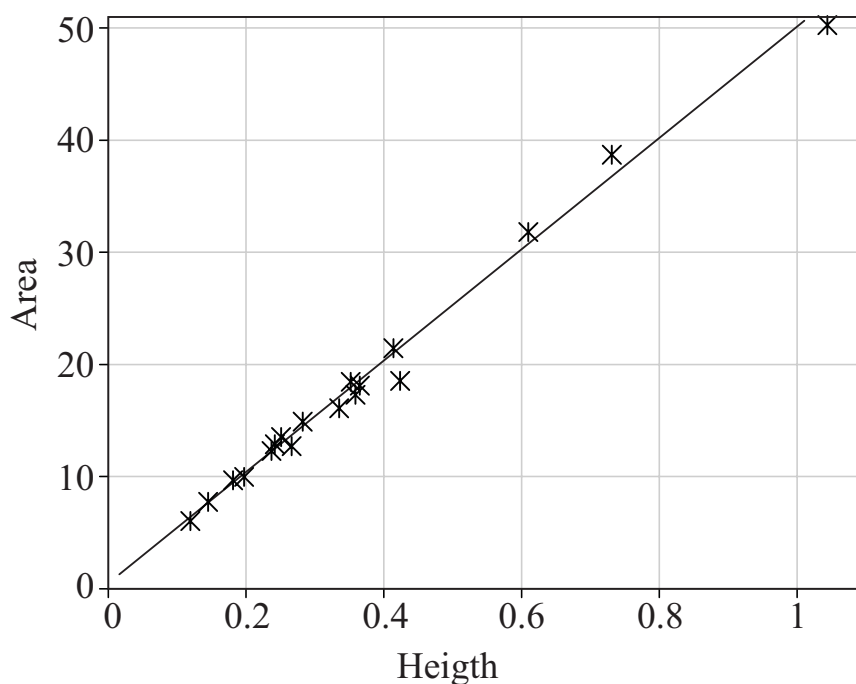
Fig. 5.22. *Comparison of the height and area of the CH-stretch vibration band at 2950–2920 cm⁻¹ in all spectra presented in Figs. 5.5–5.21. See experimental (section 5.2) for parameters.*

to a small shift in the intense lead white absorption around 680 cm⁻¹: from 681 to 678 cm⁻¹. These intensity changes and peak shift are explained by the content of neutral lead carbonate in lead white. Reference spectra ([117,144] and SDBS) show that basic lead carbonate absorbs at 3535, 778 and 681 cm⁻¹, while neutral lead carbonate, which is a normal constituent of lead white, absorbs at 2420, and 838 cm⁻¹. This indicates that the composition of lead white from different sources can be markedly different, which would be consistent with historic documentary sources.[2]

The differences between the spectra presented here and the results of the 50-years-old naturally aged lead white paint reported by Meilunas *et al*. are remarkable, especially when the stability of the spectra presented in Figs. 5.17–5.21 is considered. The most important difference is the relatively low carbonate absorption in the paint analysed by Meilunas *et al*., indicating that this paint has a much lower pigment concentration. It is indeed stated that the analysed paint had been made of a 1:1 mixture of lead white and oil. The lower amount of lead white resulted in a higher amount of oxidation products with absorptions at 3411 and 1715 cm⁻¹, as well as to an overall absorption increase in the spectral region between 1650 and 1000 cm⁻¹. A further difference is the better resolution of the peaks at 1622 and 1545 cm⁻¹. It is likely that these differences are caused by the pigment concentration in the paint.

5.4 Discussion

The large number of spectra that have been shown in this Chapter allow a classification of the different effects that pigments can have on the ageing processes in oil. A number of characteristics will be highlighted below. The broadening of the carbonyl band, which had been observed in a number of earlier studies, was shown to be due to the formation of a new carbonyl bands at 1705–1709 cm^{-1} and around 1780 cm^{-1}. The spectral location of this triplet appears to be very reproducible, but their relative intensities are dependent on the pigment present in the paint film. Another effect that can be assigned to the presence of pigments is the shift of the CH absorption bands around 3000 cm^{-1}. The most obvious effect observed in a number of paints is the formation of metal carboxylates.

5.4.1 Carbonyl bands

The carbonyl bands observed in the different spectra vary in peak width and position of the maximum absorption. Both Meilunas[37] and Hartshorn[31] have explained this by the formation of an extra, unresolved absorption peak at 1730–1700 cm^{-1} upon the drying of oil. Resolution enhancement through second derivative spectra indicates that both effects are caused by the formation of extra absorptions at 1707 and 1780 cm^{-1}. These peaks are well resolved in the second order derivative spectrum, even when no shoulders or fine structure can be seen in the raw spectra, e.g. in Figs. 5.10–5.15. Furthermore, the carbonyl peak is not hindered by masking due to absorptions of the common traditional pigments, which forms a major annoyance in traditional paint research by FTIR. Only one of the investigated pigments (Kassel earth) did disturb the analysis of the oil absorptions in the spectral region between 1700 and 1800 cm^{-1}. Therefore, this reproducible triplet may be very useful in the classification of binding media.

The absorption at 1740 cm^{-1} can be assigned to esters[103,106] that are still abundantly present in the fresh oil medium. This is confirmed by the presence of other ester peaks (1170, 1240, 1100 cm^{-1}) whenever these are not masked by pigment absorptions (Figs. 5.5–5.7, 5.9, 5.17–5.21). The intensity of this ester peak is variable, which must be related to the number of remaining ester bonds in the paint. However, a thorough quantification of the intensity would require an accurate determination of the layer thickness and the pigment content, and is not straightforward. A general impression of the intensity of the ester peak can be obtained by comparison with the asymmetric CH$_2$ stretch vibration at ~2930 cm^{-1}. The quantitative accuracy of this approach is however also questionable as the intensity of the CH stretch vibration might not be linearly related to on the amount of organic materials (see discussion below).

The 1707 cm^{-1} absorption has been assigned to the carboxylic acids, which are formed upon oxidation. This assignment seems to be confirmed by spectra (vermilion, cadmium red, iron oxide, yellow ochre, gold ochre), in which the 1707 cm^{-1} is accompanied by absorptions at 3200–2600, 1415 and 915 cm^{-1}.[106] The mere absence of the 1707 cm^{-1} peak in some of the metal soap producing pigments, (Naples yellow (Fig. 5.9), lead white (Figs. 5.17–5.21), zinc white (Fig. 5.16) and red lead (Fig. 5.8)), where the carboxylic acids obviously have reacted further to metal carboxylates, nicely confirms this assignment. No indications were found for the presence of other carbonyl groups that also absorb at ~1707 cm^{-1}. Further proof might be obtained by chemical derivatisation of aged paint material, e.g. using the method described by Mallegol.[28] If the absorption at 1707 cm^{-1} is to be assigned exclusively to carboxylic acids, it is remarkable

that is resolved from the ester absorption (1740 cm^{-1}) in only one of the spectra presented in the current study: the stand oil that has never been prepared as a paint. In all other cases, the two carbonyl peaks were not resolved in the normal infrared spectra. This suggests that the extensive changes that take place upon oil drying induces a broadening of the carbonyl peaks, obviously by the formation of several different chemical and physical environments for the carbonyl groups.

The rather small peak at 1780 cm^{-1}, which is observed in most of the presented second derivative infrared spectra, has been assigned to lactones or anhydrides. This absorption is thought to be specific for a drying oil.[37] A further carbonyl absorption at 1680 cm^{-1} is observed in the zinc white paint. This absorption has been assigned to conjugated carbonyl groups.[31]

5.4.2 Metal Carboxylates

Several complex spectral differences can be seen in the region between 1650 and 1500 cm^{-1}. Many of these can be explained by the presence of metal carboxylates. The absorption spectra of carboxylates containing long chain fatty acids and several metal ions have been accurately reported.[145] The reported value for zinc carboxylates is ~1540 cm^{-1} and a small peak at 1540 cm^{-1} is indeed found in the spectrum of zinc white paint (Fig. 5.16). However, the carboxylate absorption at 1590 cm^{-1} is much more intense. The values reported for long chain fatty acids may therefore not be correct for every type of zinc carboxylate. A number of selected reference spectra indeed illustrate that the nature of the carboxylic acid influences the spectral absorption characteristics of the metal carboxylate: Zn-stearate and palmitate (~1540 cm^{-1}),[145] Zn-lactate (1597 cm^{-1}), and Zn-oxalate (1631 cm^{-1}) (SDBS, refs. 3130, 12800 and 17155). A very interesting comparison for these absorptions is provided in the literature on ionomers, which are carboxylic acid containing polymers, normally formed by copolymerisation of ethylene and methacrylic acid. Ionomers can be neutralised by metal ions,[146] which form metal carboxylates with the carboxylic acids. Neutralisation of ionomer with lead acetate has been reported to result in infrared absorptions at 1560 cm^{-1}.[147] In another study, ionomers have been neutralised by zinc oxide, which induced infrared absorptions at 1624, 1585 and 1638 cm^{-1}. The relative intensities were found to be dependent on the amount of water absorption[146,148] and on the pressure applied to the sample.[149] Kutsumizu *et al.*[149] mention that the different absorption bands can be related to different co-ordination states of the carboxylic acids around the zinc atom, but a full assignment has unfortunately not been established yet. A better identification would not only lead to a better understanding of ionomers, but is expected to be directly applicable in aged paint, a system which is related to ionomers. This would lead to a better chemical classification of the variety of absorptions that are nowadays summarised as metal carboxylates.

5.4.3 CH stretch vibration

The intensity of the CH stretch vibrations is commonly seen as a quantitative measure of the oil content in a sample. The decreasing intensities of these peaks are interpreted accordingly as a decrease in aliphatic moieties due to the loss of volatile products. However, the amount of volatile products reported in the literature seems to be extremely high. Meilunas *et al.* mention a 60% intensity decrease of the CH stretch vibration. Rasti and Scott even report a 92% decrease of the absorption intensity at 2930 cm^{-1} (log $A_0/A_1 = 1.1$) for a vermilion pigmented paint film.[38] It seems unlikely that the loss of volatile aliphatic materials during ageing would be so extensive that it suffices to explain this effect. However, a better explanation has not yet been given. It has

been noted by Mallegol[28] that the decreasing intensity is combined with a shift of the absorptions maxima to shorter wavelengths. A shift of the CH vibrations has also been observed in the spectra reported here. The maximum absorption of ultramarine pigmented paint was found to be as high as 2945 and 2873 cm^{-1}, while the absorptions in the original oil binding medium are present at 2927 and 2855 cm^{-1}. Despite the relatively large shifts, the actual widths of the peaks remained remarkably constant, as the area of the absorption peaks changes linearly with the height (Fig. 5.22, see experimental for parameters, R=0.99). The varying intensity of the oil seriously complicates quantitative analysis of aged paint by FTIR. The absolute intensity of the CH-peaks cannot be compared objectively in the measurements reported here, as the exact amount of organic material in the light path is unknown. Furthermore, these oil components have a decreasing extinction coefficient due to hydrolysis (1740 cm^{-1}) and oxidation (2924 cm^{-1}). A valid quantitative analysis would probably require an inert internal standard.

These considerations make an assignment of the decreasing intensity to the loss of volatile material very unlikely. The direct influence of hydrolysis or metal carboxylate formation can also be ruled out. This was confirmed by measurements on ionomers, were the intensity of the CH stretch bands was found to be according to Lambert-Beer's law.[150] The origin of the hypsochromic shift of the oil medium during ageing should therefore be assigned to oxidation and possibly ring closure. These effects are known to occur in the ageing of oil,[109,129] but do not occur in ionomers. Ring closure and the resulting strain on the molecular structure are indeed known to increase the frequency of the absorption maximum of CH moieties.[103] The same is true for CH moieties close to an oxygen atom.[106] The origin of these effects is mainly located in the network fraction of the aged oil. A better understanding of these shifts may therefore become a valuable tool in the further characterisation of the polymeric fraction.

5.5   Conclusions

Several infrared spectra of traditionally prepared and naturally aged pigmented have been presented to investigate the long-term influence of the pigments on the oil medium. Reaction products of metals ions from pigments and the oil binding medium were found as metal carboxylates for a number of pigments. Other indications for reactions influenced by pigments were found in the aliphatic CH absorption at ~2930 cm^{-1} and the carbonyl absorption at ~1740 cm^{-1}. The hypsochromic shift of the CH vibration is assigned to oxidation and ring closure reactions in the network part of the oil. These shifts are especially pronounced in paints pigmented by ochres, Naples yellow and ultramarine.

The intensity of the ester peak at 1740 cm^{-1} can be greatly reduced by the presence of particular pigments, indicating hydrolysis of the triglycerides. This decreased intensity is especially clear for the zinc white and red lead paints, were the absorbance of the ester band is lower than the absorbance of the CH vibrations. Unfortunately, this relationship cannot be made fully quantitative, as the intensity of the CH vibrations is not a valid unit for the amount of oil material, as explained above.

Broadening and shifts of the carbonyl absorption have been observed in most of the aged paints. These effects are assigned to the formation of new, remarkably reproducible absorptions at 1707 ±2 cm^{-1} and 1780 ±5 cm^{-1}. The number of carboxylic acids, to which absorption at 1707

cm^{-1} is assigned, reduces upon the formation of metal carboxylates. This effect was observed for lead white, zinc white, red lead and Naples yellow. The characteristic carbonyl pattern is very useful in the investigation of oil paint, as it is normally not disturbed by any pigment absorptions.

5.6 Acknowledgements

6 CHEMICAL CHANGES IN OLD MASTER PAINTINGS: DISSOLUTION, METAL SOAP FORMATION, AND REMINERALISATION PROCESSES IN LEAD PIGMENTED PAINT LAYERS OF 17TH CENTURY PAINTINGS

A serious form of deterioration of lead pigmented paint layers was recently recognised in The Anatomy Lesson of Dr Nicolaes Tulp *by Rembrandt van Rijn (Mauritshuis inv. no. 146). Almost the entire surface of this painting shows small crater-like holes with a diameter of about 100 microns. Many of these holes are filled with whitish material that is sometimes seen to protrude. These 'protrusions' and related craters are a result of chemical changes in the composition of the underlying ground layer leading to mechanical expansion and protrusion of the newly formed substances. The phenomenon is not unique for this painting but is much more widespread. Several paintings showing the same phenomenon have been identified in the collection of the Mauritshuis. This paper focuses on a presentation of the phenomenon, by means of imaging microspectroscopic and chemical microscopic data of 'protrusions' in paintings by Albert Cuyp (*Girl with the Peaches; *MH inv. no. 829), Frans Hals (*Portrait of a Man; *MH inv. no. 982), Daniël Seghers (*Garland of flowers around an image of the Madonna; *MH inv. no. 256) and Johannes Vermeer (*Diana and her companions; *MH inv. no. 406). Presentation of macro photographs and cross-sections will be published in a companion paper by Noble, Wadum and Boon.*

In cross-section, the protrusions are seen as irregularly shaped areas consisting of whitish opaque and more transparent parts. Under UV illumination, the mass fluoresces strongly, while the transparent parts show a higher fluorescence. Finely divided, layered materials (seen especially with the Scanning Electron Microscope) suggest that precipitation of newly formed compounds has taken place. In most cases small red particles are present in or around the protrusion. Microspectroscopy of the particles identifies these particles as minium (Pb_3O_4), while SEM-EDX confirms the lead.

A general characteristic is the stunning difference in granulometry between the paint layer and the protruding mass. The original mineral matter of the paint seems to have disappeared - as if dissolved - leaving a transparent gel-like mass behind. Imaging FTIR of these 'gels' shows strong absorption in the 1510 cm^{-1} region, which is due to asymmetric vibrations of the COO^-

groups in metal carboxylates (soaps). Absorption in the 2925 cm⁻¹ region, due to CH vibrations of the fatty acid carbon chains, points to a high density of oil network derived organic substances. SEM-EDX studies demonstrate a high abundance of lead in these areas. Imaging secondary ion mass spectrometry (SIMS) in positive and negative ion mode demonstrates high concentrations of fatty acids, lead, lead-palmitate, and lead-stearate in the protruding gels.

The protrusions in the different paintings show different degrees of remineralisation. In the case of the Rembrandt painting, lead hydroxychlorides were identified, which raises questions about the source of the chloride. Lead carbonate, lead hydroxycarbonate and minium are also present as precipitates. The latter compounds were also found in the protrusions in the investigated paintings by Vermeer, Cuyp, Hals and Seghers. The most complex protrusion was discovered in a lead white/lead-tin yellow paint layer from Vermeer's Diana and her companions.

The causes for the protrusion phenomenon and the driving forces are presently unknown. Poor quality batches of lead white may be the cause for an imbalance in the paint chemistry. This might also explain the erratic occurrence of the phenomenon. We further suspect that moisture plays a crucial role in the formation of protrusions. Variable relative humidities conditions during the lifetime of the painting or introduction of water during restoration treatments may have been enough to trip a delicate balance. The precipitation of minium in the protrusions points to extremely high pH values in the paint layer in question, well beyond the thermodynamic stability of lead white.

6.1 Introduction

Small crater-like holes present in the entire surface of *The Anatomy Lesson of Dr Nicolaes Tulp,* painted by Rembrandt van Rijn in 1632, have been the subject of renewed microscopic and spectroscopic investigations. An early hypothesis of their origin proposed that the 'craters' were formed as a result of exposure to a fire in 1723, where the heat caused organic particles to migrate in the not yet completely dry paint. The microscopic studies by Noble *et al.*[151] point to chemical changes perhaps unrelated to fire damage. In cross-sections, the 'craters' appear related to changes in the composition of the underlying ground/paint layer leading to mechanical expansion and protrusion of the newly formed substances. The present study is part of an extensive survey of such phenomena in 17th century paintings performed by Noble and Wadum.[152] The focus of this paper is the determination of the infrared spectroscopic properties of the paint samples using an innovative FTIR-imaging technique. This information is correlated with imaging data from Scanning Electron Microscopy (SEM), imaging secondary ion mass spectrometry (SIMS) and visible and fluorescence microscopy. The optical examination of the pictures and their cross-sections are presented in the paper by Noble *et al.*[152] It is concluded from these studies that the protrusion phenomenon is not unique to the Rembrandt paintings but is also present in other paintings from various artists.

The protrusion phenomenon appears more pronounced in the thinly painted areas. On the surface of the painting the holes are completely round and uniform in size and shape, although due to abrasion some have a flatter profile and a more irregular contour. Some are filled with darkened material (often varnish residues), but in most cases a whitish substance protrudes. This phenomenon originates in an underlying ground/paint layer, from which a whitish mass is extruded that protrudes through the paint layers. In most of the cross-sections described by Noble *et al.*, the protrusions are irregularly shaped areas consisting of whitish opaque and more transparent parts situated in the granular matrix of the ground/paint layer. Under UV illumination, the transparent parts show a higher fluorescence compared to the opaque parts. In many cases, the protrusions contain a horizontally layered structure that suggests the precipitation of newly formed compounds. Lead white is present in the paint around the protrusions in every case. Small red particles are present in or around most of the protrusions are identified as lead oxides. Earlier FTIR-imaging and SIMS studies of *The Anatomy Lesson of Dr Nicolaes Tulp* have shown that the protruding mass consists largely of lead carboxylates of fatty acids and drying oil derived network molecules. It has been proposed that these substances are formed from an oil-rich paint or ground layer by 'dissolution' of the lead white mineral phase leaving an organically rich residue of highly oxidised drying oil components charge balanced by lead ions.[119]

Since the discovery of protrusions in *The Anatomy Lesson of Dr Nicolaes Tulp*, other examples of protrusions have been found in other paintings. Koller and Burmester,[153] Wallert[154] and White[155] all mention phenomena that resemble the protrusions found in *The Anatomy Lesson of Dr Nicolaes Tulp.* Brunnenkant[156] compared a small number of paintings having a red ground layer and found that protrusions only were present where minium (lead tetroxide) was found in the ground layer. Unn Plahter and Simonsen Plahter[157] recently revised their earlier interpretation of a gellified lumps in a cross-section of a painting by Teodoer van Baburen when new analyses pointed to the presence of lead carboxylates and minium.

Unpublished reports by the Canadian Conservation Institute (CCI) were made available that describe similar phenomena in 19th century paintings by Charles Eastlake and W. Harris.[158,159] The analytical data indicates the presence of lead soaps of palmitate, stearate, azelate and related di-acids.

The underlying study re-examines data on *The Anatomy Lesson of Dr Nicolaes Tulp* by R. van Rijn and presents new data on paintings by Cuyp, Hals, Seghers/Bosschaert and Vermeer.

6.1.1 Advanced imaging methodology

Each imaging technique has its own analytical window and spatial resolution. It is therefore of vital importance to be aware of the inherent possibilities and restrictions of each technique when data of different analytical techniques are compared. An explanation of all techniques used in this investigation is given below.

Reflection visual light microscopy reveals the stratigraphic structure, colour, and granulometry of layers in a paint cross-section with a resolution of about 1 μm. Specific layers or chemical substances in the cross-section can be highlighted by illumination with ultraviolet light and observation of the fluorescence in the visible spectrum. We developed a visible light spectrometer as an attachment to the visual light microscope that can record spectra of transmitted or reflected light with a spatial resolution of about 1 μm. An extensive explanation of the working principle of this microscopic VIS spectrometer is given in Chapter 2 of this Thesis. Visible light microscopy and spectroscopy does not provide detailed chemical information. Infrared spectroscopy on the other hand reveals chemical information on functional groups, e.g. −OH, −CH, −COC−, −C=O, −COOH, −CN. It is therefore particularly useful for the identification of organic components in paint.[37,89] Complete identification of molecules is not possible, although the chemical class of the observed compounds can normally be derived from the specific functional group absorptions. Apart from organic compounds, some inorganic groups, e.g. $-CO_3$ (carbonate) and SiO_4 (silicate) groups that absorb infrared light can be identified.

The scope of FTIR microscopy for the analysis of painting materials has been reviewed by Derrick.[43] Reflection FTIR microscopy of cross-sections presents many complications because specular reflection and diffuse reflection of the infrared light produce a mixed spectral signature of the painting materials, which is very difficult to interpret chemically. Selection of the sample spot takes place in normal visible light. The analysis is therefore a spot analysis. FTIR-imaging is a new technique that provides infrared spectra with a spatial resolution of about 6 μm from an area of about 400 by 400 μm.[66] This makes it possible to examine the spatial distribution of chemical functionalities without any prior assumptions about specific features in the cross-section.

Other kinds of chemical microscopy used in this paper are Time Of Flight-Secondary Ion Mass Spectrometry (TOF-SIMS) and Scanning Electron Microscopy (SEM) combined with Energy Disperse X-ray detection (EDX). SEM provides very high-resolution images (better than 0.01 μm). Normally, heavy atoms give a high electron emission intensity in the SEM image, while the lighter atoms result in a lower or no intensity. This is very useful in the investigation of paint cross-sections, because the pigments, usually rich in heavy atoms, can be seen with a very high resolution and contrast in the paint matrix that contains mainly low atomic weight atoms. Energy Disperse X-ray detection (EDX) is used as an attachment to the SEM and gives elemen-

tal analytical data of a spot. This technique is also more sensitive to the heavier elements. EDX is very useful in the identification of pigments. X-Ray diffraction (XRD) is used for a precise determination of molecular structure, but is only sensitive to crystalline materials.

Secondary Ion Mass Spectrometry measures the mass spectrum of a sample after desorption and ionisation of atoms and molecules with an ion beam. The sensitivity of this technique is determined by the desorption and ionisation efficiency of the sample and therefore dependent on the composition of the materials. A spatial resolution of 0.1 µm is achieved in the analysis of a cross-section reported here.

6.2 Methods and techniques

6.2.1 Sampling and embedding

Opalescent material was isolated from protrusions in Rembrandt's *Anatomy Lesson of Dr Nicolaes Tulp* (sample 39) and *Garland of Flowers around an image of the Madonna* by D. Seghers and W. Bosschaert (sample 5). The whitish material in the protrusions was removed using a scalpel. A description of sampling procedures and the position of the other paint-samples investigated is given by Noble *et al.*[152] Samples were embedded in polyester resin *Polypol* using the Easysection™ system. After an initial grinding and polishing using silicone carbide paper, the surface was dry polished using Micromesh™ cloths (final step 12 000 mesh).

6.2.2 Microscopy

Microscopic studies on cross-sections were performed on a Leica DMR microscope (Leica, Wetzlar, Germany). Normal light was provided by a 100W Halogen projection lamp. An Osram HBO 50 lamp and Leica filter D (excitation 360–425 nm, emission > 460 nm) were used for fluorescence microscopy.

6.2.3 FTIR Imaging

FTIR-imaging results were obtained using the Bio-Rad Stingray (Bio-Rad, Cambridge, USA). This system consists of a step scan interferometer (Bio-Rad FTS 6000), an infrared microscope (Bio-Rad UMA 500) and a 64×64 pixel Mercury Cadmium Telluride (MCT) focal plane array camera (Santa Barbara Focal Plane, California, USA). A detailed description of this system is given by Lewis.[66] The measurements on cross-sections were done in reflected light mode, using a ZnSe disc as a background. Transmission spectra were recorded using a Graseby Specac P/N 2550 diamond cell (Graseby Specac, Orpington Kent, UK), using the empty diamond cell as a background.

All measurements were recorded with a resolution of 16 cm^{-1} and an undersampling ratio of 4. Win-IR Pro 2.5 software (Bio-Rad) triggers both the interferometer and the WinIR 2.1 image acquisition software. The described measurements result in a data cube consisting of 4096 interferograms. Further data processing such as Fourier transformation and background correction is done using Bio-Rad Win-IR Pro software. The reflection measurements were corrected by the Kramers-Kronig transformation.

Analytical results of the FTIR-imaging system are displayed as infrared spectra and false colour images. A reflection infrared spectrum is representative for one spot (one pixel) selected

on the surface. A false colour plots show the intensity distribution of a particular infrared band on the surface. The wavenumber of that spectral band is indicated in each plot.

6.2.4 SEM-EDX

SEM-EDX measurements were performed to identify heavy elements present in pigments, dryers or other compounds. These measurements were carried out on a JEOL JSM 5900 LV scanning electron microscope scanning with a 25 kV electron beam. Samples were coated with a thin carbon coating to improve the conductivity of the sample and so prevent the accumulation of charge. EDX analyses were performed at various points throughout the cross-section by measuring the emitted X-rays with a Noran Vantage EDS-system with Pioneer Norvar detector.

6.2.5 TOF-SIMS

Time of Flight- Secondary Ion Mass Spectrometry (TOF-SIMS) measurements were performed on a TRIFT II instrument of PHI Electronics Inc. (USA).[160] The surface of the sample was scanned with a 25 keV primary ion beam from an Indium liquid metal ion gun. Positive or negative ions emitted by the primary beam were mass analysed and detected on a position sensitive detector. The surface of the sample was charge compensated with electron pulsed in between the primary ion beam pulses. A surface coating to improve conduction is not necessary.

6.2.6 Visible light imaging microspectroscopy

Visible light spectroscopic imaging studies were performed on a Leica DMRX microscope (Leica Inc., Wetzlar, Germany), equipped with a Specim Imspector V7 imaging spectrograph (Specim Inc., Oulu, Finland) and a Princeton MicroMax CCD camera (Princeton Instruments Inc., Trenton, USA). The sample movement during measurement was controlled by a DynaOptic Motion CTC-512-1 Single Axis Translation Stage (DynaOptic Motion Inc., Laguna Hills, USA). Data recording routines controlling the translation stage and the CCD camera were written in Visual basic 6.0 (Microsoft). Data processing procedures were written in Matlab 5.3 (The Mathworks Inc.). This spatially resolved spectroscopic imaging system is sensitive in the visible region (400–720 nm). It has a spectral resolution better than 5 nm and a maximum spatial resolution of about 1 μm in the current set-up.

A 50x magnifying objective was used for the experiments reported. Shutter time of the CCD camera was 18 ms, while 500 accumulations were made for every image. Spectra are corrected for dark current and background corrected using a white Teflon surface. Spectra of the orange particles were automatically selected by subtracting the images obtained at 580 and 541 nm. Pure litharge was obtained from Aldrich (Lead(II) oxide, 99.9999%), while the minium reference was taken from the Von Imhoff collection (code no. S892).

6.3 Results

6.3.1 Rembrandt's 'The Anatomy Lesson of Dr Nicolaes Tulp'

Fig. 6.1 summarises the investigations on cross-section 146/1, taken from the background in Rembrandt's *The Anatomy Lesson of Dr Nicolaes Tulp*. All plots in this figure present data on the opalescent protrusion in the same cross-section. Figs. 6.1a-c present the results of electron, visible and fluorescence microscopy; Figs. 6.1d-g display the microscopy FTIR images. Fig. 6.1h is a reflectance infrared spectrum and Figs. 6.1i-l display elemental and chemical compound maps as obtained by imaging SIMS.

Visual light microscopy (Fig. 6.1b) shows a semi-transparent, non-particulate protrusion with a diameter of about 100 µm in an opaque, light grey ground layer and a dark paint layer. The protrusion is not homogeneous, as the outer parts seem to be more transparent than the core. Under UV illumination (Fig. 6.1c) this inhomogeneity is more apparent as the transparent parts show a stronger fluorescence. On the left side of the protrusion, two small orange particles are present (see arrows in Fig. 6.1b). These red areas are not visible as discrete particles in the SEM image, but EDX showed the presence of lead in these areas.

The reflection FTIR image in Fig. 6.1d outlines the embedding material as a yellow red area due to the high carbonyl absorption of the embedding resin at 1724 cm^{-1}. The carbonyl absorption in the sample itself is low, as indicated by the blue colour of the sample in this image. Smearing of embedding medium over the sample has thus been avoided. From this image, the outline of the sample is clear which facilitates comparison with the microscopic images in Figs. 6.1a-c. Dashed white lines outline the perimeter of the protrusion.

Red high absorption regions in Figs. 6.1e and 6.1f are located within the perimeter of the protrusion. The FTIR spectrum of a point (marked * in Fig.6.1e) inside the protrusion (Fig. 6.1h) shows absorption peaks after Kramers-Kronig transformation at 2925, 1510 and 1406 cm^{-1}. Absorption at 1510 cm^{-1} (map in Fig. 6.1e) is due to asymmetric vibrations of the COO-group in metal carboxylates.[106] These metal carboxylates are carbon acid functionalities most likely from oil derived fatty acids and di-acids, in which the acidic proton is replaced by a metal ion. The metal in the carboxylates in this protrusion must be lead, as lead is the only metal found in SEM-EDX measurements. Absorption at 2925 cm^{-1} is due to CH vibrations of the fatty acids carbon chains, and is primarily observed inside the protrusion (Fig. 6.1f). The amount of aliphatic moieties in the protrusion is clearly higher than in the intact ground and the paint layer. Close comparison of images 1e and 1f shows that the highlighted area in the image at 1510 cm^{-1} is larger than in the image at 2925 cm^{-1}. The outer parts of the protrusion have lower CH bond absorption than the core. We infer that this implies that differences exist in the relative concentration of the metal carboxylate moieties and the aliphatic moieties within protrusions.

The peak seen at 1406 cm^{-1} in Fig. 6.1h is an overlay of a symmetric CO_2 stretch from metal carboxylates and a C−O stretch vibration from carbonates. The image of the 1406 cm^{-1} peak in Fig. 6.1f mainly shows the intact ground layer, where many carbonates are present as chalk ($CaCO_3$) or lead white ($PbCO_3 \cdot Pb(OH)_2$). The peak position at 1406 cm^{-1} in transmission FTIR indicates the presence of lead white.[117] An absorption at 1406 cm^{-1} in reflection FTIR also points to lead white, although chalk patches can lead to absorption shifts as is pointed out by reflection FTIR work on reference materials.[93] Presence of lead in several particles in the ground layers was proven by EDX measurements. Calcium is not found at all in this layer.

No reflection FTIR data could be obtained on the dark paint areas visible in the LM picture of Fig. 6.1b, most probably because of complete absorption of the infrared light.

Additional information on the distribution of lead, lead palmitate soaps and free fatty acids was obtained by imaging SIMS (see Figs. 6.1i, j and k). Lead, displayed by the isotope peaks at m/z 208, is highly concentrated inside the protrusion and in some smaller areas with relatively large lead white particles. Compared to the intact ground layer, lead metal carboxylates of palmitic acids are concentrated inside the protrusion as pointed out by the distribution of the mass fragment peaks of the lead salt of palmitic acid at mass m/z 461-464 (Fig. 6.1k).[119] Palmitic acid displayed in the map of mass m/z 255 (the negative parent ion of palmitic acid) is also more concentrated in the protrusion. The molecular information on these oil derived compounds correlates with the FTIR observations on the metal carboxylates, which are interpreted as lead carboxylates. Palmitic acid is present in many kinds of drying oil but it does not contain double bonds, and is therefore not build in into polymeric networks. The compound is chemically very stable however and therefore representative of the original oil binding medium.

Fig. 6.1l is the negative ion map of chlorine (mass m/z 35), which shows a remarkable resemblance to the lead distribution map. This high correlation is a result of the presence of crystalline basic lead chloride (Fiedlerite: $Pb_3Cl_4(OH)_2$), which was confirmed by X-ray diffraction studies of a small amount of sample taken from a protrusion. The origin of this rare mineral is puzzling but may be related to impurities in the lead white produced in the 17th century. The highest relative concentration for the chlorine is clearly associated with the body of the protrusion.

The following scenario for the formation of the protrusions has been proposed by Heeren and Boon:[119] the original, relatively oil-rich lead-white containing ground seems to have contained local areas where the oil paint was chemically unstable. It is not yet understood what triggers the process of chemical change that dissolves the mineral phase (i.e. the lead white). The source of the chlorine is not known, although a poor quality lead white could contain various lead hydroxychlorides.[161] After dissolution of the mineral phase, the remaining cross-linked oil network polymer appears as opalescent semi-translucent material. The metal ion cross bridging in this oil network could be significantly reduced, because the chloride anions compete for co-ordinating Pb^{2+} ions with the anionic carboxylic acid groups in the polymeric network. New mineralisation in the form of lead hydroxychloride precipitation starts off another competing reaction for lead. Consequently, the original tight ionomeric structure of the polymer system in the ground loosens up and becomes a chemical sponge for small organic compounds. Both processes could lead to a considerable increase in polymer volume and could be the main driving force for protruding eruptions. Such volume changes could be intensified by exposure to solvents during restoration.

6.3.2 Seghers' 'Garland of Flowers around an image of the Madonna'

The cross-section (256/5) taken from the black background of the *Garland of Flowers around an image of the Madonna* by Daniel Seghers and Thomas Willeboirts Bosschaert is shown in Fig. 6.2. Figs. 6.2a-c display the images obtained by electron, visual light and fluorescence microscopy. Figs. 6.2d-i are FTIR images of the cross-section. Figs. 6.2j and 6.2l represent infrared reflection spectra of the areas marked by an asterisk in Figs. 6.2f and 6.2h respectively. Fig. 6.2k is a diamond cell infrared transmission spectrum of a protrusion isolated manually from the painting.
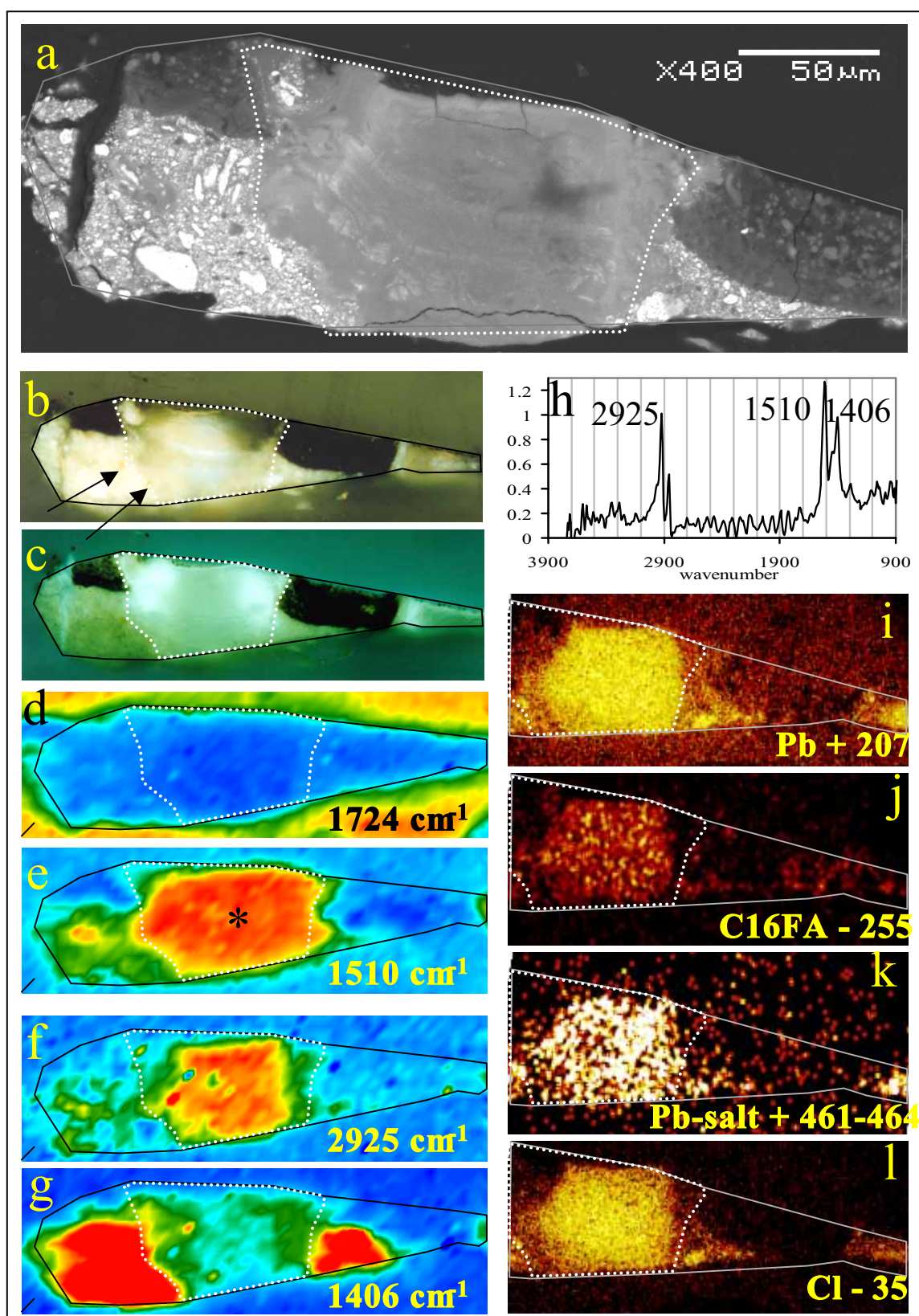
Fig. 6.1. *Microscopic and microspectroscopic analytical investigations of a paint cross section from* The anatomy lesson of Dr Nicolaes Tulp, *by Rembrandt van Rijn (MH 146/1). Dotted white line indicates the protrusion. Solid black line outlines the area of study in the cross section. (**a**) SEM image shows a protrusion as a homogeneous area in a ground layer. (**b**) Visible light microscopy shows the protrusion as a transparent mass. (**c**) Part of the protrusion shows strong fluorescence under UV illumination. (**d**) A FTIR image at 1724 cm⁻¹ outlines the embedding material. The colour map scale ranges from high (red) via medium (yellow-green) to low (blue) absorption. (**e**)-(**f**) FTIR images at 1510 and 2925 cm⁻¹ show the presence of aliphatic metal carboxylates localised in the protrusion. (**g**) FTIR at 1406 cm⁻¹ images carbonates that are mainly present in the paint layer as lead white. (**h**) FTIR reflection spectrum of a point in the protrusion (indicated * in figure 1e). The observed bands are characteristic for metal carboxylates. (**i**)-(**l**) SIMS images the distribution of lead, C16:0 fatty acid, lead salt and chlorine inside the protrusion. (see colour image at the end of this Thesis)*
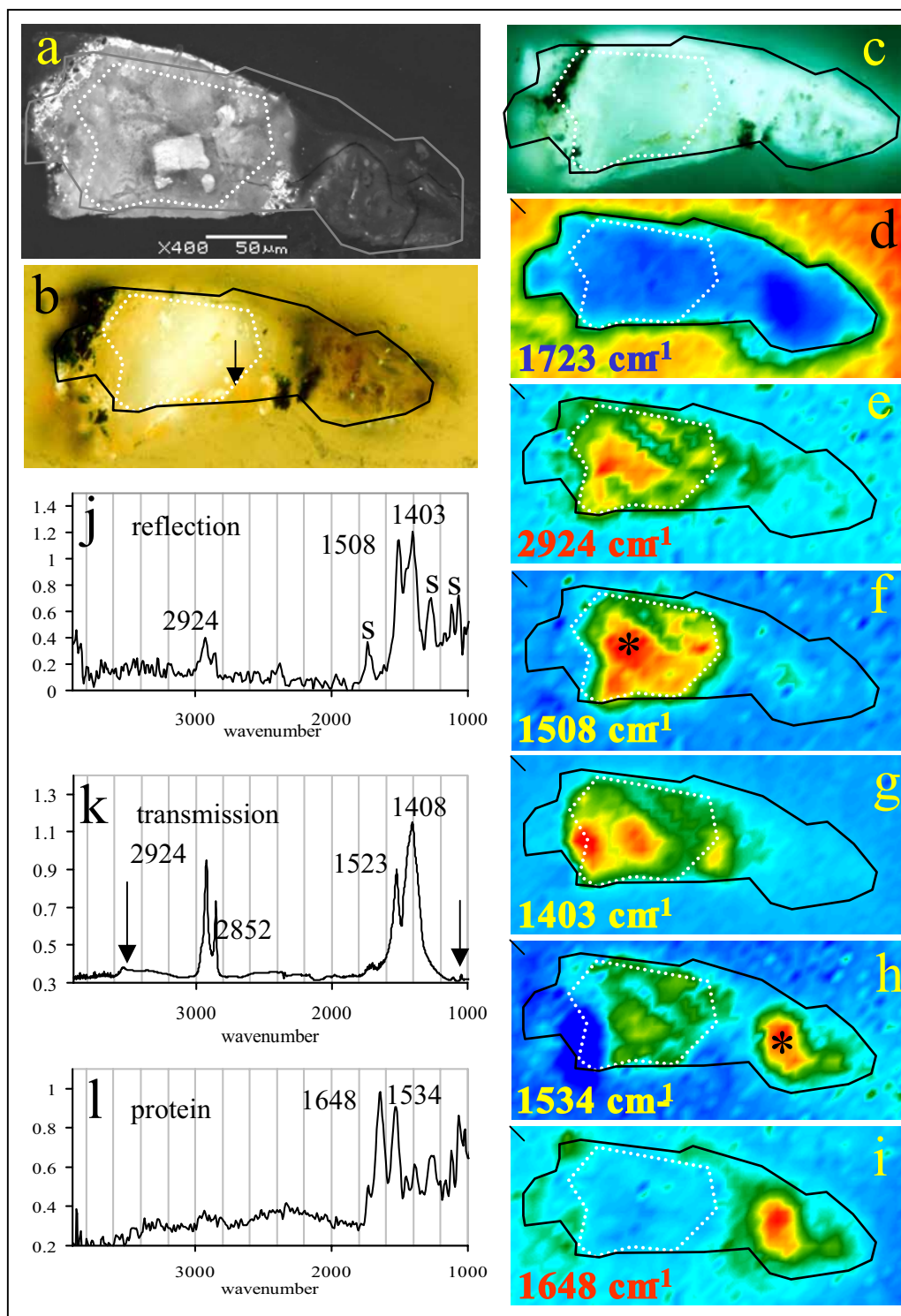
Fig. 6.2. *Microscopic and microspectroscopic analytical investigations of a cross section from* Garland of flowers *around an image of the Madonna by Seghers and Bosschaert (MH 256/5). Dotted white line indicates the protrusion. Solid black line outlines the area of study in the cross section. (a) SEM image showing a homogeneous protrusion, in which a small square particle is observed. Remaining granular paint matrix is present on the sides. (b) Visible light microscopic image. The whitish protrusion contains some orange particles (see arrow). (c) UV-fluorescence image shows fluorescence in most of this cross-section. (d) FTIR at 1724 cm⁻¹ images the outline of the embedding material. (e)-(g) FTIR images showing the presence of CH-moieties (2928 cm⁻¹), carboxylates (1508 cm⁻¹) and carbonates (1403 cm⁻¹) in the protrusions. (h)-(i) FTIR images at 1534 and 1648 cm⁻¹ highlight the brownish part on the right side of the protrusion (see Fig. 6.2b). A spectrum of the highlighted part is displayed in figure 2l. (j) Reflection FTIR spectrum of a point in the protrusion (indicated * in Fig. 6.2f). (k) Transmission FTIR spectrum of a protrusion isolated manually. The higher quality of this spectrum compared to the reflection spectrum in Fig 6.2j allows identification of the mineral basic lead carbonate (specific absorptions indicated by arrows). (l) Reflection FTIR spectrum of the brownish part (red highlighted in Figs. 6.2h and 6.2i) shows the presence of protein, probably introduced in the painting during relining. (see also coloured version at the end of this Thesis)*

The small paint sample (Fig. 6.2a) shows next to the whitish protrusion only small areas of the cream coloured ground surrounding the mass and a tiny piece of the black background on the left. The brownish part on the right, which fluoresces white under UV illumination (Fig. 6.2c), is glue from the tacking edge. Small diffuse orange particles are visible in the transparent mass of the protrusion (see arrow). An investigation by SEM using Energy Disperse X-ray analysis (EDX) shows that lead is present in the whitish protrusion as well as in the orange particles. Visible light spectra of these orange particles were obtained with the imaging spectroscopic attachment to the microscope and compared to spectra obtained from a reference minium (Pb_3O_4, red lead, Von Imhoff collection) and litharge (massicot, PbO, obtained from Aldrich). The high similarity of the spectroscopic data of the orange particles found in the painting by Seghers and the minium reference shown in Fig. 6.3 identifies the orange particles as red lead (Pb_3O_4) rather than litharge.

The reflection FTIR-image at 1723 cm^{-1} in Fig. 6.2d depicts the embedding medium by the high carbonyl absorption of the embedding medium (red) and outlines the sample circumference (blue), which can be correlated to the microscopic image. The black line in Fig. 6.2d outlines the complete paint cross-section, while the white dotted line outlines the protrusion. Images of absorption peaks at 2924 cm^{-1} (Fig. 6.2e, CH bonds), 1508 cm^{-1} (Fig. 6.2f, carboxylate), and 1403 cm^{-1} (Fig. 6.2g, carboxylate) show that these absorptions are located inside the protrusion. They are all attributed to aliphatic lead carboxylates, as EDX showed the presence of lead. The absorption peak at 1403 cm^{-1} is again an overlay of the symmetric $-CO_2$ stretch absorption in the carboxylates and the C–O stretch absorption from carbonates. This explains the differences between the images at 1508 cm^{-1} and 1403 cm^{-1} (Fig. 6.2f and 6.2g).

A reflection infrared spectrum taken from the protrusion (asterisk in Fig. 6.2f) is shown in Fig. 6.2j. In this spectrum the peaks at 2924, 1508 and 1403 cm^{-1} are clearly visible. The peaks at 1723, 1270 and around 1100 cm^{-1} (marked 's') show that on the surface of this cross-section a smearing layer of embedding medium is still present.

From this painting also a tiny sample from an isolated protrusion was available. This protrusion sample was squeezed in a diamond cell of the FTIR instrument and produced the transmission spectrum shown in Fig. 6.2k. The quality of this spectrum is better than the quality of the reflection spectrum in Fig. 6.2j. Furthermore, as no embedding material is used in this experiment the spectrum contains no IR absorptions of a smearing layer of embedding material. The peak positions are at similar frequencies in the transmission and reflection experiments, which supports the validity of the Kramers-Kronig transformation of reflection spectra. Strong absorption peaks at 2920, 2850, and 1520 cm^{-1} point to aliphatic carboxylates, i.e. lead soaps. The large absorption at 1404 cm^{-1} is assigned to a carbonate group. Because of the higher quality of the transmission spectrum, it is possible to prove the presence of lead white, based on absorptions at 3535 (OH$^-$) and 1086 cm^{-1}. Lead white in the protrusion is not the same as the lead white in the paint layer, as it does not appear as discrete particles. This could be due to partial dissolution of the existing lead white or due to formation of new lead white through recrystallisation. A possible role of chlorine in lead white mineral phases remains to be demonstrated by SIMS in the future.

The brownish part on the right side of the cross-section (Fig. 6.2b) shows absorption maxima at 1534 and 1648 cm^{-1} (cf. Figs. 6.2h en 6.2i). The brownish part is identified as a protein, based
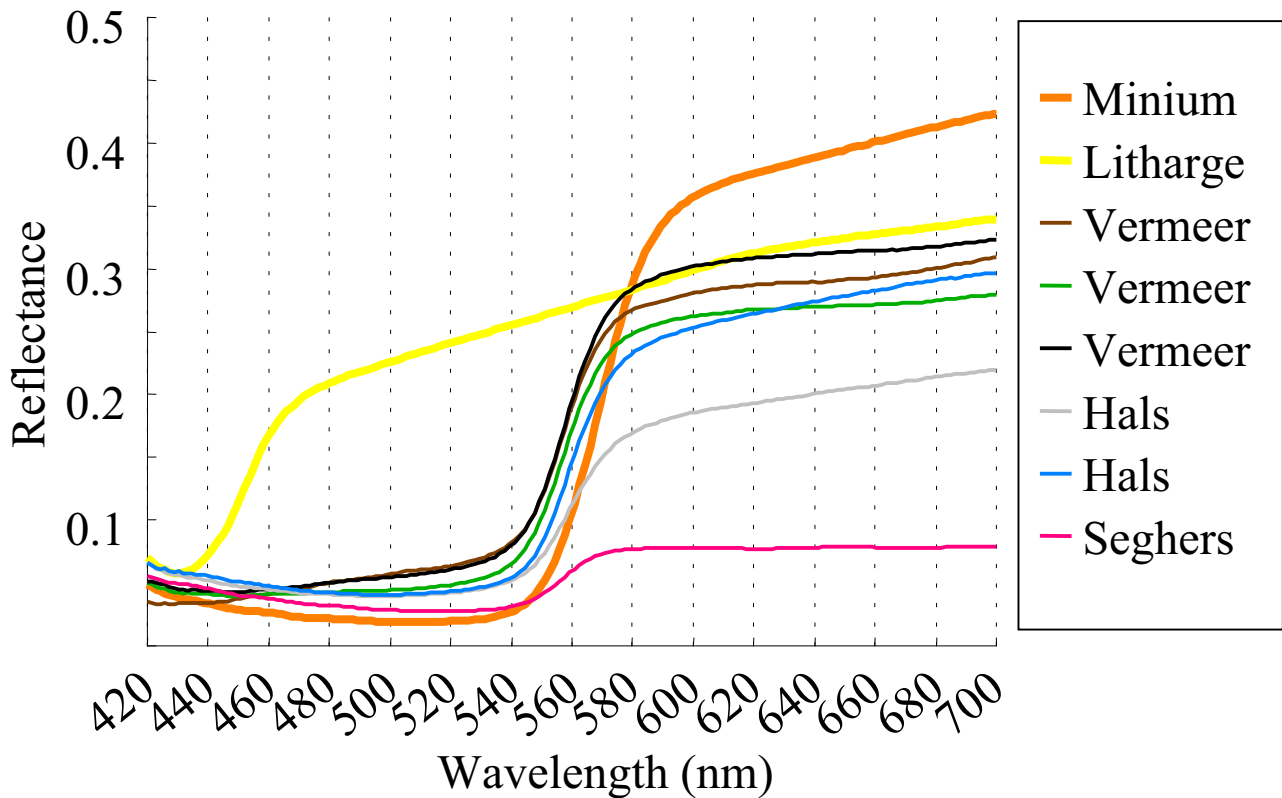
Fig. 6.3. *Visible light spectroscopy of two lead pigments and orange particles in the paintings studied. The spectra from the reference materials minium (Pb$_3$O$_4$) and litharge (PbO) are indicated by the fat orange and yellow curves, respectively. Spectral curves directly recorded from orange particles in various pain cross-sections show a sharp knee around 560 nm which identifies these particles as minium.*
(see coloured image at the end of this Thesis)

on the reflectance spectrum in Fig. 6.2k. As this proteinaceous part of the cross-section is not pigmented and the painting in question is painted in oil, this proteinaceous matter must be part of the glue introduced during relining of the painting. Intense fluorescence is not normally observed for aged proteins. No further explanation for the current observation of fluorescence was found.

6.3.3 Vermeer's 'Diana and her companions'

Fig. 6.4 shows the results of measurements on a part of a paint cross-section (406/16) taken from the background in Vermeer's *Diana and her companions*. Fig. 6.4a is the SEM image; Figs. 6.4b and 6.4c are light microscopic and UV-fluorescence images. Part of the dark undermodelling layer beneath the surface of the embedding material is outlined by a white line, which marks the border between the parts of the sample at and beneath the surface of the embedding resin. FTIR images are shown in Figs. 6.4d-h. Fig. 6.4i is an FTIR spectrum of the area marked by an asterisk in Fig. 6.4g. The visual image of the cross-section in Fig. 6.4b shows three layers. The dark paint layer contains many angular particles of smalt (Cobalt confirmed by SEM-EDX). The intermediate whitish paint layer contains lead-tin yellow, lead-white, orange particles and several relatively transparent areas. The latter are interpreted as protrusions *in statu nascendi*. The imprimatura layer is dark-coloured and finely grained. The light ground is below the embedding material. The protrusion does not erupt through the top layer but its diameter is

clearly bigger than the thickness of the paint layer from which it originates. The fluorescence image in Fig. 6.4c shows a crack in the upper paint layer (arrow), which is possibly a first step towards the protrusion of these structures through the top paint layer.
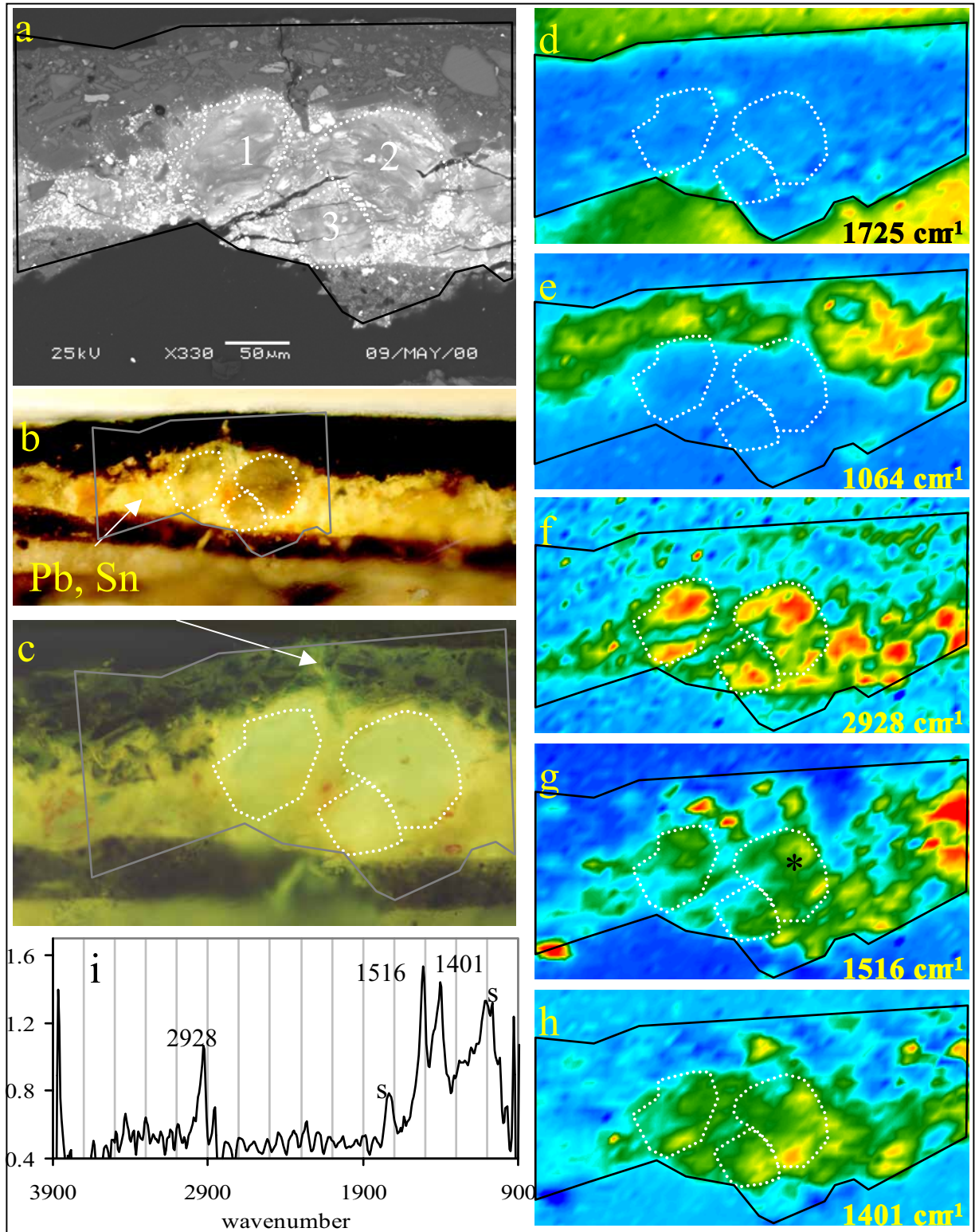
The paint layer with the protrusion is rather inhomogeneous. The SEM picture in Fig. 6.4a shows the 'protrusion' as relatively homogenous vaguely layered areas marked as 1, 2 and 3 outlined with a white dotted line for easy comparison. Between these areas particles with a high electron emission are visible as white particles in SEM image. The visual microscopic image (Fig. 6.4b) shows lead white and yellow particles in that part of the cross-section. SEM-EDX (red arrow) shows lead and tin from a lead-tin yellow pigment. The cross-section contains also many orange to red coloured pigment particles near the protrusion. A large cluster of orange particles is seen in light microscopy on the left hand side. These orange crystals were not found as separate entities in the SEM image, implicating that their secondary electron emission is similar to that of the adjacent lead-containing matrix. These particles are identified as minium on the basis of their visible light spectrum (Fig. 6.3) and their lead content determined by EDX.

The FTIR images in Figs. 6.4d to 4h show an area of observation by the FTIR microscope that is smaller than the LM and SEM maps. The outline of the protrusion found in the SEM picture is also plotted in these images for easy comparison. The absorption map at 1064 cm^{-1} presented in Fig. 6.4e is due to silicates from smalt in the upper paint layer. Smalt was identified on the basis of Cobalt found in many particles in this layer by EDX.

The absorption maps at 2928 cm^{-1}, 1516 cm^{-1} and 1401 cm^{-1} (Figs. 6.4 f, g, h) point to the presence of aliphatic carboxylates in the intermediate white paint layer in question. The spectrum in Fig. 6.4i taken from protrusion 1 shows the different characteristic carboxylate peaks at 2925, 1516 and the combined lead white/metal carboxylate peak at 1401 cm^{-1}. Comparison of the white dotted outlined protrusions from the SEM picture with those in the FTIR images demonstrates that the aliphatic carboxylates are not restricted to the transparent areas, but are also prominent in other parts of the paint film. This suggests that the conversion of the original paint to the present composition is not confined to the transparent areas 1-3. A possible scenario is that an original lead white and lead-tin yellow paint has been converted by 'dissolution' of this paint producing a lead carboxylate rich composition with local residues of the original mineral pigments and newly formed mineral matter. Examples of the latter are in our view the orange minium particles that appear near the borders and partly inside the transparent protrusion areas.

6.3.4 Cuyp's 'Girl with the peaches'

Results from analytical microscopic investigations on a cross-section taken from the *Girl with the peaches* by Albert Cuyp are shown in Fig. 6.5. Sample 829/1 is taken from the flesh colour, and consists of a relatively homogenous fine-grained yellowish flesh layer broken up by a protrusion area. The SEM image in Fig. 6.5a zooms in on the protrusion and the intact flesh paint layer on the left and right hand sides of the cross-section. The flesh paint consists of a poorly sorted mass of pigment particles. A tiny amount of residual grey ground is present on the left side of the protrusion. Inside the protrusion defined particles are absent; cloudy areas with clear differences in secondary electron emission density are seen instead. SEM-EDX only shows lead in the high intensity emission parts of the protrusion. As lead is the only heavy element observed inside the protrusion, intensity differences are interpreted to be depending on the relative lead concentration.

a

1

2

3

25kV   X330   50μm   09/MAY/00

b

Pb, Sn

c

i

1.6

1.2

0.8

0.4

2928

1516   1401

S

S

3900   2900   1900   900

wavenumber

d

1725 cm^{-1}

e

1064 cm^{-1}

f

2928 cm^{-1}

g

*

1516 cm^{-1}

h

1401 cm^{-1}

Both figures: see also coloured version at the end of this Thesis

*Left-hand image: **Fig. 6.4.** Microscopic and microspectroscopic analytical investigation of a cross section from Vermeer's* Diana and her companions *(MH 406/16). Dotted white line indicates the protrusion. Solid black line outlines the area of study in the cross section. (**a**) The SEM image shows 3 more or less separated protrusions (numbered 1-3) that are homogeneous and without granular pigments. (**b**) Visual light microscopy reveals presence of many orange particles in this cross section, especially in a cluster on the left side of the protrusion. The bright paint layer contains lead and tin (EDX data). (**c**) The UV- fluorescence image shows the beginning of a craquelure in the top-paint layer (white arrow). Some red particles are visible around the fluorescing protrusions. (**d**) FTIR at 1725 cm^{-1} images the outline of embedding material. (**e**) The FTIR image at 1064 cm^{-1} localises silicates. This is probably due to smalt, as EDX confirms the presence of cobalt in this layer. (**f**)-(**h**) FTIR images at 2928, 1516 and 1401 cm^{-1} indicate that carboxylates are present in the protrusions, but they are not so strictly localised in the protruding masses and also present in other parts of the paint layer. (**i**) Reflection FTIR spectrum of a point in the protrusion (indicated * in Fig. 6.4g). Peaks marked S are indicative for a smearing layer of embedding material.*
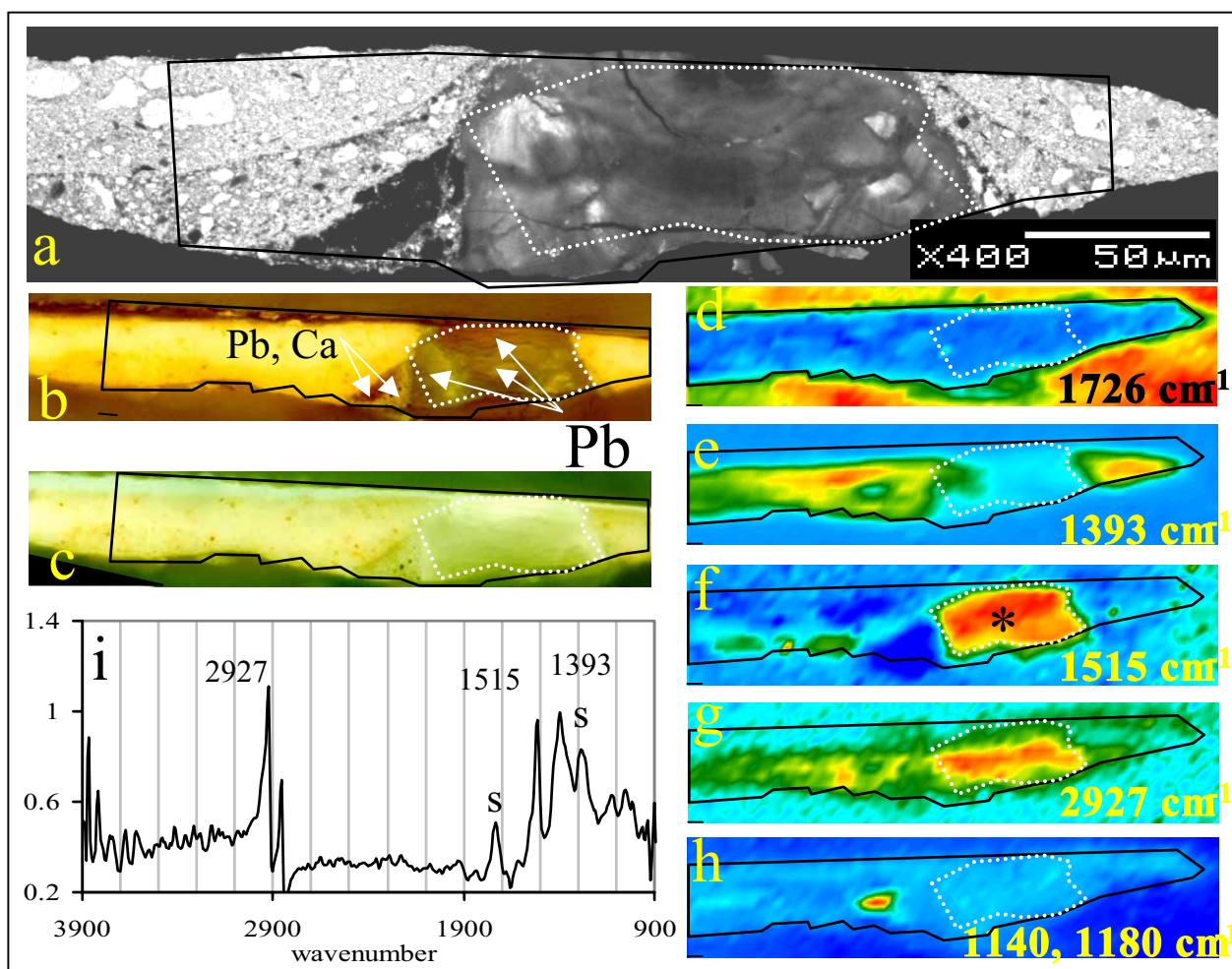

Fig. 6.5. *Microscopic and microspectroscopic analytical investigations of a cross section from Cuyp's* Girl with the peaches *(MH 829/1). Dotted white line indicates the protrusion. Solid black line outlines the area of study in the cross section. (**a**) SEM image shows that the paint layer characterised by a very detailed pigment particle distribution is completely replaced by the protrusion with a dramatically different granulometry. (**b**) Visual light microscopy of this yellow paint layer reveals that the protrusion is not completely homogeneous. EDX identifies only lead in the protrusion, while lead and calcium were found in small remnants of the ground layer. (**c**) UV-fluorescence microscopy shows the similarity between fluorescence of the small varnish layer on top of the paint layer and the top part of the protrusion. (**d**) FTIR at 1726 cm^{-1} images the outline of embedding material. (**e**) FTIR image at 1393 cm^{-1} localises the carbonates in the intact paint layer. (**f**)-(**g**) FTIR images at 1515 and 2927 cm^{-1} show that carboxylates (1515 cm^{-1}) and C-H moieties are found mainly in the protrusion. The C-H stretch vibration is also observed in the intact paint layer. (**h**) The image at 1140 cm^{-1} shows a small region in which silicates are found. Similar results were obtained at 1180 cm^{-1}. (**i**) Reflection FTIR spectrum of a point in the protrusion (indicated * in Fig. 6.5f).*

Opaque whitish areas inside the protrusion visible in the light microscopic images (Fig. 6.5b) correlate with the high emission lead enriched areas in the SEM picture. UV-fluorescence microscopy reveals a fluorescent varnish layer on top of the paint (Fig. 6.5c). The top part of the protrusion also shows a relatively high fluorescence. Small remnants from the grey ground layer are present on the left side of the protrusion. EDX demonstrated both lead and calcium on this position, presumably from lead white and chalk.

Fig. 6.5d shows the FTIR image of the embedding medium, outlining the circumference of the sample (black line). This outline is also plotted in the other FTIR images (5e-5h) to enable their mutual comparison. The FTIR image in Fig. 6.5e shows the distribution of carbonates (1393 cm^{-1}). This image closely resembles the light microscopic distribution, where the distribution of carbonates corresponds to the opaque area. Comparison with the outline shows that the unpigmented varnish layer on top of the paint layer is devoid of carbonates. The transparent matter in the protrusion has a very specific FTIR image at 1515 cm^{-1} pointing to metal carboxylates (Fig. 6.5e). The circumference of the 1515 cm^{-1} map is reproduced in the other FTIR images with a white dotted line. The metal carboxylates are very pronounced in the protrusion. The image of the absorption by CH vibration of aliphatic carbon chains at 2927 cm^{-1} in Fig. 6.5f shows aliphatic moieties in the protrusion as well as in parts of the paint layer. The protrusion shows maxima in the FTIR maps of aliphatic moieties and metal carboxylates pointing to lead soaps as the body of the transparent matter in the cross-section. This interpretation is confirmed by the FTIR spectrum (Fig. 6.i). Additionally, a strong absorption at 1393 cm^{-1} is present pointing to carbonates inside the protrusion mass. The cloudy patches with a higher electron density must be due to lead carbonates or lead hydroxycarbonates, since lead is the only cation detected by EDX.

Comparison of the 2927 cm^{-1} map to the outline of the sample shows that the varnish layer does not reflect much IR radiation at 2927 cm^{-1} although an unpigmented varnish layer usually contains many CH functionalities. In our experience, it is difficult to obtain FTIR reflection spectral data on resins in specular reflectance. The varnish on top of the protruding mass seems to have penetrated the metal soap mass as deduced from the UV fluorescence picture (Fig. 6.3c). The FTIR image of 2927 cm^{-1} is affected by this varnish as the distributions of metal carboxylates (1515 cm^{-1} map) and aliphatic CH vibrations do not match at the top of the protruding mass.

6.3.5 Hals's 'Portrait of a man'

Fig. 6.6 summarises the results of investigations on cross-section 928/2 taken from the thin dark drapery in the *Portrait of a man*, painted by Frans Hals. An almost rectangular relatively transparent mass resembling the protrusions in the examples above is present in a thick cream coloured ground layer protruding through the dark paint layer (Fig. 6.6b). Above this are several layers of varnish, dirt, and overpaint. The SEM picture in Fig. 6.6a shows the cream ground layer as a poorly sorted granular mass of lead white particles with a relatively homogenous protrusion within. The protrusion shows a layered structure in the bottom part and almost no structure in the top part. The varnish layer is not observed in the SEM image (Fig. 6.6a), as it contains no heavy elements. Lead is the only element observed by SEM-EDX in the ground layer and the transparent material of the protrusion. One circular dark particle seen as a dark
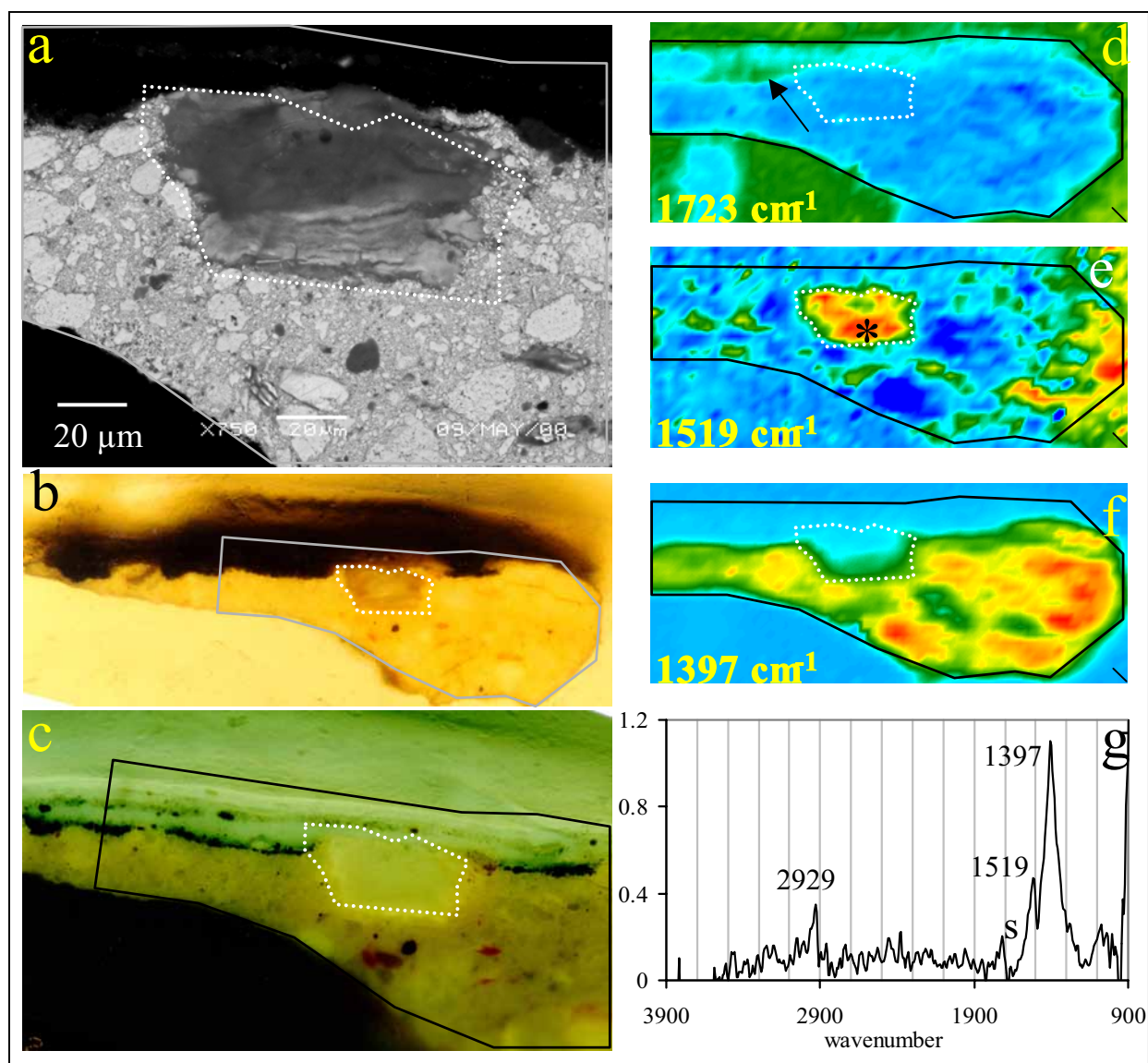
Fig. 6.6. *Microscopic and microspectroscopic analytical investigations of a cross section from Hals's* Portrait of a man *(MH 928/2). Dotted white line indicates the protrusion. Solid black line outlines the area of study in the cross section. **(a)** SEM image shows a layered structure in the bottom of the mainly transparent protrusion. Particle size distribution in the protrusion is completely different from the distribution in the intact paint layer. **(b)** Visible light microscopic image of the same cross section. The protrusion is indicated by a white dotted line. **(c)** The protrusion and varnish layers fluorescence in UV light. **(d)** FTIR at 1723 cm^{-1} images the outline of embedding material (black line). The thick varnish layer shows a small amount of absorption (see arrow). **(e)** FTIR image at 1519 cm^{-1} clearly highlights the protrusion, where lead carboxylates are localised. **(f)** FTIR image at 1397 cm^{-1} shows high absorption of carbonates in the paint layer. Varnish layers are not highlighted. **(g)** Reflection FTIR spectrum of a point in the protrusion (indicated * in Fig. 6.6e).*
(see also the coloured version at the end of this Thesis)

brown spot in the cream ground (Fig. 6.6b) contains iron and manganese and is interpreted as a small addition of umber.

The dark semi-transparent varnish layer clearly consists of several layers when observed in UV-fluorescence mode (Fig. 6.6c). In and around the protrusion small orange particles are present. Visible light spectroscopy identifies these as minium (Fig. 6.3).

The FTIR image at 1723 cm^{-1} from the embedding material shows the circumference of the sample (Fig. 6.6d). In addition, some evidence for the varnish layer can be seen in this image (arrow) as a result of IR absorptions from acidic and ketone functionalities. The 1519 cm^{-1} metal carboxylate absorption is imaged in Fig. 6.6e, and is maximal in the protrusion. It is remarkable how well the outline of this map follows the contours of the protruding mass in the SEM picture. A density difference at the top in the SEM protrusion picture is also observed as a low absorption in the metal carboxylate FTIR map. The carbonate absorption map at 1397 cm^{-1} from lead white (Fig. 6.6f) mainly highlights the paint layer. The bottom part of the protrusion however also contains carbonates that correspond to more opaque areas seen in visible light.

The horizontal pattern observed in the bottom part of the protrusion by SEM (Fig. 6.6a) could very well be newly precipitated lead white or lead carbonate and so explain the increased carbonate absorption observed in this position.

Fig. 6.6i shows a typical infrared spectrum of the protruding mass. Compared to the spectra obtained from the other cross-sections (Figs. 6.1g, 2i, 4i and 5i) discussed earlier, the peak positions are similar but the peak intensities are quite different. In this protrusion the absorption of metal carboxylates at 1519 cm^{-1} is considerable lower than the carbonate peak at 1397 cm^{-1}, while the CH absorption is very low. This suggests that the degree of remineralisation of this protrusion is much higher than in the other cases. The map of aliphatic moieties of this sample is rather unspecific and suggests that the surface of the sample may be contaminated.

6.4 Discussion

Protrusions appear as opalescent, partly transparent globules in the cross-sections. In normal light microscopy, no or very few pigment particles can be seen inside the protrusions, even if the protrusion appears embedded in a coloured layer. The grain size distribution in the paint layer and the protruding mass differs substantially. It appears that the mineral matter in the paint layer has 'dissolved'. Light microscopy, and particularly SEM shows that residual or new mineral phases with a relatively homogeneous grain size distribution are present. Protrusions are areas with a clearly distinct texture and chemistry that differ greatly from the surrounding paint.

The extensive analysis of cross-sections from the different paintings provides a consistent image of the chemical constituents in the protrusions. It is clear from FTIR-imaging data that metal carboxylates are present in all protrusions investigated. DTMS and SIMS identify the carboxylic acid groups as stearic and palmitic acid derived from the drying oil in the paint. EDX and SIMS measurements identify the metal to be lead, probably derived from lead white, which is found in the residual ground/paint layer around every protrusion.

Lead soaps are not introduced into the paint as such, but have developed as a result of the ageing of lead white oil paint. Lead white will act as a catalyst in the oxidation and cross-linking of the unsaturated triglycerides of drying oil. Cross-linked oil is de-esterified upon ageing.[19,105,108]

New ionic bonds between acid groups of the residual oil network polymer and dissolved lead ions form an ionomeric structure in which lead acts as the main co-ordinating ion. These ionomers are confined to the surface of the mineral matter and the interstitial pore space. The relatively large accumulation of lead soaps, which act as colloidal gels in the paint layers, points to major changes in the local chemical environment. Dissolution of the mineral phase inside a paint must lead to very high local concentration of lead and other substances.

SIMS revealed the presence of chlorine inside the protrusions in the case of *The Anatomy Lesson of Dr Nicolaes Tulp*. Until the pending SIMS research on the cross-sections from the other paintings presented in this paper is carried out, it is unclear whether *The Anatomy Lesson of Dr Nicolaes Tulp* is a special case. Chlorine could be a normal contamination of 17th century lead white, because the production process is far from well defined. We have observed chlorine strongly associated with intact lead white in SIMS data from other 17th century paintings. It is therefore possible that Rembrandt used a bad batch of lead white paint. However, it is not yet clarified if the presence of chlorine affects the paint during the life-time of the painting.

X-ray diffraction studies of an isolated protrusion revealed the presence of fiedlerite, i.e. a water-soluble basic lead chloride. Fiedlerite is a water soluble substance, and therefore one wonders how it has survived the water based lining procedure and the rain water exposure that are part of the history of this painting.[151] Related chlorine containing lead corrosion minerals exist and a more precise distribution map of lead-chloride compounds would be desirable.

Dissolution of the mineral phase of the paint would release this chlorine as chloride. It is clear from the SIMS data that a relatively large amount is presently concentrated in the protruding mass. The lead hydroxychlorides are highly concentrated in the protrusion as finely divided particles and have a banded structure reminiscent of Liesegang precipitation bands. Such bands point to concentration gradients of lead and chloride inside the gel of the protrusion. Further studies on the presence of chlorine in protrusions in other paintings will be performed to investigate whether chloride is present and plays an active role in the gellification process. Lead hydroxychlorides are not the only new mineral phases inside protrusions. Carbonates, indicated by the FTIR data of all protrusions, are assigned to new precipitation products of lead white or related lead carbonates. In an infrared spectrum of one protrusion that could be isolated manually, lead white, i.e. basic lead carbonate was positively identified. Although the presence of lead white inside the protrusions is clearly shown by FTIR spectroscopy, the SEM images indicate that it is present in an entirely different form compared to the lead white of the intact paint layer. For example, the pigment particles of the original paint layer in the painting by Cuyp show poorly sorted angular lead white particles. Lead white inside the protrusion occurs as cloudy masses of amorphous or extremely finely divided particles that are homogeneously distributed. The same phenomenon is also obvious in the other protrusions investigated. We infer that dissolution of the mineral phase of the original paint layers has occurred and new mineralisation in the form of basic lead carbonate and lead hydroxychloride precipitation is taking place in the residual lead soap gel.

Another indication for remineralisation is the presence of lead oxides. Diffuse orange particles seen in and around most protrusions were identified as minium (Pb_3O_4) by EDX and visible light spectroscopy. These particles were always found in close proximity to lead carboxylate protrusions and in many cases in paint layers where no red lead would be anticipated. Contrary

to the interpretation of Plahter[157] and Brunnenkant[156] we hypothesise that these red lead particles were not added to the paint as such, but are newly formed after dissolution of the original lead white paint.

These new mineralisation processes provide clues on the chemical environment inside the protrusions, which determines the course of the demineralisation process. The stability of mineral matter in different chemical environments can be derived from thermodynamical data. Garrels and Christ[162] developed this methodology for the calculation of the stability field of corrosion products on top of ore deposits. The influence of the electrical Nernst potential (Eh), the acidity (pH) and the partial CO_2 pressure on the stability of mineral phases have to be taken into account. Eh-pH diagrams show that lead oxides (minium and massicot) are the most stable mineral phases in a highly alkaline environment (pH > 12). Also basic lead carbonate (lead white, hydrocerussite) is found to be in a stable form at high pH values (>10).

We conclude from the mineralisation towards these products that the environment in and around the protrusion is very basic, with pH values exceeding pH 10. It is likely that the dissolution of the lead white mineral phase provides the OH^- moieties that lead to these high pH-values.

The driving force for the dissolution of the original paint layer is unknown. We infer that impure lead white may have a different thermodynamic stability under the conditions that have developed. This aspect, combined with a relatively high binding medium content of the affected ground/paint layer and exposure to relatively wet conditions, may be enough to trip the balance. The phenomenon is not typically limited to one particular spot in the paintings; in some cases the whole painting is affected equally. The globular aspect of protrusions suggests that they grow and affect their immediate environment. There is no indication that the process is presently halted. The products found inside the protrusion are a result of remineralisation of the compounds that were present in the paint and became available through de-esterification of the drying oil triglycerides and the dissolution of lead white particles. The composition of the original mineral pigments, the morphology of the protrusion, the nature of the remineralisation products and their distribution provide important information about the phenomenon. In further research, we hope to clarify the process that triggers the dissolution of the mineral lead white and leads to the formation of protrusions. However from our investigations presented here, it is clear that this triggering process has occurred in many paintings and plays an important part in the ageing process of paintings. Paintings respond in various ways to the external and internal environment, and should be considered as chemically dynamic systems. The awareness that organic substances in paintings are vulnerable is growing. Mineral phases and metal co-ordinated organic networks appear to be equally sensitive to chemical change. Some paintings have still not reached completely stable conditions even after hundreds of years.

Are we presently looking at the top of the iceberg?

It is difficult to say at this moment whether other opalescent globules observed in paintings by other investigators[153,154,156] are comparable to the protrusions described here. It is likely that this is the case considering the very similar characteristics for protrusions we found in a large number of paintings. We expect that more paintings will be found that show this same 'disease'. However, more comparative studies with the same analytical techniques are necessary. Further studies on how to reconstruct this phenomenon in simulated paintings are planned.

6.5 Acknowledgements

7   Metal carboxylates in the grounds of 19th century preprimed canvases used by F. Church

This Chapter describes the investigation of several samples from two primed but unfinished canvases found at Olana, the former home of the 19th century American painter Frederic Church. Different kinds of defects have been observed on these canvases: formation of protrusions, efflorescence, and ground staining. Several analyses were performed on the surface of a part of these unfinished paintings and on several microscopic samples taken from these canvases, such as the ground layer, isolated protrusions, and isolated efflorescence. These samples were analysed by various techniques, such as optical microscopy, FTIR, FTIR-imaging, DTMS, GC-MS, SIMS, and SEM-EDX. The ground layer is a complex system consisting of layers pigmented by chalk, lead white/chalk and lead white. The material found in protrusions and efflorescence contain large amounts of lead carboxylates and do not have a significant network fraction. It is hypothesised that protrusions and efflorescence are formed upon phase separation of the mobile, saturated fatty acids from the oxidised oil network. This hypothesis was confirmed by a pilot experiment, in which lead white transformed into lead carboxylates quantitatively on reaction with fatty acids.

7.1 Introduction

Severe deterioration effects disturb the visual appearance of many 19th century American paintings and form a serious threat for this important part of the cultural heritage of the United States.[163] Several of these paintings were and still are immensely popular, e.g. *Niagara* and *Heart of the Andes* by Frederic Edwin Church (1826-1900), the most famous American landscape painter of mid-19th century.

One of these deterioration effects is the formation of accumulated masses of lead carboxylates. Lead carboxylates are formed after reaction of carboxylic acids derived from the oil medium and lead ions, which become available due to degradation or dissolution of lead containing materials, e.g. lead white or lead acetate. Agglomerations of these lead carboxylates form transparent whitish masses, which fluoresce under UV illumination. Expansion of the masses makes the white material visible on the paint surface and deforms the paint layer extensively. These phenomena are very similar to the protrusions described in the previous Chapter of this Thesis.[118,152] This similarity suggests that the presence of protrusions is not confined to 17th century Dutch paintings and instigated the research described in this Chapter.

Another form of deterioration frequently observed in Hudson River School paintings is ground staining, the appearance of dark coloured patches in the image.[164] Ground staining can have a significant impact on the tonality of these translucent paintings. The effect of ground staining must have developed relatively quickly, as it is known that Frederic Church observed it himself.[164] He assigned the presence of stains to the use of lead acetate dryer, as ground staining developed on a painting in which this dryer was certainly used. Another reason for the appearance of ground staining might be that the painting materials used by this group of painters were imported from Europe, as they were not produced locally. The accusation that Europeans sold inferior pigments to far-away America has been made,[165] but it might also be that colourmen conscientiously altered export materials, especially primed canvases, to enable the long-term rolling and storing necessary for transport overseas. Microscopic investigations by Dwyer assigned the darkening to an increased and variable translucency of the ground layer, due to chemical alteration of the lead white: the upper particles of this pigment, which is normally opaque, had been transformed into transparent crystals.[166] The longer path length and therefore higher absorbance of incident light in a more transparent medium explains the darker appearance of stained patches.

The third and most apparent effects found in 19th century American paintings is the formation of efflorescence or bloom (cf. Fig. 7.1). Efflorescence is the appearance of white or bluish white film on the surface of the oil painting.[128,167] Analogies have been drawn with the formation of whitish material on chocolate, wax objects, and leather. Several analyses of efflorescence have been presented in the literature, and different kinds of materials have been found on the surface of the paint, e.g. plasticizers from synthetic resins, organic pigments,[128,168] wax like material,[169] fatty acids and/or their soaps,[167,170] sulphates, and lead chloride.[171]

All these deterioration phenomena were recognised recently on two primed, but unfinished canvases in the archive at Olana, home of F. Church, located just outside Hudson, New York.[164] Marks on the back of the canvases indicate that they were purchased from one of the regular suppliers of Church. This implies that the canvases are valid models for the priming material in

Hudson River School paintings. Furthermore, it is very well possible that the deterioration of the priming layer causes the defects observed in many 19th century American paintings. In that case, a very large group of paintings with serious restoration problems is represented by these unfinished paintings, which stresses the necessity of their investigation. The canvases provide an excellent opportunity to investigate the origin of the deterioration in detail, as the paint system of these unfinished paintings is relatively simple compared to normal multi-layered paintings. Furthermore, their art historical value is limited and relatively large samples can be taken for research. Several samples from these canvases were investigated using multiple analytical techniques. This paper presents the results of optical microscopy, Scanning Electron Microscopy with Energy Disperse X-ray detection (SEM-EDX), Fourier Transform Infrared spectroscopy (FTIR), FTIR-imaging, Direct Temperature resolved Mass spectrometry (DTMS), Gas Chromatography-Mass Spectrometry (GC-MS) and Secondary Ion Mass Spectrometry (SIMS). The focus of this article will be the description of the paint system and the elucidation of the mechanisms that lead to the described defects, especially efflorescence and protrusions.

Source	Sample	Sample prep.	Technique
122	1 and 2: intact paint	Embedded	FTIR, SEM
122	3 and 4: paint and protrusion	Embedded	FTIR
122	Paint	Diamond cell	FTIR
		Etoxide/BSTFA	GC-MS
			DTMS
122	Ground	Diamond cell	FTIR
		Etoxide/BSTFA	GC-MS
			DTMS
NA	Ground	Etoxide/BSTFA	GC-MS
			DTMS
122	Protrusion	Diamond	FTIR
			DTMS
122	Efflorescence	Diamond	FTIR
			DTMS

Tabel 7.1. Overview of the dissected samples analysed in the presented study.

7.2 Experimental

Samples

Canvases OL1984.NA and OL1984.122 were found at Olana (Hudson, New York). OL.NA is a primed but unused canvas, measuring 78.5 cm (selvage to selvage) by 74 cm. It has a plain tabby weave having 18 warp and weft threads per cm. Canvas OL1984.122 has a similar cream coloured priming, which is partly covered by a brown imprimatura. Some pieces of these canvases (~1 cm^2) were made available for research. These could be directly measured by SIMS, FTIR (specular reflectance and ATR), and SEM-EDX. Samples were taken for analysis by FTIR (transmission), DTMS, GC-MS, and for the preparation of embedded cross-sections. Sampling was carried out using a stereomicroscope and a fine scalpel. Table 7.1 presents an overview of these samples. The cross-sections were embedded in Technovit 2000LC (Heraeus Kulzer, Wehrheim, Germany) and polished with Micromesh® polishing cloths (Scientific Instrument Services Inc., Minnesota). The samples of the other parts (protrusions, efflorescence, ground and imprimatura) were isolated manually. The whitish efflorescence material has a waxy appearance and is not soluble in water, ethanol, or hexane. It can however be displaced easily with some mechanical force.

Microscopy

A Leica DMRX analytical microscope (Leica Inc., Wetzlar, Germany) was used for visual light microscopy.

SEM-EDX

A XL30 SFEG SEM (FEI company, Eindhoven, The Netherlands) and a EDAX EDX system were used for the SEM-EDX analysis. The accelerator voltage of the system was 22 kV. The sample was carbon coated to ensure good conducting properties of the surface.

DTMS

Samples of typically 20 to 60 μg were homogenised in ethanol using a mini-glass mortar. Aliquots of the obtained suspension or extracted materials were applied onto the analytical filament and dried *in vacuo*. DTMS analyses were performed on a Jeol SX-102 double focussing mass spectrometer (B/E) using a direct insertion probe equipped with a Pt/Rh (9/1) filament (100 micron diameter). The probe filament was temperature programmed at a rate of 0.5 A/min to an end temperature of about 800 °C. Compounds were ionised at 16 eV under electron ionisation conditions in an ionisation chamber kept at 180 °C. Masses in the range of m/z 20–1000 were analysed with a cycle time of 1 second. The results were processed using a JEOL MP-7000 data system.

GC-MS

Samples were derivatised by a two-step procedure to determine the degree of hydrolysis of the oil paint system. Discrimination between esterified and free fatty acids is achieved by their subsequent labelling. The first derivatisation step transethylates all esterified fatty acids, e.g.

triacylglycerols and waxes. In a subsequent reaction free and metal-bound acid as well as hydroxy groups are silylated. The experimental procedure is detailed by Van den Berg *et al.*[19]

TOF-SIMS

Time of Flight- Secondary Ion Mass Spectrometry (TOF-SIMS) measurements were performed on a TRIFT II instrument of PHI Electronics Inc. (USA).[160,172] The surface of the sample was scanned with a 25 keV primary ion beam from an Indium liquid metal ion gun, which has a final beam diameter of about 100 nm. The triple ESA ion focussing system guarantees a spatial resolution of at least 1 micron at a mass resolution of about 5000. Positive or negative ions emitted by the primary beam were mass analysed and detected. The surface of the sample was charge compensated with electrons pulsed in between the primary ion beam pulses.

FTIR

FTIR spectra were acquired by a Bio-Rad FTS-6000 spectrometer (Nowadays Digilab, Cambridge, MA, USA), equipped with an UMA 500 infrared microscope and a MCT detector. Samples were squeezed in a Graseby Specac P/N 2550 diamond anvil cell (Graseby Specac, Orpington Kent, UK). Spectra were recorded at a spectral resolution of 4 cm⁻¹, a mirror speed of 5 kHz, an UDR (undersamling ratio) of 2, and accumulation of 100 spectra. ATR spectra were acquired using a Bio-Rad slide-on ATR accessory connected to the 15× objective of the UMA 500 microscope.

Imaging-FTIR

Imaging-FTIR data were acquired using the Bio-Rad Stingray, combining the mentioned spectrometer and microscope to a 64×64 MCT camera. Spectra from cross-sections were recorded in reflection mode with a 16 cm⁻¹ spectral resolution, a step-scan frequency of 1 Hz, and an UDR of 4. The spectra were transformed to absorbance-like spectra by the Kramers-Kronig transformation which is part of the Bio-Rad Win-IR Pro software. A more detailed explanation of this system is provided in Chapter 4 of this Thesis.

Chemicals

GC-MS: Sodium ethoxide 21 wt% solution in denatured ethanol (approximately 99%) was obtained from Sigma-Aldrich Chemie Bv. (Zwijndrecht, The Netherlands). Bis-(trimethylsilyl)trifluoroacetamide, containing 1% trimethylchlorosilane, was purchased from Fluka (Zwijndrecht, The Netherlands). Pilot experiment: Xylene and stearic acid were obtained from Aldrich. Cremser white was obtained from Kremer Pigmente. Lead white and a small excess of stearic acid were kept for 5 minutes in refluxing xylene. The reaction product was allowed to cool, and washed with hexane on a filter to remove excess stearic acid. The white residue was analysed by FTIR using a diamond cell.

7.3 Results

7.3.1 General description of the paint system

A macro-photo of the surface of OL1984.122 is displayed in Fig. 7.1. Efflorescence and protrusions cover large parts of the surface and partly mask the brownish imprimatura layer. The efflorescence is mainly present in distinct patterns that coincide with the canvas structure.

The layer structure of this unfinished painting was investigated from a cross-section. Visual light microscopic images of sample OL1984/3 are shown in Fig. 7.2. The cross-section contains a thick (75 µm) white priming. The lower part of the ground layer is more transparent than the opaque layers that were applied later. A thin (~1 µm), dark imprimatura is present on top of the priming. The presence of the transparent part in the middle of cross-section OL1984/4 (arrow) indicates that a protrusion was successfully included in the sample. The layer structure of the intact paint is consistent for all four paint cross-sections.
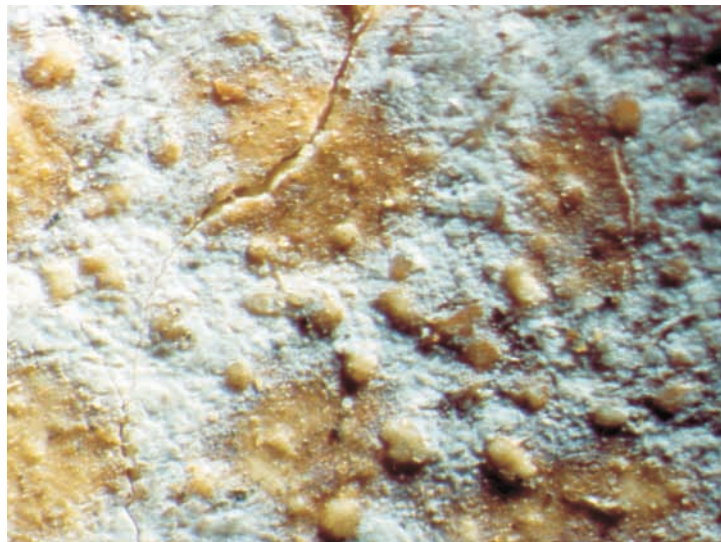

Fig. 7.1. *Macrophoto of the paint surface of OL1984.122. (see coloured version at the end of this Thesis)*
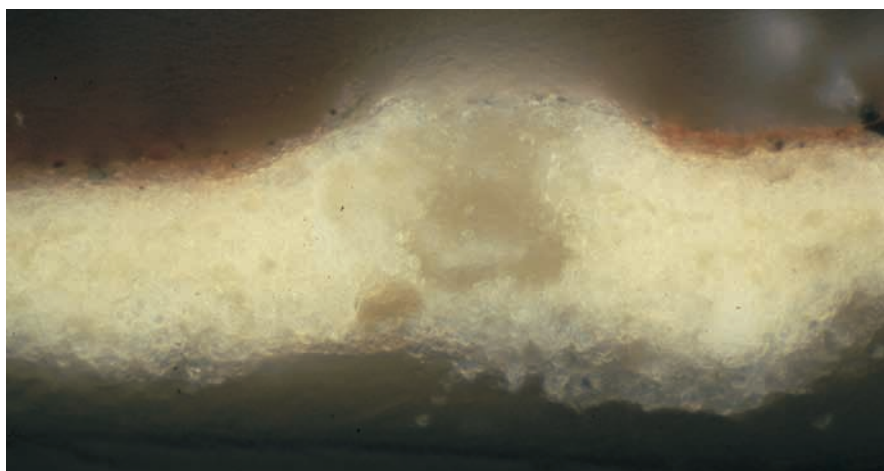

Fig. 7.2. *Optical microscopy of embedded paint cross section OL1984.122/3.*
(see coloured version at the end of this Thesis)

The identity of the pigments and their distribution was investigated by SEM-EDX. A backscattered SEM image of sample OL1984/1 is shown in Fig. 7.3A. The cross-section is a multi-layered system, containing at least four superimposed paint layers, numbered 1-4. The ground layers (1-3) have an increasing backscatter intensity towards higher layers. This can be explained by the elemental analysis (Figs. 7.3b-d), which shows the presence of mainly calcium (Ca) in layer 1, a mixture of Ca and lead (Pb) in layer 2, and the exclusive presence of Pb in layer 3. The ground layers further contain some silicon containing particles. This complex layer structure has been described before.[164] The thin brown imprimatura (marked 4) is present on top of this stack of layers and also contains Ca and Pb. Aluminium (Al, see Fig. 7.3d), Silicon (Si), and phosphor (P) are also found in this layer.

A general overview of the functional groups in the paint was obtained by FTIR. Figs. 7.4 A and B show transmission infrared spectra of the ground and imprimatura layers from OL1984.122 squeezed in a diamond anvil cell. The spectrum of the ground layer in Fig. 7.4A shows the presence of both lead white (3539, 1400 and 683 cm^{-1}) and calcium carbonate (2519, 1400 and 874 cm^{-1}). The broad and intense shoulder at 1540 cm^{-1} is assigned to metal carboxylates. Carboxylic acids (3200–2600 cm^{-1} and 1700 cm^{-1}) are hardly present. The CH vibrational bands have a low intensity, a round appearance, and absorption maxima at 2940 and 2872 cm^{-1}. They are unlike the intense and sharp peaks found in fresh drying oils (2926, 2855 cm^{-1}, see Fig. 5.2).
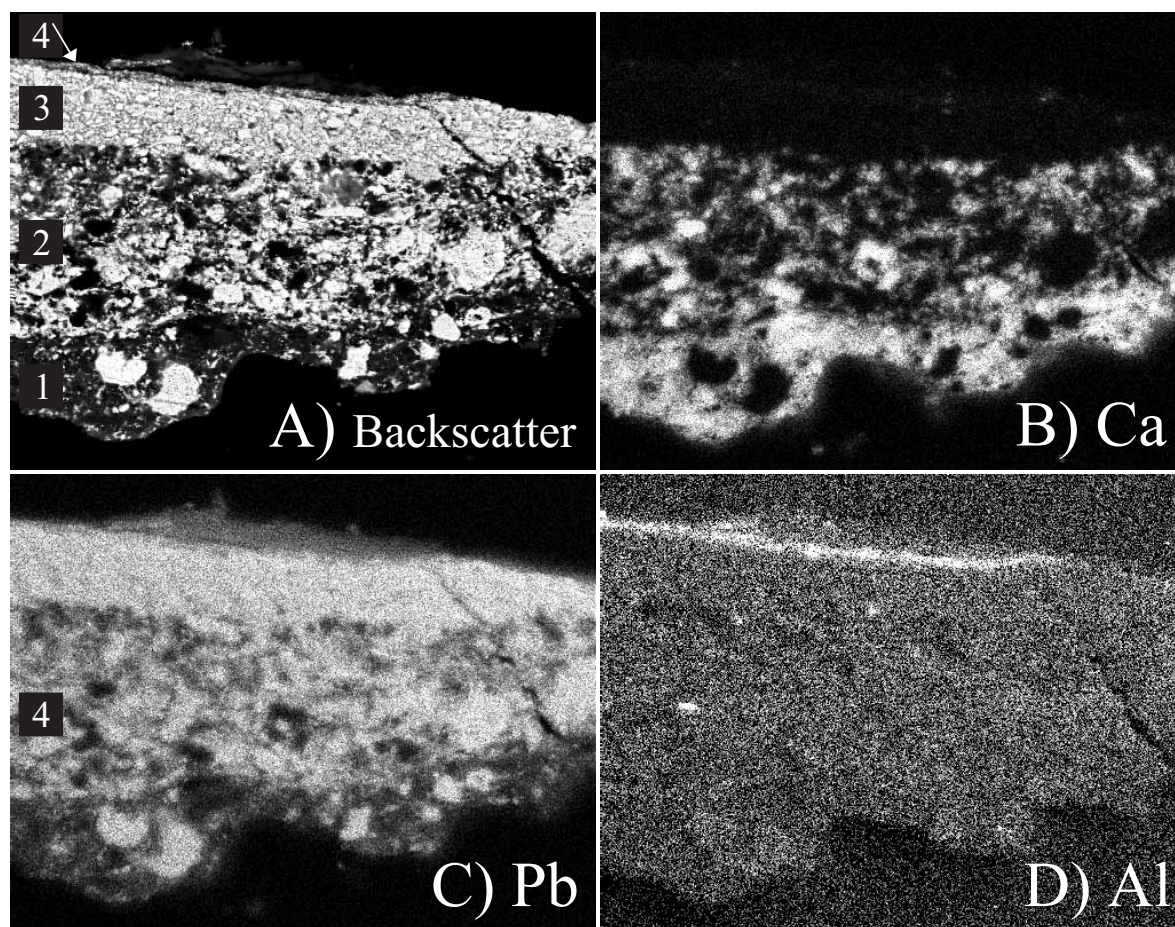

Fig. 7.3. *SEM-EDX results of embedded paint cross section OL1984.122/1. (A) Backscatter SEM image. (B)-(D) EDX maps of calcium, lead and aluminium respectively.*

Small silicate peaks are present around 1100 cm^{-1}.

The dark paint layer (Fig. 7.4B) contains lead white (3537, 1415 and 685 cm^{-1}; lead confirmed by SEM-EDX). The presence of Ca, P, Fe, Al and Si in the brown imprimatura, identified by EDX, indicate that the brown pigments in this layer are bone black (calcium phosphate) and iron oxide. The CH stretch vibration bands in this spectrum are also low (2952 and 2871 cm^{-1}). The mere absence of absorption at 1540 cm^{-1} indicates that lead carboxylate formation has occurred only to a very limited degree compared to the priming layer.

A thin section of a paint cross-section was made to improve the spatial resolution of the FTIR measurements. This was considered necessary, as the different priming layers are very difficult to separate by scalpel due to their small colour differences (cf. Fig. 7.2). The results of FTIR-imaging analyses on the thin slice are shown in Fig. 7.5. The three images show the different layers that can be distinguished in this cross-section. The 4th layer (cf. Fig. 7.3A) is too thin to be resolved by FTIR. Unfortunately, only a small remnant of the lead white layer is present on the right side of the image. The major part has been lost in the polishing process. The corresponding
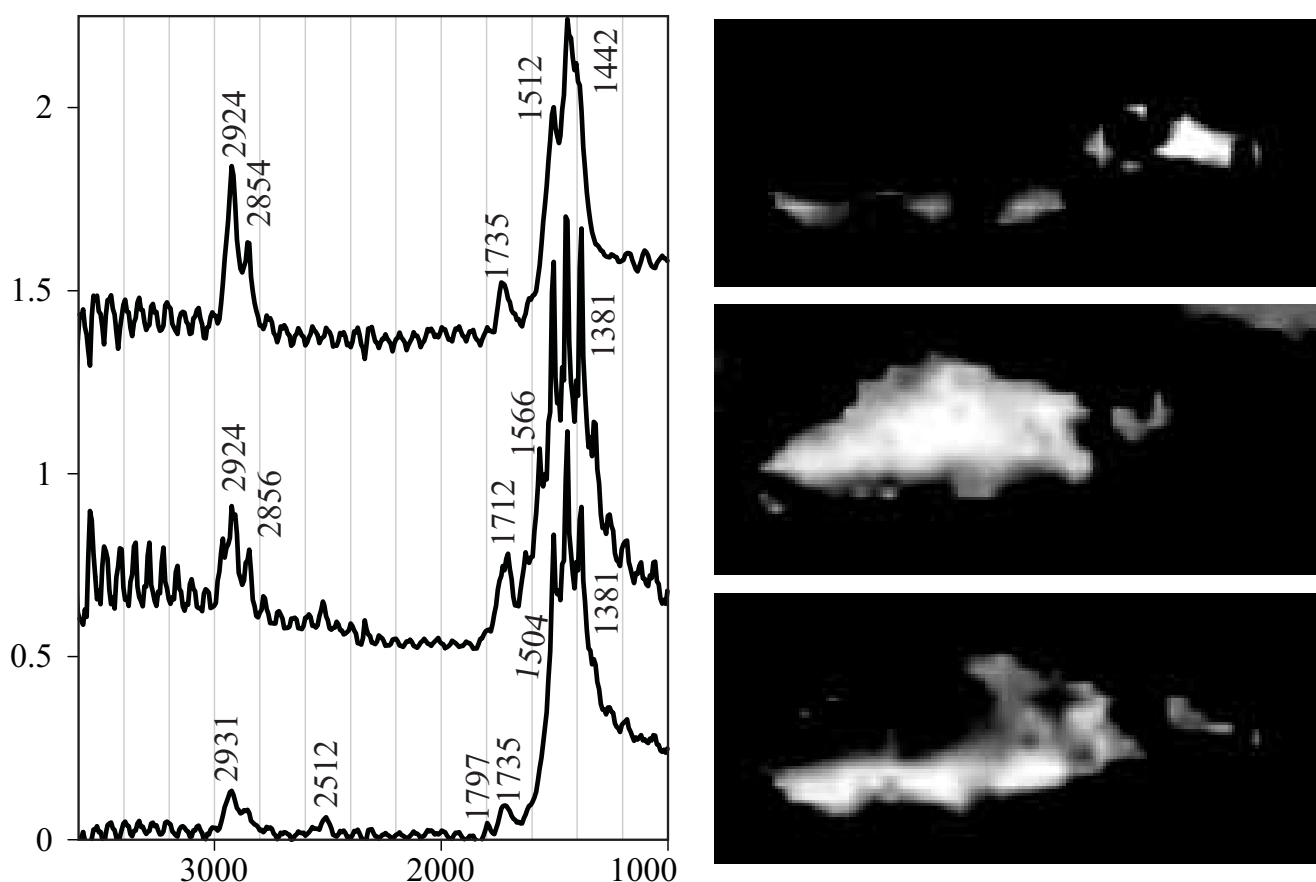

Fig. 7.5. Results of Imaging-FTIR on a thin cross-section of OL1984.122, prepared by the KBr polishing method. The spectra in the FTIR data-set were clustered on the basis of their high similarity by the projection algoritm (see Chapter 2 of this Thesis). The locations of the different clusters is highlighted in the score-plots on the right, and the mean spectrum of the highlighted part is shown in the spectrum alongside the score-plot.

Right-hand image: Fig. 7.4. Results of transmission FTIR of different dissected samples from OL1984.122, analysed in a diamond cell. (A) White priming. (B) Dark imprimatura. (C) Protrusion material. (D) Efflorescense.
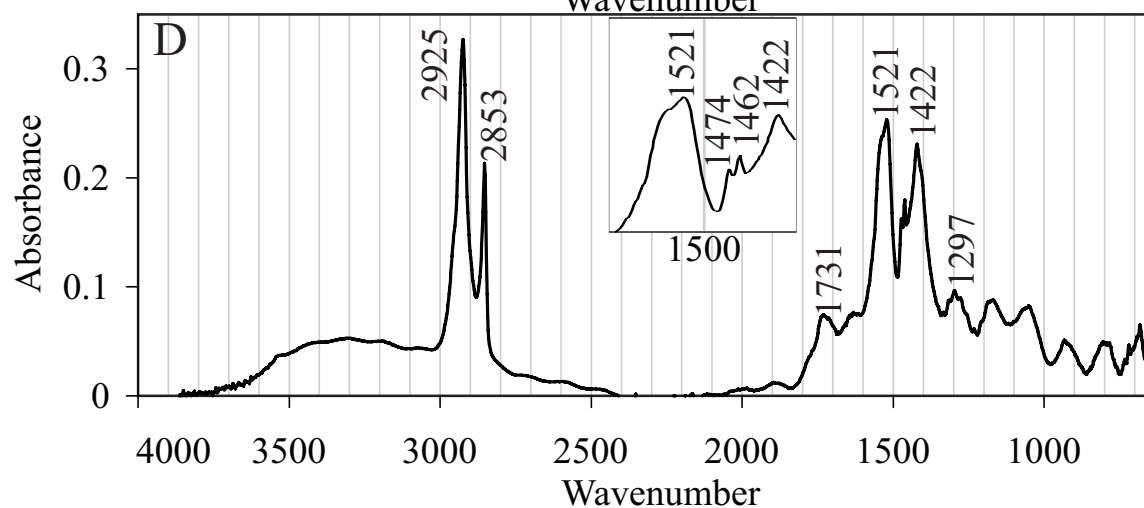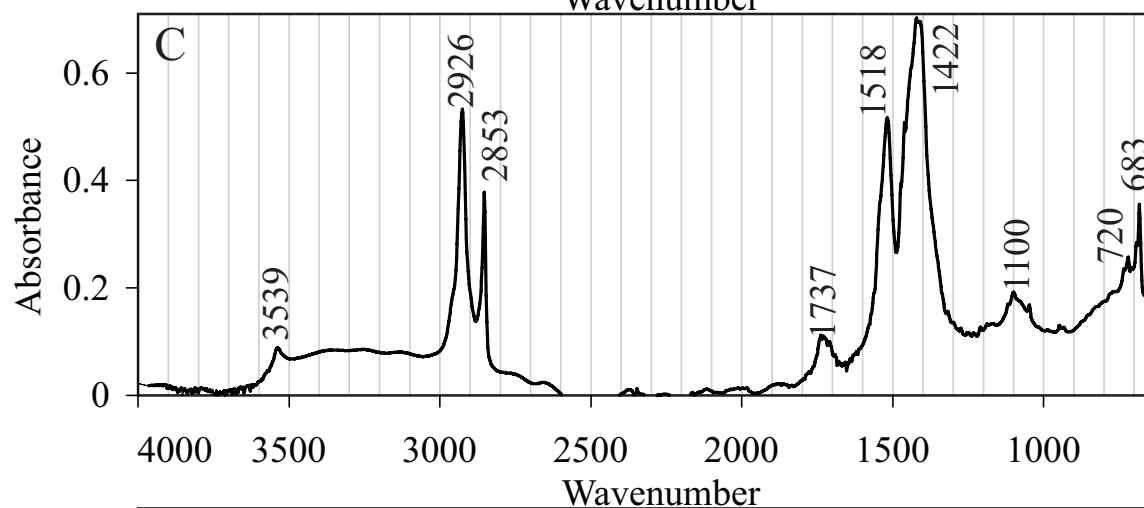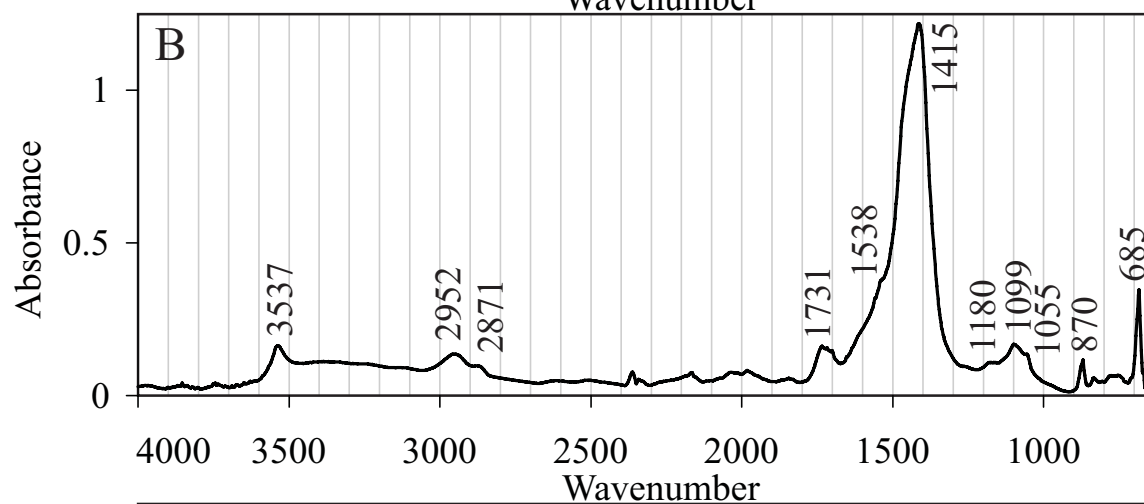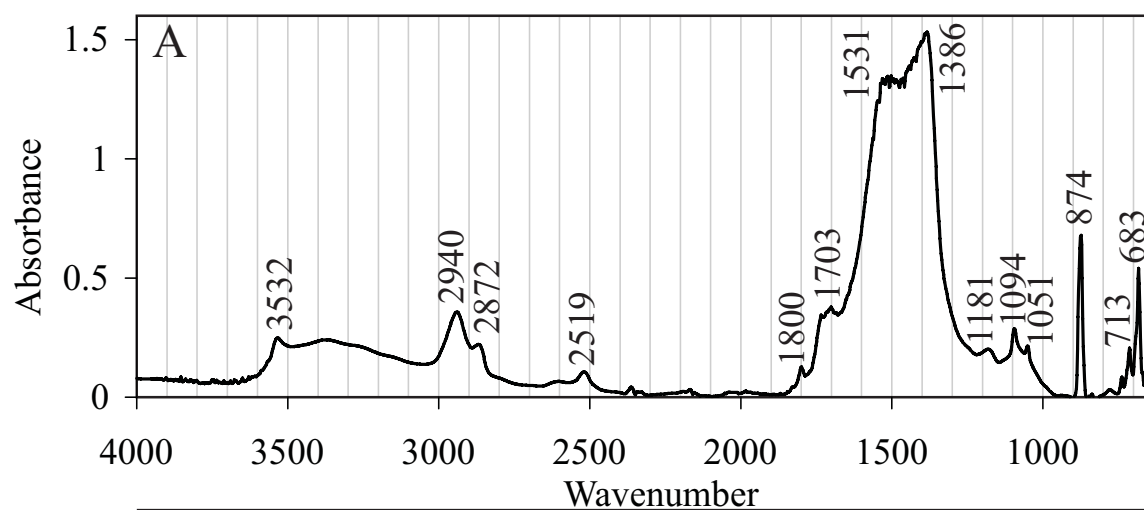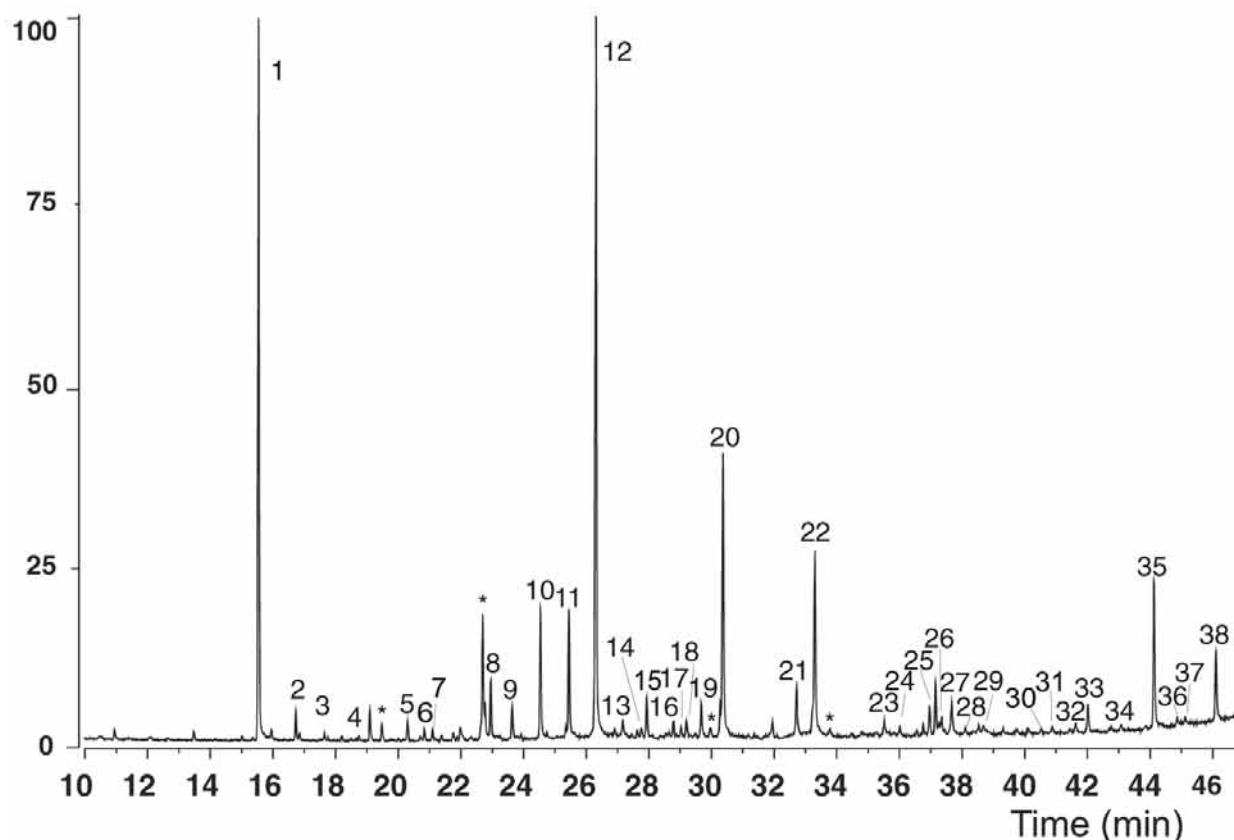
Fig. 7.6. Total ion chromatogram of the cream-coloured ground layer of OL.NA after transethylation and trimethyl silylation derivatisation in combination with GC-MS using an on-column injector. Temperature program: 50(2)-6-320. Peak numbers correspond to Table 7.2.

spectrum shows clear carbonate (1442 cm^{-1}) and carboxylate (1512 cm^{-1}) absorptions. The carbonyl absorption (1735 cm^{-1}) is rather low compared to the CH absorption (2924 and 2854 cm^{-1}, which indicates a low number of ester-bonds. The middle layer shows a broad carbonate absorption with a number of sharp peaks on top. These peaks (1566,1504, 1445, and 1381 cm^{-1}) are equally spaced, at about 60 cm^{-1}. A similar splitting is seen on the peaks on the left side of the spectrum. These effects are probably due to interference or an instrumental artefact and heavily affect the presented spectra. Therefore, a detailed interpretation is impossible. A similar effect is seen in the spectrum of the lower layer. Nevertheless, the presence of calcium carbonate in this layer can be concluded from subtle absorptions at 2512 and 1799 cm^{-1}. Unfortunately, these spectra do not allow a binding medium identification.

A chemical identification of the organic components in the paint was carried out by GC-MS. Results of the GC-MS measurements of the priming in OL1984.NA are presented in Fig. 7.6. The identification of the main components is presented in Table 7.2. Palmitic (C_{16}, label 19,20) and stearic (C_{18}, 21,22) acid are present in a ratio typically for linseed oils (P/S = 1.48). A range of oxidised C_{18} fatty acids (25-27) and di-acids (C_4-C_{10}, 2, 4-6, 8-18) are present as well. Azelaic acid (11,12), a C_9 dicarboxylic acid is the most abundant of these products. The relatively high amounts of other di-acids (C_8, C_{10}, 9, 10, 13, 15) are typical for a heat-treated oil. Traces of a series of even-carbon numbered long chain fatty acids (C_{20}-C_{30}, 23, 24, 28-31, 34, 36, 37, 39) and even-numbered alcohols (C_{26}-C_{30}, 33, 35, 38) indicate the presence of bees wax esters. Longer

Label	Retention Time	Compound	TMS Ethers [a]	Ester Bound
1	15.5	glycerol	1, 2, 3	
2	16.7	C4 di-acid		–
4	18.7	C5 di-acid		–
5	20.3	C4 di-acid	2	–
8	22.8	C7 di-acid		–
9	23.6	C8 di-acid		+
10	24.6	C8 di-acid		–
11	25.5	C9 di-acid		+
12	26.3	C9 di-acid		–
13	27.2	C10 di-acid		+
15	27.7	C10 di-acid		–
19	29.6	C16 FA		+
20	30.4	C16 FA		–
21	32.7	C18 FA		+
22	33.3	C18 FA		–
25	36.7–37.0	Oxo-C18 FA	8, 9, 10 mixture	
26	37.3	C18 FA	9, 10	+
33	42.0	C26 alcohol		
35	44.1	C28 alcohol		
38	46.1	C30 alcohol		

Table 7.2. *List of main compounds identified in the cream-coloured ground layer of sample OL.NA after transethylation/trimethyl silylation and GC-MS analysis using on-column injection. Identification is based on the 70 eV mass spectrum.*
[a] Position of alcohol groups, derivatised to TMS ethers. Data according to Van den Berg et al.[23]

Scans	Components
10–30	Fatty acids: **256** (C_{16}), **284** (C_{18}), **312** (C_{20}), **340** (C_{22}) Unidentified: **243**, **258**
30–45	Esters: **239** (C_{16}), **267** (C_{18}) Fatty acids: **312** (C_{20}), **340** (C_{22}), **368** (C_{24}), **382** (C_{25}), **396** (C_{26})
60–70	Oil network polymer and lead white: **44** (CO_2)
72–85	Oil paint: **91** (Aromatic pyrolysis product)
85–110	Lead white: **44** (CO_2), **206–208** (Pb)

Table 7.3. *Marker compounds identified by DTMS of the ground layer of OL1984.NA. DTMS results shown in Fig. 7.7.*

fatty acids and alcohols were not analysed as the GC-run was terminated before their elution. The degree of hydrolysis can be calculated from the relative amounts of ethylated and trimethylsilylated compounds.[19] The average degree of hydrolysis was found to be 88% for the components derived from the oil binder. Waxes are hydrolysed less severely than the paint. Samples taken from the imprimatura of OL1984.122 were also measured by this procedure. The results from this measurement are very similar to the results obtained from the ground layer, as presented in Fig. 7.6.

The physical state of the various components was studied by DTMS. Results of DTMS on the white priming layer of OL1984.NA are shown in Fig. 7.7. Assignment of several peaks is presented in Table 7.3. A TIC (total ion current) trace is shown as insert in Fig. 7.4A. This is an unusual desorption profile for an aged oil paint because of the high amount of volatile matter (scans 10-50). Free and esterified fatty acids of the oil network and waxes are detected at lower temperatures (scans 10-30, spectrum not shown). The appearance of long-chain material at scans 30-35 confirms the identification of bees wax by GC-MS. However, the source of wax is not clear, as this canvas has not been lined. A broad envelope of several low molecular weight pyrolysis products forms a typical pattern for oil network degradation products at scans 72-85 (Fig. 7.7B). DTMS results of the priming of OL1984.122 (results not shown) are similar to the results of OL.NA. The compounds identified in the imprimatura of OL1984.122 are also similar, but the TIC trace of this paint indicates that a lower amount of volatile products is present.

7.3.2 Protrusions

Fig. 7.2 shows an optical microscopic image of cross-section OL1984/3. The protrusion in this sample is visible as an expanded and transparent area. The mass has erupted through the thin imprimatura. The absence of imprimatura on top of the protrusion explains its good visibility at the paint surface (cf. Fig. 7.1).

The results of FTIR-imaging on paint cross-section OL1984/4 are presented in Fig. 7.8. The four plots in this Figure provide an overview of the intensities of the absorption peaks at four different wavenumbers, which are indicated in the plots. The brightness of the grey colour in these plots indicates the intensity of the corresponding peak. The intensity plot of the ester absorption at 1729 cm^{-1} (Fig. 7.8A) shows an outline of the sample due to absorption of the embedding medium. The broad carbonate ($CaCO_3$ or lead white) band at 1403 cm^{-1} is primarily observed in the intact paint layer (Fig. 7.8B). Figs. 7.8C and D highlight the protrusion because of their absorption at 1510 cm^{-1} and 2927 cm^{-1}, which are assigned to asymmetrical carboxylate and CH stretch vibrations. These reflection infrared imaging results indicate that the protrusions observed are comparable to the protrusions described for 17th century Dutch paintings.[118]

One of the protrusions was isolated manually and measured by FTIR in the transmission mode using a diamond cell (Fig. 7.4C), as reflection spectra of inhomogeneous materials such as paints suffer from low signal to noise ratios (S/N) and are difficult to interpret quantitatively (cf. Chapter 3 of this Thesis). Peaks at 1422, 3539, and 683 cm^{-1} indicate the presence of lead white in the protrusion. The intense, well resolved peaks for lead carboxylates (1518 cm^{-1}) and the sharp CH bands (2920 and 2853 cm^{-1}) confirm the results of reflection imaging data (cf. Fig. 7.8).

The results of DTMS on another manually separated protrusion are shown in Fig. 7.9 and interpreted in Table 7.4. The TIC-curve, shown as insert in this figure, shows a multiple-peak
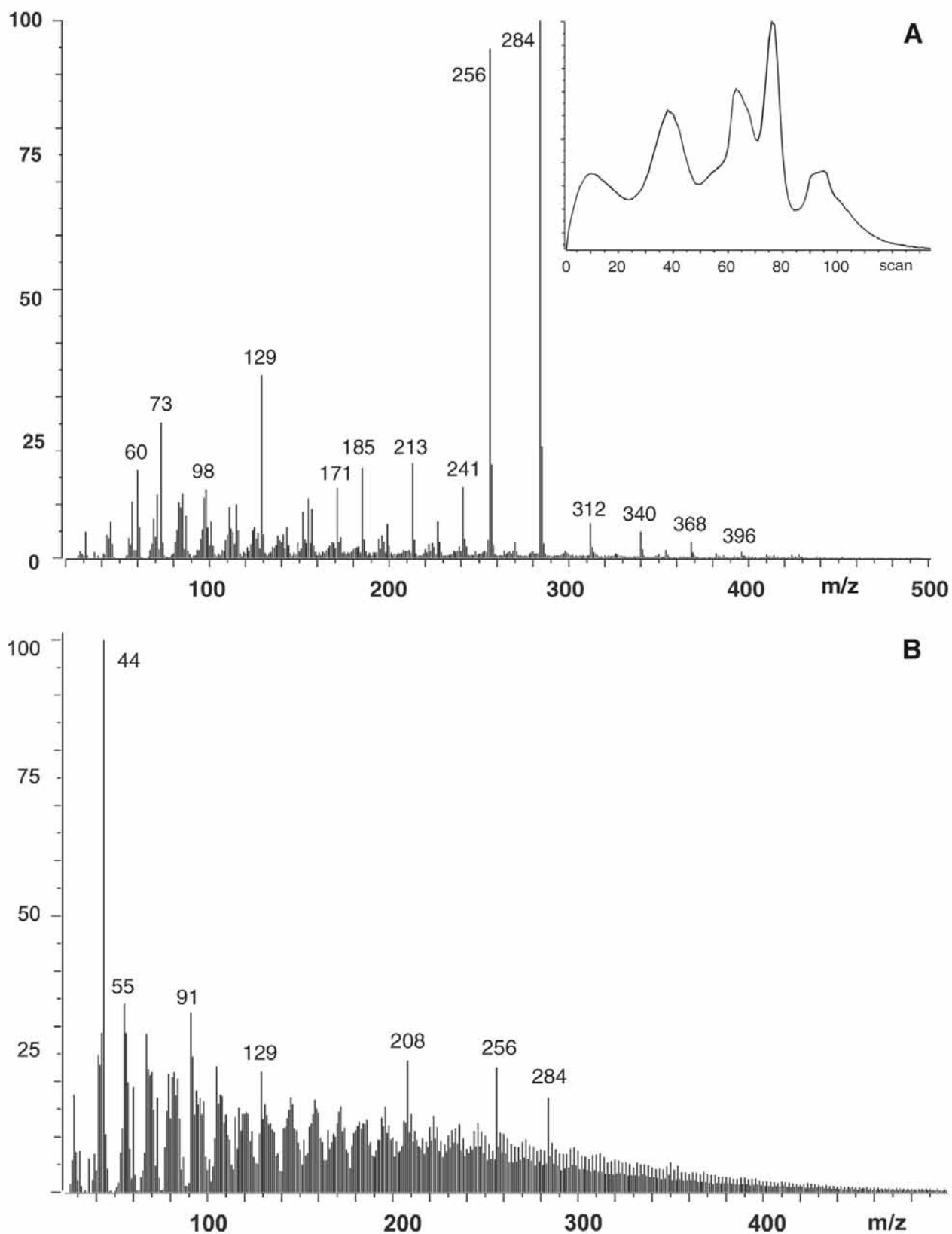
Fig. 7.7. *DTMS summation spectrum of OL1984.NA.* (**A**) *scans 30-45, insert: TIC, and* (**B**) *scans 72-85.*

desorption profile. Free fatty acids are observed at low temperatures (scan <50), while the desorption of lead soaps at higher temperature (scans 50-60) is indicated by the peaks at m/z 463 ($C_{15}H_{31}COOPb$) and 491($C_{17}H_{35}COOPb$). The TIC profile shows no distinct signal in the region where normal aged paint shows pyrolysis of the oil network (scans 70-80). Traces of lead are detected at high temperatures (scans >80).
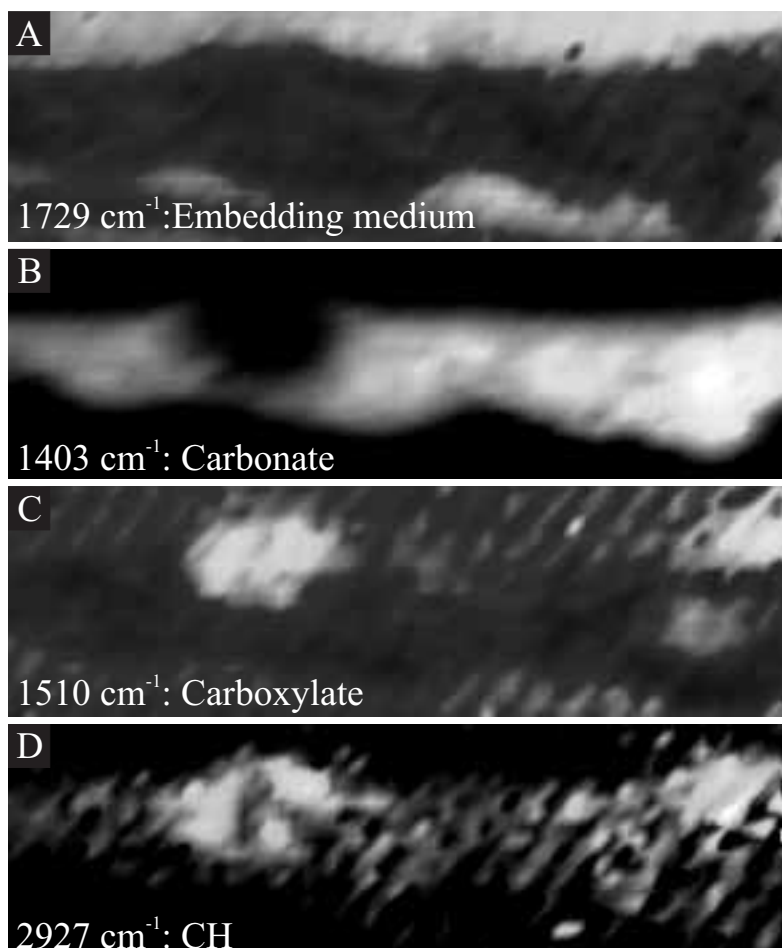

Fig. 7.8. *Imaging-FTIR imaging of embedded paint cross-section OL1984.122/3. White representation in these images implies a high absorption at the wavenumber indicated in the figure.*

Scans	Components
10–30	Fatty acids: **256** (C_{16}), **284** (C_{18}), **312** (C_{20}), **340** (C_{22})
50–60	Lead carboxylates: **463** (C_{16}), **491** (C_{18})
> 60	Lead white: **206–208** (trace Pb), **44** (CO_2), No oil polymers

Table 7.4. *Marker compounds identified by DTMS of a protrusion isolated from OL1984.NA. DTMS results shown in Fig. 7.9.*
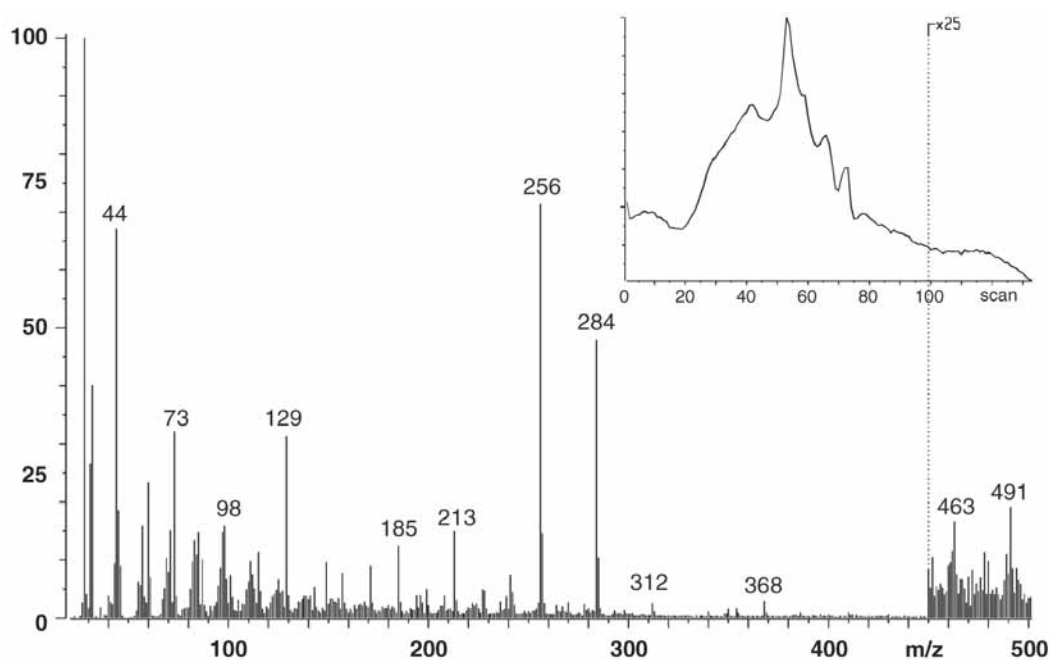
Fig. 7.9. DTMS summation spectrum of scans 50-60 of a protrusion in paint OL.NA. Insert: TIC. Interpretation of this analysis is presented in Table 7.4.

7.3.3 Efflorescence

Efflorescence can hardly be analysed in cross-section, as it is present only in a thin layer, easily damaged by embedding. Therefore, surface analyses were carried out directly on the surface of a small part of OL1984.122. The efflorescence pattern could easily be found in a backscattered SEM-image (see Fig. 7.10A), as it has a lower backscatter intensity than the uncovered imprimatura. This lower backscatter intensity is caused by a high carbon content (C, Fig. 7.10B) in the efflorescence. Other elements are more abundantly present in the imprimatura (Pb, O, Al, Si, Ca, Fe). The intensity plots for O and Al are shown in Figs. 7.10 C and D.

FTIR was applied to characterise the organic functional groups in the efflorescence. A microscopic ATR crystal was used to acquire transmission infrared spectra directly from the surface of the paint without the need for sampling. However, the high carbonate absorption (1400 cm^{-1}) in the ATR spectra (not shown) indicates that not only material from efflorescence is sampled, but also from the intact paint. The pressure applied on the ATR crystal for optimal contact with the sample might very well have displaced the pliable efflorescence layer. Therefore, the efflorescence on the surface of OL1982.122 was also measured using specular reflectance. The resulting spectrum, part of which is shown in Fig. 7.11, has a relatively poor overall quality, but nicely shows the mere absence of carbonates (1400 cm^{-1}) and carboxylic acids. Instead, the most pronounced features of this spectrum are the large carboxylate absorptions (1541, 1516, 1416 cm^{-1}). The CH bend vibrations give rise to two sharp, nicely resolved peaks at 1473 and 1462 cm^{-1}. The CH stretch vibrations show two sharp peaks (2922 and 2851 cm^{-1}, outside the spectral region presented). These sharp peaks indicate the presence of mainly non-oxidised, saturated fatty acids. These results were confirmed by a transmission spectrum of manually isolated efflorescence, shown in Fig. 7.4D. Intense and sharp CH absorptions (2925, 2853, 1474, 1462, and possibly 720 cm^{-1}) and metal carboxylates absorptions (1520 and 1422 cm^{-1}) also dominate this
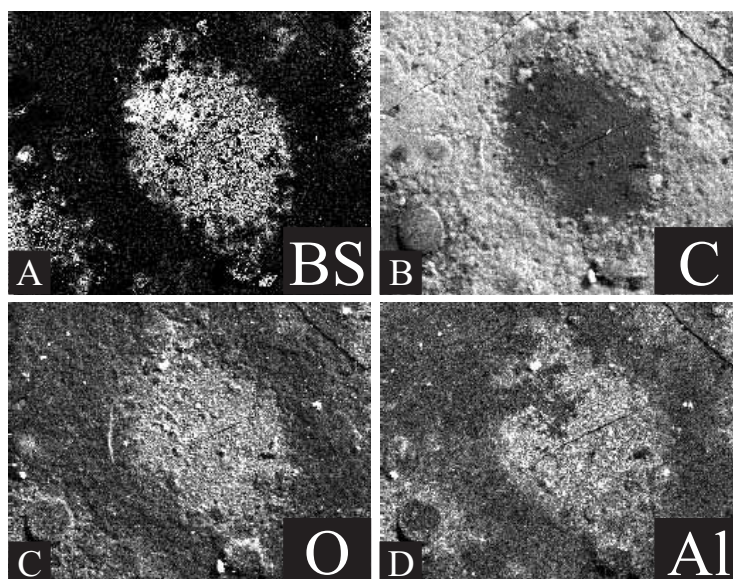
Fig. 7.10. *Results of SEM-EDX directly on the paint-surface of OL1984.122 (compare to optical image in Fig. 7.1.). (A) Backscatter SEM image. (B)-(D) EDX maps of carbon, oxygen and aluminium respectively.*
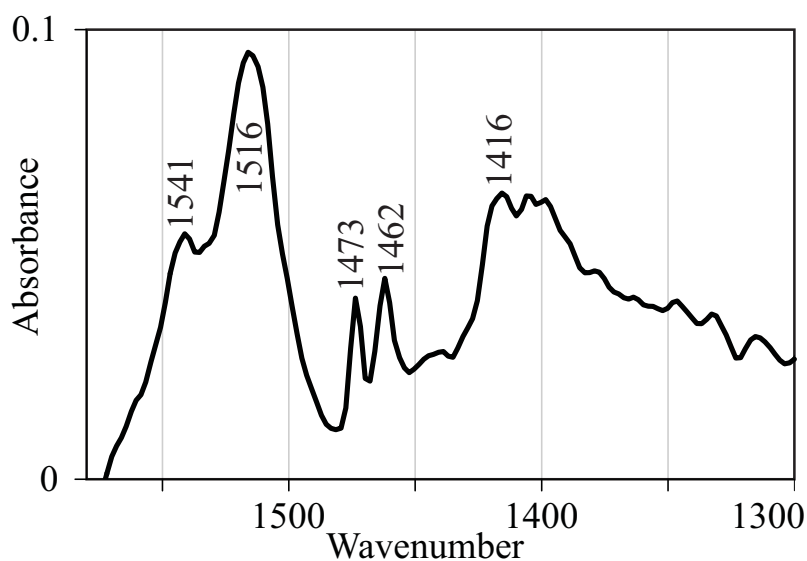

Fig. 7.11. *Specular reflectance FTIR spectrum directly on the paint surface of OL1984.122.*

spectrum. This spectrum shows that the amounts of free carboxylic acids and esters (1710–1740 cm^{-1}) are small, while the amount of lead white (681, 3535 cm^{-1}) is negligible. The broad peaks on the long wavelength side of the spectrum are probably due to interference. The EDX and FTIR measurements clearly show the abundant presence of lead carboxylates in the efflorescence layer. The sharp absorption peaks for the various CH vibrations indicate a homogeneous, non-oxidised, and non-polymerised aliphatic fraction.

DTMS analysis of the efflorescence isolated from the ground layer of sample OL1984.122 (see Fig. 7.12 and Table 7.5) indicates that it consists mainly of relatively volatile components. Fatty acids are desorbed at low temperatures. Lead soaps, as observed at higher temperatures,
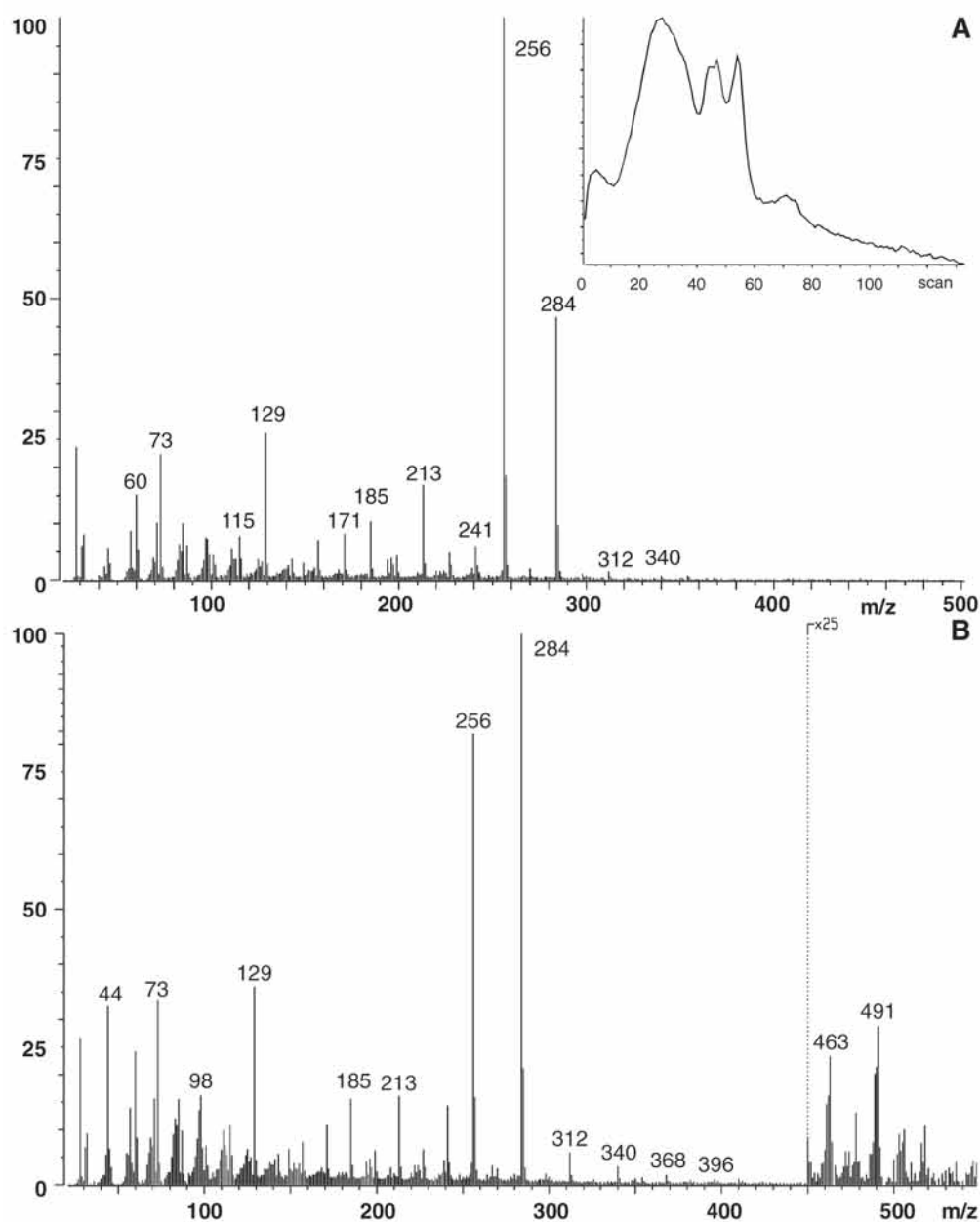
Fig. 7.12. *DTMS summation spectrum of efflorescence on surface OL1984.122.* **(A)** *Scans 1-25, insert: TIC.* **(B)** *Scans 33-50.*

Scans	Components
1-25	Fatty acids: **256** (C_{16}), **284** (C_{18}), **312** (C_{20}), **340** (C_{22})
20-30	Diacylglycerols: **550** (C_{16}, C_{16}), **578** (C_{16}, C_{18}), **606** (C_{18}, C_{18}) Wax esters: **648**, **676**, **704**
33-50	Lead carboxylates: **463** (C_{16}), **491** (C_{18}), **239** ($C_{15}H_{31}CO^+$), **267** ($C_{17}H_{35}CO^+$)
> 60	**206–208** (Pb), **44** (CO_2), No network pyrolysis

Table 7.5. *Marker compounds identified by DTMS of efflorescence isolated from OL1984.122. DTMS results shown in Fig 7.9.*

are rarely seen in an aged paint system and indicate that appreciable amounts of saturated lead soaps are present in the efflorescence material. There is no indication for pyrolysis products of oil from network constituents.

SIMS was applied to directly analyse inorganic and organic materials directly from the upper surface of the paint layer. Results from OL1984.122 are presented in Fig. 7.13. Ions indicative for palmitic and stearic fatty acids are seen at m/z 255 (C_{16}) and 283 (C_{18}). Both free and esterified fatty acids are known to produce these ions in SIMS.[173] Saturated fatty acids are also observed in the positive mode at m/z +257 (C_{16}+H) and m/z +285 (C_{18}+H). SIMS-studies on reference materials (results not shown) indicated that these ions derive from free or metal bound fatty acids rather than from esterified fatty acids, as esters would also give rise to acylium ions [R−C≡O]$^+$. Mono- and diacylglycerols esters are however observed at m/z 313 (C_{16}), 341 (C_{18}), 369 (C_{20}), 397 (C_{22}), 551 (C_{16}, C_{16}), 579 (C_{16}, C_{18}), and 607 (C_{18}, C_{18}). Lead soaps and their basic forms are observed at m/z 463 (C_{16}-Pb), 491 (C_{18}-Pb), 685 (C_{16}-PbOPb) and 713 (C_{18}-PbOPb), with a typical lead isotopic distribution. These findings confirm the observation of lead soaps of saturated fatty acids, as hypothesised on the basis of EDX, FTIR and DTMS.

The most abundant peaks in the positive mode spectrum are due to inorganic lead oxides and lead hydroxides (430 (Pb_2O), 654 (Pb_3O_2), 878 (Pb_4O_3), 225 (PbOH), 447 (Pb_2O_2H), 671 (Pb_3O_3H), etc). These compounds most likely originate from lead white due to thermal processes induced by the primary ion beam. A similar reduction of lead has been observed when irradiating lead white with a Nd: YaG laser.[174] PbO clusters of unknown identity are observed above mass 1000 with a mass increment of 224 (PbO).

7.4 Discussion

7.4.1 Paint

The investigated canvases have been prepared with a number of ground layers. A rationale for the complex layer structure of the priming, shown by the backscattered SEM image in Fig. 7.3, has been described before.[164] These layers cannot be dissected accurately using a scalpel, as their colour is very similar. Therefore, a mixture of these layered has been analysed in cases were an isolated sample is needed. GC-MS measurements indicated a preheated linseed oil, in which 88% of the original ester bonds in the oil have been hydrolysed. Both GC-MS and DTMS show the presence of fatty acids in the paint system (Figs. 7.4 and 7.5). The relative amounts of the free fatty acids is however low, as they are hardly seen in FTIR measurements. Instead, FTIR indicates that the priming layer contains a considerable amount of carboxylates (Fig. 7.6A). The amount of metal carboxylates is not homogeneous throughout the paint system. The infrared spectrum of the imprimatura (Fig. 7.6B) shows a far lower amount of carboxylates than the priming (Fig. 7.6A). This might be caused by different qualities of the lead white, as well as differences in the thickness, drying time, and/or paint composition. The extensive lead soap formation in the ground layer must go along with a dissolution of lead white particles and hence a reduced scattering power of the paint. This will lead to a longer effective path length of light in the priming layer, especially when deeper, transparent chalk/distemper layers are penetrated. These provide a good indication for the cause for ground staining, although an extensive comparison between stained and unstained parts of a painting is left for future research. Dwyer stated
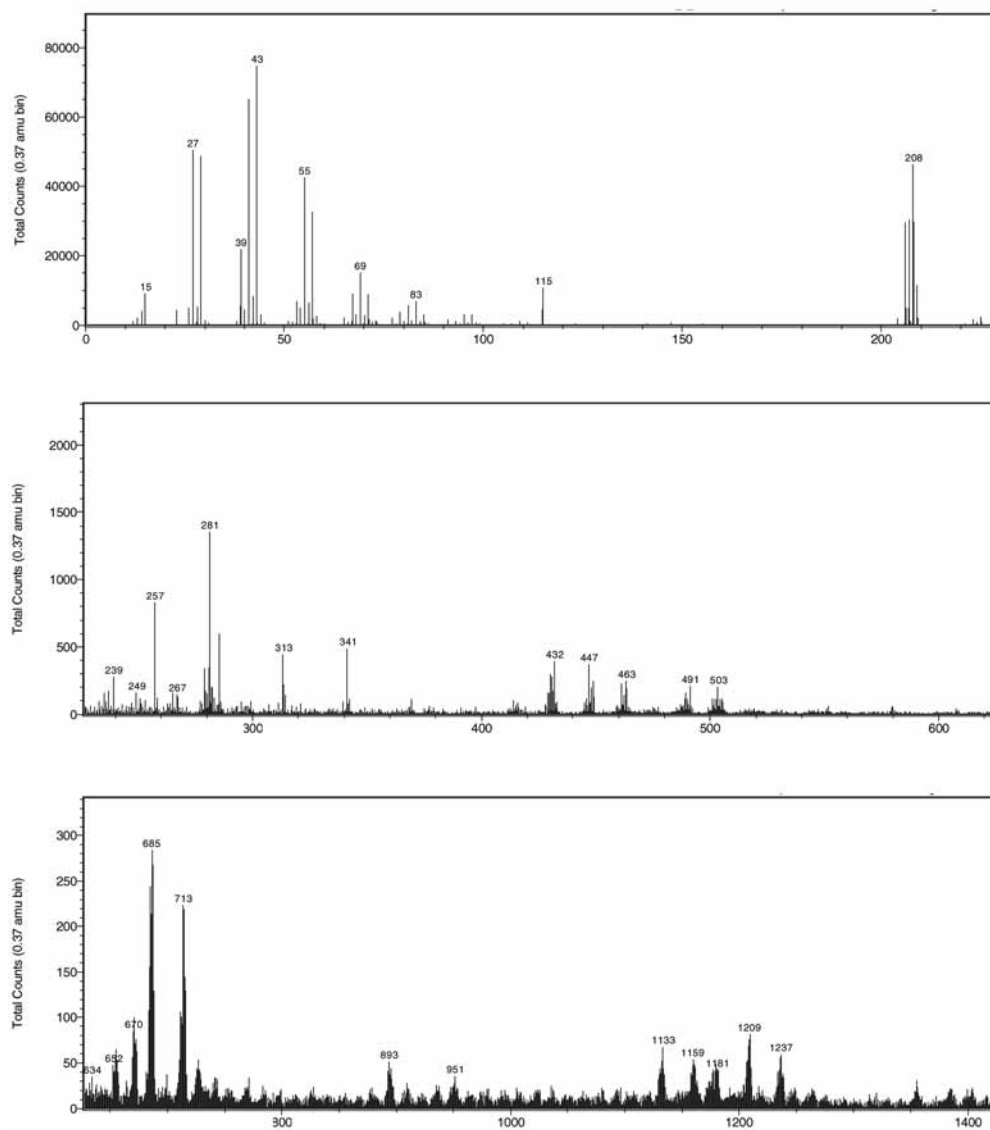
Fig. 7.13. *SIMS spectrum of the surface of sample OL1984.122.* **(A)** *Mass range m/z 0-230.* **(B)** *Mass range m/z 230-620.* **(C)** *Mass range m/z 625-1425.*

that ground staining is the result of transformation of lead white into transparent crystals.[166] It could very well be that she actually observed protrusions, far before this name was given to this phenomenon.

7.4.2 Protrusions and Efflorescence

Several measurements on protrusions and bloom indicate that these phenomena have important similar characteristics. Both were found to contain high amounts of saturated lead carboxylates (DTMS). The carboxylate absorptions found by FTIR (Figs. 7.4 C and D) are narrow peaks, exactly on the literature value for saturated lead carboxylates (1515 cm^{-1}).[145] They are unlike the broad shoulder found for the carboxylates in the intact paint (Fig. 7.4A). Also the CH absorptions in bloom and protrusions (narrow, 2925, 2853 cm^{-1}) strongly differ from the intact paint (broad, 2940, 2872 cm^{-1}). In fact, the CH absorptions in bloom and protrusions resemble the sharp absorptions of fresh linseed oil (2928 and 2866 cm^{-1}). The infrared spectral changes upon artificial ageing of drying oil have been detailed by Mallegol.[27,28] This work reports a shift in band position (to ~2950 cm^{-1}) and an absorption intensity drop (60%) of the original intensity upon artificial ageing of an oil film. Rasti and Scott even report a 92%-decrease of absorption intensity at 2930 cm^{-1} ($\log A_0/A_1 = 1.1$) for a vermilion pigmented paint film.[38] It is unlikely that the loss of volatile aliphatic materials during ageing suffices to explain this decrease, but a better explanation has not yet been given. It is proposed here that extensive oxidation and polymerisation of the oil system reduces the intensity of CH vibration peaks (cf. Chapter 5 of this Thesis). The aliphatic absorptions of protrusions and efflorescence are still intense, sharp, and at the original position, suggesting a non-oxidised organic fraction. This is confirmed by DTMS, which showed the abundant presence of saturated fatty acids, but no or very little evidence for the presence of an oil network (Figs. 7.9 and 7.12). It is concluded that efflorescence originates from the exudation of saturated fatty acids in the paint. The expanded volume of protrusions (Figs. 7.1 and 7.2) indicates that they are caused by clustering of these saturated materials. Both mechanisms basically are phase separations, for which mobility of the involved materials is necessary. Saturated fatty acids are indeed mobile, as they do not take part in the network formation.[108] These mobile materials can form a considerable part of the paint system, as linseed oil normally contains about 10% saturated fatty acids, 85% of which has been hydrolysed from glycerol (GC-MS results in Fig. 7.5). Furthermore, the mobile fraction can also include other molecules that are not trapped in the oil network, such as wax esters.

A spontaneous phase separation would violate the second law of thermodynamics and therefore an energetic driving force must be present. Teixeira[175] mentions a phase separation upon partial polymerisation in a mixture of monomers and other molecules, a system very similar to the mobile fraction in aged oil paint. The imbalance in aged oil will be increased by differences in polarity of the mobile and the stationary phase of the paint. The mobile fraction of saturated fatty acids is relatively apolar, while the polarity of the oil network increases due to the formation of oxygen containing moieties, such as carboxylic acids, aldehydes and ketones. A mismatch in polarity between mobile and stationary phases in paint might very well be the driving force for a phase separation and hence the direct reason for instabilities like protrusion formation and efflorescence.

Lead white might act as a nucleation or immobilisation site and thereby trigger the process of protrusion formation. A pilot test carried out indeed shows that lead white can be transformed

easily into lead stearate upon reaction with stearic acid. An FTIR spectrum of the reaction product (Fig. 7.14) shows the complete absence of carbonate absorption, indicating that the lead white reacted quantitatively. The spectrum shows absorption peaks for the lead carboxylate groups (1541, 1522 cm^{-1}) and aliphatics (2960, 2828, 2853, 1475, 1462, 735, 720 cm^{-1}). The small features at 1475 and 1462 cm^{-1} confirm the similarity of the synthesised lead stearate (Fig. 7.14) and the compounds present in the efflorescence (Figs. 7.4D and 7.11). The pilot experiment was carried out in boiling xylene, which is far above the temperatures to which normal paintings are normally exposed. However, the described reaction was finished quantitatively within a few minutes, and it seems likely that similar reactions also will take place at lower temperatures, albeit at a lower rate.

The mechanism for the formation of protrusions and efflorescence described above provides a sound explanation for a number of observed characteristics. The previous Chapter of this Thesis describes a common feature of protrusions: the high absorption of the CH stretch vibration at 2925 cm^{-1}.[118] The high intensity of these absorptions, also observed in Fig. 7.8, is confirmed by the transmission measurements in Fig. 7.4 and is due to the aggregation of organic materials in protrusions. This aggregated material is mostly saturated, and is therefore not affected by the loss of CH absorption intensity associated with oxidation. The high abundance of saturated fatty acids also explains the remarkable observation of lead stearate and lead palmitate in the DTMS results (Figs. 7.9 and 7.12). The presence of lead carboxylate materials further explains the observed insolubility of the efflorescence.
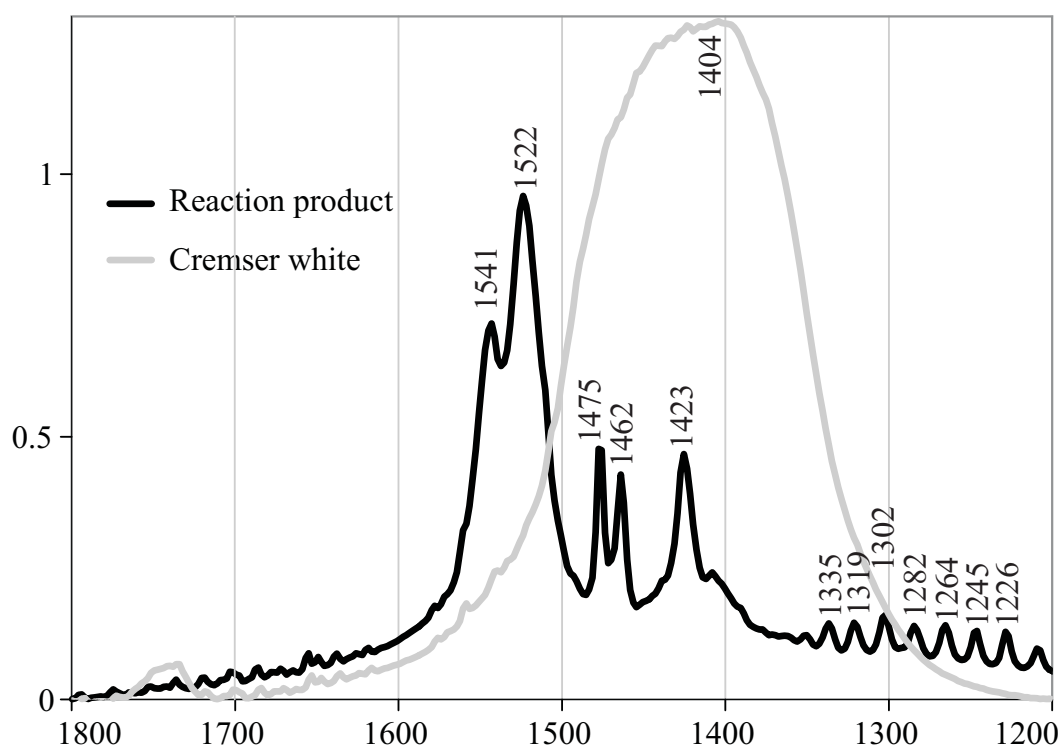

Fig. 7.14. *Infrared analysis of the products of the reaction between stearic acid and lead white (black spectrum). The grey spectrum shows a normal lead white spectrum as a reference.*

An important next question is what the conditions could be that lead to efflorescence and/or protrusions. A detailed quantitative answer to this question cannot be based on the presented results, but the proposed mechanism provides some clues on the circumstances that can increase the sensitivity of paint.

The carboxylate formation is dependent on the availability of metal ions and free fatty acids. The metal ions can only be dissolved from a pigment particle, if the specific pigment is sensitive for free fatty acids, in a way similar to lead white (cf. Fig. 7.14). Pigments are normally abundantly present in paint and therefore the availability of free fatty acids is thought to determine the final reaction rate. The amount of free fatty acids is dependent on numerous factors. An important factor is the relative amount of oil originally present in the paint. Another factor inherent in the paint is the absence of sufficient trapping potential for the fatty acids released by hydrolysis upon ageing. Part of the fatty acids form lead soaps in the lead white containing layers, another part reaches the surface where it forms efflorescent material. Esterified fatty esters begin to play a role in phase separation and metal carboxylate formation after their hydrolysis from glycerol. Certain pigments, e.g. lead white, can accelerate hydrolysis. Furthermore, hydrolysis is enhanced by temperature and humidity, which partly explains the frequent observation of these instabilities in paintings that are stored in the humid and warm climate of the New York region. The high local temperature might also lead to a high mobility of the fatty acids through the paint layer and thereby reduce the time needed for phase separation. We propose that the manufacturers of the preprimed canvas were applying a medium rich ground with a low buffering capacity.

Summarising, the formation of bloom and protrusions in the present cases is mainly caused by the high amounts of free fatty acids released in the paint. The high levels of fatty acids are due to the high amount of binding medium in the paint, and probably increased by the presence of metals, and the humid and warm climate in which the paint has resided. The capacity of the paints to trap these high amounts of fatty acids in the normal way, as well as the evaporation from the surface of the painting is clearly insufficient. The accumulation of fatty acids in the paint layer enables the extensive lead carboxylate formation due to reaction with lead white particles, similar to the pilot experiment presented in Fig. 7.14. This trapping immobilises the fatty acids. Protrusions are formed on places where the rate of carboxylate formation is high. The reason for these non-homogeneous reactions can be explained by phase separation of the mobile fatty acids. Autocatalysis of the reaction between lead white and fatty acids might be another hypothesis, but no indications were found for such a process. Efflorescence can be explained by the carboxylate formation of fatty acids, after accumulation of these surface-active compounds on the surface of the painting.

7.5 Conclusions

This study focusses on the investigation of different deterioration effects found in 19th century American paintings, i.e. efflorescence, protrusions and ground staining. It is shown that efflorescence and protrusions are caused by an instability in the ground layer. This instability causes a phase separation between saturated fatty acids and the oil network. The isolated fatty acids mostly react to lead carboxylates. The correlated degradation of the lead might cause the ground staining effects. The presented study confirms the similarity of the protrusions found in the 19th century canvas to those observed before in several 17th century paintings. The proposed mechanism for the formation of these protrusions is therefore considered to be valid also in these cases. The dissolution of lead white might provide an explanation for the increased transparency of the ground layer and hence to the defect called ground staining. A closer investigation of this effect is however left for further research.

7.6 Acknowledgements

8   ZINC SOAP AGGREGATE FORMATION IN 'FALLING LEAVES (LES ALYSCAMPS)' BY VINCENT VAN GOGH

Surface defects have been found recently in Falling Leaves (Les Alyscamps)*, painted by Vincent van Gogh in the autumn of 1888. These defects have been analysed to comprehend their nature and origin. Embedded cross-section and isolated samples of this painting have been investigated by microscopy, infrared spectroscopy, and FTIR-imaging, SEM-EDX, DTMS. The analyses show that the material found in the defects consist of aggregated masses of zinc carboxylates, which sometimes contain zinc white (ZnO). The carboxylic acid part of the zinc carboxylates consist of saturated fatty acids. The paint in which these defects are found contains lead chromate, barium sulphate (baryte), calcium sulphate (gypsum) in an oil binding medium. Traces of zinc were found throughout the paint layer. The mobility of metal soaps in this paint layer was demonstrated by an FTIR study of the paint after squeezing in a diamond anvil cell.*

8.1 Introduction

Routine investigation of *Falling Leaves (Les Alyscamps)*, painted by Vincent van Gogh in the autumn of 1888 (Fig. 8.1, Kröller Müller Museum, Otterlo, the Netherlands, inv. no. 224, F486), revealed the presence of small defects in the extended orange regions of this painting. These thousands of surface defects look like small whitish or transparent spots in the paint surface. In some cases, a whitish mass is literally pressed out of a crack in the paint surface (see Fig. 8.2). These extrusions occurred only after the latest varnish application, because the varnish is cracked open by the extruding matter, which is deposited on the varnish surface.

The phenomenon of material protruding from a paint surface has recently been investigated in several 17th century Dutch paintings.[118,152] In these paintings, accumulated masses of a whitish material protrude through the surface of paint layers and thereby manifest themselves on the surface of the painting. These so-called 'protrusions' clearly differ from the original paint, as they are devoid of pigment particles and have a transparent appearance. Furthermore, they show clear fluorescence upon illumination with ultraviolet radiation. Chemical analysis showed that these transparent masses mainly consist of lead carboxylates, i.e. molecules that contain an ionic bond between lead ions and carboxylic acids. It has been concluded that the metal ions originate from the lead white pigments, which dissolve in the paint layer. Carboxylic acids are formed in paint by oxidation of unsaturated fatty acids[131] or hydrolysis of esterified fatty acids. Fatty acids are not immediately available in fresh paint and the time needed for hydrolysis can be several decades.[19] The research described in the previous Chapter of this Thesis indicates that hydrolysed saturated fatty acids (palmitic and stearic acid) are the most important carboxylic acids in protrusions found in a 19th century painting. The presence of similar defects in other 19th century paintings has also been found by other investigators.[158,159]

The similarities of the 17th and 19th century protrusions to the defects found in the orange paint of *Falling Leaves (Les Alyscamps)* suggests that they are caused by a similar mechanism, and maybe by the same compounds, i.e. metal carboxylates. The present work aims at a verification or rejection of this hypothesis by a detailed analysis of the paint and especially the materials found in the defects.

8.2 Experimental

Samples

The paint samples examined in this paper are taken from *Falling Leaves (Les Alyscamps)*, painted in 1888 by Vincent van Gogh (Museum Kröller Müller, Otterlo, the Netherlands, Inv. no. KM224). A summary of the analysed samples is presented in Table 8.1. Their sample positions are indicated in Fig. 8.1. Sample 224/2a is embedded in Technovit 2000LC (Heraeus Kulzer, Wehrheim, Germany) and polished with Micromesh® (Scientific Instrument Services Inc.) polishing cloths. Thin samples necessary for transmission FTIR and transmission optical microscopy were obtained by squeezing a sample in a Graseby Specac p/n 2550 diamond cell (Graseby Specac, Orpington, Kent, UK).
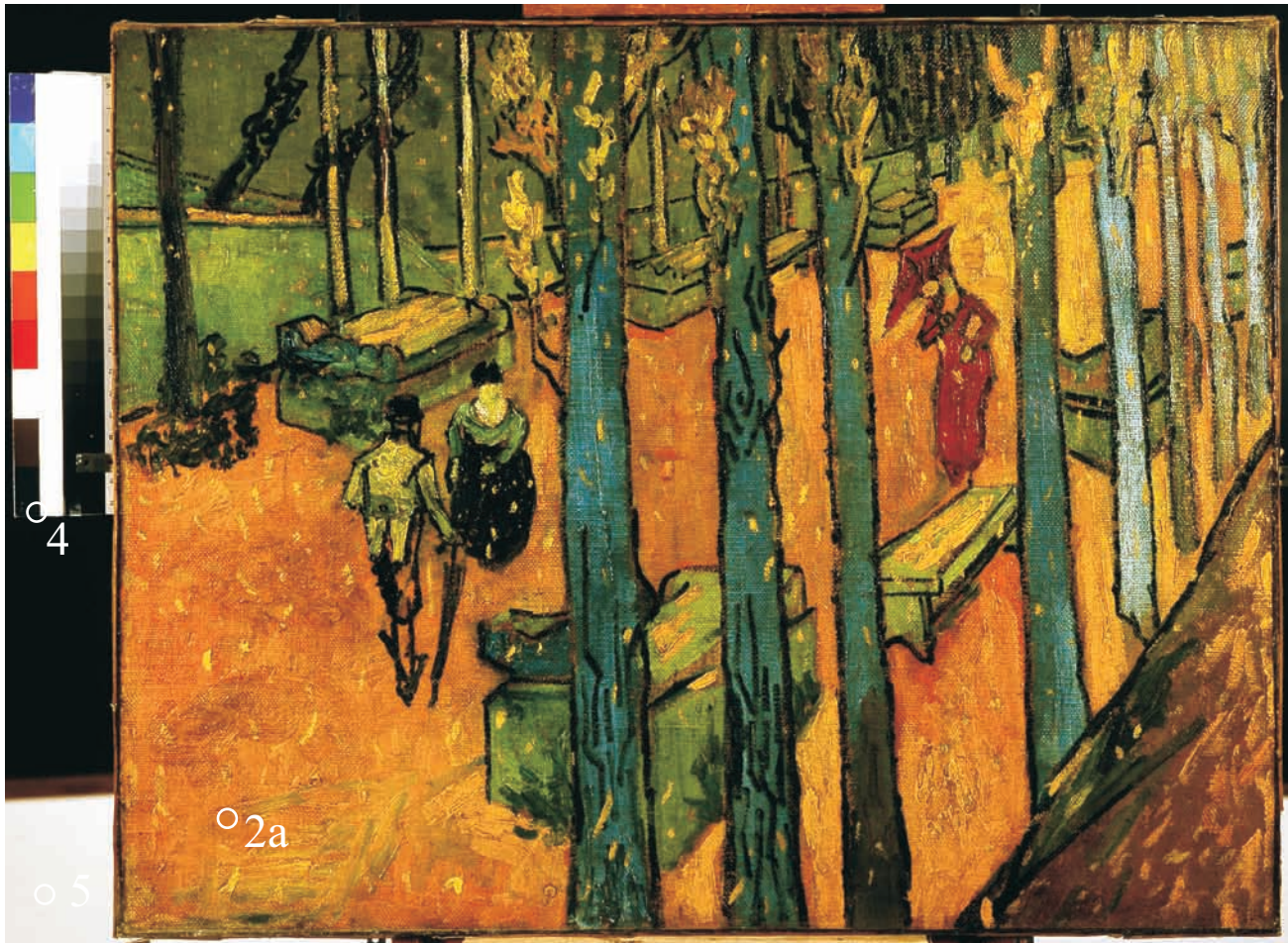
Fig. 8.1. Falling Leaves (Les Alyscamps) *by Vincent van Gogh, 1888 (Museum Kröller-Müller, Otterlo, the Netherlands, Inv. Km224, F486)*
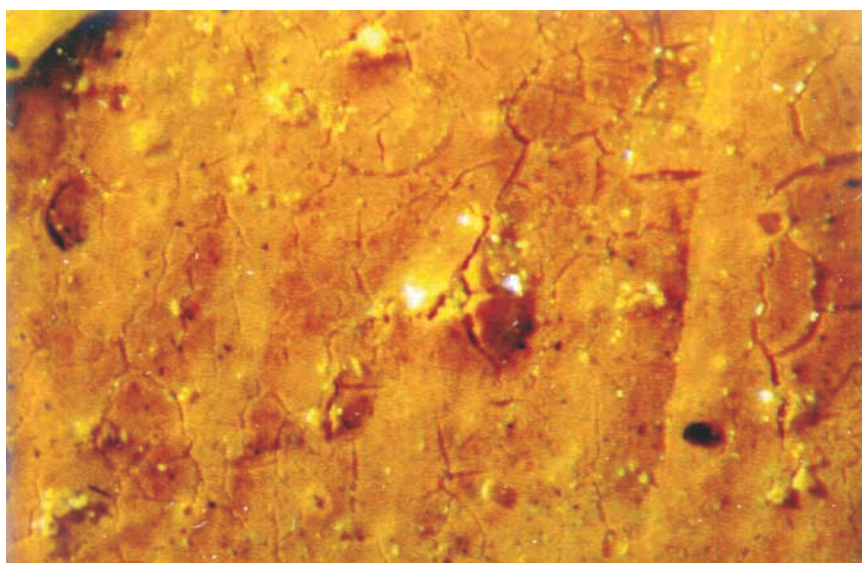*(coloured version at the end of this Thesis)*

Fig. 8.2. *Macro-photograph of a detail in the orange paint surface of* Falling Leaves (Les Alyscamps).
(coloured version at the end of this Thesis)

Microscopy

A Leica DMRX analytical microscope (Leica Inc., Wetzlar, Germany) was used for visual light microscopy. An XL30 SFEG SEM (FEI company, Eindhoven, the Netherlands) equipped with an EDAX EDX system was used for the SEM-EDX analysis. The accelerator voltage of the system was 22 kV. The sample was carbon coated to ensure good conducting properties of the surface.

FTIR

FTIR spectra were acquired by a Bio-Rad FTS-6000 spectrometer (Nowadays Digilab, Cambridge, MA, USA), equipped with a Bio-Rad UMA 500 infrared microscope and an MCT detector. Single point spectra were recorded at a spectral resolution of 4 cm^{-1}, a mirror speed of 5 kHz, and an UDR (undersamling ratio) of 2. 100 spectra were accumulated to optimise the Signal-to-Noise ratio (S/N).

FTIR-imaging

FTIR-imaging data were acquired using the Bio-Rad Stingray, combining the FTS 6000 spectrometer and infrared microscope mentioned above with a 64×64 MCT camera.[66,75] Analysis of the embedded cross-section was carried out in reflection mode. Reflection spectra were recorded with a 16 cm^{-1} spectral resolution, a step-scan frequency of 1 Hz, and an UDR of 4. The spectra were transformed to absorbance-like spectra by the Kramers-Kronig transformation, which is part of the Bio-Rad Win-IR Pro software. Transmission spectra were recorded using the same apparatus at a spectral resolution of 8 cm^{-1}. The different spectra in the data-sets were clustered using the projection-method described in Chapter 2 of this Thesis. This algorithm calculates the similarity between a single spectrum selected from the normalised data-set and the other spectra in the data-set by means of a dot product. Spectra with a high similarity are clustered and the location of three clusters is visualised using RGB-plots. The (not-normalised) spectra within a single cluster are subsequently averaged to increase the signal to noise ratio. All projection and visualisation algorithms were developed in Matlab 5.2 (The Mathworks, Inc., Natick, MA, USA).

DTMS

Samples of typically 20 to 60 μg were homogenised in ethanol using a mini-glass mortar. Aliquots of the obtained suspension or extracted materials were applied onto the analytical filament and dried *in vacuo*. DTMS analyses were performed on a Jeol SX-102 double focussing mass spectrometer (B/E) using a direct insertion probe equipped with a Pt/Rh (9/1) filament (100 micron diameter). The probe filament was temperature programmed at a rate of 0.5 A/min to an end temperature of about 800 °C. Compounds were ionised at 16 eV under electron ionisation conditions in an ionisation chamber kept at 180 °C. Masses in the range m/z 20–1000 were analysed with a cycle time of 1 second. The results were processed using a JEOL MP-7000 data system.

Sample	Position	Pretreatment	Measurement
KM224/2a	Cross-section	Embedded	SEM-EDX Imaging-FTIR
KM224/4	Paint/protrusion	Diamond cell	FTIR, Imaging-FTIR
KM224/5	Paint	Diamond cell	FTIR, Imaging-FTIR DTMS
KM224/6	Varnish	Diamond cell	FTIR DTMS
KM224/prot	Protruded material	Diamond cell	FTIR
KM224/relining	Relining material	Diamond cell	FTIR DTMS

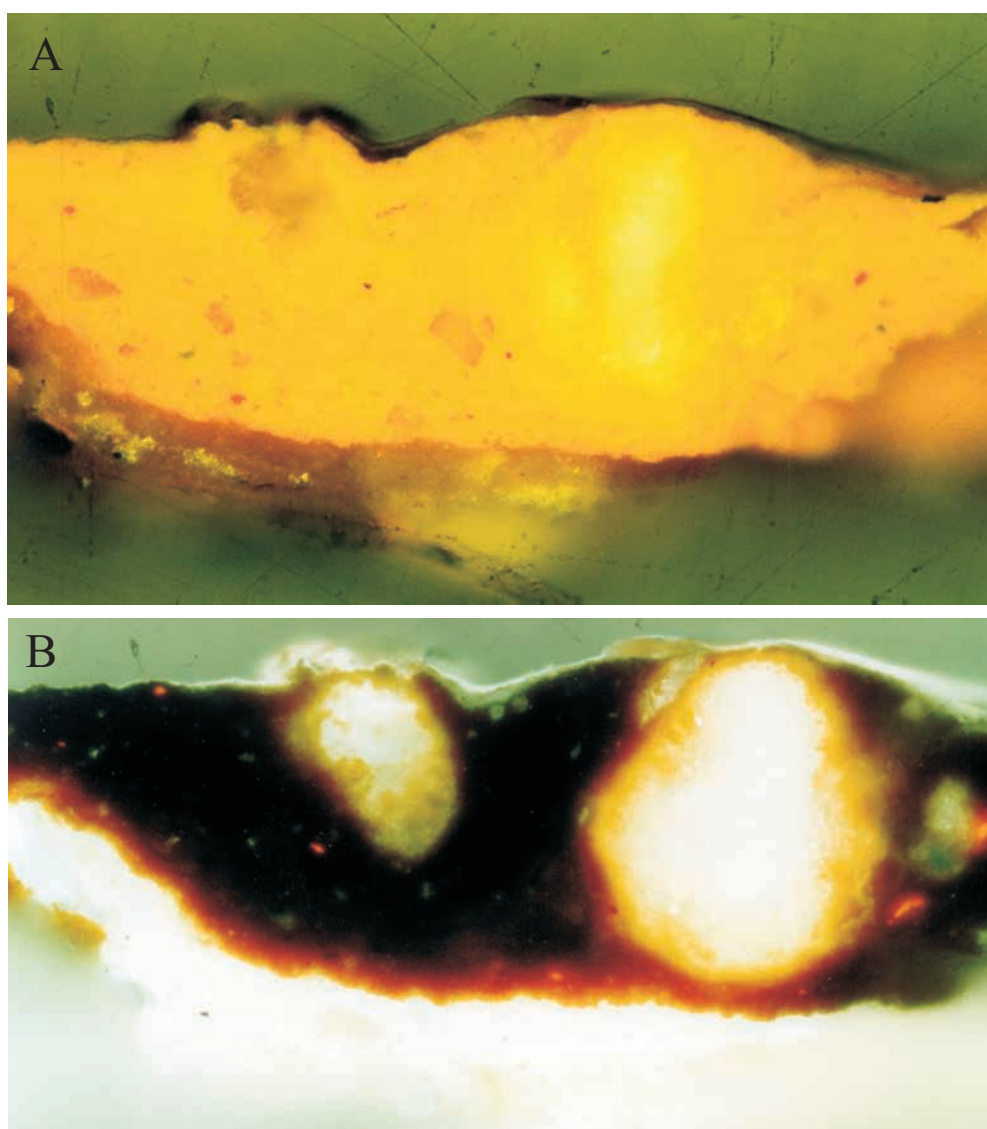***Table 8.1.*** *Overview of the dissected samples analysed in the presented study.*

Fig. 8.3. *Microscopic images of cross-section KM224/2a, taken from KM224. (**A**) Visual light microscopy. The numbers in this image indicate the positions where single point EDX spectra have been recorded. (**B**) Fluorescence microscopy of this cross-section. (see also the coloured version at the end of this Thesis)*

8.3 Results and discussion

8.3.1 Microscopy

The transparent masses were observed in the extensive orange paint areas in the painting by optical microscopy (Fig. 8.2). This orange paint contains many of these defects, especially in the thicker parts of the paint layer. In some cases, the transparent material completely stands upright through a crack in the paint layer. More regularly, the transparent material is seen in a slight elevation in the paint. Sample 2a was taken to include one of these defects and includes some of this whitish material. Optical microscopy of cross-section KM224/2a (Fig. 8.3a) shows a thick (~150 μm) bright orange paint layer on top of a transparent dark ground layer (~30 μm). Two large transparent globules and several smaller dark orange particles are visible in the paint. The globules can be seen clearly upon UV-illumination of the sample (Fig. 8.3b), as they are highly fluorescent, contrary to the surrounding paint. The orange paint layer is thicker near the positions of the globules, suggesting that the surface of the paint has been pushed upwards due to the volume increase of these globules. The globules are not covered by paint, which explains their visibility on the surface of the painting. The fluorescence image shows a light orange structure along the edges of the aggregate, which indicates a sparse presence of pigment particles in this region. The inverse effect, a brighter area in the paint near the aggregates and the ground layer, is also observed. This effect is due to the penetration of fluorescence light into the paint layer.

Cross-section KM224/2a was investigated by SEM-EDX to obtain a higher spatial resolution and allow elemental analysis. A scanning electron image (backscattered electrons) is displayed in Fig. 8.4A. The orange paint is visible as a bright layer, indicating the presence of heavy atoms. The ground layer, varnish layer and the transparent globules are visible as darker regions. A detailed structure is present in the bigger globule on the right. The elemental composition of this cross-section was investigated by single point EDX and EDX mapping. The different EDX plots are shown in Figs. 8.4B-I. The element maps and the backscattered image are obtained in a single measurement, so the images comprise exactly the same area. The bright orange layer contains high amounts of lead (Pb) and chromium (Cr) with a very similar distribution (Fig. 8.4B-C), which indicates that this orange paint layer contains a lead chromate pigment. Barium (Ba) is found in discrete particles in the paint layer (Fig. 8.4D), suggesting the presence of barium sulphate (baryte, $BaSO_4$). Unfortunately, this map cannot be correlated to the map of sulphur (Fig. 8.4E), as the intense X-ray emission of Pb is very close to the S emission lines. This causes a high background signal throughout the paint layer and completely masks the baryte particles. The barite identity of these particles was confirmed by single point EDX measurements. The particles discernible in the sulphur plot (Fig. 8.4E) do correspond perfectly to the Ca particles in the paint layer (Fig. 8.4F), suggesting that small quantities of calcium sulphate (gypsum, $CaSO_4$) are present in the paint. Calcium (but not sulphur) is also found in the ground layer, most likely due to the presence of calcium carbonate.

The transparent globules contain carbon (C), zinc (Zn), and oxygen (O). The presence of C suggests that the transparent masses contain a relatively high percentage of organic material. This image further indicates the presence of a third, smaller globule near the ground layer (arrow in Fig. 8.4I). Zn is present in all three globules, but has the highest abundance in the bigger one on the right. A closer examination of this big transparent part shows the presence of two separate fractions. The centre part of the protrusion shows the combined presence of Zn and O. This part
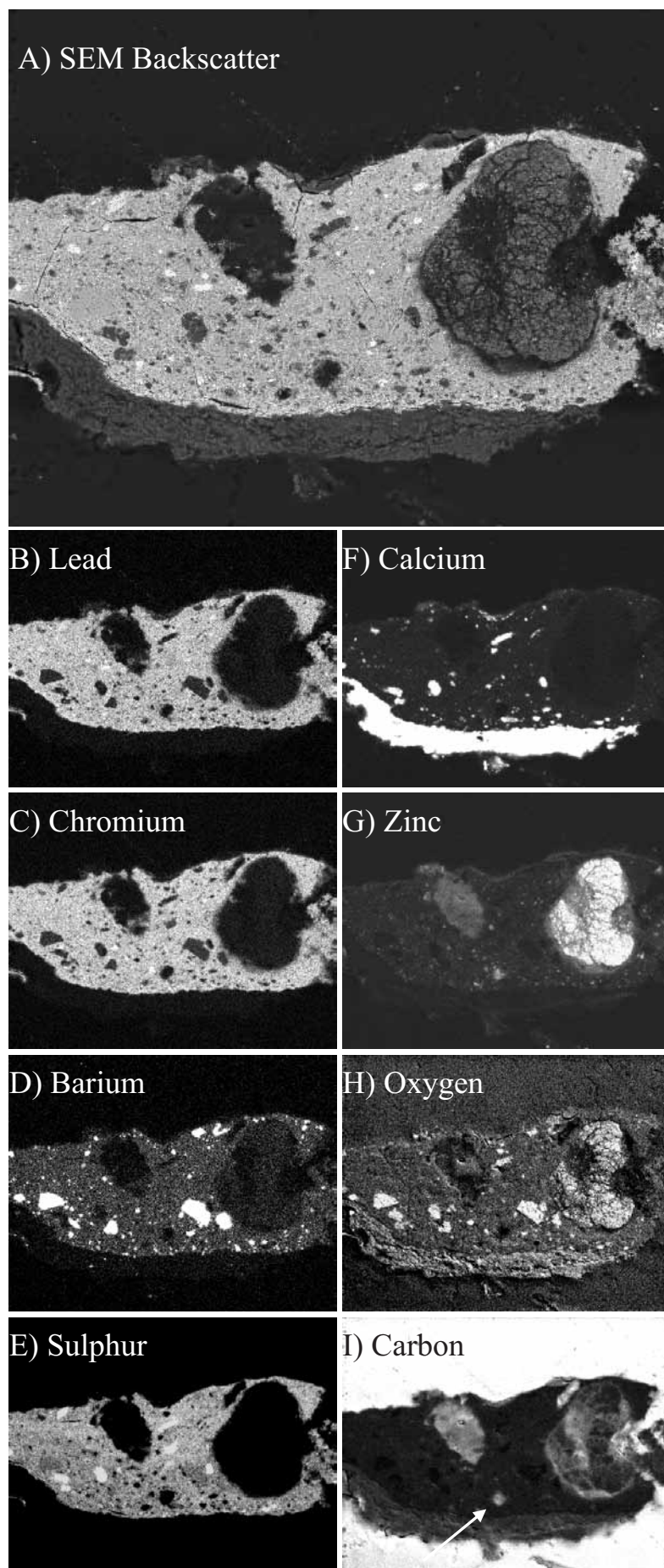
Fig. 8.4. SEM-EDX of paint cross-section KM224/2a.
(A) Backscatter SEM image;
(B)-(I) EDX-maps for different elements, as indicated in the figures.

is also visible in the backscatter SEM image (Fig. 8.4A) as a highly structured region. The left and right sides of this globule contain less Zn and O, but a clearly higher abundance of C (Fig. 8.4I). This globule clearly contains two different fractions: a mainly organic part and a part that contains more inorganic materials. The most likely inorganic material present is zinc oxide (ZnO). The EDX-plot in Fig. 8.4G further shows that Zn is present throughout the paint layer, albeit it in a lower abundance compared to the transparent globules. The presence of Zn in these areas was confirmed by a single point EDX measurement.

8.3.2 Imaging-FTIR

The elemental analysis indicated the abundant presence of organic materials in the protrusion areas. The same embedded cross-section was investigated by FTIR-imaging to yield a more specific chemical description. The obtained imaging data-set was processed by a clustering algorithm to enable a fast and easy distinction between different areas in the sample. This algorithm quantifies the similarity of all spectra in the imaging data-set to a single, user-selected spectrum. The quantified similarity can be presented as a score-plot. Fig. 8.5A presents the score plots for three different regions: paint (presented in red), ground (green), and embedding medium (blue). The obtained information on the location can easily be used to combine the corresponding spectra in order to obtain a single spectrum with a high S/N (signal to noise ratio) that is representative for the complete cluster. An averaged spectrum of the embedding medium area, outlined in blue in Fig. 8.5A is presented as the lower spectrum in Fig. 8.5C. While not directly important in the analysis of the paint, this spectrum is kept as a reference to recognise a potential smearing layer of embedding medium on top of the sample. The green colour in Fig. 8.5A represents the ground layer. The absorbance maximum of the carbonate peak in the corresponding spectrum (Fig. 8.5C, 1419 cm^{-1}) exceeds 5 and is truncated to ascertain the readability of the other spectra in Fig. 8.5C. The presence of carbonate confirms the presence of calcium carbonate, as was already indicated by the SEM-EDX results (see Fig. 8.4F). The spectrum shows a small absorption at 1658 cm^{-1}, which can be assigned to a proteinaceous binder, most likely animal glue. Unfortunately, the amide-II absorption, which would confirm this assignment, is masked by the carbonate absorption. The carbonyl absorption (1743 cm^{-1}) is not expected in a glue layer. It can be assigned to dislocated glycerol esters from the paint or wax esters introduced during the relining of the painting. Contamination by embedding medium seems unlikely in this case, as the embedding medium was found to absorb at 1728 cm^{-1} rather than at 1740 cm^{-1}. Furthermore, the other embedding medium peaks (1072, 1149, 1234 cm^{-1}) are absent.

The orange paint is represented in red in Figs. 8.5A and B. Most of the absorptions in this spectrum are due to organic moieties, as the inorganic lead chromate pigment has no active infrared absorptions in the analysed spectral region. Furthermore, this pigment needs a relatively large amount of oil (20–25%) to form a workable paint.[176] The CH vibrations (2931, 2862 and 1458 cm^{-1}) indicate the presence of aliphatic materials, while the absorption at 1740 cm^{-1} is again assigned to glycerol or possibly wax esters. The intense absorption at 1543 cm^{-1} and the shoulder at 1400 cm^{-1} are characteristic for metal carboxylates. The exact position of the asymmetric carboxylate peak at 1540 cm^{-1} indicates a zinc carboxylate,[145] but the presence of other carboxylates cannot be excluded. The absorption at 1064 cm^{-1} is due to $BaSO_4$, which is present throughout the paint layer with a dispersion finer than spatial resolution of FTIR-imaging. Some

larger lumps of baryte particles can be resolved, and these are represented in green in Fig. 8.5B. The corresponding spectrum ('sulphate' in Fig. 8.5C) shows an intense (truncated) sulphate absorption (1072 cm^{-1}). The presence of both finely distributed and coarser baryte particles is confirmed the EDX map in Fig. 8.4D.

The blue-coloured parts in Fig. 8.5B show that the reflectance infrared spectra of the transparent globules are clearly distinguished from the spectra of the normal paint by the applied clustering method. The most notable difference is the complete absence of sulphate absorptions (1064 cm^{-1}) in the spectrum of the protrusion. Furthermore, the asymmetric metal carboxylate absorption (1404 cm^{-1}) is a distinct peak, instead of a shoulder. Finally, the CH stretch absorptions appear to be intenser and slightly shifted to lower energy (2924 and 2851 cm^{-1} instead of 2931 and 2857 cm^{-1}). These shifts and peak broadening are assigned to oxidation in the paint layer, which obviously did not take place in the transparent globule (cf. Chapter 5 of this Thesis).

8.3.3 Manually isolated samples

The possibility to study embedded paint cross-section by FTIR-imaging provides a powerful and versatile method to investigate paint at a relatively high spatial resolution. The spectral quality of the results is however compromised as a result of the reflection mode of data collection, as shown in Chapter 3 of this Thesis. Therefore, several samples were manually isolated and investigated by transmission FTIR and DTMS to complement the results obtained by reflection FTIR-imaging. The sampling positions of the different samples are indicated in Fig. 8.1.

The infrared spectra of materials separated manually from *Falling Leaves (Les Alyscamps)* are shown in Fig. 8.6. The upper spectrum in this figure is isolated material from a transparent globule. The spectrum (A) shows aliphatic CH vibrations at 2924, 2851 and 1468 cm^{-1}. The obtained spectrum is similar to the spectrum obtained by reflection FTIR (Fig. 8.5C). In the transmission measurement, a number of narrow peaks can be resolved for both the asymmetric (1593, 1551, and 1532 cm^{-1}) and the symmetric (1410 and 1400 cm^{-1}) metal carboxylate vibrations, due to the higher spectral resolution of the measurement. The transmission spectrum of isolated paint (KM224/5) shows large absorptions for $PbCrO_4$ (856 cm^{-1}) and $BaSO_4$ (1102 cm^{-1}), ester (1739 cm^{-1}) and hydroxyl (~3400) groups, all of which are smaller or completely absent in the isolated globule (top spectrum). The aliphatic absorptions in the paint are slightly shifted to 2931 and 2857 cm^{-1}, while a clear fingerprint of metal carboxylates (1551, 1413 cm^{-1}) is found.

An additional chemical analysis of sample KM224/5 was obtained by DTMS. The results of DTMS measurements are summarised in Table 8.2. The ratio of palmitic and stearic acid in KM224/5 indicates the use of walnut oil. However, the use of the more expensive walnut oil for a yellow area would be surprising. It is therefore assumed that the P/S ratio of the oil is due to a mixture of cheaper oils or is affected by use of additives, a common practice during the 19th century. Bees wax, also found in the paint layer, might be one of these additives. However, its presence in the paint layer can also be explained by impregnation of the bees wax introduced during the relining of this painting. The ions indicative for lead and sulphur are due to the lead chromate pigment and the barium sulphate filler. The presence of carbon dioxide ions can be explained by the decarboxylation of metal carboxylates. The presence of potassium in the paint is confirmed by EDX, but its source is unknown.
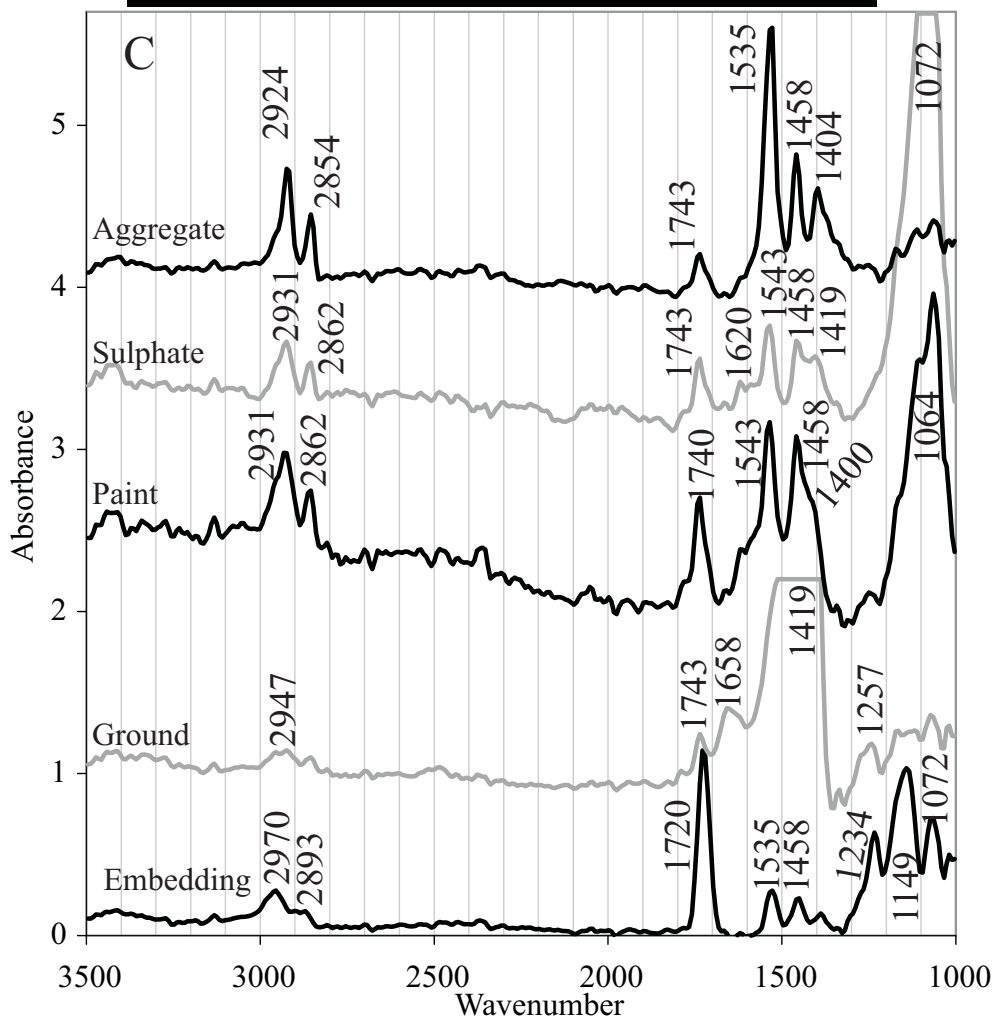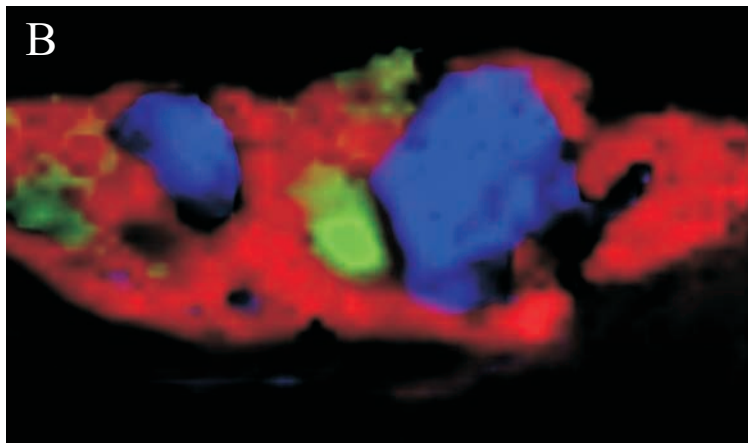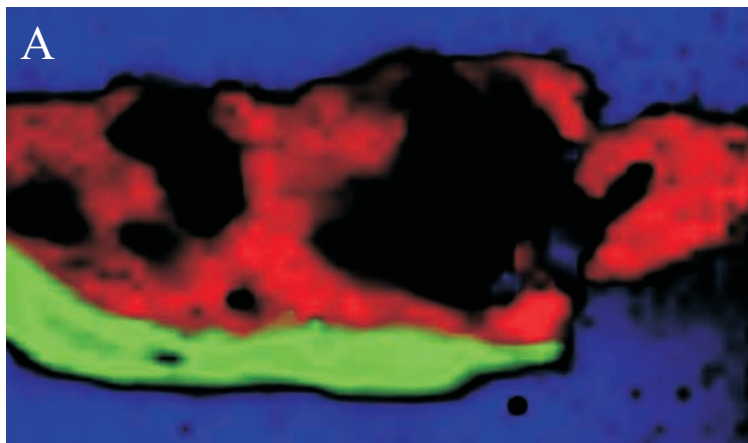
*Left-hand image: **Fig. 8.5.** Imaging FTIR of KM224/2a. The spectra in the FTIR data-set were clustered by the projection algorithm on the basis of their high similarity (See Chapter 2 of this Thesis). The locations of the clusters are highlighted in the score-plots. (**A**) Score plots of three different clusters showing the paint layer (red), the ground layer (green) and the embedding medium (blue). (**B**) Score plots of three different clusters showing the paint layer (red), sulphate-rich parts in the paint layer (green) and the aggregate (blue). (**C**) Mean spectra of each of the clusters shown in A and B. (see also the coloured version at the end of this Thesis)*
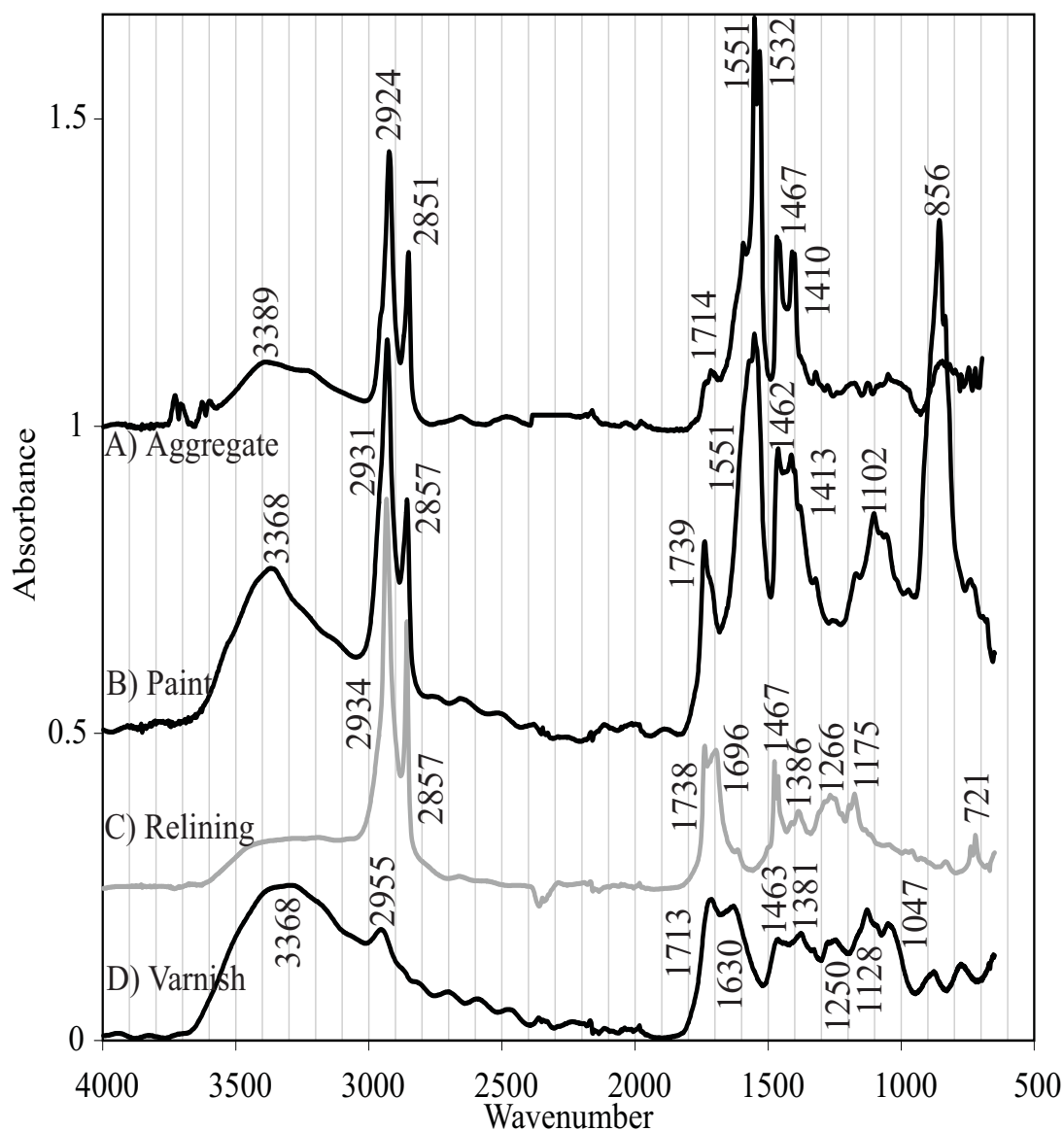

***Fig. 8.6.** Transmission FTIR spectra of manually separated samples from KM224, prepared in a diamond anvil cell, show spectra of isolated material from (**A**) an aggregate, (**B**) the paint layer, (**C**) the relining material, and (**D**) the varnish.*

The relining material is identified as a mixture of bees wax and diterpenoid resin. Wax is indicated by narrow aliphatic peaks at 2932, 2857, 1476, 1463, and 721 cm^{-1} in the FTIR spectrum (Fig. 8.6) and by the observation of peaks at m/z 592 620, 648, 676, 704, and 732 in DTMS (Table 8.2). The presence of the aged diterpenoid resin is indicated by infrared absorptions at 1693, 1613, 1263, and 1175 cm^{-1} and by mass peaks at m/z 257, 285, 302, 315.

The varnish layer (KM224/6) is sampled on a position where the uneven varnish layer is relatively thick and allows physical separation. The lower spectrum in Fig. 8.6 is recorded from this sample. Metal carboxylates, which are present throughout the paint, are not observed in this spectrum, indicating that the sample was well separated from the paint layer. This spectrum indicates the presence of a resin (1250, 1130, and 1047 cm^{-1}) and shows extensive oxidation (OH at ~3300, C–O at 1100–1300 cm^{-1}). Analysis by DTMS indeed showed the presence of triterpenoids.

Sample KM224/4 was squeezed in the diamond anvil cell to allow transmission FTIR. Figs. 8.7AB show visual light and fluorescence microscopic images of the sample after squeezing. The sample clearly shows three different regions, numbered 1-3 in Fig. 8.7A. These regions were measured individually using a diaphragm in one of the image planes of the infrared microscope. The location of the diaphragm in the different measurements is indicated by the coloured squares in Fig 8.7A.

Region 1 represents the varnish layer, as it is completely transparent and contains no scattering particles. Manual sampling of the thin varnish layer is difficult, but this layer can very well be analysed after squeezing of a larger sample. The spectrum of region 1 (Fig. 8.7C) suggests the presence drying oil, as indicated by the characteristic glycerol-ester triplet at 1170, 1244 and 1110 cm^{-1}. The oil containing varnish on this position is remarkably different from the isolated triterpenoid varnish (lower spectrum of Fig. 8.6) and suggests that different kinds of unpigmented layers are present. These different unpigmented layers might have been applied during successive varnish applications. However, the oil part can also be explained by the presence of a nourishing or oiling-out layer. A more accurate observation of the fluorescence image of sample KM224/2a (Fig. 8.3B) seems to confirm the presence of two different layers on top of the paint layer, as the fluorescing resin layer seems to be separated from the paint layer by an intermediate layer. However, more samples would be needed for a definite interpretation of these results.

Region 2 represents the paint layer, as it has a dark colour in transmitted light (Fig. 8.7A), which indicates scattering and absorption by pigment particles. The infrared spectrum obtained for this region is similar to the paint spectrum (KM224/5) displayed in Fig. 8.6, and shows a clear chromate absorption at 854 cm^{-1}. The spectrum of region 3 is similar to this spectrum, except for the absence of inorganic materials (sulphates and chromates) and a broadening of the absorptions around 1500 cm^{-1}. It can therefore not be assigned to materials from one of the transparent globules, in which these absorptions are clearly narrower (Fig. 8.6A). Furthermore, the spectrum is very different from the spectra of the varnish layers shown in Figs. 8.6D and 8.7C (part 1), and the spectrum of the ground layer shown in Fig. 8.5. The most likely explanation for this layer is therefore that it has been squeezed out of the paint layer by the pressure that has been applied in the diamond cell. This extruded area 3 was further investigated by FTIR-imaging.

Imaging-FTIR of this sample (KM224/4) indicated that this area (nr. 3) is not homogeneous.

Sample	Observed masses (interpretation)
KM224/5	**256** (palmitic), **284** (stearic), **592, 620, 648, 676, 704, 732** (bees wax), **206-208** (Pb), **64** (S_2/SO_2), **44** (CO_2), **39** (K)
KM224/6	123, 191, 248 (triterpenoids)
KM224/relining	**257, 285, 302, 315** (diterpenoids), **592, 620, 648, 676, 704, 732** (bees wax)

Tabel 8.2. *Interpretation of the results of DTMS on different samples taken from* Falling Leaves (Les Alyscamps).
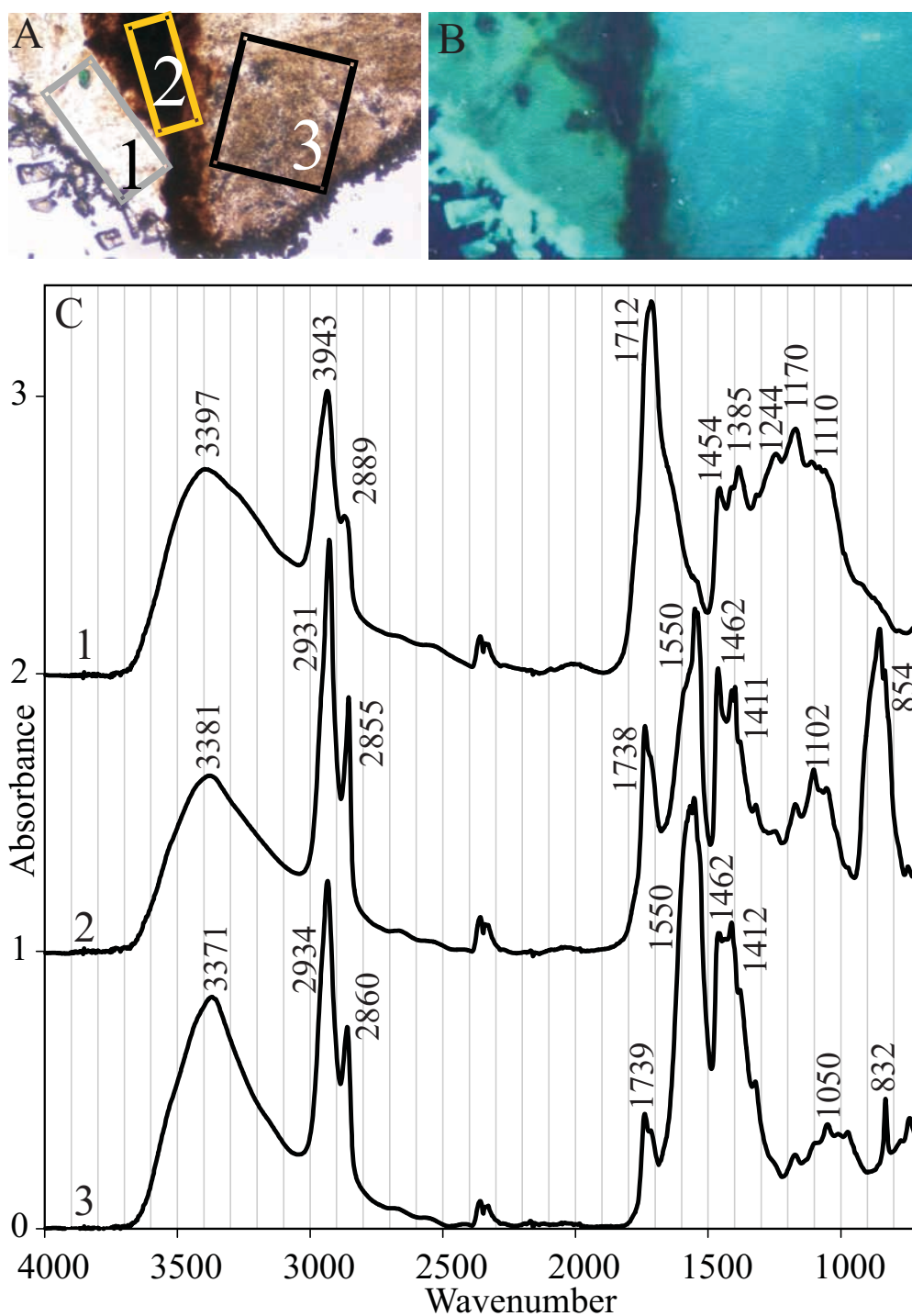

Fig. 8.7. *Microscopy and transmission FTIR spectra of a manually separated, inhomogeneous sample KM224/4). (A) Visual light microscopic image of the sample after squeezing in the diamond cell. (B) Fluorescence image of the same sample. (C) Infrared Spectra of the regions 1-3 indicated in A. (see at the end for a coloured version)*
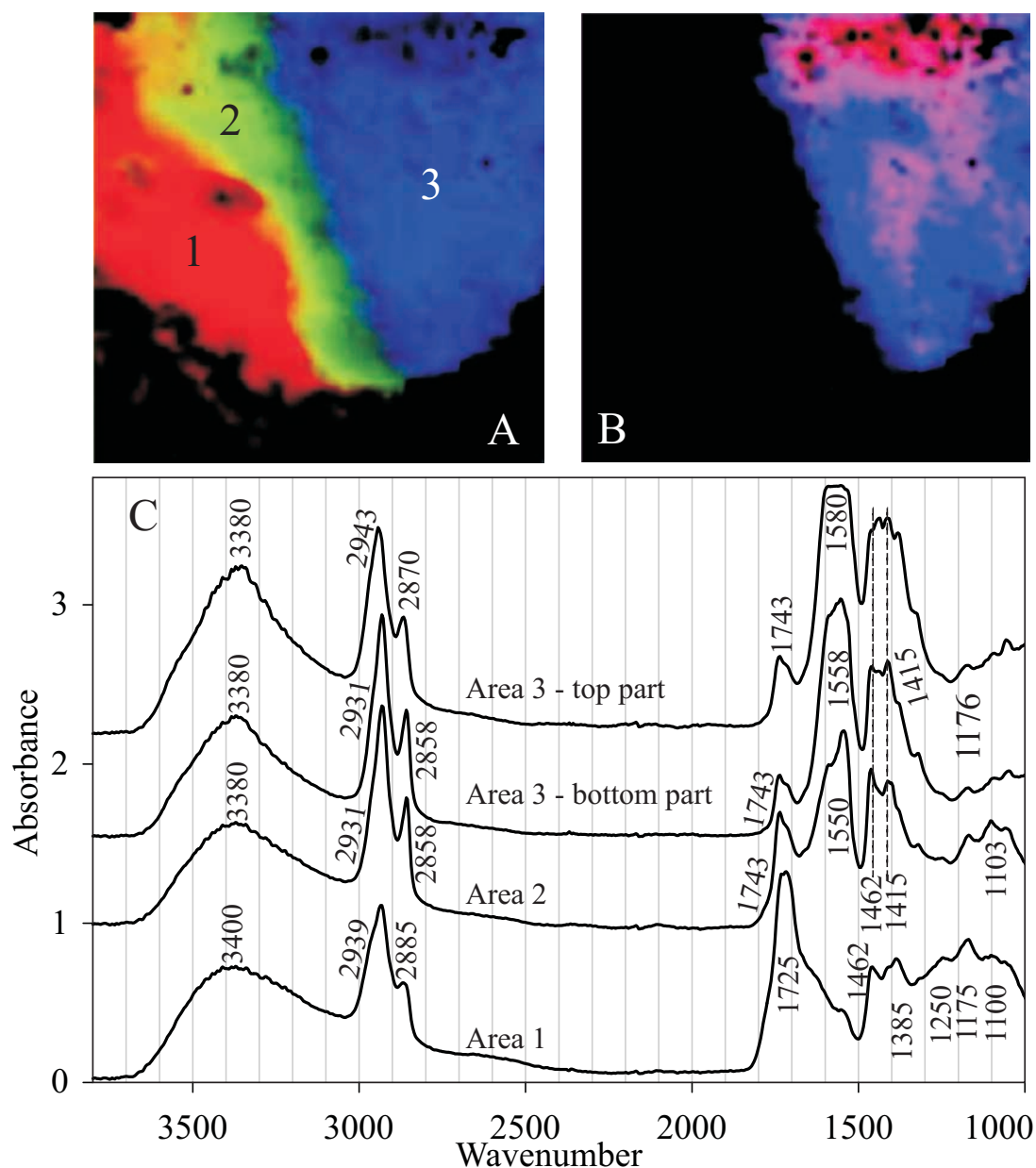
Fig. 8.8. *Imaging-FTIR of KM224/4 (same sample as Fig. 8.7). The spectra in the FTIR data-set were clustered by the projection algorithm on the basis of their high similarity (see Chapter 2 of this Thesis). The locations of the clusters are highlighted in the score-plots. (A) Score plots of three different clusters showing the areas 1, 2, and 3 (see Fig. 8.7a) as red, green and blue respectively. (B) Score plot of the clusters showing the upper and lower part of area 3 (See Fig. 8.7a). (C) Averaged spectra of the clusters shown in Figs. 8.8A and B.*
(see also the coloured version at the end of this Thesis)

Data processing was performed as described before. The obtained clusters (Fig. 8.8A) correlate well to the visual image shown in Fig. 8.7A and the corresponding spectra (Fig. 8.8C) are comparable to the spectra obtained for the single point measurements (Fig. 8.7C). Unfortunately, the lead chromate pigment absorption (854 cm^{-1}) is invisible for the imaging system due to the restricted spectral sensitivity of the infrared camera. Fig. 8.8A shows that the top part of region 3 (blue in Fig. 8.8A) did not take part in the clustering. The deviation of the spectrum in this top part was first found using multivariate techniques (results not shown), but can also be visualised by the projection method, as shown in Fig. 8.8B. The corresponding spectra (Fig. 8.8C) show a rather large shift in the energy of the CH stretch vibration. These are positioned at 2943 and 2870 cm^{-1} in the top part, compared to 2931 and 2858 cm^{-1} for the bottom part. Furthermore, the asymmetric carboxylate has become a featureless plateau between 1550 and 1600 cm^{-1}, while the symmetric carboxylate absorption (~1400 cm^{-1}) is not resolved from the CH bending absorption (1462 cm^{-1}). Similar effects have been assigned to oxidation and polymerisation of the oil binding medium (see Chapter 5 of this Thesis). The material extruded by the paint is thus partly oxidised. The different fractions seem to have separated due to the pressure applied in the diamond cell. The clear and easy separation of the paint materials suggests that a rather high fraction of the paint is flexible or even mobile. This observation is important to explain the mechanism of aggregation that leads to the formation of the various transparent globules. Phase separation, the mechanism proposed as the driving force for the formation of protrusions in the previous Chapter of this Thesis, implies the existence of a mobile fraction. The squeezing experiment clearly shows that such a flexible and mobile metal carboxylate fraction is present in the paint of *Falling Leaves (Les Alyscamps)*.

8.5 Conclusions

The transparent material found in the surface defects of *Falling Leaves (Les Alyscamps)* mainly consists of zinc carboxylates. The infrared spectra of the carboxylates contain very distinct and narrow peaks for the CH vibrations. The fatty acids involved are clearly not or hardly affected by the oxidation, which is broadening the absorption peaks in the spectra of paint (Fig. 8.6, cf. Chapter 5). The involved carboxylic acids are therefore most likely saturated, non-polymerised fatty acids. This is very similar to the description of protrusions in 17th and 19th century lead white paints, as described in the previous Chapters in this Thesis. It is therefore concluded that both are formed by a similar mechanism: the aggregation through phase separation of mobile, apolar, saturated fatty acids. In this case however, these fatty acids are not connected to lead, but to zinc ions. The Zn compound found in one of the aggregates consists of ZnO based on the combined presence of Zn and O found in the EDX maps (Figs. 8.4GH), and the absence of characteristic infrared absorptions of sulphates or carbonates inside the aggregates. The combined use of lead chromate and zinc white pigments by Van Gogh is not unlikely, and it has been reported before.[177] Nevertheless, zinc white is not necessarily the original source of zinc, as it might very well be derived from other zinc containing compounds in the paint. Possible other sources are the chromate pigment, which can contain small quantities of zinc chromate in addition to lead chromates. Furthermore, white vitriol (zinc sulphate) might have been used as a drier.[2] Lithopone, a mixture of barium sulphate and zinc sulphide, is less likely as

a zinc source, as the distributions of Zn and Ba do not show any correlation.

The Zn carboxylates are not only present in the aggregates, but appear to be abundantly present throughout the paint layer. In fact, the differences between the infrared spectra of the aggregate and normal paint are small (Figs. 8.6AB). The main differences are the presence of inorganic materials (baryte, 1102 cm^{-1}, lead chromate 856 cm^{-1}), and a higher amount of intact glycerol esters (1739 cm^{-1}) in the paint. Furthermore, a higher level of oxidation in the paint is indicated by the absorption at 3100–3500 cm^{-1} and a broadening of the carboxylate peaks at 1551 and 1413 cm^{-1}.

Despite these small differences, it is clear that carboxylates form a major constituent of the intact paint. The present Zn content of the lead chromate paint seems to be very low (Fig. 8.4G). It is remarkable that the Zn concentration in one of the observed aggregates is higher than in the intact paint. The large unevenness in Zn concentration suggests a certain mobility of zinc compounds. The potential mobility material in the paint was clearly shown by the squeezing experiment in the diamond anvil cell. A solid paint would be expected to result in a crumbled, but reasonably homogeneous layer. Instead, clearly separated areas were found, which shows that part of the metal soap fraction was squeezed out, indicating its mobility. The high amount of mobile materials observed in this study can be explained by a relatively high amount of oil needed to make a workable paint from chromate pigment (> 20–25% [176]).

Direct indications for the mobility of metal carboxylates have not been found in the previous Chapters, in which lead carboxylates have been investigated. It is indeed very well possible that the metal ions might have a profound effect on the properties of the metal carboxylates. In fact, similar effects have been observed in partly neutralised ionomers. These properties also explain the differences in the visual appearance between the Zn and Pb aggregate material. The higher mobility might very go along with a higher pliability of the Zn carboxylates and thereby explain the squeezing out of the aggregated material.

The mobility of the paint materials can be further increased during varnish application. The effect of the triterpenoid varnishes themselves is considered small, but the fluids used to apply the resin might very well accelerate the phase separation by an increase in the mobility of the materials. The varnish application of *Falling Leaves (Les Alyscamps)* might thus have acted as a trigger in the growth of the aggregates.

The aggregates have a profound impact on the visual appearance of the painting due the extensive expansion. A small calculation indicates that complete transformation of ZnO (M = 81.4, d = 5.6) to zinc palmitate (M = 575.4, d = 1.10) leads to a volume increase of factor 36. This large volume increase explains the extensive damage that zinc soap formation can have on a painting. Unfortunately, the clustering of saturated fatty acids and soap formation cannot be reversed. However, it might be possible to reduce the velocity of the formation of these aggregates by lowering the temperature and minimising the exposure to moisture and solvents.

8.6 Acknowledgements

References

1. Encyclopædia Brittanica I, *The New Encyclopædia Brittanica*, Vol. 1, Chicago, 1992.
2. Carlyle L, *The Artist's Assistant, Oil Painting Instruction Manuals and Handbooks in Britain 1800-1900 with Reference to Selected Eighteenth-Century Sources*. Archetype Publications, London, 2001.
3. Koller M, Das Staffeleibild der Neuzeit. In: *Farbmittel, Buchmalerei, Tafel- Und Leinwandmalerei*, Vol. 1 (Ed. Reclam P), Philipp Reclam jun., Stuttgart, 1984, p. 261-434.
4. Bomford D, Brown C and Roy A, *Art in the Making; Rembrandt*. National Gallery Publications Limited, London, 1988.
5. Van Asperen de Boer JRJ, An Introduction to the Scientific Examination of Paintings, *Nederlands Kunsthistorisch Jaarboek* **26:** 1975, p. 1-40.
6. Dran J-C, Calligaro T and Salomon J, Particle-Induced X-Ray Emission. In: *Modern Analytical Methods in Art and Archaeology*, Vol. 155 (Eds. Ciliberto E and Spoto G), John Wiley & Sons, New York, 2000, p. 135-166.
7. Saunders D and Kirby J, Light-Induced Colour Changes in Red and Yellow Lake Pigments, *National Gallery Technical Bulletin*: 1994, p. 75-97.
8. Leona M and Winter J, Fiber Optics Reflectance Spectroscopy: A Unique Tool for the Investigation of Japanese Paintings, *Studies in Conservation* **46(3):** 2001, p. 153-162.
9. Van Asperen de Boer JRJ, *Infrared Reflectography, a Contribution to the Examination of Earlier European Paintings*, Thesis: Universiteit van Amsterdam, 1970.
10. Châtelet A, *Jean Prévost Le Maître De Moulins*, Monographies. Gallimard, Paris, 2001.
11. Mrusek R, Fuchs R and Oltrogge D, Spectral Windows on the Past - a New Reflectographic Method for Analysis of Book Illuminations and Historical Manuscripts, *Naturwissenschaften* **82(2):** 1995, p. 68-79.
12. Mansfield JR, Sowa MG, Majzels C, Collins C, Cloutis E and Mantsch HH, Near Infrared Spectroscopic Reflectance Imaging: Supervised vs. Unsupervised Analysis Using an Art Conservation Application, *Vibrational Spectroscopy* **19(1):** 1999, p. 33-45.
13. Walmsley E, Metzger C, Fletcher C and Delaney JK, Evaluation of Platinum Silicide Cameras for Use in Infrared Reflectography. In: *Preprints ICOM Committee for Conservation, 10th Triennial Meeting, Washington, 1993*, p. 57-62.
14. Van der Weerd J, Heeren RMA and Van Asperen de Boer JRJ, A European 640 X 486 PtSi Camera for Infrared Reflectography. In: *Le dessin sous-jacent et la technologie dans la peinture. Colloque XIII, La Peinture et le Laboratoire. Procédés. Méthodologie. Applications, Leuven, 1999* (Eds. Van Schoute R and Verougstraete H), Uitgeverij Peeters, p. 231-243.
15. Fabbri M, Picollo M, Porcinai S and Bacci M, Mid-Infrared Fiber-Optics Reflectance Spectroscopy: A Noninvasive Technique for Remote Analysis of Painted Layers. Part I: Technical Setup, *Applied Spectroscopy* **55(4):** 2001, p. 420-427.
16. Mills J and White R, Analyses of Paint Media, *National Gallery Technical Bulletin* **4:** 1980, p. 65-68.
17. Mills JS, The Gas Chromatographic Examination of Paint Media. Part I. Fatty Acid Composition and Identification of Dried Oil Films, *Studies in Conservation* **11:** 1966, p. 92-108.
18. Sutherland K, The Extraction of Soluble Components from an Oil Paint Film by a Varnish Solution, *Studies in Conservation* **45:** 2000, p. 54-62.
19. Van den Berg JDJ, Van den Berg KJ and Boon JJ, Determination of the Degree of Hydrolysis of Oil Paint Samples Using a Two-Step Derivatisation Method and on-Column GC/MS, *Progress in Organic Coatings* **41(1-3):** 2001, p. 143-155.
20. Van der Doelen GA and Boon JJ, Artificial Ageing of Varnish Triterpenoids in Solution, *Journal of Photochemistry and Photobiology A-Chemistry* **134:** 2000, p. 45-57.
21. Boon JJ, Analytical Pyrolysis Mass-Spectrometry - New Vistas Opened by Temperature-Resolved in-Source Py-Ms, *International Journal of Mass Spectrometry and Ion Processes* **118:** 1992, p. 755-787.
22. Van den Brink O, Boon JJ, O'Connor PB, M.C. D and Heeren RMA, Matrix-Assisted Laser Desorption/Ionization Fourier Transform Mass Spectrometric Analysis of Oxygenated Triglycerides and Phosphatidylcholines in Egg Tempera Paint Dosimeters Used for Environmental Monitoring of Museum Display Conditions, *Journal of Mass Spectrometry* **36(5):** 2001, p. 479-492.
23. Van den Berg JDJ, *Analytical Studies on Traditional Linseed Oil Paint*, Thesis: University of Amsterdam, 2002.

24. Boon JJ, Keune K, van der Weerd J, Geldof M and Van Asperen de Boer JRJ, Imaging Microspectroscopic, Secondary Ion Mass Spectrometric and Electron Microscopic Studies on Discoloured and Partially Discoloured Smalt in Cross-Sections of 16th Century Paintings, *Chimia* **55(11):** 2001, p. 952-960.

25. O'Connor RT, Recent Progress in the Applications of Infrared Spectroscopy to Lipid Chemistry, *Journal of The American oil Chemists' Society* **38:** 1961, p. 648-659.

26. Honn FJ, Bezman IL and Daubert BF, Infrared Absorption of Hydroxy Compounds in Autoxidizing Linseed Oils, *Journal of the American Chemical Society* **71:** 1949, p. 812-816.

27. Mallegol J, Gonon L, Lemaire J and Gardette JL, Long-Term Behaviour of Oil-Based Varnishes and Paints 4. Influence of Film Thickness on the Photooxidation, *Polymer Degradation and Stability* **72(2):** 2001, p. 191-197.

28. Mallegol J, Gardette JL and Lemaire J, Long-Term Behavior of Oil-Based Varnishes and Paints I. Spectroscopic Analysis of Curing Drying Oils, *Journal of the American Oil Chemists Society* **76(8):** 1999, p. 967-976.

29. Ma K, van de Voort FR, Sedman J and Ismail AA, Stoichiometric Determination of Hydroperoxides in Fats and Oils by Fourier Transform Infrared Spectroscopy, *Journal of the American Oil Chemists Society* **74(8):** 1997, p. 897-906.

30. O'Neil LA, Application of Infrared Spectroscopy to the Study of the Drying and Yellowing of Oil Films, *Paint Technology* **27(1):** 1963, p. 44-47.

31. Hartshorn JH, Time-Lapse Infrared Spectroscopic Investigation of Alkyd and Linseed Oil Cure, *Journal of Coatings Technology* **54:** 1982, p. 53-61.

32. Lazzari M and Chiantore O, Drying and Oxidative Degradation of Linseed Oil, *Polymer Degradation and Stability* **65:** 1999, p. 303-313.

33. Rheineck AE, Peterson R and Sastry GM, Attenuated Total Reflectance Studies on Drying Oil Films, *Journal of Paint Technology* **39(511):** 1967, p. 484-489.

34. Odlyha M, Investigation of the Binding Media of Paintings by Thermoanalytical and Spectroscopic Techniques, *Thermochimica Acta* **269/270:** 1995, p. 705-727.

35. Hedley G, Odlyha M, Burnstock A, Tillinghast J and Husband C, A Study of the Mechanical and Surface-Properties of Oil Paint Films Treated with Organic-Solvents and Water, *Journal of Thermal Analysis* **37(9):** 1991, p. 2067-2088.

36. Simunkova E, Brothankova-Bucifalova J and Zelinger J, The Influence of Cobalt Blue Pigments on the Drying of Linseed Oil, *Studies in Conservation* **30:** 1985, p. 161-166.

37. Meilunas RJ, Bentsen JG and Steinberg A, Analysis of Aged Paint Binders by FTIR Spectroscopy, *Studies in Conservation* **35:** 1990, p. 33-51.

38. Rasti F and Scott G, The Effects of Some Common Pigments on the Photo-Oxidation of Linseed Oil-Based Paint Media, *Studies in Conservation* **25:** 1980, p. 145-146.

39. Luxan MP and Dorrego F, Reactivity of Earth and Synthetic Pigments with Linseed Oil, *Jocca-Surface Coatings International* **82(8):** 1999, p. 390.

40. Learner T, The Use of FT-IR in the Conservation of Twentieth Century Paintings, *Spectroscopy Europe* **8(4):** 1996, p. 14-19.

41. Van't Hul-Ehrnreich EH, Infrared Microspectroscopy for the Analysis of Old Painting Materials, *Studies in Conservation* **15:** 1970, p. 175-182.

42. Low MJD and Baer NS, Application of Infrared Fourier Transform Spectroscopy to Problems in Conservation, General Principles, *Studies in Conservation* **22:** 1977, p. 116-128.

43. Derrick MR, Infrared Microspectroscopy in the Analysis of Cultural Artifacts. In: *Practical Guide to Infrared Microspectroscopy* (Ed. Humecki HJ), Marcel Dekker, Inc, New York, 1995, p. 287-322.

44. Carbo RTD, Reig FB, Adelantado JVG and Martinez VP, Fourier Transform Infrared Spectroscopy and the Analytical Study of Works of Art for Purposes of Diagnosis and Conservation, *Analytica Chimica Acta* **330:** 1996, p. 207-215.

45. Dunkerton J and White R, The Discovery and Identification of an Original Varnish on a Panel by Carlo Crivelli, *National Gallery Technical Bulletin* **21:** 2000, p. 70-75.

46. Derrick MR, Stulik DC, Landry JM and Bouffard SP, Furniture Finish Layer Identification by Infrared Linear Mapping Microspectroscopy, *Journal of the American Institute of Conservation* **31:** 1992, p. 225-236.

47. Mills JS and White R, *The Organic Chemistry of Museum Objects*, Arts and Archaeology. Butterworth-Heinemann Ltd, Oxford, 1994.

48. Shearer JC, Peters DC, Hoepfner G and Newton T, FTIR in the Service of Art Conservation, *Analytical Chem-*

istry **55(8):** 1983, p. 874a-880a.

49. Pouchert CJ, *The Aldrich Library of FT-IR Spectra*, Vol. 1-3. Aldrich Chemical, Milwaukee.

50. Wehling B, Vandenabelee P, Moens L, Klockenkamper R, Von Bohlen A, Van Hooydonk G and De Reu M, Investigation of Pigments in Medieval Manuscript by Micro-Raman Spectroscopy and Total Reflection X-Ray Fluorescence Spectrometry, *Microchim. Acta* **130:** 1999, p. 253-260.

51. Vandenabeele P, Wehling B, Moens L, Dekeyzer B, Cardon B, Bohlen Av and Klockenkamper R, Pigment Investigation of a Late-Medieval Manuscript with Total Reflection X-Ray Fluorescence and Micro-Raman Spectroscopy, *Analyst* **124:** 1999, p. 169-172.

52. Clark RJH, Cooksey CJ, Daniels MAMA and Withnall R, Indigo, Woad, and Tyrian Purple: Important Vat Dyes from Antiquity to the Present, *ENDEAVOUR* **17(4):** 1993, p. 191-199.

53. Castillejo M, Martin M, Silva D, Stratoudaki T, Anglos D, Burgio L and Clark RJH, Analysis of Pigments in Polychromes by Use of Laser Induced Breakdown Spectroscopy and Raman Microscopy, *Journal of Molecular Structure* **550-551:** 2000, p. 191-198.

54. Burgio L and Clark RJH, Library of FT-Raman Spectra of Pigments, Minerals, Pigment Media and Varnishes, and Supplement to Existing Library of Raman Spectra of Pigments with Visible Excitation, *Spectrochimica Acta Part A-Molecular and Biomolecular Spectroscopy* **57(7):** 2001, p. 1491-1521.

55. Bell SEJ, Bourguignon ESO, Dennis AC, Fields JA, McGarvey JJ and Seddon KR, Identification of Dyes on Ancient Chinese Paper Samples Using the Subtracted Shifted Raman Spectroscopy Method, *Analytical Chemistry* **72(1):** 2000, p. 234-239.

56. Vandenabeele P, Weling B, Moens L, Edwards H, De Reu M and Van Hooydonk G, Analysis with Micro-Raman Spectroscopy of Natural Organic Binding Media and Varnishes Used in Art, *Analytica Chimica Acta* **407:** 2000, p. 261-274.

57. Halpine S, M., Amino Acid Analysis of Proteinaceous Media from Cosimo Tura's 'the Annunciation with Saint Francis and Saint Louis of Toulouse', *Studies in Conservation* **37:** 1992, p. 22-38.

58. Vallance SL, Singer BW, Hitchen SM and Townsend J, The Analysis of Proteinaceous Artists's Media by High Performance Liquid Chromatography, *LC-GC International***:** 1997, p. 48-53.

59. Maugard T, Enaud E, Choisy P and Legoy MD, Identification of an Indigo Precursor from Leaves of Isatis Tinctoria (Woad), *Phytochemistry* **58(6):** 2001, p. 897-904.

60. Muizebelt WJ, J.C. H, Nielen MWF, Klaasen RP and Zabel KH, Crosslink Mechanisms of High-Solids Alkyd Resins in the Presence of Reactive Diluents, *Progress in Organic Coatings* **40:** 2000, p. 121-130.

61. Pages O, Legendre B, Odlyha M and Craig D, Phase Miscibility in Oil/Resin Mixtures: A Study by FTIR and Thermomechanical Analysis, *Thermochimica Acta* **287(1):** 1996, p. 53-70.

62. Plesters J, Cross-Sections and Chemical Analysis of Paint Samples. Tables for Identification of Pigments, *Studies in Conservation***:** 1955-1956, p. 134-155.

63. Plesters J, Cross-Sections and Chemical Analysis of Paint Samples, *Studies in Conservation* **11:** 1956, p. 110-157.

64. McCrone WC, The Microscopical Identification of Artists' Pigments, *J. ICC-Covodeder Group 7* **Nos. 1& 2:** 1982, p. 11-34.

65. Johansson T and Pettersson A, Imaging Spectrometer for Ultraviolet near Infrared Microspectroscopy, *Rev.Sci.Instrum.* **68(5):** 1997, p. 1962-1971.

66. Lewis EN, Treado PJ, Reeder RC, Story GM, Dowrey AE, Marcott C and Levin IW, Fourier Transform Spetroscopic Imaging Using an Infrared Focal Plane Array Detector, *Analytical Chemistry* **67(19):** 1995, p. 3377-3381.

67. Burka EM and Curbelo R, Imaging ATR Spectrometer, United States patent, nr. US006141100A, Bio-Rad Laboratories.

68. Ebizuka N, Wakaki M, Kobayshi Y and Sato S, Development of a Multichannel Fourier Transform Spectrometer, *Applied Spectroscopy* **34(34):** 1995, p. 7899-7906.

69. Williams KPJ, Pitt GD, Batchelder DN and Kip BJ, Confocal Raman Microspectroscopy Using a Stigmatic Spectrograph and CCD Detector, *Applied Spectroscopy* **48(2):** 1994, p. 232-235.

70. Barbillat J, Dhamelincourt P, Delhaye M and DaSilva E, Raman Confocal Microprobing, Imaging and Fiberoptic Remote-Sensing - a Further Step in Molecular Analysis, *Journal of Raman Spectroscopy* **25:** 1994, p. 3-11.

71. Price DV, Reading M, Hammiche A and Pollock HM, Micro-Thermal Analysis: Scanning Thermal Microscopy and Localised Thermal Analysis, *International Journal of Pharmaceutics* **192:** 1999, p. 85-96.

72. Price DM, Reading M, Caswell A, Hammiche A and Pollock JM, Micro-Thermal Analysis: A New Form of A-

nalytical Microscopy, *Microscopy and Analysis* **1998(TA247):** 1998.

73. Schueler BW, Time of Flight Mass Analysers. In: *Imp P Publications and Surface Spectra Limited* (Eds. Vickerman JC and Briggs D), 2001

74. Caprioli RM, Farmer TB and Gile J, Molecular Imaging of Biological Samples: Localization of Peptides and Proteins Using MALDI-TOF-MS, *Analytical Chemistry* **69(23):** 1997, p. 4751-4760.

75. Van der Weerd J, Brammer H, Boon JJ and Heeren RMA, Fourier Transform Infrared Microscopic Imaging of an Embedded Paint Cross-Section, *Applied Spectroscopy* **56(3):** 2002, p. 275-283.

76. Mühlethaler B and Thissen J, Smalt. In: *Artists' Pigments, a Handbook of Their History and Characteristics*, Vol. 2 (Ed. Roy A), Oxford University Press, Washington, 1993, p. 113-130.

77. Geladi P and Grahn H, *Multivariate Image Analysis*. John Wiley & Sons, Chichester, 1996.

78. Herbst W and Hunger K, *Industrial Organic Pigments, Production, Properties, Applications*. VCH Verlagsgesellschaft MBH, Weinheim, 1997.

79. Boon JJ, Keune K and Learner T, Identification of Pigments and Media from a Paint Cross-Section by Direct Mass Spectrometry and High-Resolution Imaging Mass Spectrometric and Spectroscopic Techniques. In: *ICOM CC Science symposium, Rio de Janeiro,* submitted *2002*.

80. Carbo MTD, Martinez VP, Adelantado JVG, Reig FB and Moreno M, Fourier Transform Infrared Spectroscopy and the Analytical Study of Sculptures and Wall Decoration, *Journal of Molecular Structure* **410:** 1997, p. 559-563.

81. Shearer G, Use of Diffuse Reflectance Fourier Transform Infrared Spectroscopy in Art and Archaeological Conservation. In: *Recent Advances in the Conservation and Analysis of Artifacts* (Ed. Black J), Summer Schools Press, London, 1987, p. 253-256.

82. Derrick MR, Stulik DC and Landry JM, *Infrared Spectroscopy in Conservation Science*, Scientific Tools for Conservation. The Getty Conservation Institute, Los Angeles, 1999.

83. Krishnan K, Hill SL and Brown RH, FT/IR Spectroscopy Using Diffuse Reflectance and a Diamond Cell, FTS/IR application note, no. 33, Digilab (Bio-Rad).

84. Fitzpatrick J, The Evolution of Diamond ATR Microsampling, *Internet Journal of Vibrational Spectroscopy (www.ijvs.com)* **3(3)(4):** 1999.

85. Griffiths PR and de Haseth JA, *Fourier Transform Infrared Spectroscopy*, Chemical Analysis, Vol. 83. John Wiley & Sons, New York, 1986.

86. Laver M and Williams RS, The Use of a Diamond Cell Microsampling Device for Infrared Spectrophotometric Analyses of Art and Archaeological Materials, *Journal for the International Institute for Conservation-Canadian Group* **3(2):** 1978, p. 34.

87. Bruni S, Cariati F, Casadio F and Toniolo L, Spectrochemical Characterization by Micro-FTIR Spectroscopy of Blue Pigments in Different Polychrome Works of Art, *Vibrational Spectroscopy* **20(1):** 1999, p. 15-25.

88. Gay MC, Essais d'Identification et de Localisation des Liants Picturaux par des Colorations Spécifiques sur Coupes minces, *Annales du Laboratoire de Recherche des Musées de France*, 1970, p. 8-24.

89a. Pilc J and White R, The Application of FTIR Microscopy to the Analysis of Paint Binders in Easel Paintings, *National Gallery Technical Bulletin* **16:** 1995, p. 73-95.

89b. Langley A and Burnstock A, The analysis of layered paint samples from modern paintings using FTIR microscopy, ICOM committee for conservation, 12th triennal meeting, Lyon 1999, preprints, vol 1, James and James, London, p. 234-241.

90. MacKenzie WS and Adams AE, *Color Atlas of Rocks and Minerals in Thin Section*. Wiley Publishers, 1996.

91. Van Heel ACS, *Inleiding in De Optica*. Martinus Nijhoff, 's Gravenhage, 1958.

92. Harbecke B, Application of Fourier's Allied Integrals to the Kramers Kronig Transformation of Reflectance Data, *Applied Physics A* **40:** 1986, p. 151-158.

93. Salisbury JW and Wald A, The Role of Volume Scattering in Reducing Spectral Contrast of Reststrahlen Bands in Spectra of Powdered Minerals, *ICARUS* **96:** 1992, p. 121-128.

94. Krishnan K, Applications of the Kramers Kronig Dispersion Relations to the Analysis of FTIR Specular Reflectance Spectra, FTS/IR application note, no. 51, Digilab (Bio-Rad).

95. Hopfe V, Korte EH, Klobes P and Grählert W, Optical Data of Rough-Surfaced Ceramics: Infrared Specular and Diffuse Reflectance Versus Spectra Simulation, *Applied Spectroscopy* **47(4):** 1993, p. 423-429.

96. Van de Hulst HC, *Multiple Light Scattering, Tables, Formulas, and Applications*. Academic Press, London, 1980.

97. Judd DB and Wyszecki G, *Theories of Color Vision*, Color in Business, Science and Industry. John Wiley and

Sons Inc., New York and London, 1963.

98. Wülfert S, *Der Blick Ins Bild Lichtmikroskopische Methoden zur Untersuchung von Bildaufbau, Fasern und Pigmenten*, Bücherei des Restaurators, Vol. 4. Ravensburger Buchverlag Otto Maier GmbH, Ravensburg, 1999.

99. Hammiche A, Pollock HM, Reading M, Claybourn M, Turner PH and Jewkes K, Photothermal FT-IR Spectroscopy: A Step Towards FT-IR Microscopy at a Resolution better than the Diffraction Limit, *Applied Spectroscopy* **53(7):** 1999, p. 810-815.

100. Anderson MS, Infrared Spectroscopy with an Atomic Force Microscope, *Applied Spectroscopy* **54(3):** 2000, p. 349-352.

101. Noble D, FT-IR Pas Steps up to Depth Profiling, *Analytical Chemistry* **66(14):** 1994, p. 757-760.

102. Wahls MWC and Leyte JC, Step-Scan FT-IR Photoacoustic Studies of a Double-Layered Polymer Film on Metal Substrates, *Applied Spectroscopy* **52(1):** 1998, p. 123-127.

103. Colthup NB, Daly LH and Wiberley SE, *Introduction to Infrared and Raman Spectroscopy*. Academic Press, New York, 1964.

104. Edwards HGM, Drummond L and Russ J, Fourier Transform Raman Spectroscopic Study of Prehistoric Rock Paintings from the Big Bend Region, Texas, *Journal of Raman spectroscopy* **30(6):** 1999, p. 421-428.

105. Van den Berg JDJ, Van den Berg KJ and Boon JJ, Chemical Changes in Curing and Ageing Oil Paints. In: *ICOM-CC 12th Triennial Meeting, Lyon,* August 29-September 3 *1999* (Ed. Bridgland), p. 248-253.

106. Smith B, *Infrared Spectral Interpretation, a Systematic Approach*. CRC Press, London, 1999.

107. Chalmers JM, Everall NJ and Ellison S, Specular Reflectance: A Convenient Tool for Polymer Characterisation by FTIR-Microscopy?, *Micron* **27(5):** 1996, p. 315-328.

108. Boon JJ, Peulvé SL, Van den Brink OF, Duursma MC and Rainford D, Molecular Aspects of Mobile and Stationary Phases in Ageing Tempera and Oil Paint Films. In: *Early Italian Paintings Techniques and Analysis, Maastricht, 1997* (Eds. Bakkenist T, Hoppenbrouwers R and Dubois H), Limburg Conservation Institute, p. 32-47.

109. Wexler H, Polymerization of Drying Oils, *Chemical Reviews* **64(6):** 1964, p. 591-611.

110. Van der Doelen GA, Van den Berg KJ and Boon JJ, Comparative Chromatographic and Mass-Spectrometric Studies of Triterpenoid Varnishes: Fresh Material and Aged Samples from Paintings, *Studies in Conservation* **43(4):** 1998, p. 249-264.

111. Boon JJ and Van der Doelen GA, Advances in the Current Understanding of Aged Dammar and Mastic Varnishes on the Molecular Level. In: *Varnish, Material-Aesthetics-History, International Colloquium, Braunschweig, 1998*, AdR, p. 92-104.

112. Brammer H, Rembrandts Ganzfiguriges Herrenportrait: eine Stellungnahme zur jungsten Restaurierung und ein Bericht über neue Erkentnisse, *Journal of Art Technology and Conservation* **2:** 1992, p. 223-240.

113. Crocombe R, A. and Compton SV, The Design, Performance and Applications of a Dynamically-Aligned Step-Scan Interferometer, FTS/IR application note, no. 82, Digilab (Bio-Rad).

114. Nussenzveig HM, *Causality and Dispersion Relations*, Mathematics in Science and Engineering, Vol. 95. Academic Press, New York, 1972.

115. Groen K, Investigation of the Use of the Binding Medium by Rembrandt, *Journal of Art Technology and Conservation* **12:** 1997, p. 207-227.

116. Hermesdorf PFJM and Schnackenburg B, Rembrandts Ganzfiguriges Herrenportrat, *Restauro* **2:** 1992, p. 85-95.

117. Gettens RJ, Kühn H and Chase WT, Lead White. In: *Artists' Pigments: A Handbook of Their History and Characteristics*, Vol. 2 (Ed. Roy A), Oxford university Press, Washington, 1993, p. 67-82.

118. Van der Weerd J, Boon JJ, Geldof M, Heeren RMA and Noble P, Chemical Changes in Old Master Paintings: Dissolution, Metal Soap Formation and Remineralization Processes in Lead Pigmented Paint Layers of 17th Century Paintings., *Journal of Art Technology and Conservation* **In Press:** 2001.

119. Heeren RMA, Boon JJ, Noble P and Wadum J, Integrating Imaging FTIR and Secondary Ion Mass Spectrometery for the Analysis of Embedded Paint Cross-Sections. In: *ICOM, 12th Triennial Meeting Lyon, Lyon, 1999*, James, p. 228-233.

120. Jacobsen AE and Gardner WH, Zinc Soaps in Paints, Zinc Oleates, *Industrial and Engineering Chemistry* **33(10):** 1941, p. 1254-1256.

121. Heeren RMA, Van der Weerd J and Boon JJ, FTIR Imaging Spectroscopy for Organic Surface Analysis of Embedded Paint Cross-Sections. In: *Fifth International Conference on Optics Within Life Sciences OWLS V, Crete, 1998* (Eds. Fotakis C, Papazoglou TG and Kalpouzos C), Springer, p. 179-182.

122. Gombrich EH, *Eeuwige Schoonheid*. De Haan, Houten, The Netherlands, 1992.

123. Wallert A, *From Tempera to Oil Paint : Changes in Venetian Painting 1460 - 1560*. Rijksmuseum Amsterdam, Amsterdam, 1998.

124. Muizebelt WJ, Donkerbroek JJ, Nielen MWF, Hussem JB, Biemond MEF, Klaasen RP and Zabel KH, Oxidative Crosslinking of Unsaturated Fatty Acids Studied with Mass Spectrometry, *Journal of Mass Spectrometry* **31(5):** 1996, p. 545-554.

125. Porter NA, Lehman LS, Weber BA and Smith KJ, Unified Mechanism for Polyunsaturated Fatty Acid Autoxidation. Competition of Peroxy Radical Hydrogen Atom Abstraction, β-Scission, and Cyclization, *Journal of the American Chemical Society* **103:** 1981, p. 6447-6455.

126. Porter NA, Mechanisms for the Autoxidation of Polyunsaturated Lipids, *Acc. Chem. Res.* **19:** 1986, p. 262-268.

127. Swern D, Scanlan JT and Knight HG, Mechanism of the Reactions of Oxygen with Fatty Materials. Advances from 1941 through 1946, *Journal of The American Oil Chemists' Society***:** 1948, p. 193-200.

128. Hess M, Hamburg HR and Morgans WM, *Hess's Paint Film Defects*. Chapman and Hall, London, 1979.

129. Sebedio JL and Grandgirard A, Cyclic Fatty Acids: Natural Sources, Formation During Heat Treatment, Synthesis and Biological Properties, *Progress in Lipid Research* **28:** 1989, p. 303-336.

130. Chan HWS and Coxon DT, Lipid Peroxides. In: *Autoxidation of Unsaturated Lipids* (Ed. Chan HWS), Academic Press, London, 1987, p. 17-50.

131. Grosch W, Reactions of Hydroperoxides - Products of Low Molecular Weight. In: *Autoxidation of Unsaturated Lipids* (Ed. Chan HWS), Academic Press, London, 1987, p. 95-139.

132. Figge K, Dimeric Fatty Acid[1-14C] Methyl Esters. I. Mechanisms and Products of Thermal and Oxidative-Thermal Reactions of Unsaturated Fatty Acid Esters - Literature Review, *Chem. Phys. Lipids* **6:** 1971, p. 164-182.

133. Frilette VJ, Drying Oil and Oleoresinous Varnish Films, Increase in Acidity on Ageing, *Industrial and Engineering Chemistry* **38:** 1946, p. 493-496.

134. Osawa Z, Role of Metals and Metal-Deactivators in Polymer Degradation, *Polymer Degradation and Stability* **20:** 1988, p. 203-236.

135. Susi H and Byler DM, Protein Structure by Fourier Transform Infrared Spectroscopy: Second Derivative Spectra, *Biochemical and Biophysical Research Communications* **115(1):** 1983, p. 391-397.

136. Arrondo JLR, Muga A, Castresana J and Goni FM, Quantitative Studies of the Structure of Proteins in Solution by Fourier-Transform Infrared-Spectroscopy, *Progress in Biophysics & Molecular Biology* **59(1):** 1993, p. 23-56.

137. Mossoba MM, McDonald RE, Roach JAG, Fingerhut DD, Yurawecz MP and Sehat N, Spectral Confirmation of Trans Mono-Unsaturated C-18 Fatty Acid Positional Isomers, *Journal of the American Oil Chemists Society* **74(2):** 1997, p. 125-130.

138. Ma K, Van de Voort FR, Ismail AA and Sedman J, Quantitative Determination of Hydroperoxides by Fourier Transform Infrared Spectroscopy with a Disposable Infrared Card, *Journal of the American Oil Chemists Society* **75(9):** 1998, p. 1095-1101.

139. Wainwright IN, Taylor JM and Harley RD, Lead Antimonate Yellow. In: *Artists' Pigments 1, a Handbook of Their History and Characteristics*, Vol. 1 (Ed. Feller RL), Cambridge University Press, Washington, 1986, p. 219-254.

140. Grissom CA, Green Earth. In: *Artists' Pigments 1, a Handbook of Their History and Characteristics*, Vol. 1 (Ed. Feller RL), Cambridge University Press, Washington, 1986, p. 141-167.

141. Languri G, *Thesis in Preparation*, Thesis: University of Amsterdam, in prep.

142. Feller RL and Johnston-Feller RM, Vandyke Brown. In: *Artists' Pigments: A Handbook of Their History and Characteristics*, Vol. 3 (Ed. West Fitzhugh E), Oxford University Press, Washington, 1997, p. 157-190.

143. Kühn H, Zinc White. In: *Artists' Pigments 1, a Handbook of Their History and Characteristics*, Vol. 1 (Ed. Feller RL), Cambridge University Press, Washington, 1986, p. 141-167.

144. Kühn H, Bleiweiss und seine verwendung in der Malerei II, *Farbe und Lack* **73(3):** 1967, p. 209-213.

145. Matura R, Divalent Metal Salts of Long Chain Fatty Acids, *Journal of the Chemical Society of Japan* **86:** 1965, p. 560-572.

146. Ishioka T, Infrared Spectral Change in a Zinc Salt of an Ethylene-Methacrylic Acid Ionomer on Water-Absorption, *Polymer Journal* **25(11):** 1993, p. 1147-1152.

147. Zeng ZH, Wang SH and Yang SH, Synthesis and Characterization of PbS Nanocrystallites in Random Copolymer Ionomers, *Chemistry of Materials* **11(11):** 1999, p. 3365-3369.

148. Ishioka T, Shimizu M, Watanabe I, Kawauchi S and Harada M, Infrared and EXAFS Study on Internal Structural Change of Ion Aggregate in a Zinc Salt of Poly(Ethylene-Co-Methacrylic Acid) Ionomer on Water Absorption, *Macromolecules* **33(7):** 2000, p. 2722-2727.

149. Hashimoto H, Kutsumizu S, Tsunashima K and Yano S, X-Ray Absorption Spectroscopic Studies on Pressure-Induced Coordination-Structural Change of a Zinc-Neutralized Ethylene-Methacrylic Acid Ionomer, *Macromolecules* **34(5):** 2001, p. 1515-1517.

150. Kutsumizu S, Instrumental Analysis Center, Gifu University, Yanagido 1-1, Gifu 501-1193, Japan. Personal communication.

151. Middelkoop N, Noble P, Wadum J and Broos B, *Rembrandt onder het Mes: De Anatomische Les van Dr Nicolaes Tulp ontleed*. Six Art Promotion, Amsterdam, Den Haag, 1998.

152. Noble P, Wadum J and Boon JJ, Mechanical Changes in Old Master Paintings: Surface and Cross Sectional Analyses of Protrusions Found in Lead-Pigmented Ground and Paint Layers of 17th Century Paintings, *ArtMatters* **1:** 2002.

153. Koller J and Burmester A, Cleaning, Retouching and Coatings. In: *IIC, Brussels, 1990*, p. 141.

154. Wallert A, *Still Lifes: Techniques and Style, the Examination of Paintings from the Rijksmuseum*, Vol. 1. Waanders Publishers, Zwolle, Amsterdam, 1999.

155. White R, Van Dyck's Paint Medium, *National Gallery Technical Bulletin* **20:** 1999, p. 88.

156. Brunnenkant K, Falscher Glanz?, *Journal of Art Technology and Conservation* **17:** 1999.

157. Plahter LE and Plahter US, The Young Christ among the Doctors by Teodoer Van Baburen Technique and Condition of a Dutch Seventeenth Century Painting on Canvas. In: *Conservare Necesse Est. Festskrift Til Leif Einar Plather, IIC Nordic Group*, 1999, p. 42-67.

158. Sirois J, Miller D and Moffatt E, Analysis of Transparent White Inclusions Protruding from the Surface of the Painting 'Portrait of Admiral Sir J. Ross', Analytical Research Services Report, 3017.2, 005, 346, Canadian Conservation Institute.

159. Sirois J and Williams S, Analysis of Transparent White Inclusions Protruding from the Surface of the Painting 'Portrait of Surgeon James Heron Conroy', Analytical Research Services Report, 3017.1, Canadian Conservation Institute.

160. Schueler B, Sander P and Reed DA, A Time-of Flight Secondary Ion Microscope, *Vacuum* **41:** 1990, p. 1661-1664.

161. Edwards R, Gillard RD and Williams PA, Studies of Secondary Mineral Formation in the $PbO-H_2O-HCl$ System, *Mineralogical Magazine* **56:** 1992, p. 53-65.

162. Garrels RM and Christ CL, *Solutions, Minerals and Equilibria*. Harper & Row, London, 1965.

163. Zucker J, Painting Conservator, Bureau of Historic Sites, Office of Parks Recreation and Historic Preservation. Personal communication.

164. Zucker J, From the Ground Up: The Ground in 19th-Century American Pictures, *Journal of the American Institute of Conservation* **38(1):** 1999, p. 3-20.

165. Kemp W, *The Desire of My Eyes: The Life and Work of John Ruskin*. Fararr, Straus and Giroux, 1990.

166. Dwyer D, John F. Kensett's Painting Technique. In: *John F. Kensett: An American Master* (Eds. Driscoll JP and Howat JK), Metropolitan Museum of Art, New York, 1985

167. Ordonez E and Twilley J, Clarifying the Haze. Efflorescence on Works of Art, *Analytical Chemistry* **69(13):** 1997, p. A416-A422.

168. Van Loo M, Physical Chemistry of Paint Coatings, *Official Digest***:** 1956, p. 1126-1156.

169. Pearlstein E, Fatty Bloom on Wood Sculpture from Mali, *Studies in Conservation* **31(2):** 1986, p. 83-91.

170a. Koller J and Burmester A, Blanching of Unvarnished Modern Paintings: A Case Study on a Painting by Serge Poliakoff. In: *Cleaning, Retouching, and Coatings: Technology and Practice for Easel Paintings and Polychrome Sculptures,* Brussels, 1990, p. 138-143.

170b. Williams RS, Blooms, Blushes, Transferred Images and Moldy Surfaces: What are these disfiguring Accretions on Art Works?, The International Institute for Conservation - Canadian group, 14th Annual Conference, Toronto, 1988.

170c. Burnstock A, Caldwell M, Odlyha M, A technical examination of surface deterioration of Stanley Spencer's Paintings at Sandham Memorial Chapel, ICOM Committee for Conservation. 10th triennial meeting, Washing

ton, DC, 1993, (ed. Bridgland J), Inernational Council of Museums Committe for Conservation, Paris: p. 231-238

171. Hill GVG, The Mechanism of the Formation of Crystalline Bloom on Paint Films, *J. Oil Col. Chem. Assoc.* **57:** 1974, p. 342-344.

172. Schueler BW, Microscope Imaging by Time-of-Flight Secondary Ion Mass Spectrometry, *Microsc. Microanal. Microstruct.* **3:** 1992, p. 119-139.

173. Vickerman JC and Briggs D, TOF-SIMS: Surface Analysis by Mass Spectrometry. In: *Imp Publications and Surfacee spectra Limited* (Eds. Vickerman JC and Briggs D), 2001, p. 789.

174. Pouli P, Emmony DC, Madden CE and Sutherland I, Analysis of the Laser-Induced Reduction Mechanism of Medieval Pigments, *Applied Surface Science* **173:** 2001, p. 252-261.

175. Teixeira PIC and Mulder BM, Cell Dynamics Model of Droplet Formation in Polymer-Dispersed Liquid Crystals, *Physical Review E* **53(2):** 1996, p. 1805-1815.

176. Kühn H and Curran M, Chrome Yellow and Other Chromate Pigments. In: *Artists' Pigments 1, a Handbook of Their History and Characteristics*, Vol. 1 (Ed. Feller RL), Cambridge University Press, Washington, 1986, p. 187-218.

177. Leighton J, Reeve A, Roy A and White R, Vincent Van Gogh's 'a Cornfield, with Cypresses', *National Gallery Technical Bulletin* **11:** 1987, p. 42-59.

Summary

Artists have used paint to express themselves for thousands of years. Paintings form an important part of our cultural heritage, but many questions regarding their chemical composition, ageing and correct conservation remain to be answered. The analysis of paintings presents a number of challenges because of the high complexity of these multi-layered, inhomogeneous, and impure systems. Many of the current analytical techniques require the dissection of a physical sample and therefore restrict the accuracy with which the original position of a sample can be determined. The distinction of different sections within a sample can be greatly improved by a spatially resolved analysis of paint cross-sections using imaging techniques. This Thesis focuses on the development and application of spectroscopic imaging techniques for paint research. Chapter 1 provides a short introduction into the composition of a painting, followed by an overview of the most important non-destructive and destructive analytical techniques. The remainder of this Thesis can be divided into three sections: development and evaluation of different imaging techniques and sample preparation methods (Chapters 2, 3, 4), the characterisation of several naturally aged paints from test panels (Chapter 5), and the investigation of samples from various paintings by the application of several imaging and other techniques (Chapter 6,7,8).

A VIS-imaging (visual light microspectroscopic imaging) system has been built, tested and applied to several paint cross-sections (Chapter 2). The presented technique provides the possibility to acquire visual light spectra with a maximum spatial resolution of about 1 μm. Visual light spectra of different traditional and modern pigments that can hardly be discriminated by normal microscopy show distinctly different features. This imaging technique has proven to be effective for distinguishing the visual light spectra of several 17th century blue pigments. It was possible to recognise the spectral characteristics of smalt, even in partly or completely discoloured particles. Analysis of paint cross-sections by VIS-imaging is easy and does normally not require sample preparation.

Analysis of cross-sections by FTIR and FTIR-imaging provides a higher chemical specificity, but the experimental procedure for sample preparation is not straightforward. Several commonly used and newly developed sample preparation techniques are evaluated in Chapter 3. Transmission spectra of physically dissected samples yield high-quality infrared spectra, but limit the spatial resolution to about 50 μm. Smaller details can be analysed individually when the applied sample preparation method leaves the layer structure intact, for example when a sample is embedded in a synthetic resin. Specular reflectance measurements of these paint cross-sections compromise the chemical specificity, as the obtained spectral quality is rather poor. Other techniques to allow the acquisition of higher quality spectra from embedded cross-sections (diffuse reflection, microscopic ATR, microtomy, Raman spectroscopy) however were not successful. A new sample preparation technique for making thin sections by polishing of paint cross-sections embedded in KBr provides the best combination of high spatial resolution and high spectral quality.

Chapter 4 describes a study of a paint cross-section of Rembrandts *Portrait of a standing man* (Staatlichen Gemälde Galerie Kassel, GK 239). FTIR imaging of this cross-section identified and localised different compounds such as lead white, calcium carbonates, and metal carboxylates in the layers of this sample. These findings could be correlated well to SEM-EDX

analyses and art historical evidence. The most interesting feature of this specimen was a discoloration that was observed in large parts of the described painting. The hypothesis on the nature of this discoloured paint layer is the increased porosity of the upper paint layer due to the loss of binding medium was proposed to explain this effect.

Chapter 5 provides an overview of the ageing processes involved in the drying of oil and naturally aged oil paint. The initial reactions in a drying oil were monitored by FTIR spectroscopy. A large number of naturally aged paints were analysed to evaluate the long-term influence of pigments on the ageing of oil. The most significant effects of pigmentation are the acceleration of hydrolysis of ester bonds (most pronounced for paint made with minium or zinc white), changes in the effects of oxidation (in paint with ochre or ultramarine) and the formation of metal carboxylates (in paints with lead white, zinc white, Naples yellow, or minium).

The final part of this Thesis focuses on the observation and further analysis of a paint defect found in several 17th and 19th century paintings by the Dutch painters Van Rijn, Seghers and Bosschaert, Cuyp, Vermeer, Hals (Chapter 6) and Van Gogh (Chapter 8) and the American painter Church (Chapter 7). These defects are visible as ~100 μm diameter homogeneous aggregates of a transparent material. Isolated samples and cross-sections taken through these defects in the five 17th century Dutch paintings were investigated by FTIR, FTIR-imaging, SEM-EDX, VIS-imaging, and SIMS. These studies indicated the presence of metal carboxylates in the aggregated material. Different remineralised compounds were found in this metal carboxylate matrix, e.g. minium, basic lead carbonate, and basic lead chloride (fiedlerite). Very similar defects were found in a primed but unfinished canvas that was found in the archives of Olana, the former home of the 19th century American painter Frederic Church. Samples from these canvases were investigated by the techniques mentioned above as well as by GC-MS and DTMS. The results imply that the defects are formed in the priming, which consists of different layers pigmented by chalk and/or lead white. The material found in protrusions contains large amounts of lead carboxylates of mainly saturated fatty acids, but appears to lack an ionomeric oil network fraction. It is hypothesised that protrusions are formed upon phase separation of the mobile, saturated fatty acids from the oxidised oil network and the subsequent reaction of these fatty acids to lead carboxylates. This hypothesis was supported by a pilot experiment, in which lead white transformed into lead carboxylates quantitatively upon reaction with fatty acids. The unfinished canvases found in Olana are also affected by efflorescence, the exudation of a material on the surface of the painting. The compounds identified in the efflorescent material are very similar to those of protrusions, and it is hypothesised that they are formed by a similar mechanism.

Similar protrusions were found in *Falling Leaves (Les Alyscamps)* by Vincent van Gogh. These protrusions formed in a paint containing lead chromate, calcium sulphate is paint mainly consist of zinc carboxylates. The carboxylic acid part of these protrusions also consists mainly of saturated fatty acids, similar to the lead based protrusions. Evidence was found for the mobility of the involved zinc components, probably induced by a higher pressure or temperature. This implies that the aggregation may have occurred after formation of the zinc carboxylates.

Samenvatting

Kunstenaars uiten zich al duizenden jaren met behulp van verf. Schilderijen vormen een belangrijk deel van ons cultureel erfgoed, maar de kennis over hun chemische samenstelling, veroudering en conservering is nog verre van compleet. Schilderijen zijn complexe systemen om te bestuderen: ze bestaan vaak uit meerdere verflagen, die op hun beurt weer bestaan uit mengsels van verscheidene, niet geheel zuivere materialen.

Veel van de huidige analytische technieken kunnen slechts los monstermateriaal analyseren. Daarmee wordt de precisie waarmee een bepaalde laag of een bepaald deeltje geanalyseerd kan worden gereduceerd tot de precisie waarmee die deelstructuur bemonsterd kan worden. De analyse van kleinere structuren binnen een monster kan sterk verbeterd worden door verf dwarsdoorsneden te bestuderen met plaatsoplossende technieken. Dit Proefschrift beschrijft de ontwikkeling en toepassing van verschillende plaatsoplossende technieken om verf te analyseren. Hoofdstuk 1 beschrijft de globale opbouw van een schilderij, gevolgd door een overzicht van de meest gebruikelijke technieken om schilderijen te analyseren. Het overige deel van dit Proefschrift bestaat uit drie delen: ontwikkeling en evaluatie van verschillende plaatsoplossende z.g. *imaging* technieken en methoden om monsters voor te bereiden voor een meting (Hoofdstukken 2, 3, 4), de analyse van verfmonsters uit verschillende testpanelen (Hoofdstuk 5) en de analyse van monsters uit diverse schilderijen met verscheidene imaging- and andere technieken (Hoofdstukken 6, 7, 8).

Een VIS-Imaging (microscopisch zichtbaar-licht imaging) systeem is ontwikkeld, getest, en gebruikt voor de analyse van verschillende verfdwarsdoorsneden (Hoofdstuk 2). Met deze techniek kunnen zichtbaar licht spectra van een vlak monster opgenomen worden met een maximale plaatsresolutie van ongeveer 1 μm. Zichtbaar licht spectra van verschillende traditionele and moderne pigmenten zijn duidelijk te onderscheiden en toe te kennen, ook wanneer directe identificatie met behulp van normale microscopie vrijwel onmogelijk is. Als voorbeeld onderzochten we een aantal 17^e eeuwse blauwe kleurstoffen. Smalt kon zelfs herkend worden in volledig ontkleurde toestand. Analyse van verfdwarsdoorsneden met VIS-imaging is relatief eenvoudig, en speciale monstervoorbereiding is normaliter niet nodig.

Informatie met een grotere chemische specificiteit werd verkregen met Fourier transform infrarood spectroscopie (FTIR) en FTIR-imaging. Een goede monsterpreparatie voor deze analysetechniek is essentieel. Daarom worden verschillende bekende en nieuw ontwikkelde preparatietechnieken geëvalueerd in Hoofdstuk 3. Transmissie spectra van geïsoleerde monsters zijn doorgaans kwalitatief erg goed, maar structuurelementen kleiner dan ongeveer 50 μm zijn nauwelijks toegankelijk met deze methode. Kleinere details kunnen individueel geanalyseerd worden door de laagstructuur van het monster intact te laten, bijvoorbeeld door een dwarsdoorsnede in te bedden in synthetische hars. De spectra, die verkregen worden door directe analyse van deze dwarsdoorsneden met speculair gereflecteerd licht, zijn echter niet optimaal, wat de mogelijkheden voor een chemische interpretatie beperkt. Andere methoden om betere spectra van een ingebed monster verkrijgen zijn niet gelukt (diffuse reflectie, microscopische ATR, microtomie, Raman spectroscopie). Een nieuw ontwikkelde monsterpreparatietechniek, die gebruik maakt van dunne doorsneden verkregen door het polijsten van een dwarsdoorsnede ingebed in KBr, leidde tot de meest geslaagde combinatie van goede spectra en een hoge

plaatsresolutie.

Hoofdstuk 4 beschrijft de analyse van een verfdwarsdoorsnede van Rembrandts *Portret van een staande man* (Staatlichen Gemälde Galerie Kassel, GK 239). FTIR-imaging resultaten van deze dwarsdoorsnede zijn gebruikt om verschillende materialen, zoals loodwit, calcium carbonaat, en metaal carboxylaten, te identificeren en te localiseren. De resultaten verkregen met FTIR-imaging zijn vergeleken met SEM-EDX analyses en kunsthistorische gegevens. De meest interessante eigenschap van dit monster is de gedeeltelijke ontkleuring van de verflaag. Als hypothese voor deze ontkleuring werd een toegenomen porositeit van de verflaag voorgesteld, wat veroorzaakt kan zijn door verlies van het bindmiddel.

Hoofdstuk 5 geeft een overzicht van de verouderingsprocessen, die optreden in drogende olie en verf, die op natuurlijke wijze verouderd is. De initiële reacties in een drogende olie zijn gevolgd met FTIR spectroscopie. Daarnaast zijn een groot aantal natuurlijk verouderde verven onderzocht om veranderingen op lange termijn te onderzoeken, met name de invloed van pigmenten op de veroudering van het bindmiddel. De belangrijkste effecten die gevonden werden zijn de katalyse van de hydrolyse van esterbindingen (vooral bij verf met zinkwit of rood lood (loodmenie)), veranderingen in het oxidatieproces (in verf met okers of ultramarijn) en de vorming van metaalzepen (loodwit, zinkwit, Napels geel of loodmenie verf).

Het laatste deel van dit Proefschrift beschrijft het onderzoek naar defecten die gevonden werden in 17e en 19e eeuwse schilderijen van Hollandse schilders als Van Rijn, Seghers en Bosschaert, Cuyp, Vermeer, Hals (Hoofdstuk 6), Van Gogh (Hoofdstuk 8) en de 19e eeuwse Amerikaanse schilder Church (Hoofdstuk 7). De onderzochte defecten bestaan uit homogene aggregaten van transparant materiaal met een diameter van ongeveer 100 mm). Geïsoleerde monsters en dwarsdoorsneden van de vijf 17e eeuwse Hollandse schilderijen waarin dit fenomeen gevonden werd, zijn geanalyseerd met FTIR, FTIR-imaging, SEM-EDX, VIS-imaging, en SIMS (Hoofdstuk 6). De aggregaten blijken grotendeels uit metaalcarboxylaten te bestaan met lood als metaalion. In de metaalcarboxylaat matrix zijn verschillende mineralen neergeslagen, zoals loodmenie, basisch loodcarbonaat, and basisch loodchloride (fiedleriet). Vergelijkbare defecten werden gevonden in een gegrondeerd, maar onvoltooid werk van de 19e eeuwse Amerikaanse schilder Frederic Church (Hoofdstuk 7). Verschillende monsters van dit doek werden geanalyseerd met de bovenstaande technieken aangevuld met GC-MS en DTMS. De grondering bestaat uit meerdere lagen die loodwit en/of kalk bevatten. Het materiaal dat in de protrusies gevonden werd, bevat vooral loodcarboxylaten van verzadigde vetzuren. Een ionomere olienetwerk fractie lijkt niet aanwezig te zijn. De hypothese voor het ontstaan van deze defecten, protrusies genaamd, is een fasenscheiding van de mobiele, verzadigde vetzuren van het geoxideerde olienetwerk, en de daaropvolgende reactie van deze vetzuren tot loodcarboxylaten. Deze hypothese werd ondersteund door een experiment waarin loodwit kwantitatief tot loodzepen bleek te reageren met vetzuren. De wittige uitslag of "bloom", die ook op dit onvoltooide werk gevonden werd, vertoond een grote gelijkenis met de materialen in de protrusies. De huidige hypothese is dat beiden door een vergelijkbaar mechanisme ontstaan.

Vergelijkbare protrusies werden gevonden in *Vallende bladeren (Les Alyscamps)*, geschilderd door Vincent van Gogh (Hoofdstuk 8). In dit geval hebben de defecten zich gevormd in een verf van loodchromaat, calciumsulfaat, barium sulfaat en zeer waarschijnlijk zinkwit. De protrusies in deze verf bestaan uit zinkcarboxylaten, waarvan het organische deel ook in dit geval

voornamelijk uit verzadigde vetzuren bestaat. Er zijn aanwijzingen gevonden dat zinkcarboxylaten in de verflaag mobiel zijn onder invloed van een hogere druk of temperatuur. In dit geval is het dus mogelijk dat de aggregatie is opgetreden na de vorming van de zinkcarboxylaten.

Dankwoord

Ik kan mij nog heel goed herinneren hoe ik zo'n 4½ jaar geleden voor het eerst achter de FTIR zat, en met een stapeltje artikelen probeerde uit te zoeken wat ik nu eigenlijk ging doen. En nu ineens ligt daar een boekje met in het groot mijn naam voorop. Tussendoor is er heel wat gebeurd en ben ik op vele momenten geholpen en bijgestuurd. Al die personen die daarin bijgedragen hebben ben ik dankbaar. Ze hebben mijn tijd op AMOLF tot een nuttige en goede tijd gemaakt.

Ron, jouw grondig fysisch inzicht is regelmatig gebruikt om onverklaarbare dingen duidelijk te maken. Ik heb veel geleerd over het gemak waarmee verschillende apparaten uit elkaar te halen of aan elkaar te knopen zijn; iets wat nog regelmatig van pas komt. Bovenal, je uitbundige enthousiasme waarmee mijn soms wat sarcastische kijk op tegenvallende resultaten weer in het juiste perspectief gezet werd, bleek op een aantal momenten hard nodig. Helaas snap ik nog steeds niet waarom je rondjes draait als je maar aan één kant van een kano peddelt.

Jaap, de kritische blik op verkregen resultaten, het vermogen al die verschillende technieken naast elkaar te leggen en daar de relevante info uit te halen zijn een voorbeeld geweest. Wat me bovenal bij zal blijven is je tomeloze inzet in de laatste periode. De laatste sessies, tot diep in de nacht, waren vruchtbaar. Ik reken het tot één van mijn betere resultaten dat je nu veel positiever over IR denkt dan een jaar of vier terug.

Een ander groots resultaat is het computergebruik van mijn gewaardeerde co-promotor, Prof. Van Asperen de Boer. Het grootste deel van onze samenwerking was gericht op de IRR. Deze experimenten, en laat ik de daarbijbehorende uitjes naar musea en kerken niet vergeten, verenigden het nuttige zeer goed met het aangename. Daarnaast wil ik u hartelijk bedanken voor de lessen over schilderijen, verf, lagenopbouw en onderzoekstechnieken.

De collega's die als vraagbaak gediend hebben, hebben mij voor veel wankele interpretaties behoed. Ik denk vooral aan Jorrit van den Berg, die al veel langer en beter in de chemie van drogende olie thuis was. Vaak ben ik bij hem binnengelopen: "Jorrit, ik zie A, kan dat B betekenen?". En steevast was het antwoord: "Ehh, dat ligt niet zo gemakkelijk, want dat kan inderdaad B zijn, maar vergeet ook C en D niet. En ik moet E en F nog even nakijken". Zo langzamerhand ben ik op die manier toch ingewijd in de moeilijke olie-chemie. Ook de enorme mogelijkheden van data-analyse die Gert Eijkel uit een computer kan trekken hebben me enorm geholpen. Het is jouw verdienste dat ik de matrix-bestanden en berekeningen nu redelijk doorzie, en kan gebruiken. Het kost wel eens wat moeite om een probleem zo interessant te formuleren dat je er daadwerkelijk energie in stopt. Maar vervolgens zijn Fourier-transformaties toch ook minstens zo interessant als borrels....

In de loop der jaren heb ik verschillende mensen ingewerkt op 'mijn' FTIR. De nuttige kant daarvan is dat er een discussie over de interpretatie op gang komt. Vooral Muriel en Annelies hebben zich vol overgave op de spectroscopie gestort. Beiden hebben mij ook flink wat over microscopie en pigmenten bijgebracht, waarvoor hartelijk dank.

En dan natuurlijk de vele andere collega's die mijn verblijf hier verder opgefleurd hebben. Ik denk dan aan Georgiana Languri, Oscar van den Brink, Sander Koster, Petra Novotna, Gisela van der Doelen, Olga Katsibiri, Stefan Luxembourg, Lidwien Speleers, Jerre van der Horst, Marc Duursma, Marieke van Veen, Theo van Diepen, Frank Hoogland, Beatrice Marino, Tania